TECHNICAL REPORT

Remediation and Treatment Technology Development and Support for DOE Oak Ridge Office: EFPC Model Update, Calibration and Uncertainty Analysis

Date submitted:

March 1, 2013

Principal Investigators:

Leonel E. Lagos, Ph.D., PMP®
David Roelant, Ph.D.

Florida International University Collaborators:

Lilian Marerro, MS Candidate, (DOE Fellow)
Georgio Tachiev, Ph.D., PE
Angelique Lawrence, MS, GISP
Hector R. Fuentes, PhD

Submitted to:

U.S. Department of Energy
Office of Environmental Management
Under Grant # DE-EM0000598

Applied Research Center
Florida International University

EXECUTIVE SUMMARY

This research continues previous efforts to correlate the hydrology of East Fork Poplar Creek (EFPC) and Bear Creek with the long term distribution of mercury within the overland, subsurface, and river sub-domains. An integrated surface-subsurface flow and mercury transport model (MIKE SHE and MIKE 11) was modified to reduce computational time and resources, predict flow discharges and total mercury concentration at key monitoring stations under various hydrological and environmental conditions, and include the reactive transport mercury exchange within sediments and porewater (ECOLAB) through the watershed. Historical precipitation, groundwater levels, river discharges, and mercury concentrations were retrieved from government databases and incorporated at various points throughout the domain in the form of boundary conditions. Sensitivity analysis results show the general trend between the organic partition coefficient and the total mercury present. Duration and probability exceedance curves detail the relationship between discharges and mercury loads at various stations throughout EFPC.

TABLE OF CONTENTS

LIST OF TABLES

LIST OF FIGURES

LIST OF ACRONYMS

ARC	Applied Research Center
DHI	Danish Hydraulic Institute
DOE	Department of Energy
EFPC	East Fork Poplar Creek
EPA	Environmental Protection Agency
FDC	Flow Duration Curve
FDI	Flow Duration Interval
foc	Fraction Organic Carbon
LDC	Load Duration Curve
MHL	Melton Hill Lake
NPDES	National Pollution Discharge Elimination System
OREIS	Oak Ridge Environmental Information System
ORNL	Oak Ridge National Laboratory
ORR	Oak Ridge Reservation
TMDL	Total Maximum Daily Load
TSS	Total Suspended Solids
USGS	United States Geologic Survey
WCS	Watershed Characterization System

LIST OF VARIABLES

difv	Diffusion coefficient in water
dz	Thickness of the actual layer in computational grid
dzds	Thickness of diffusion layer in sediment
dzwf	Average thickness water film that metals have to diffuse through
$f_{biot \cdot difw}$	Factor for diffusion due to bioturbation
K_d	Partitioning coefficient for mercury between particulate matter and water
K_{ds}	Partitioning coefficient for mercury between sediment and pore water
ks	Desorption rate in sediment
	Adsorption rate [d^{-1}]
	Desorption rate [d^{-1}]
por_s	Porosity of sediment
S_{HM}	Dissolved Mercury Concentration in Water
S_{HMS}	Dissolved mercury concentration in sediment pore water
X_{HM}	Adsorbed mercury concentration in water
X_{HMS}	Adsorbed mercury concentration in sediment
X_{SED}	Mass of sediment
Vs	Settling velocity [m/d]
Vc	Critical current velocity for initiation of the movement [m/s]
RR	Re-suspension rate [$g/m^2.d$]
PPR	Particle production rate [$g/m^2.d$]

1. INTRODUCTION

The United States Department of Energy (DOE) decontamination and decommissioning activities of industrial, radiological and nuclear facilities seek to restore environmental conditions of contaminated sites to accepted levels designated by local, state and federal regulations. The East Fork Poplar Creek (EFPC) Watershed, shown in Figure 1, is located in the state of Tennessee and represents one of many contaminated sites. EFPC has been severely impacted by the release of more than 100 metric tons of elemental mercury as a byproduct of nuclear processing activities employed in the lithium-isotope separation process used in the production of nuclear fusion weapons during the 1950's [**1**].

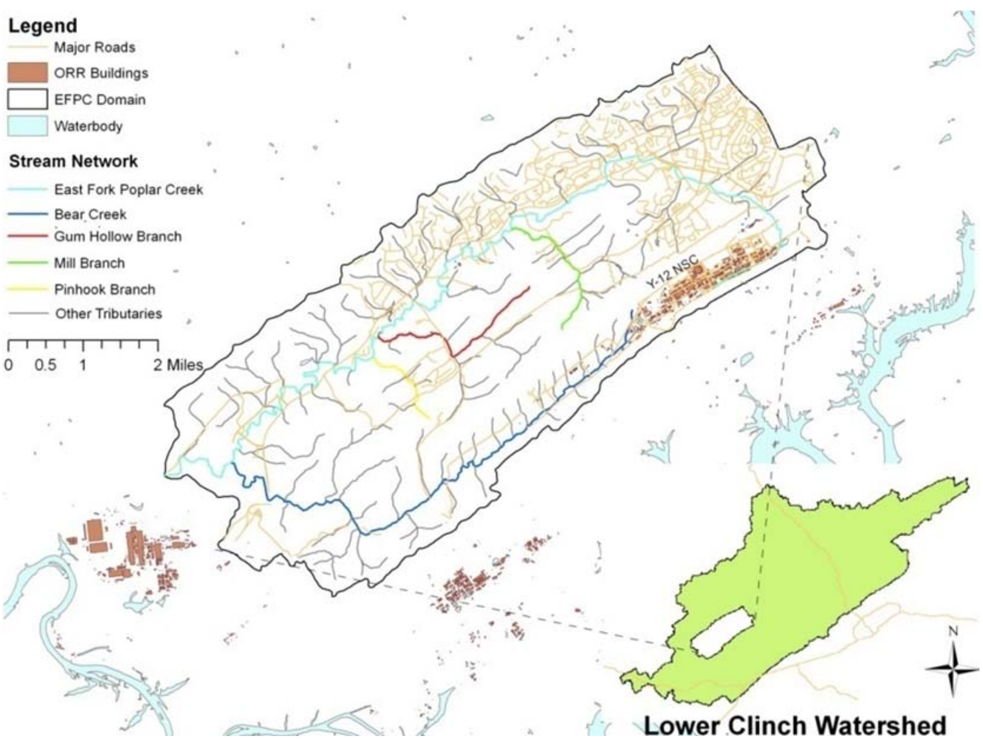

Figure 1 East Fork Poplar Creek watershed and stream network.

Studies have identified over 77,000 kg of mercury present in the upper 10 feet of soils along a 15-mile long stretch of EFPC [**2**]. Mercury is present in the sediment, surface water, groundwater, and infrastructure in the National Security Complex (Y-12) area and in the upper reaches of EFPC [**2**]. Mercury releases into the creek ceased in 1963; nonetheless, the pollution continues to spread. Although remediation strategies have been implemented since the problem's inception, the issue of mercury contamination continues to prevail.

Figure 2 Mercury present in sub-surface soil samples from Oak Ridge [**3**].

The state of Tennessee continues to list portions of the EFPC as not supporting their designated use classifications such as aquatic life, irrigation, livestock watering, wildlife, and recreation due to mercury contamination [**4**]. Streams and lakes in violation of one or more water quality standards within the state of Tennessee are described in the 303 (d) list. Portions of this list are summarized in the table below for streams near the Oak Ridge Reservation. Shown in Table 1, contaminated streams relevant to the present study include 9.7 impaired miles of EFPC within Roane County, and 11.3 miles within Anderson and Roane. Approximately 141 acres of the Poplar Creek Embayment, Watts Bar Reservoir, within Roane County are also contaminated.

Table 1 Streams in violation of water quality standards

Water Body ID	Waterbody Impacted	County	Miles/Acres Impaired
TN06010207026 – 0600	Bear Creek	Roane	10.87
TN06010207026 – 1000	EFPC	Roane	9.7
TN06010207026 – 2000	EFPC	Anderson/Roane	11.3
TN08010208009 - 1000	Poplar Creek	Haywood/Fayette	23.6
TN08010208011 - 2000	Bear Creek	Fayette	7.9
TN08010209021 – 0110	Bear Creek	Shelby/Tipton	14.5
TN05130104050 - 0100	East Branch Bear Creek	Scott	5.7
TN05130104050 - 1000	Bear Creek	Scott	2.6
TN06010102003 – 0500	Bear Creek	Sullivan	4.6
TN08010204004 - 0100	Bethel Branch	Dyer/Gibson	30.4
TN06010207001 - 0100	Poplar Creek Embayment, Watts Bar Reservior	Roane	141 ac

Elemental mercury dissolves and oxidizes to mercuric ion under environmental conditions resulting in increased mobility of mercury due to its increased solubility. Higher concentrations of mercury and suspended solids have been recorded as a byproduct of higher volumes and higher stream velocities during and post flood events [**5**]. Mercury present in surface water is converted to various forms. Mercury particles may settle with sediments, may be consequently diffused into the water column, re-suspended, or hidden within sediments until a hydrological event disturbs the particles and reignites the complex cycle through which it is recycled [**5**]. Mercury is released from bed sediments as bed layer particles are re-suspended. Mercury exchange occurs between the water column and sediment as well as between the dissolved and adsorbed phases of mercury via adsorption-desorption processes [**6**]. Methylmercury is the most toxic form of mercury because it can accumulate at a faster rate within organisms in comparison to the rate at which it can be eliminated; as takes longer for organisms to remove it from their systems [**7**]. Effects are dependent upon the chemical form and type of exposure. The mercury within the EFPC system is continuously recycled by the surrounding environment, making the successful implementation of remediation strategies difficult to execute.

Mercury contamination in the environment represents a health concern for wildlife, as well as humans [**7**]. Studies have shown a correlation between total mercury concentration within the creek and methylmercury concentrations and long term bioaccumulation and biomagnifications. Understanding the processes by which mercury is transported and recycled within the EFPC environment is an essential step towards complying with applicable and relevant or appropriate requirements (ARARs) in the DOE's Record of Decision (ROD) Phase I and Phase II [**8**] [**9**].

Total Maximum Daily Load (TMDL) studies, identify the sources of pollutant in a stream, quantify the amount, and recommend appropriate action to be taken in order for the stream to no longer be polluted. Further analysis and modeling of the area is necessary so that TMDLs studies may be developed in the future.

Previous efforts to model the hydrological environment and mercury transport dynamics within the Oak Ridge Reservation include the major contributions made by Long (2009) and Cabrejo (2011). Long created a baseline model capable of simulating the hydrology and mercury transport throughout the entire EFPC Watershed. Cabrejo focused on a subsection of the watershed known as Upper East Fork Poplar Creek, and instead considered as factors adding to the total mercury concentration, the diffusive transport between the water column and sediment pore water and the adsorption-desorption processes between dissolved mercury and suspended matter in the water column. This research combines both methods by incorporating ECOLAB to simulate the fate and transport of mercury at the water and sediment interface throughout EFPC.

In this report, results for simulated discharges, contaminant concentration levels, and mercury loads are presented in the form of timeseries. Probability distribution curves were developed for each set of timeseries. Flow, discharge and load duration curves were developed for various hydrological regimes.

2. BACKGROUND

Models are generally categorized as stochastic or deterministic, and further classified as conceptual or empirical depending on their ability to obey the physical laws. Stochastic models are dependent upon random variables dominated by a probability distribution function. In deterministic models all the input parameters are known within a specific certainty range. Modeling tools have been used extensively to simulate system dynamics. For instance, MIKE SHE/MIKE 11 modeling systems have been applied by the South Florida Water Management District (SFWMD) in an integrated approach that successfully simulates wetland dynamics as part of the Everglades Nutrient Removal (ENR) project [**10**]. The models have also been applied in Broward County to develop an Integrated Water Resources Master Management Plan (IWRMMP) [**11**].

Other studies employed computer models to emphasize the significance of sediments and suspended matter in contaminant transport. A study performed by the North Carolina Department of Natural Resources revealed that 75% of the total mercury load present in the Cashie River Watershed resulted from eroded sediments [**12**]. A study on the "Development of a Mercury Speciation, Fate and Biotic Uptake (BIOTRANSPEC) Model", applied to the Lohatan Reservoir in Nevada, showed that 90% of the mercury released into the system was maintained within the sediments and constituted a continuous source of pollution [**13**]. Similarly, Cabrejo analyzed how mercury within the sediment serves as a continuous source of pollution within portions of the Y-12 National Security Complex, a sub-domain of the EFPC Watershed [**5**]. A study simulating flow and mercury transport in upper portions of EFPC also confirmed that for the sub-domain, a large portion of the mercury in the river is present as mercury bound to sediment particles [**6**]. These studies summarize the importance of the adsorption-desorption process in mercury contaminated environments, especially when the contaminant has an affinity to sorb to soils in the sediment bed layer.

2.1 Site Description

The geological characteristics of the EFPC watershed, its tributaries' attributes, and vegetation cover have been extensively described by Long [**14**]. This section serves as a summary of efforts previously executed in characterizing the site since the project's inception.

East Fork Poplar Creek (EFPC) is located within the Oak Ridge Reservation (ORR) in the state of Tennessee, in the counties of Roane and Anderson. The reservation houses three major US Department of Energy facilities within 14,260 ha. These include the Y-12 National Security Complex, the East Tennessee Technology Park (ETTP) or K-25 complex, and the Oak Ridge National Laboratory. EFPC watershed is a sub-watershed of the larger Poplar Creek watershed; one of four sub-watersheds of the Lower Clinch River watershed (Hydrologic Unit Code (HUC) 06010207). The EFPC watershed domain area covers approximately 29.7 square miles.

An estimated 88 square miles of streams and tributary branches have been identified within the domain. Bear Creek and EFPC are two small rivers with a length of more than 12,500 kilometers in length. As shown Figure 1, Gum Hallow Branch, Mill Branch, and Pinhook Branch represent other tributaries of significant length. As can be observed from the figure, EFPC is recharged by Bear Creek, Gum Hollow Branch, Mill Branch, and Pin Hook Branch in addition to 30 unnamed tributaries. These tributaries were all included in the model.

Geological formations beneath ORR include primary group formations recognized as: the Knox (OCk), Rome (Cr), Chickamauga (Och), and Conasuaga (Cc), Sequatchie Formation (Os), Fort Payne Chert (Mfp), Rockwood Formation (Sr), Copper Ridge Dolomite (Ccr), Maynardville Limestone (Cmn). The Knox aquifer and the Chickamauga Group are the dominant hydrologic units in which flow is controlled by solution conduits, leaky confining units in which flow is dominated by fractures and relatively low hydraulic conductivity.

Landcover includes intensive agriculture, urban and industrial, or areas of thick forest. White oak forests, bottomland oak forests, and sycamore-ash-elm riparian forests are the common forest types, and grassland barrens intermixed with cedar-pine glades also occur here.

3. RESEARCH OBJECTIVE

The purpose of this research is to correlate the hydrology of the EFPC and Bear Creek with the long term distribution of mercury within the overland, subsurface, river, and vadose zone sub-domains. Previous modeling efforts; which originally included only the upper portions of EFPC were extended to include the entire EFPC, down to station EFK 6.4 and the Bear Creek. Modeling software MIKE SHE, MIKE11, and ECOLAB were combined in a comprehensive package that models the flow, transport, and mercury exchange within sediment layers. The model considers the most significant parameters and processes of flow and mercury transport for the study site by incorporating a flow, advection, dispersion, water quality and sedimentation (ECOLAB) module. The research includes an analysis of spatial and temporal patterns as a result of variations of selected properties of the sub domain and also emphasizes the stochastic modeling of the system. The impact of sedimentation within the mercury recycling process was assessed through a series of simulations. This component was analyzed in greater detail within this study through the incorporation of a sedimentation layer module (ECOLAB), which addresses the dissolved mercury in the water, the adsorbed mercury concentration on suspended matter, the dissolved mercury in sediment pore water, and the adsorbed mercury in the sediment.

The model is intended to serve as a useful remediation tool since the site will be characterized using relevant historical records for precipitation, groundwater levels, and river discharges obtained from the Oak Ridge Environmental Information System (OREIS) and the Oak Ridge National Laboratory (ORNL) databases, which will be incorporated into the model in the form of boundary or calibration conditions. The incorporation of the ECOLAB module is expected to better characterize the mercury processes in the EFPC environment since mercury species are known to diffuse from contaminated sediment pore water to creek water in the form of diffusive transport.

4. RESEARCH METHODOLOGY

The following approach was applied in modifying and executing the hydrology and transport model developed in support of the DOE's remediation strategies for the EFPC watershed. These techniques expand upon previous modeling efforts including the diffusive transport between the water column and sediment pore water, and the adsorption-desorption processes between dissolved mercury and suspended matter in the water column as part of the total mercury concentration. The integrated surface/subsurface model was built using the numerical package, MIKE (MIKE 11 coupled with MIKE SHE and ECOLAB), developed by the Danish Hydraulic Institute (DHI). The sedimentation module, which originally included UEFPC, was extended to include the entire EFPC, down to EFK 6.4 and the Bear Creek. The sedimentation and water quality module were extended to the entire EFPC watershed in the following phases:

1. The water quality and sedimentation module (ECOLAB) was extended for Bear Creek and for the remaining section of EFPC (downstream of Station 17) to include EFK 6.4.

2. Water quality, transport related, and sediment related parameters, such as carbon partitioning coefficient, adsorption rates of mercury species to sediment particles and water molecules, re-suspension rate of sediments, settling velocity of suspended particles, and critical current velocity for sediment re-suspension were estimated from literature, such as DOE reports of field surveys, laboratory experiments reported by FIU or other research institutes, and referenced publications.
3. Simulations were executed for a range of significant input parameters to correlate stochastic hydrologic events with mercury distribution patterns.
4. The extended EFPC model was calibrated using observed total suspended solids and total mercury concentration timeseries (including dissolved and adsorbed mercury concentrations) recorded at the key stations downstream of Station 17 (EFK 23.4). The calibration procedures consisted of:
    a. Identifying the significant input parameters in the water quality module. This step was carried out for the UEFPC model and the significant parameters were identified. There are two major sets of input parameters associated with the water quality modeling:
        1. Transport-related parameters including carbon partitioning coefficient and adsorption coefficients; and
        2. Sediment-related parameters including the re-suspension rate, critical current velocity, settling velocity for the suspension of sediment particles, and particle production rate along the creek.
5. Model simulations using observed total suspended solids and total mercury concentration timeseries were analyzed using a range of correlations, including:

a. Timeseries plots of observed and simulated values for flux or state variables.
b. Flow duration curves (FDC) and probability exceedances.
c. Mercury probability exceedances.
d. Load duration curves.

6. The approach implemented for data processing from ORNL includes:
   a. Data processed for validity and categorized into spreadsheets.
   b. New stations were added to GIS maps of the site.
   c. Timeseries files were developed and input into the model.
   d. Model nodes, cross-sections, and boundaries were modified as necessary due to the addition of new observation stations.

5. MODEL OVERVIEW

The model includes the main components of the hydrological cycle and contaminant transport; groundwater flow and transport (3D saturated and unsaturated), overland flow, flow in rivers, precipitation, and evapotranspiration. The model enables full dynamic coupling of surface and subsurface flow processes which allows calculations of water and contaminant exchange between the land, rivers, and the groundwater. By providing detailed spatial information and characteristics including hydrological and transport properties in the four sub-domains, Saturated Zone (SZ), Unsaturated Zone (UZ), Overland Flow (OL), and Transport in Streams (OC), the model provides accurate water and contaminant mass balance for the domain. MIKE SHE and MIKE 11 are used to simulate and assess the impact of hydrological events on mercury contamination. The processes simulated by each module (MIKE 11, MIKE SHE, and ECOLAB) in the EFPC model are shown in Figure 3 and explained in greater detail within the subsequent sections. Figure 28 in the Appendices of this report, provides a conceptual schematic based on the EFPC model modular set up. The diagram denotes the various pathways of interaction among the MIKE SHE, MIKE 11, and ECOLAB modules and list the numerical engines associated at each level of computation.

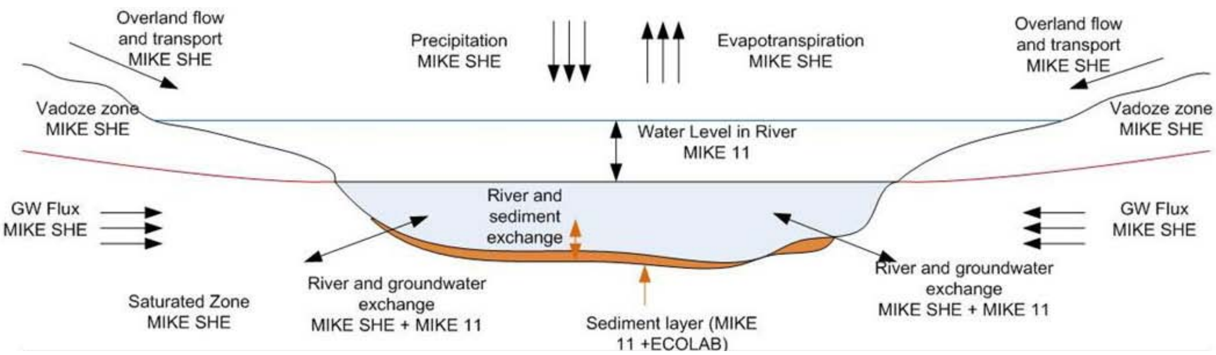

Figure 3 Processes simulated by MIKE modules.

5.1 MIKE 11 and MIKE SHE

MIKE 11 is a one-dimensional river flow and transport model that requires longitudinal profiles, cross-sections, Manning's numbers, and other hydrodynamic parameters [**15**]. It uses the dynamic Saint Venant equations to determine river flow and water levels. The complete nonlinear equations of open channel flow (Saint-Venant) can be solved numerically between all grid points at specified time intervals for given boundary conditions. In addition to this fully dynamic description, other descriptions are also available to choose from including high-order, fully dynamic, diffusive wave, kinematic wave, quasi-steady state, and kinematic routing (Muskingum, Muskingum-Cunge).

MIKE SHE is a fully integrated model for the 3D simulation and linkage of hydrologic systems including overland, subsurface, and river flows. It has been successfully applied at multiple scales, using spatially distributed and continuous climate data to simulate a broad range of integrated hydrologic, hydraulic, and transport problems. MIKE SHE represents the the two-dimensional overland, one-dimensional unsaturated zone, three-dimensional saturated and vadose zone flow and transport components [**16**]. The hydrologic processes are described based on physical laws such as the conservation of mass, energy and momentum. MIKE SHE couples several partial differential equations that describe flow in the saturated and unsaturated zones with the overland and river flow. Different numerical solution schemes are then used to solve the different partial differential equations for each process. A solution to the system of equations associated with each process is found iteratively by use of different numerical solvers.

The model enables MIKE SHE and MIKE 11 Hydrodynamic (HD) modules to interact through branches or stream reaches defined within the domain. This coupling allows for one-dimensional simulation of river flows and water levels through the fully dynamic Saint Venant equations. Hydraulic control structures, area-inundation modeling, dynamic overland flooding flow in relation to the MIKE 11 river network, and the dynamic coupling of surface and sub-surface flow is simulated. Floodplain flooding is simulated by first establishing the floodplain through the MIKE SHE topography and then activating the direct overbank spilling option in MIKE 11 while simultaneously restricting cross-sections to the main channel. The cross-sections defined in MIKE 11 are used to calculate the river water levels and volumes. Consistency with topographical elevations is of extreme importance since the bank elevation is the primary reference for cell flooding. River and groundwater exchange is modeled by defining the river in contact with the aquifer. In this case, the water exchange between MIKE 11 and MIKE SHE is performed through a river-link cross section. The river cross-sections link is a function of Conductance (C), the grid node, and river link.

5.2 ECOLAB

ECOLAB is an equation solver for the sedimentation and exchange of mercury within sediments, suspended particles, pore water and dissolved mercury species [**17**]. An ECOLAB template can be developed by the user to model the ecological processes as required by any specific project; however, some templates have already been developed by DHI in the areas of water quality (17 templates), heavy metal transport (1 template), eutrophication (3 templates), and xenobiotics (1 template). For the modeling of mercury fate and transport in EFPC, the heavy metal transport template of ECOLAB is used coupled with both MIKE-11 and MIKE-SHE to simulate the interaction of mercury species with the sediment particles and water molecules in the creek. The heavy metal template describes the adsorption/desorption of mercury to suspended matter, the sedimentation of sorbed mercury to the streambed, as well as re-suspension of the settled mercury. It also includes exchange of mercury between particulates of the bed sediment and the interstitial waters of the bed. The diffusive exchange of dissolved mercury in the water and in the interstitial waters is also considered.

6. MODEL THEORY

6.1 MIKE 11

The one-dimensional numerical engine used to compute flow within the hydrodynamic (HD) module employs the Saint Venant Equations under various assumptions. The model disregards variations in density within the flow medium (water). Flow within rivers or streams are assumed to be parallel to the reach bottom. Moreover, water movement perpendicular to the flow direction of the stream is disregarded. These simplifications lead to the modified Saint Venant equations shown below; constituting the numerical foundation of the HD module.

$$\frac{\partial q}{\partial x} + \frac{\partial A_{fl}}{\partial t} = q_{in}$$

$$\frac{\partial q}{\partial t} + \frac{\partial\left(\alpha \frac{q^2}{A_{fl}}\right)}{\partial x} + gA_{fl}\frac{\partial h}{\partial x} + gA_{fl}I_f = \frac{f}{\rho_w}$$

The continuity equation; shown first above, emphasizes the conservation of mass within stream sections. The second equation expresses the conservation of momentum. The variables q, A_{fl}, q_{in}, h, a, I_f, *f*, and r_w respectively represent the discharge, cross-sectional area, lateral inflow per unit length, water level, the momentum distribution coefficient, friction slope, momentum forcing, and water density.

6.2 ECOLAB

ECOLAB was incorporated into the model through the Advection or AD module. The set of transport equations governing the advective ECOLAB dynamics are shown below in their non-conservative form:

$$\frac{\partial c}{\partial t} + u\frac{\partial c}{\partial x} + v\frac{\partial c}{\partial y} + w\frac{\partial c}{\partial z} = D_x\frac{\partial^2 c}{\partial z^2} + D_y\frac{\partial^2 c}{\partial z^2} + D_z\frac{\partial^2 c}{\partial z^2} + S_c + P_c$$

The variables c, u,v,w, D_x, D_y, D_z, S_c, and P_c represent the ECOLAB state variables concentration, flow velocity components, dispersion coefficients in the x, y, and z direction, sources and sinks, and ECOLAB processes. The transport equation is modified as:

$$\frac{\partial c}{\partial t} = AD_c + P_c$$

The rate of change in concentration as a byproduct of advection dispersion is accounted by the term AD_c. Per DHI, the ECOLAB solver calculates the concentration at each time step through an explicit time-integration where AD_c is constant at each time step. The ECOLAB module is capable of performing the explicit time-integration using various methods. These methods include the Euler, Runge Kutta 4, and Runge Kutta with quality check. The newly added ECOLAB module within EFPC was set to perform the explicit-time integration using the Runge Kutta 4th order. This method was selected because it has higher accuracy. As illustrated within the scientific manual the function:

$$y_{n+1} = y_n + h \cdot f(x_n, y_n)$$

is solved in the four steps shown below:

$$k_1 = h \cdot f(x_n, y_n)$$

$$k_2 = h \cdot f\left(x_n + \frac{h}{2}, y_n + \frac{k_1}{2}\right)$$

$$k_3 = h \cdot f\left(x_n + \frac{h}{2}, y_n + \frac{k_2}{2}\right)$$

$$k_4 = h \cdot f(x_n + h, y_n + k_3)$$

$$y_{n+1} = y_n + \frac{k_1}{6} + \frac{k_2}{3} + \frac{k_3}{3} + \frac{k_4}{6} - O(h^5)$$

The solution y is obtained from x_n to x_{n+1} and equivalent to $x_n + h$.

In addition to the internal computational processes described, mercury transport processes in ECOLAB are defined by specifying the following:

- Dissolved mercury in the water (S_{HM})
- Adsorbed mercury concentration on suspended matter (X_{HM})
- Dissolved mercury in the sediment pore water (S_{HMS})
- Adsorbed mercury in the sediment (X_{HMS})

S_{HM} is the byproduct of mercury exchange between suspended solids and the water column. This exchange is mainly driven by the organic carbon partitioning coefficient (K_d), indicating the contaminant's affinity towards the soil phase. Dissolved mercury is computed using the following set of interconnected equations:

$$\frac{dS_{HM}}{dt} = -adss + dess + difv$$

$$adss = k_w K_d S_{HM} TSS$$

$$dess = k_w X_{HM}$$

$$difv = \frac{f_{biot(difw)}\left(\frac{S_{HMS}}{(pors)(dzds)} - S_{HM}\right)}{(dzwf + dzds)dz}$$

The equations above clearly represent the relation between adsorption (adss), desorption (dess), and diffusive transfer (difv). The variables k_w, K_d, *TSS*, $f_{biot(difw)}$,*pors*, *dzwf* and *dz* are equivalent to the desorption rate (d^{-1}), partitioning coefficient for mercury (m^3 H_2O/gDW), total suspended solids concentration (g DW/m^3 bulk), factor for diffusion due to bioturbation (dimensionless), thickness of diffusion layer in sediment (m), and thickness of the computational grid layer (m) respectively.

X_{HM}, the adsorbed mercury concentration on suspended matter within the water column results from mercury being absorbed by both the suspended solids and particles re-suspended by the river bed layer, and eliminating the mercury desorbed from suspended solids into water column, and also those adsorbed by settling particles.

$$\frac{dX_{HM}}{dt} = adss - dess - sev + resv$$

$$sev = \frac{v_s X_{HM}}{dz}$$

$$resv = \frac{RR \frac{X_{HMS}}{X_{SED}}}{dz}$$

Sev and resv represent the sedimentation and re-suspension of particles. V_s defines the settling velocity (m/d) of suspended solids. RR denotes the re-suspension rate (gDW/m^2/d). X_{SED} is the sediment mass gDW/m^2). These equations assume that the current speed is greater than the critical speed responsible for initiating movement.

S_{HMS} is calculated based on the equations below:

$$\frac{dS_{HM}}{dt} = -adss + dess - difv$$

$$adss = k_s K_{ds} S_{HMS} \frac{X_{SED}}{dzs.por_s}$$

$$dess = k_s X_{HMS}$$

The desorption rate in sediment (d-1), metal partitioning coefficient between particulates and water (m^3 H_2O/gDW), sediment porosity (m^3 H_2O/ m^3 bulk), are given by k_s, K_{ds}, and por_s. The variables in the above equations have been defined earlier in this section.

X_{HMS} is calculated using the following:

$$\frac{dX_{HMS}}{dt} = adss - dess - sev + resv$$

$$adss = k_s K_{ds} S_{HMS} \frac{X_{SED}}{dzs.por_s}$$

$$sev = v_s X_{HM}$$

$$resv = \frac{RRX_{HMS}}{X_{SED}}$$

7. EFPC MODEL OVERVIEW AND IMPROVEMENTS

The EFPC model originally developed by Long has been extended and improved throughout the course of this study. The model has been extended to include observation stations not previously considered. This was performed upon evaluating the most recent publicly available historical data for the site. Boundary conditions were created based on a merger between the previously existing EFPC model boundary file and the Y-12 model boundary file. The boundary conditions were updated for point sources within the hydrodynamic and advection module. Links to mercury and flow timeseries were also established.

Simulation specifications have been evaluated and updated to decrease the computational time within the model's pre-processing, water movement, and water quality phases. For example, vegetation data input format has been changed from shape to gridded codes; increasing the model's preprocessing speed. River cross-sections were also examined and modified to ensure consistency in bed level elevations at the branch junctions and thus reduce numerical instabilities. The following sections provide an overview of the input parameters used and changes implemented.

7.1 Data Extraction and Processing

The Oak Ridge Environmental Information System (OREIS) is a centralized, standardized, quality-assured, and configuration-controlled environmental data management system belonging to the U. S. Department of Energy (DOE). The environmental data retrieved from the OREIS database for the purposes of this research include known quality measurement and spatial data from groundwater, surface water, sediment, and soil. The spatial data was extracted by utilizing the OREIS Spatial Query Tool. The interface is shown in the figure below.

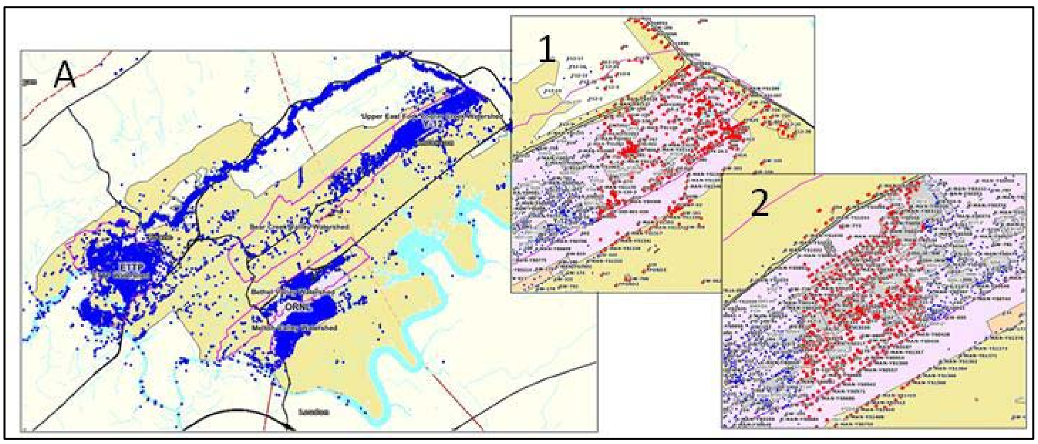

Figure 4 OREIS spatial query tool (A), and sample segments extracted (1) - (2).

During the data extraction process, the domain was divided into 16 sub segments in an effort to minimize the time and computer resources spent in the data extraction process. The data was initially extracted in the form text files. It was archived into Excel spreadsheets, converted into appropriate units, formatted as timeseries, and added to the model as additional observation stations. Stations 2236AQ06, 3538250, 3215AQ05, 3904AQ04, EFK 13.8, 5313AQ03, EFK 18.2, 6262AQ02, and 6361AQ01 shown on the map below were initially identified as potential observation stations to be added to the model. Additional stations considered but discarded based on the invalid declaration of the OREIS validation qualifier include PCM 5.5-1, PCM 5.5-2, PCM 5.5-3, PCM 5.5-4, PCM 5.5-5, PCM 6.0, PCM 6.5, PCM 7.0, LASD01, and CCSD01.

Ultimately, 3538250, EFK 13.8, and EFK 18.2 were the only new discharge (flow rates measurements) stations with sufficient data to be included in the model. The relative location of processed field stations and stations added to the model are shown in Figure 29. Specific coordinates are maintained confidential.

7.2 Model Domain, Topography

The domain/study area, shown as the red outline in Figure 5, was defined by the USGS as Hydrologic Unit Code 060101070302. GIS files for the domain, USGS observation stations, streams, water bodies such as lakes, and topography were inserted into the model in the form of either shapefiles, or MIKE Zero shell extensions (dfs0, dfs1, or dfs1). Figure 5 (A), shows an overlay of these files as it appears within the model's display section. Surface elevations were originally embedded in the model in the form of a dfs2 extension file. These surface elevations are measured in meters. Figure 5 (B), (C), and (D), show GIS shapefiles for soil imperviousness, and vegetation. These files were introduced in MIKE SHE and prepared by previous members of the Applied Research Center - Environment and Water Resources Group during the initial stages of model development. Refer to Long [**14**] for a more detailed explanation of their assembly.

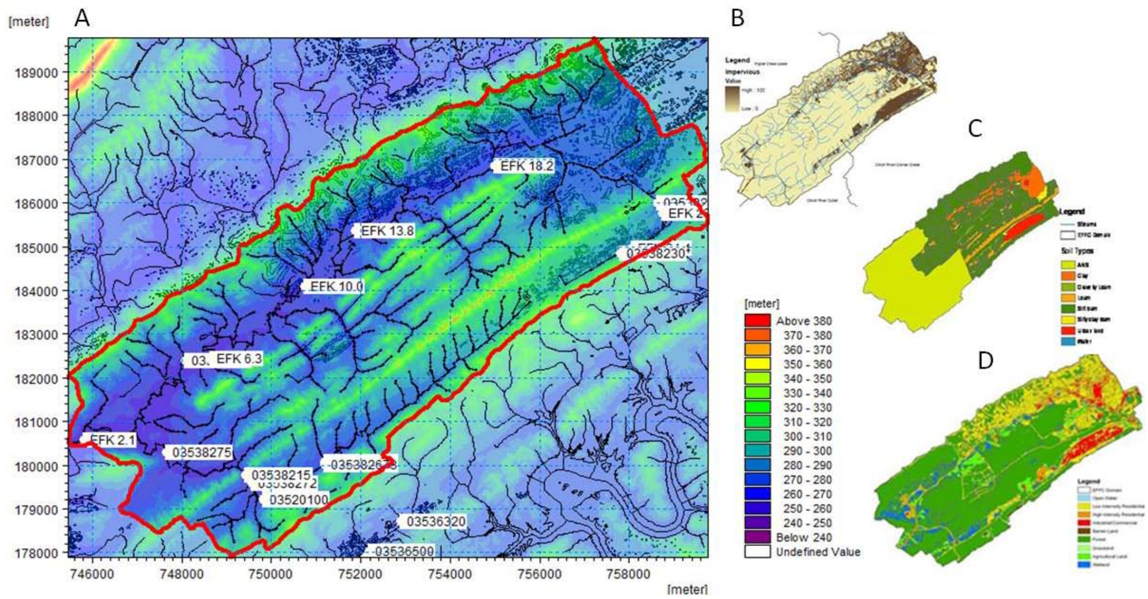

Figure 5 Image overlay of observation stations, streams, water bodies, and topography (A), imperviousness (B), soil type (C), and land use (D).

7.3 Climate

Hydrological climate patterns such as precipitation, snowmelt and evapotranspiration form part of the climate sub-section within MIKE SHE. The precipitation component of the model determines surface water flows and defines the basics for the groundwater table. The precipitation timeseries is presented as a rate in the form of mm/day from 1/1/1950 through 12/31/2008. The module MIKE SHE will only use the precipitation data within the user-specified time period. It must be noted that snow melt is not included as a sub-component of the climate since the precipitation values reported in the timeseries already account for frozen precipitation.

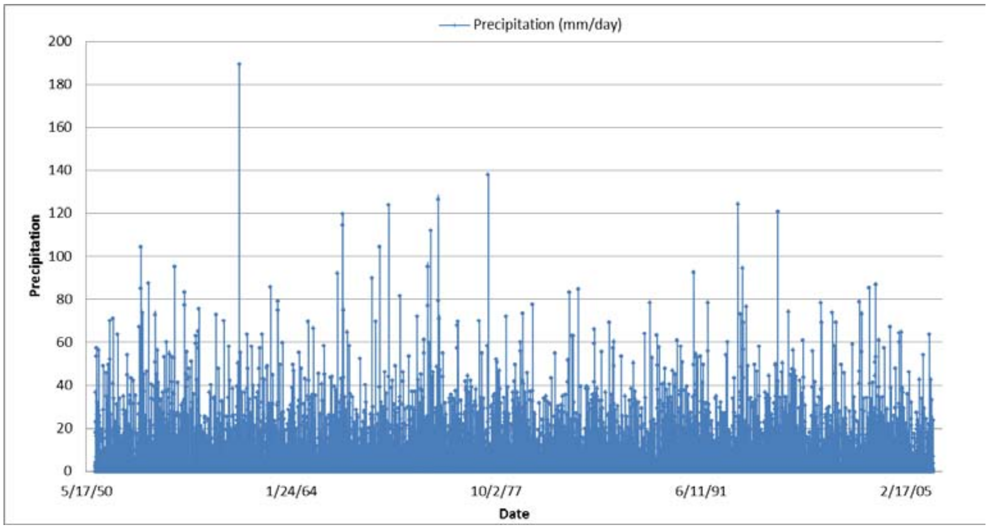

Figure 6 Precipitation timeseries data for 1/1/1950 to 12/31/2008.

The evapotranspiration (ET) component of the model is dependent upon meteorological and vegetative data as it must predict evapotranspiration due to rainfall interception by canopy, canopy drainage to soil surface, evaporation from plant and soil surface, and water uptake by roots. A spatially uniform constant value of 2.01168 mm/day is observed based on records for the state of Tennessee [**14**]. The model adjusts ET based on the leaf area index and root depth specified under land use.

7.4 Land Use

The land use consists of vegetation maps with assigned Leaf Area Index (LAI) constants and Root Depth (RD) values obtained from USGS. LAI and RD spatially adjust the reference ET stated previously. The table below depicts the gridded codes and their classification along with assigned LAI, RD and Manning's M (1/n).

GRID CODE	CLASS	LAI	RD (mm)	M
11	Open water	0	0	50
21	Developed, Open Space	3	2000	50
22	Developed, Low Intensity	2.5	2000	20
23	Developed, Medium Intensity	2	2000	10
24	Developed, High Intensity	1.5	2000	7
31	Barren Land, Rock, Sand, Clay	1.31	4000	11
41	Deciduous Forest	5.5	2000	10
42	Evergreen Forest	5.5	1800	9
43	Mixed Forest	5.5	2400	10
52	Shrub, Scrub	2.08	2500	20
71	Grassland, Herbaceous	1.71	1500	29
81	Pasture, Hay	1.71	1500	30
82	Cultivated Crops	3.62	1500	27
90	Woody Wetlands	6.34	2000	10
95	Emergent Herbaceous Wetlands	6.34	2400	22

Table 2: Land Usage Classifications

7.5 Saturated Zone

The saturated zone includes subsurface drainage where the distribution of hydrogeologic parameters is assigned via geological layers. A layer from 0 meters to 30 meters below ground level exists and another from 30 to 100 meters below ground surface. These set a two-layer surficial aquifer profile for the site. Parameters influencing saturated flow are considered in this section. A horizontal hydraulic conductivity, vertical hydraulic conductivity, specific yield, and specific storage of 1.0 e^{-04} m/s, 1.0 e^{-05} m/s, 0.2 and 3.0 $x10^{-5}$ formed part of the original model and remain unchanged in the current version. The drainage level was assumed -1.0 m relative to the ground, and the drainage time constant has been preset to $1.0x10^{-6}$ sec^{-1} based on calibration and uncertainty analysis performed by previous modelers [**14**].

7.6 Unsaturated Zone

The unsaturated zone employs the Van Genuchten algorithm in the computation of the water content and hydraulic conductivity of the soil based on defined parameters. The total saturated water content, capillary head, and the alpha-empirical constant, and M-empirical constant must be specified in order for the algorithm to compute the soil water content. As discussed in greater detail within the MIKE SHE Unsaturated Zone Model Theory, the hydraulic conductivity is expressed as a ratio between the hydraulic conductivity for given water content and the saturated hydraulic conductivity. Input parameters from literature for the Upper and Lower Aquifer Hydraulic Conductivity and curves are summarized in Table 3 and Table 4. The retention and conductivity curves are shown in Figure 7.

Retention Curve Parameters									
Upper Layer					Lower Layer				
θ_s	θ_r	α	n	m	θ_s	θ_r	α	n	m
0.41	0.057	0.124	2.28	0.5614	0.43	0.089	0.01	1.23	0.1869

Table 3: Parameters of the Retention and Hydraulic Conductivity Curves Retention

Hydraulic Conductivity Curve Parameters									
Upper Layer					Lower Layer				
K_s	α	n	Shape factor	m	K_s	α	n	Shape factor	m
4.05e-5	0.124	2.28	0.5	0.5614	1.95e-7	0.01	1.23	0.5	0.1869

Table 4: Parameters of the Retention and Hydraulic Conductivity Curves

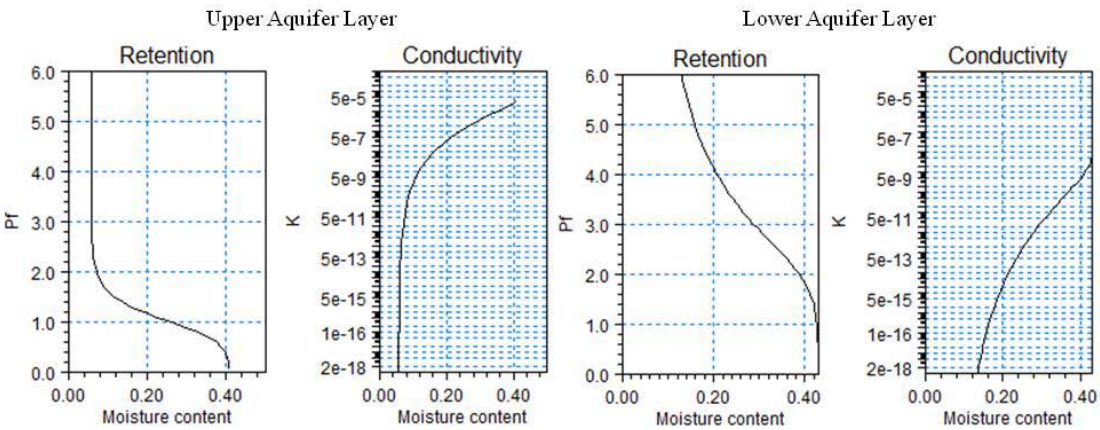

Figure 7 Retention and Hydraulic Conductivity Curves for the Upper and Lower Aquifer Layers

7.7 Overland Flow

Drainage in the overland zone is routed downhill based on adjacent drain levels. If drain flow is produced it is routed to the recipient point using a linear reservoir routing technique based on a pre-processor generated reference system that utilizes the slope of the drains calculated from the drainage levels in each cell.

7.8 Channel/River Flow

Water flow is simulated in MIKE 11 via a 1-dimensional engine directly linked to the network geometry. The network developed for the EFPC model consists of reaches, nodes, grid points, and cross-sections. The river and stream network for the domain area is shown below. It consists of 112 branches/ MIKE SHE links, and 1086 nodes. Cross-sections are set to allow for overbank spilling. The left and right bank elevations and bed layer are consistent with topography files. Resistance (Manning's M) values range between 10 and 20 throughout the domain.

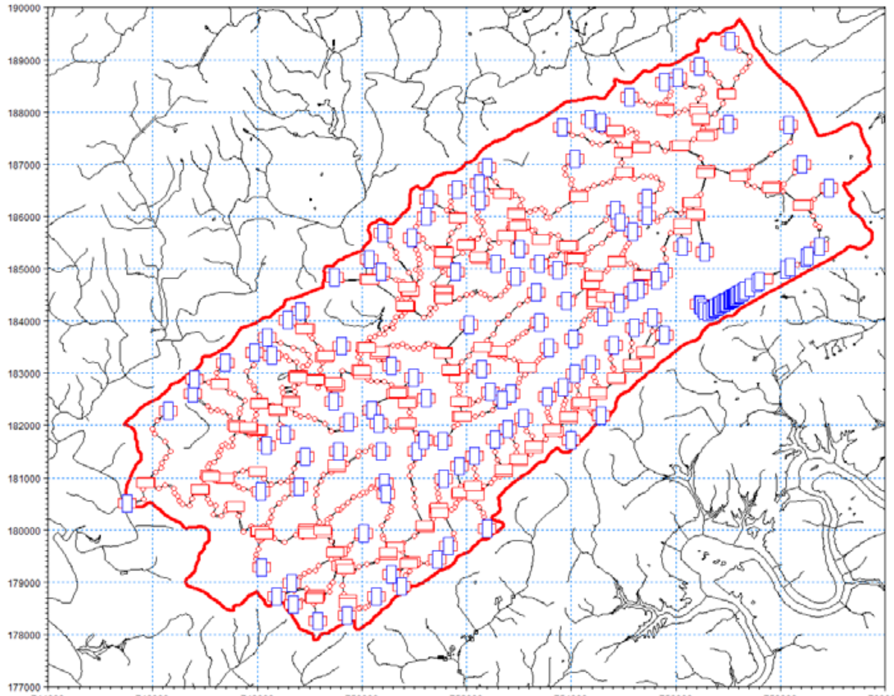

Figure 8 River network with point nodes, boundary conditions and cross-sections.

7.8.1 Boundary Conditions

The watershed model consists of well defined boundary conditions. The boundary conditions guide the interaction between the model domain and the surrounding external areas. Open boundary conditions were paired with additional boundary point sources to simulate the hydrology of the natural environment as well as the most significant anthropological alterations to the site.

The EFPC model was modified by adding Outfalls (point sources) to the boundary file in both the Hydrodynamic (HD) and Advection (AD) modules. The newly developed boundary conditions file for the modules consists of a merger between the previously existing EFPC Model boundary file and the Y-12 Model. The new boundary condition files consist of a total of 157 branches of which 42 were declared point sources. These point sources listed in the Appendices section of this report include discharge and mercury timeseries for the hydrodynamic and advection modules.

7.8.2 Cross-Sections

The cross-sections are a 2-dimensional intersection of the stream. These are perpendicular to the stream direction. As described within the MIKE 11 user manual, the geometry of the cross-section defines the volume of water for a specific water level at the cross-section. Alternatively, the user-specified resistance defines the easiness of flow through the stream. Cross-sections were generated for EFPC using a raw data approach requiring left and right bank elevations along with bed elevations. The raw data is automatically processed within the model during simulations. Storage width, flow area, resistance number, and hydraulic radius values are generated for each cross-section during the pre-processing stages of the simulation.

The original EFPC model had numerical instabilities within the MIKE 11 module as the water depth within the original set of cross-sections was routinely exceeding the allowable cross -sections depth. These numerical instabilities were eliminated by adding more cross-sections. The final network file used in simulations is shown in Figure 9, and reveals all the model cross-sections included within the domain. All cross-sections were checked for consistency in the left and right bank elevations, and bed layer elevation against available topography elevation maps for the site. Furthermore, overbank spilling was allowed in all cross-sections.

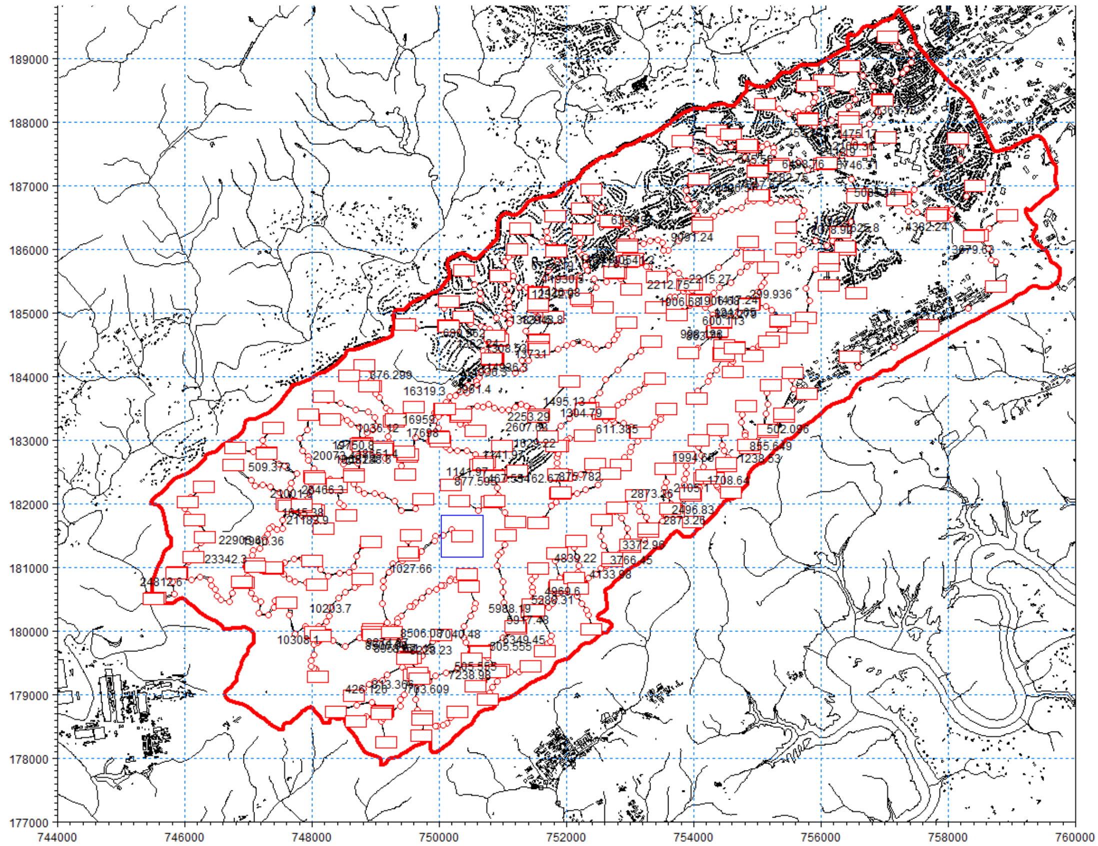

Figure 9: Overview of all river cross-sections in the model.

River cross-sections within the model were generalized as trapezoidal. A model snapshot depicting a detailed schematic of a river cross-section for EFPC is shown at chainage 0.000. Cross-sections downstream of the EFPC branch are also shown in gray in Figure 10.

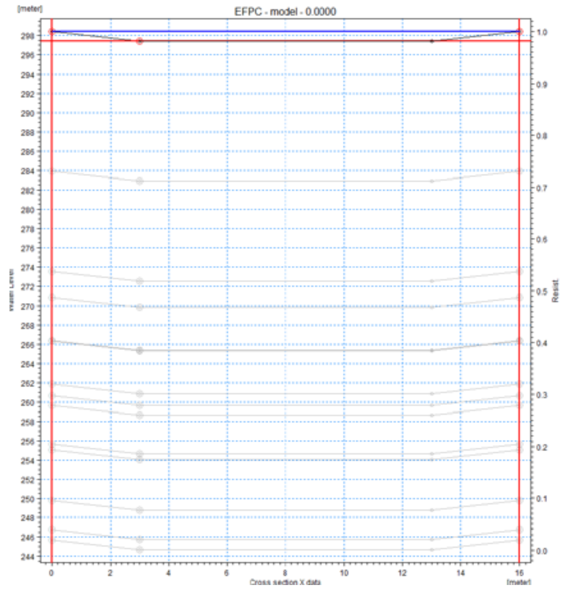

Figure 10 Detailed schematic of river cross-section for EFPC at chainage 0.000 and subsequent chainages downstream

7.9 ECOLAB

The activated ECOLAB module within the Advection Component of Rivers and Lakes currently contains 6 state variables, 11 auxiliary variables, 16 constants, 15 processes, 3 forcing, and 11 derived outputs. The description of the ecosystem state variables is formulated via a series of ordinary coupled differential equations describing the rate of change of each state variable within the ecosystem. Mercury, adsorbed mercury, dissolved mercury in sediment, adsorbed mercury in sediment, suspended solids, and mass of sediment constitute the state variables. Model constants account for the organic-carbon partitioning coefficient, desorption rate in both water and sediment, the fraction of organic carbon in suspended solids (ss) and sediment, thickness of the water film, the ratio between the thickness of diffusion layer in sediment, factor for diffusion as a byproduct of bioturbation, molecular weight of heavy metal, density and porosity of dry sediment, settling velocity of suspended solids, re-suspension rate, particle production rate, and critical current velocity for sediment re-suspension. The forcing used to represent external variables affecting the ecosystem under analysis includes the current speed, total water depth, and thickness of the computational layer. These components are summarized in the table below.

State Variables	Value	Constants	Value
Mercury	0.01 mg/l	Organic-carbon partitioning coefficient	50000 l/kg
Adsorbed mercury	0.1 mg/l	Desorption rate in water	1 day^{-1}
Dissolved mercury in sediment pore water	0.1 g/m^2	Desorption rate in sediment	0.1 day^{-1}
Adsorbed mercury in sediment	10 g/m^2	Fraction of organic carbon in SS	0.1
Suspended solids	50 mg/l	Fraction of organic carbon in sediment	0.2
Mass of sediment	10000 g/m^2	Thickness of water film	0.1 mm
Forcing		Mole weight of heavy metal	92 g/mole
Thickness computational grid layer	2 m	Density of dry sediment	250 kg/m^3 bulk
Total water depth	8 m	Porosity of sediment	0.8 m^3 H_20 / m^3 Bulk
Current speed	0.2 m/s	Settling velocity of SS	0.1 m/day

Table 5: Summary of ECOLAB Input

8. RESULTS

A variety of simulations have been executed with the purpose of calibrating the recently modified model for flow and mercury. The model network is shown in Figure 11. Field stations considered for flow and mercury calibration purposes are shown (EFK 23.4, 03538250, 03538273, 03538270, and 03538673) as well as their model computational counterparts (EFPC 3209.9, EFPC 03538250, BC 8728.87, BC 7700.06, BC 6168.82).

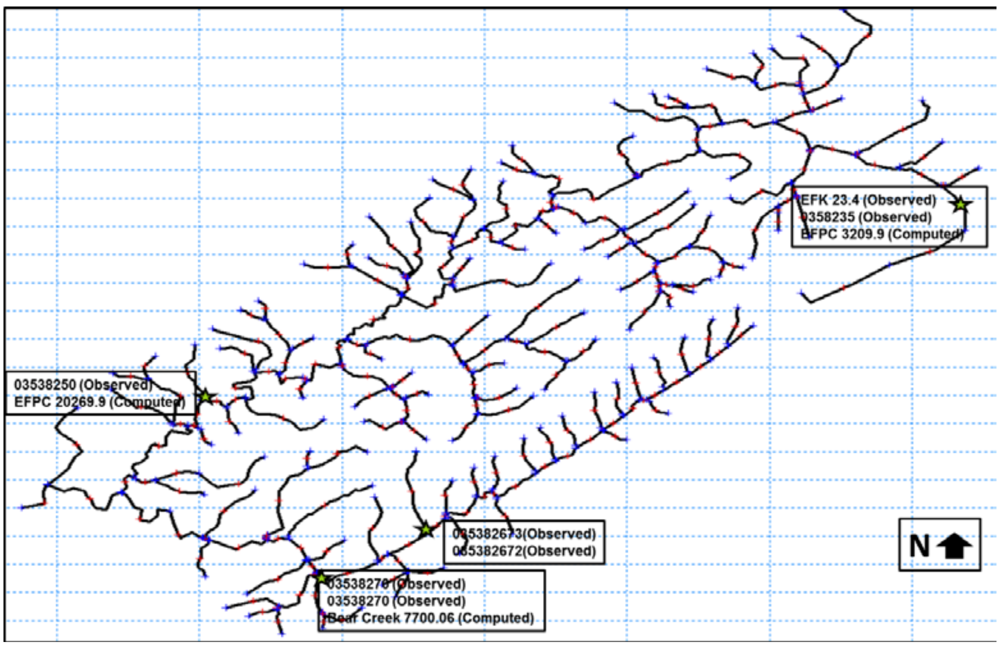

Figure 11 Model network highlighting the stations discussed in the results.

Flow and load duration curves represent a valid tool for the analysis of data. These methods of analysis were used to effectively calibrate the model. A flow duration curve reveals the relationship between the magnitude of the flow and the frequency in a particular stream. Load duration curves were developed by multiplying the daily mean flow by the measured concentration of suspended solids. LDCs for mercury were also developed by multiplying the daily mean flow by the observed concentration of mercury in the water. The discharge and mercury timeseries shown in the graphs that follow reveal variations in discharge and mercury concentrations at various points throughout EFPC and Bear Creek being primarily driven by hydrological events.

8.1 Flow Module Results

The average flow of 0.281 m^3/s computed from the timeseries for EFPC 3209.9 was compared to the average recorded field value of 0.363 m^3/s for Station 17. The simulated discharge timeseries for EFPC 3209.9 exhibited a 22.6% difference in average flow for a 15-year simulation period when compared to field records at Station 17. Discrepancies among the computed and observed average flow is smaller at other points throughout the watershed. For example, downstream EFPC at computational node EFPC 20731.6, the average flow was 1.22 m^3/s while the recorded value for USGS station 03538250 was 1.41 m^3/s. In this case, a 13.5% error between computed and observed average flow values was exhibited. In reality, flow at Station 17 is not solely dependent upon hydrological events that magnify discharges at a given time. This section of EFPC is heavily influenced by discharges from regulated outfalls.

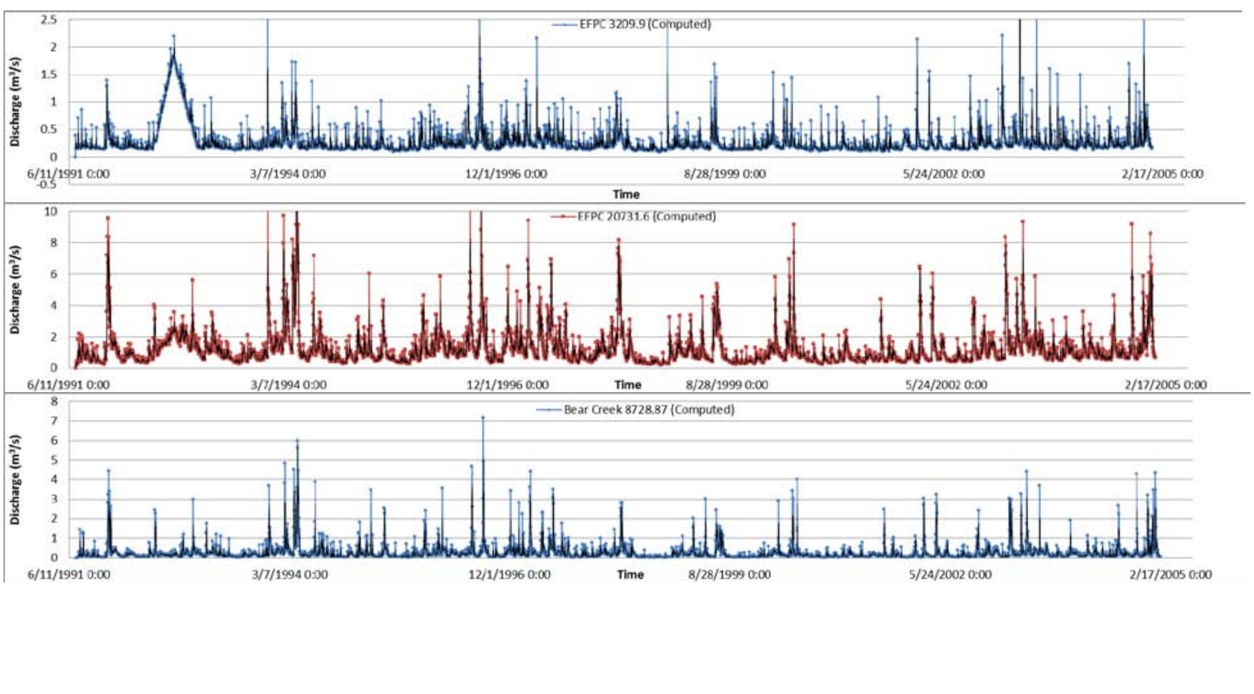

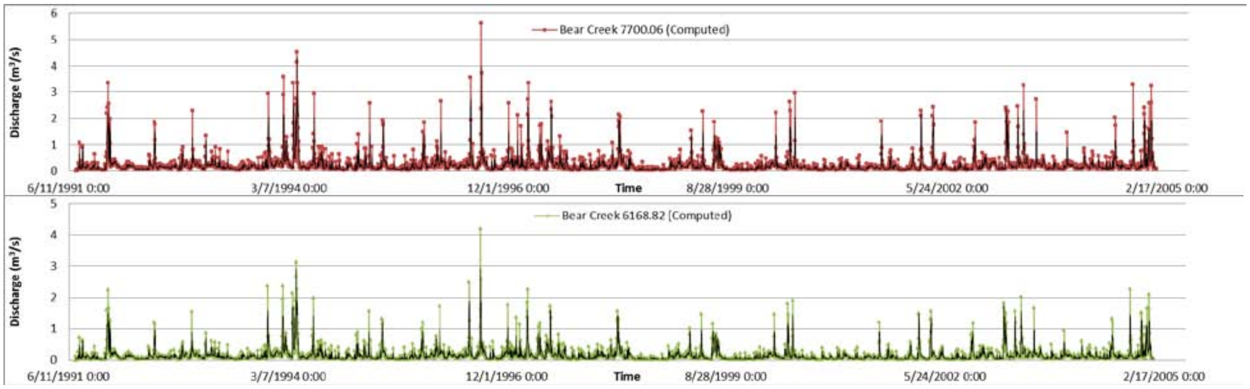

Figure 12 Computed discharges downstream EFPC and Bear Creek for various model nodes (EFPC 3209.9, EFPC 20731.6, BC 20731.6, BC 8728.87, BC 7700.06, and BC 6168.82).

Discharges from such regulated outfalls can thus be a contributing factor; amplifying the differences between computed and observed average flow at Station 17 and EFPC 3209.9. Simulated average flow for Bear Creek at chainage 8728.28, 7700.06, and 6168.82 were 0.279 m^3/s, 0.215 m^3/s, and 0.156 m^3/s, respectively. This was comparable to the observed average flow of 0.253 m^3/s, 0.212 m^3/s, and 0.143 m^3/s for USGS stations 03538273, 03538270, and 03538672.

The model reveals general trends consistent with measured data. The average flow increases downstream EFPC and Bear Creek. Figure 13 compares the computed discharges at EFPC 3209.9 to observed records at station EFK 23.4. A flow duration curve (FDC) shown in Figure 14 was generated to depict the relationship between the magnitude and frequency of daily stream flow for both computed and observed records.

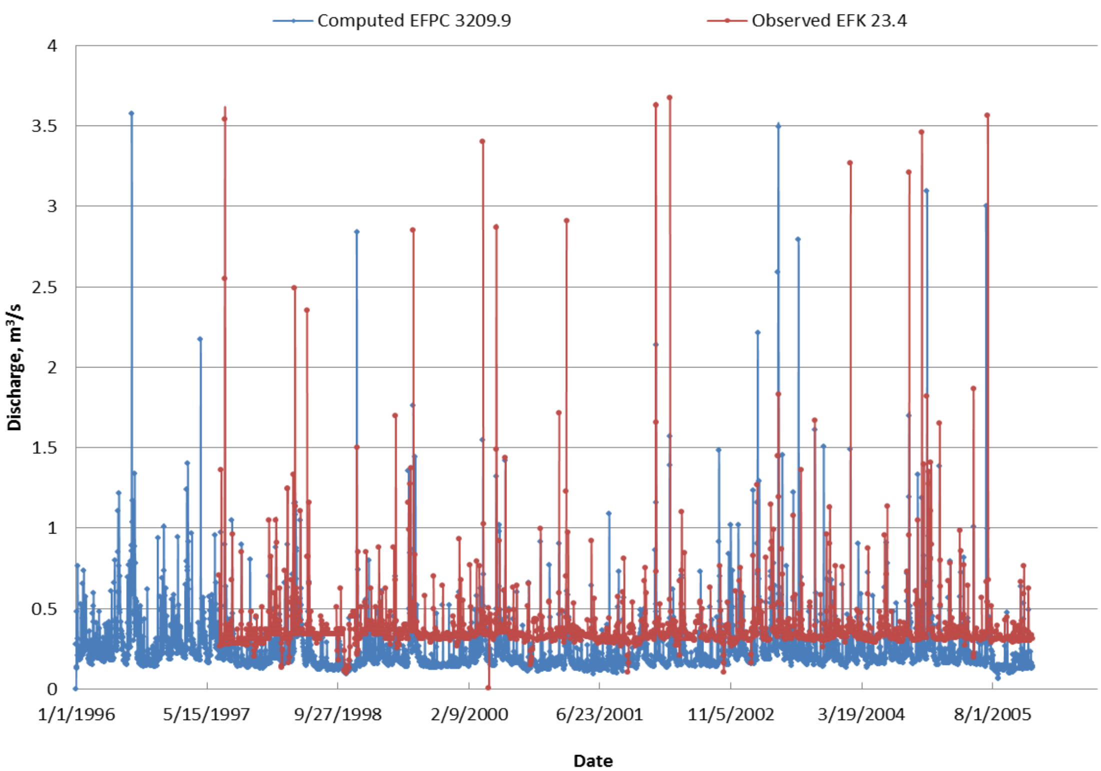

Figure 13 Comparison of discharges timeseries at EFPC 3209.9(computed) and EFK 23.4 (observed).

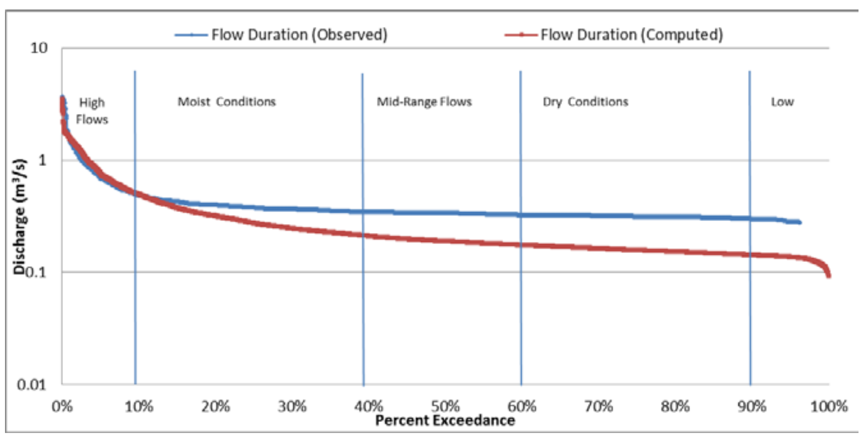

Figure 14 Comparison of flow duration curves for EFPC 3209.9 (computed) and EFK 23.4 (observed).

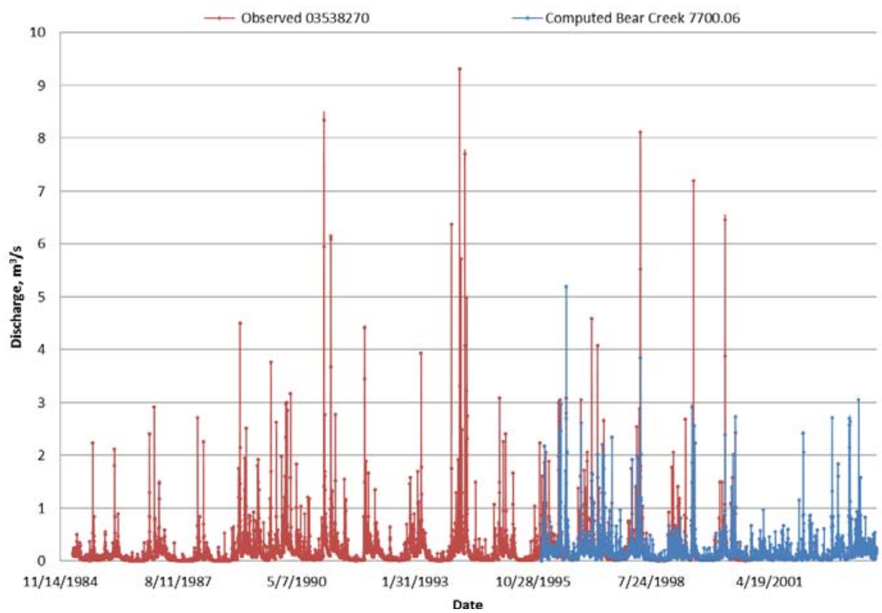

Figure 15 Comparison of discharges timeseries at Bear Creek 7700.06 (computed) and 03538270(observed).

Similarly, the computed discharges at Bear Creek 7700.06 were compared to USGS station 03538270 in Figure 15. Observed and computed discharges at this station show an excellent match. Flow duration curves are also shown in Figure 16 through Figure 18. These images reveal the model's ability to best simulate flow or discharges during high flow, moist-conditions, and mid-range flows. Dry conditions and low flow regimes establish a greater margin of error and numerical instability.

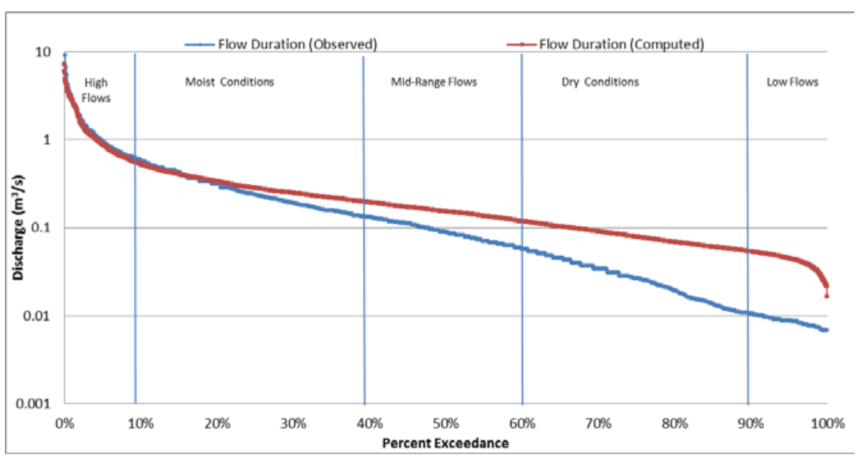

Figure 16 Comparison of flow duration curves for BC8728.87 (computed) and 03538273 (observed).

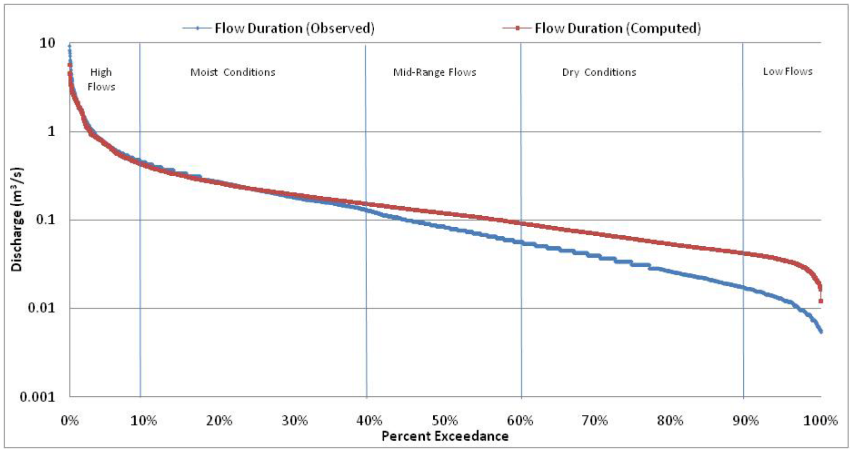

Figure 17 Comparison of flow duration curves at Bear Creek 7700.06 (computed) and 03538270(observed).

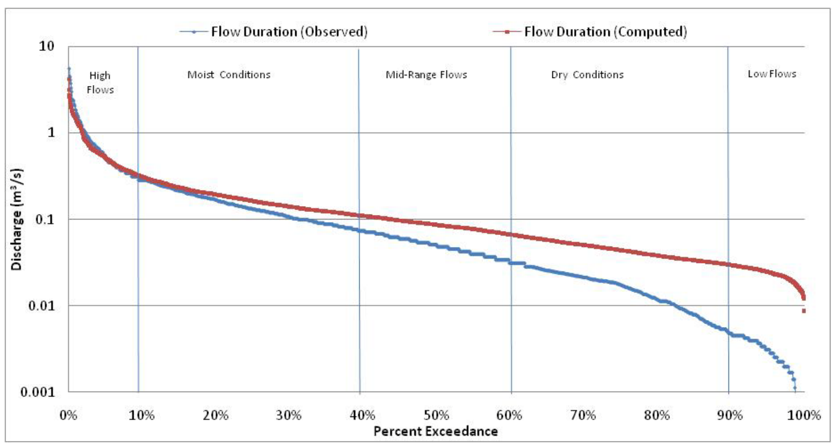

Figure 18 Comparison of flow duration curves at Bear Creek 7700.06 (computed) and 03538270(observed).

8.2 Water Quality Module Results

Simulated mercury timeseries are shown in Figure 19 for computational nodes downstream EFPC and Bear Creek that overlap with field stations. Simulated average mercury concentrations for Bear Creek at chainage 8728.28, 7700.06, and 6168.82 were 1.6 µg/L, 2.2 µg/L, and 2.9 µg/L, respectively. Mercury concentrations appear to decrease upstream Bear Creek. The slightly higher average mercury concentration of 2.9 µg/L computed at BC 8728.28 could be attributed to its proximity to East Fork Poplar Creek as previous studies hypothesize on the potential of mercury particulates to be carried downstream during extreme hydrological events. In the case of EFPC, the model initially over estimated the mercury concentration at Station 17 reporting 186 μg/L when the recorded average was 0.89 μg/L. At EFPC 20731.6, the average mercury concentration was 13.7 μg/L. Since EFK 23.4 or Station 17 is the only station with significant mercury data, extensive calibration efforts were thus implemented within the model's computational dynamics to achieve more realistic results for mercury concentrations at observed Station 17 and computed EFPC 3209.9.

Probability exceedance curves are a classical way for regulators to understand the system in terms of the various flow regimes exhibited. Figure 22 shows the probability exceedances for computed and recorded mercury concentrations prior to the implementation of mercury calibration efforts for EFPC 3209.9 and EFK 23.4. Similarly, Figure 23 depicts the post-calibration mercury concentration probability exceedances for the same station. Figure 23 reveals a much better correlation between the field records and the simulated results at Station 17. As can be observed in Figure 22, the post calibration load was improved by orders of magnitudes.

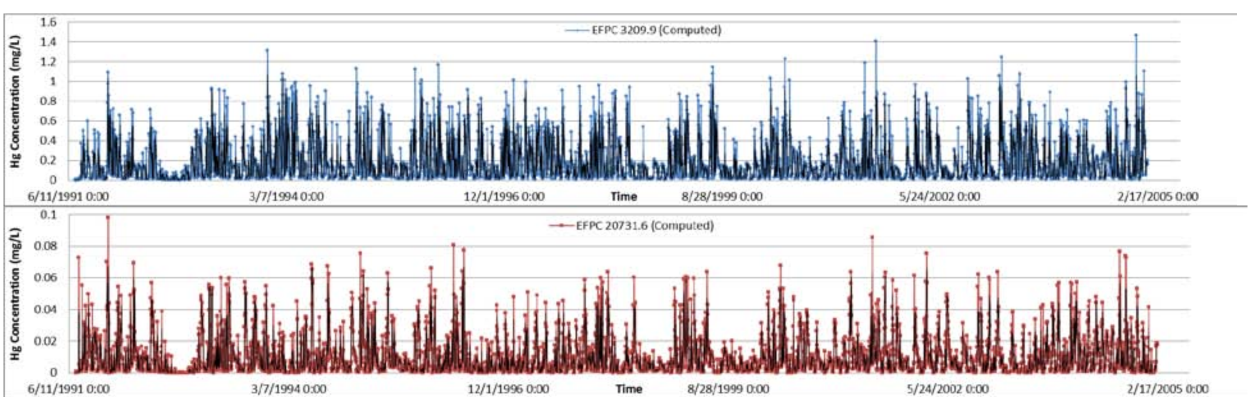

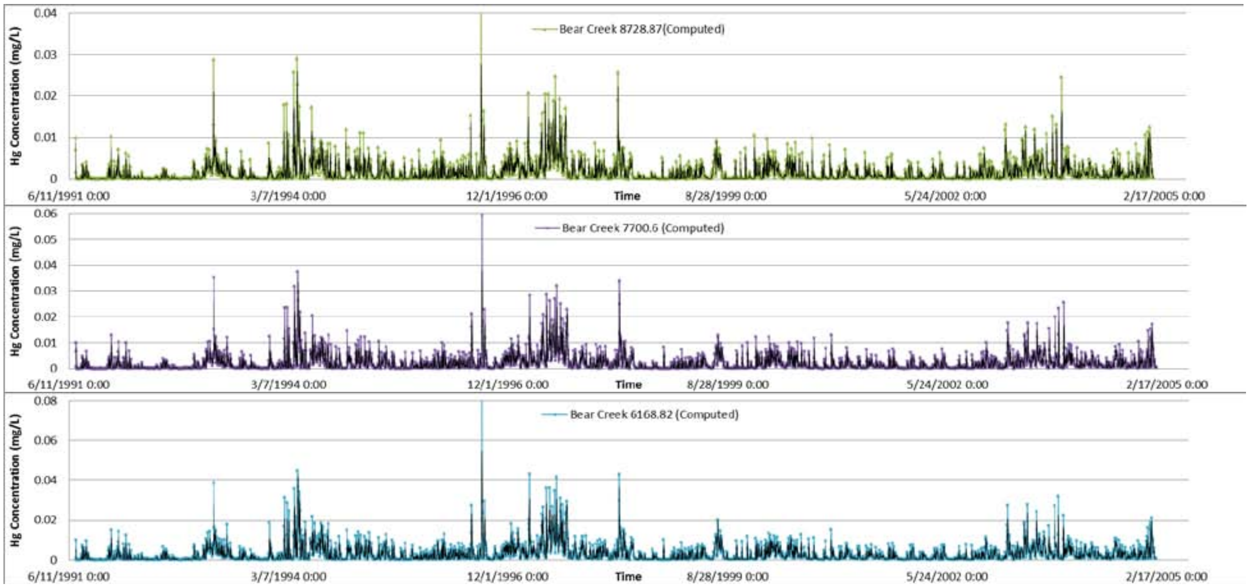

Figure 19 Computed mercury concentrations downstream EFPC and Bear Creek for various model nodes (EFPC 3209.9, EFPC 20731.6, BC 20731.6, BC 8728.87, BC 7700.06, and BC 6168.82).

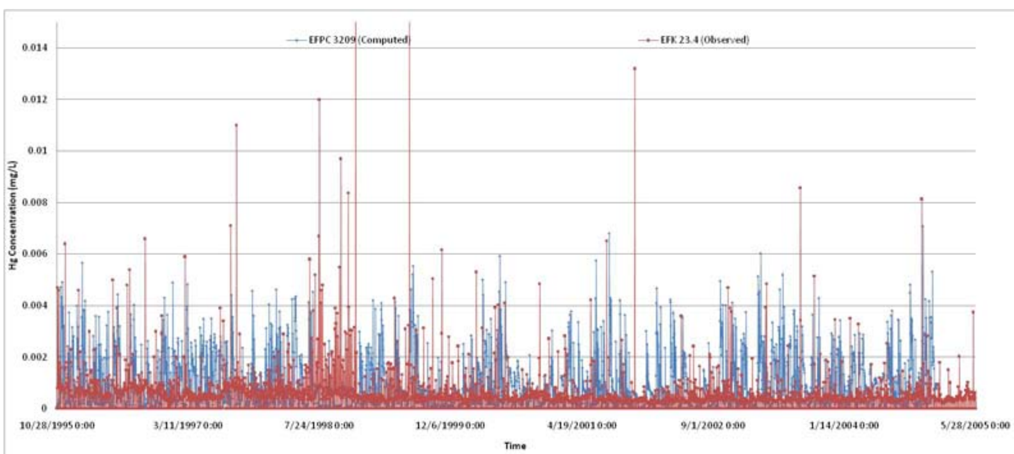

Figure 20 Comparison of mercury timeseries at EFPC 3209.9 (computed) and EFK 23.4 (observed).

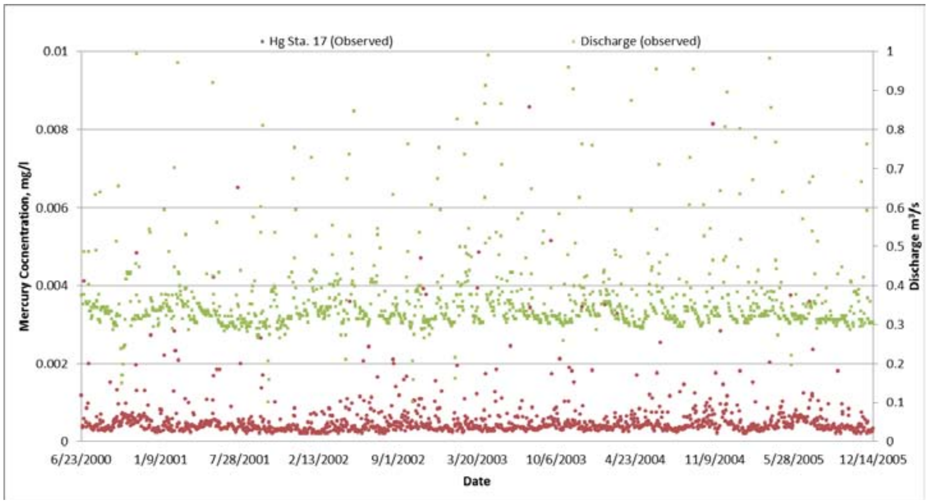

Figure 21 Measured mercury concentrations and discharges at Station 17.

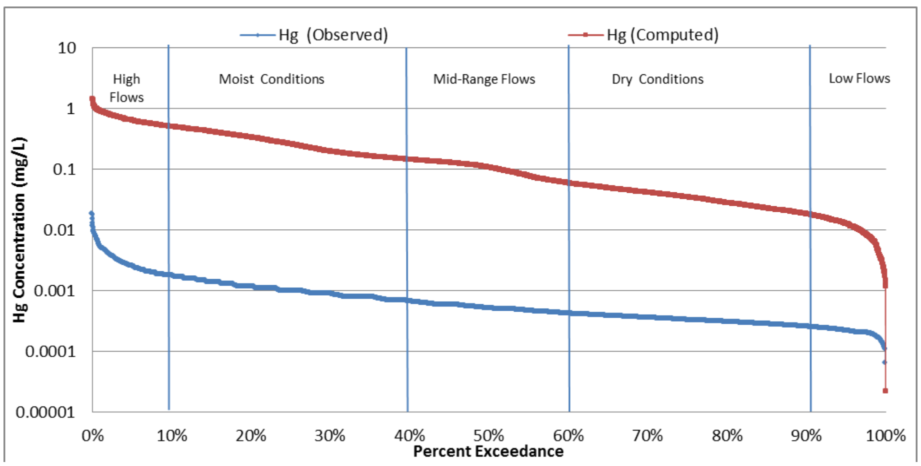

Figure 22 Comparison of pre-calibration mercury concentration probability exceedances for EFPC 3209.9 (computed) and EFK 23.4 (observed).

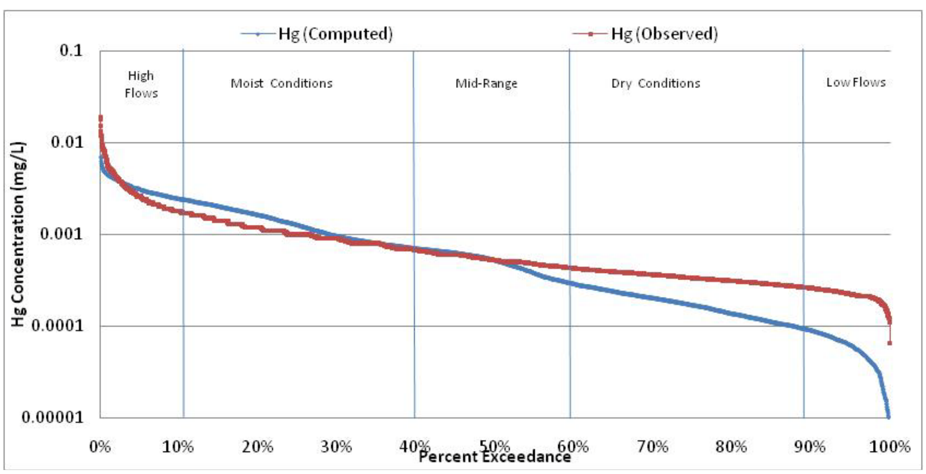

Figure 23 Comparison of post-calibration mercury concentration probability exceedances for EFPC 3209.9 (computed) and EFK 23.4 (observed).

The daily flow rates and observed concentration were used to obtain daily load estimates in an attempt to identify seasonal trends, compare one location to another, and serve as a future tool for the development of water quality goals. Computed and observed load duration curves (LDCs) were thus created for the previously discussed field records and model stations. These images are shown in Figure 24 through Figure 26. The LDC for model station EFPC 3209.9 and field station EFK 23.4 provides a general trend consistent with the one previously reveal by the FDCs. For the loads, similarly to the discharges, the model is best able to simulate the observed for high flow, mid-range flow, and moist conditions. The mercury loads appear to be attenuated downstream EFPC (Figure 25). This pattern is not of significance at Bear Creek (Figure 26) as variations of load duration curves are minor throughout Bear Creek.

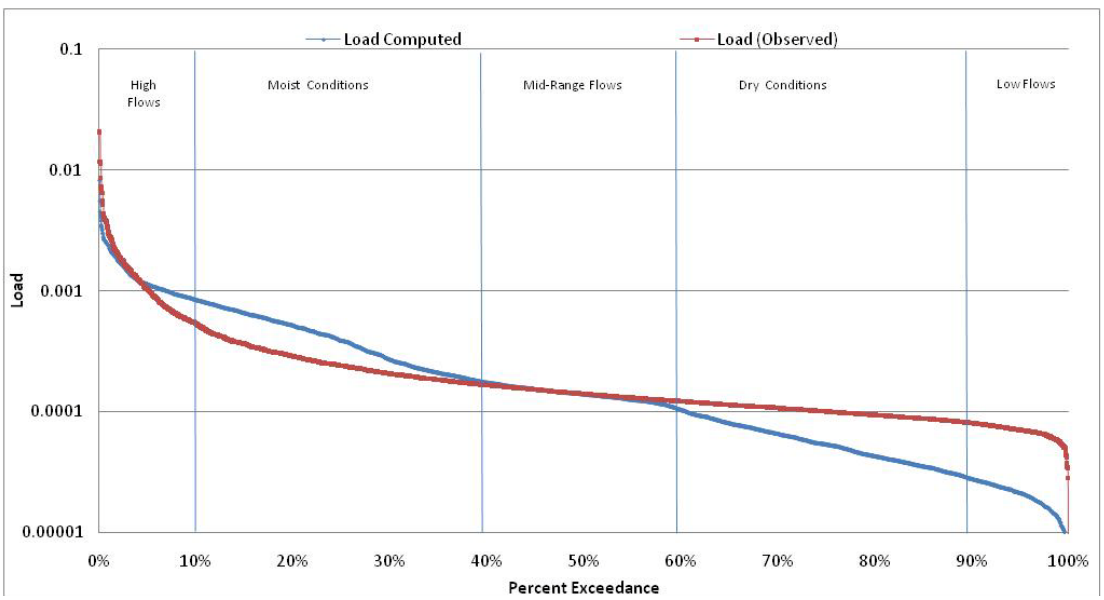

Figure 24 Comparison of load duration curves for EFPC 3209.9 (computed) and EFK 23.4 or Sta. 17 (observed).

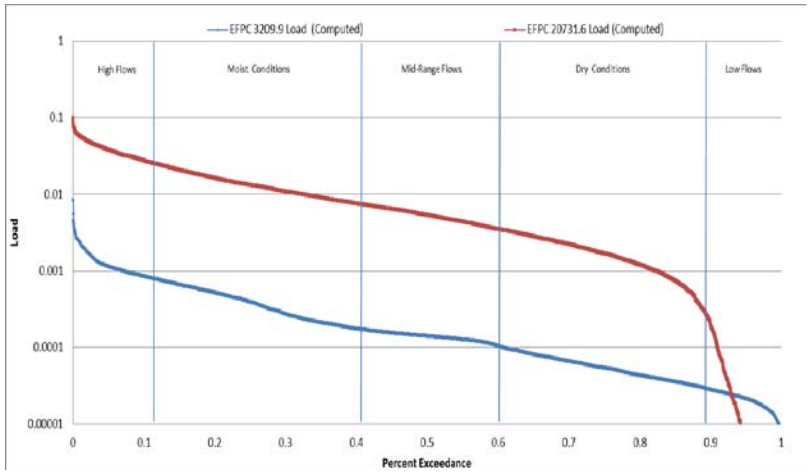

Figure 25 Comparison of load duration curves for computed model stations EFPC 3209.9 and EFPC 20731.6.

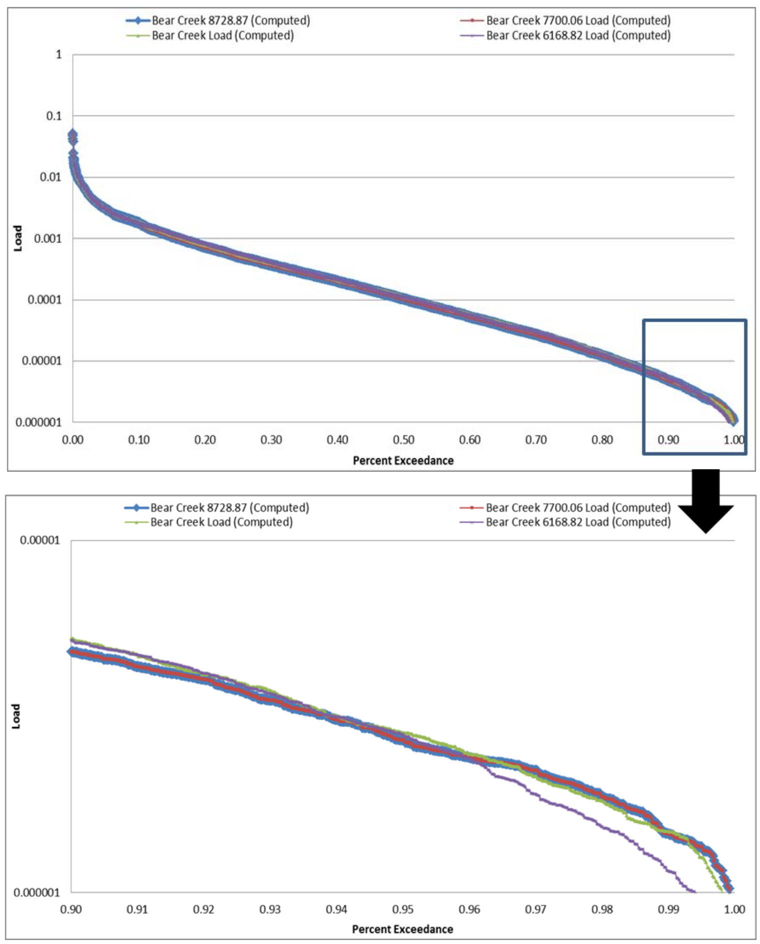

Figure 26 Load duration curves downstream Bear Creek.

Profiles were generated for the major streams (East Fork Poplar Creek, Bear Creek, Gum Hallow Branch, Mill Branch, and Pinhook Branch) in addition to evaluating mercury concentrations and mercury loads downstream EFPC and Bear Creek. The profiles were used to analyze fluctuations in mercury concentrations as a function of time and identify how these fluctuations relate to hydrologic events. Figure 27 reveals a sample profile for EFPC. Figure 28 and Figure 29 portray the simulated mercury concentrations dowstream EFPC per corresponding hydrological event for time-step November 11, 1995 and January 6, 1996. The maximum mercury concentration reached within the simulated period is shown in red. A comparison of the mercury profile downstream the selected branch with the precipitation pattern (Figure 29), reveals that during high flood events mercury concentration decreases due to dilution. However, post hydrological events, the mercury concentration levels increase (Figure 28).

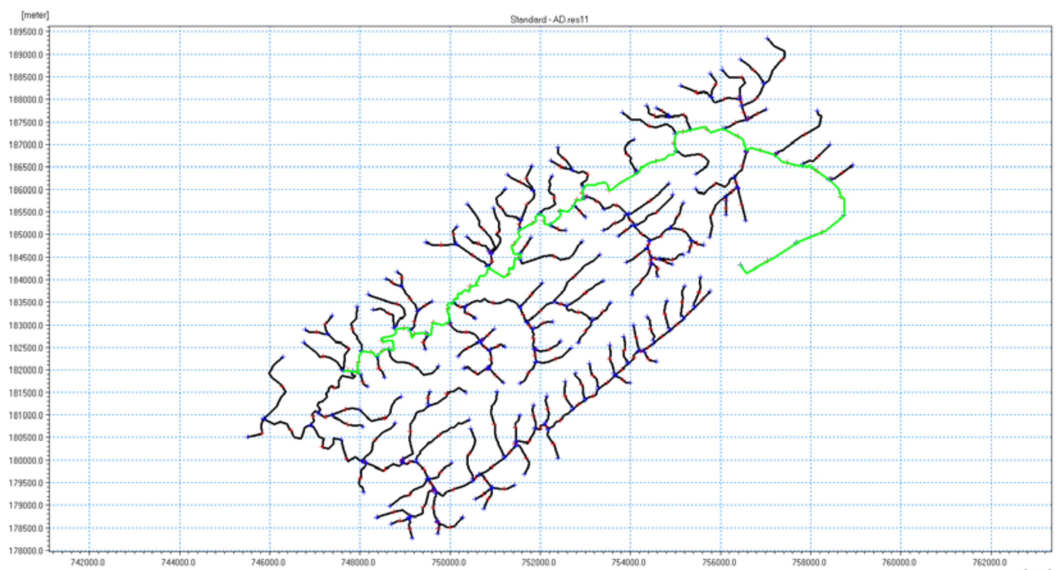

Figure 27 Model river network depicting physical path within watershed of the mercury profile showcased in subsequent figures.

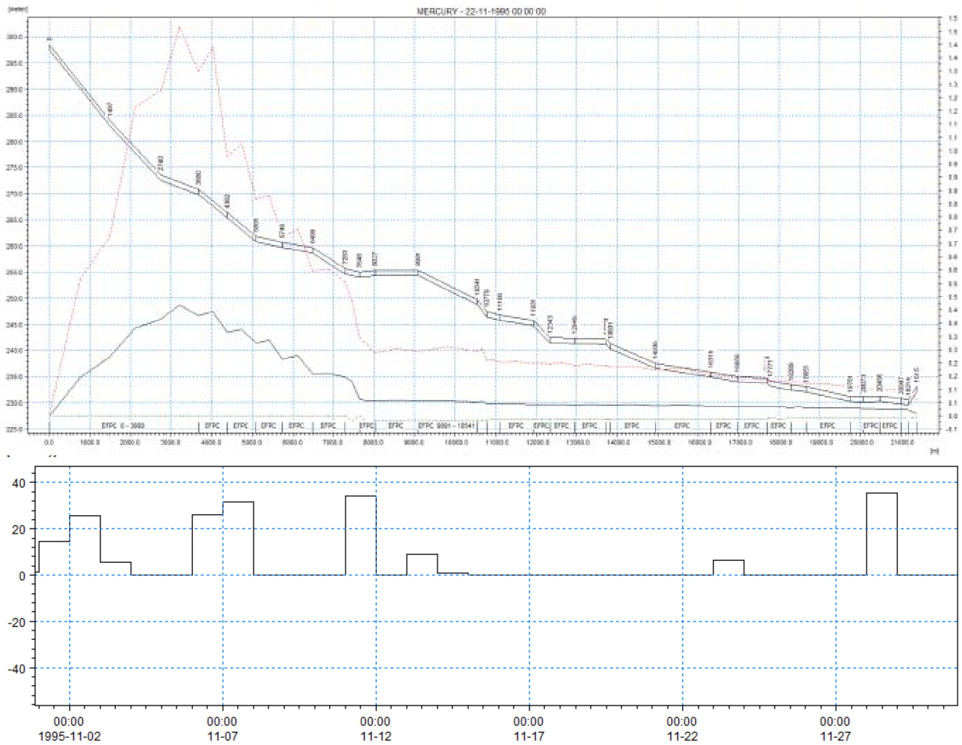

Figure 28 Simulated mercury concentrations downsteam EFPC per corresponding hydrological event for November 22, 1995.

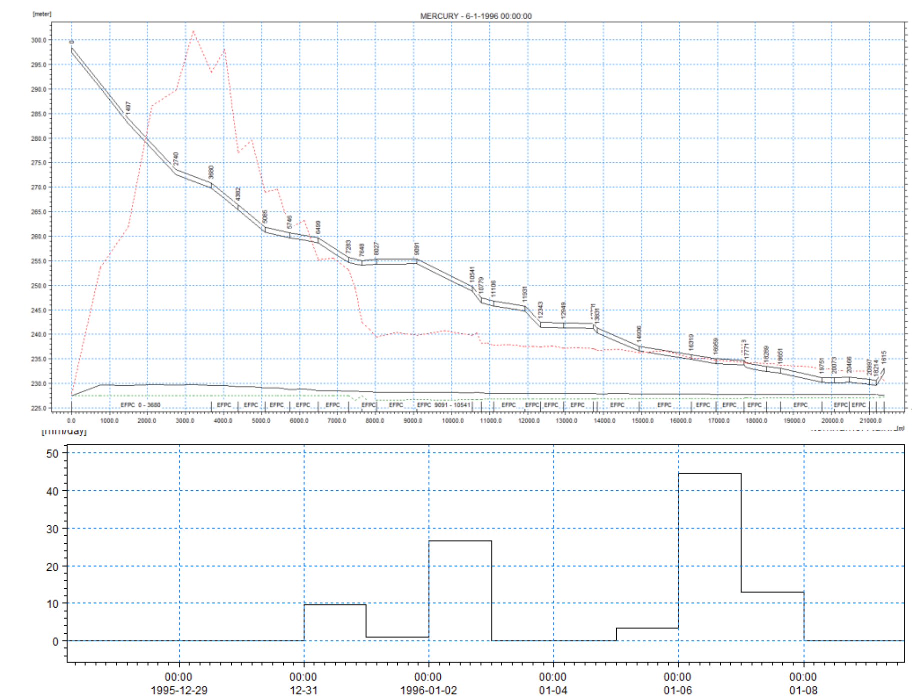

Figure 29 Simulated mercury concentrations downsteam EFPC with corresponding hydrological event in Figure 33 for January 6, 1996.

Total suspended solids patterns were also investigated for Station 17. The same process applied for analyzing the flow and mercury timeseries, generating probability exceedance curves, and LDCs were implemented when evaluating total suspended solids. Figure 32 compares the observed and computed trends of TSS loads with the mercury loads at Station 17.

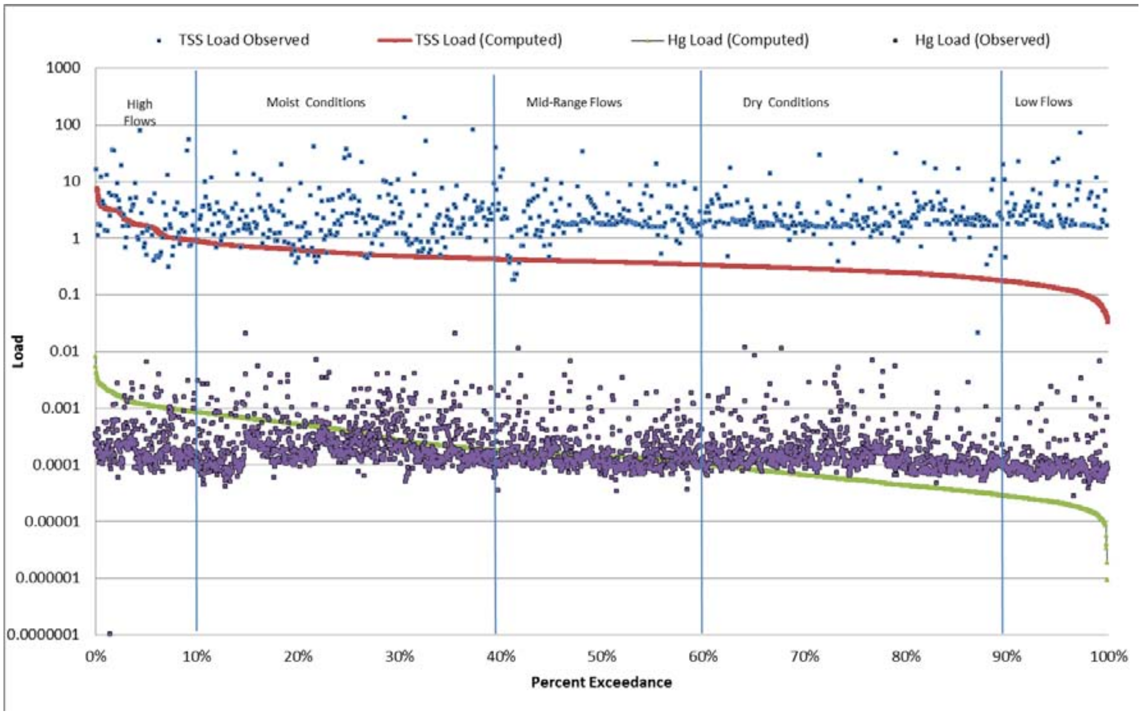

Figure 30 Observed and computed TSS load and mercury concentration load for observed and computed station 17

8.3 Sensitivity Analysis

The sensitivity of the organic partition coefficient (K_d) within the water quality sorption processes was evaluated to establish how total mercury concentrations computed within the water quality module are impacted by variations of this parameter. The organic partition coefficient parameter was varied. The K_d values used include 0.001 m^3/g, 0.025 m^3/g, 0.050 m^3/g, 0.500 m^3/g, and 5 m^3/g. Figure 30 shows the variability caused by each K_d within the mercury concentration timeseries for a 1-year period (2001 - 2002). As shown in the image, the pattern within the timeseries is maintained yet the baseline mercury concentration and peak extent is accentuated. The relationship between the organic partition coefficient and the average daily load at Station 17 is best described as logarithmic (Figure 31).

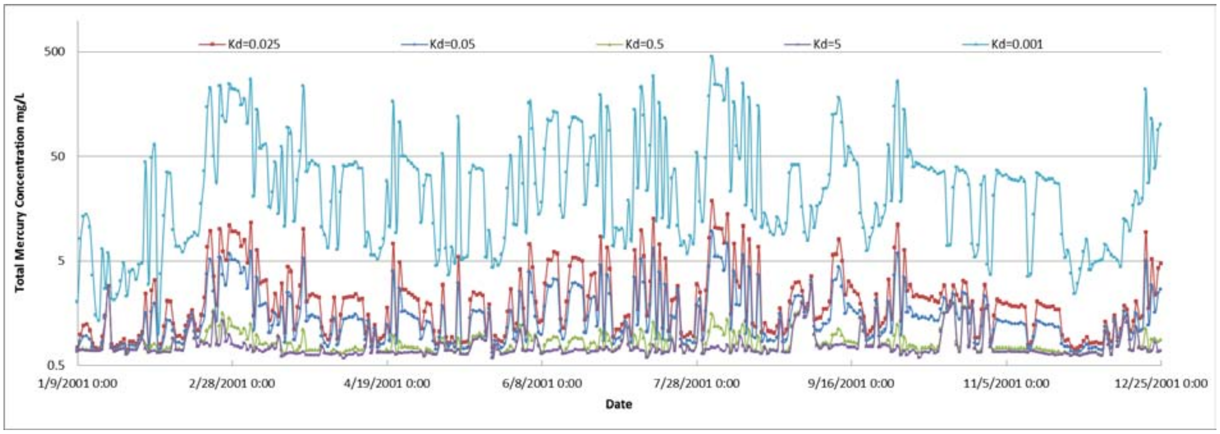

Figure 31 Total mercury timeseries depicting sensitivity to organic partition coefficient (K_d) for various simulations.

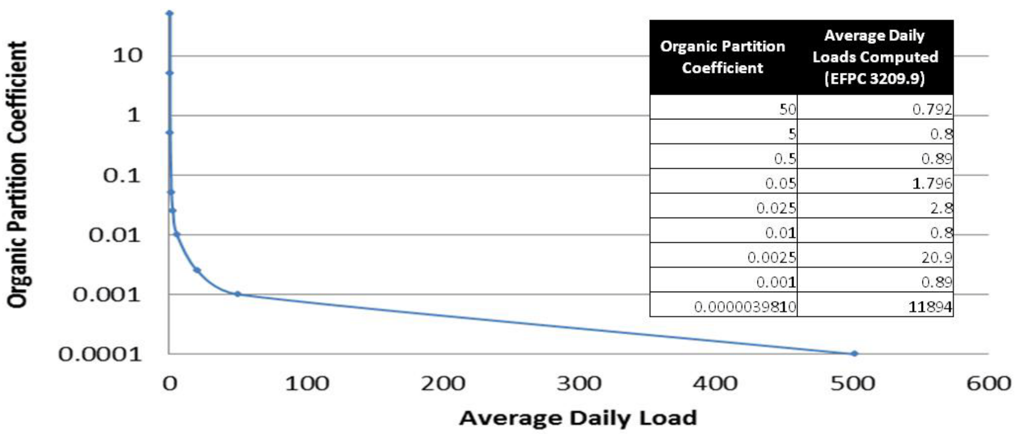

Organic Partition Coefficient	Average Daily Loads Computed (EFPC 3209.9)
50	0.792
5	0.8
0.5	0.89
0.05	1.796
0.025	2.8
0.01	0.8
0.0025	20.9
0.001	0.89
0.0000039810	11894

Figure 32 Observed trend between average daily loads and K_d.

9. CONCLUSIONS

A working model of East Fork Poplar Creek has been developed and optimized to execute flow and water quality simulations throughout the various zones of the sub-domain, including the sediment layer through the implementation of ECOLAB. The model is capable of simulating the entire hydrological cycle. It has been calibrated for various observation stations included in the model. The water quality and sedimentation modules were extended to include the entire EFPC, down to station EFK 6.4 and the Bear Creek. Water quality, transport, and sediment related parameters have been updated based on DOE experimental reports and journal publications. Simulations were executed for a range of input parameters to correlate stochastic hydrologic events with mercury distribution patterns and total suspended solid pattern at Station 17. The simulations were analyzed using a range of techniques, primarily comparative schematics of timeseries plots, probability exceedance curves, and load duration curves.

10. REFERENCES

[1] R.R. Turner and G.R. Southworth, *"Mercury-Contaminated Industrial and Mining Sites in North America: an Overview with Selected Case Studies in Mercury Contaminated Sites," R. Ebinghaus, R. R. Turner, L. D. de Lacerda, O. Vasiliev, and W. Salomons (Eds.)*. Berlin: Springer-Verlag, 1999.

[2] F. X. Han, Y. Su, D. L. Monts, C. A. Waggoner, and M. J. Plodinec, "Binding, distribution, and plant uptake of mercury in a soil from Oak Ridge, Tennessee, USA.," *Science of The Total Environment*, vol. 368, no. 2-3, pp. 753-768, September 2006.

[3] Remediation of Mercury and Industrial Contaminants Applied Research Initiative. (2013, February) Oak Ridge National Laboratory. [Online]. http://www.esd.ornl.gov/romic_afrc/field_characterization.shtml

[4] Tennessee Department of Environment and Conservation, "2008 303 (d) List," Division of Water Pollution Control Planning and Standards Section, 2008.

[5] E. Cabrejo, "Mercury Interaction with Suspended Solids at the Upper East Fork Poplar Creek, Oak Ridge, Tennessee.," Florida International University, Environmental Engineering Department, Miami, Master Thesis 2011.

[6] S. Malek-Mohammadi, G. Tachiev, E. Cabrejo, and A. Lawrence, "Simulation of Flow and Mercury Transport in Upper East Fork Poplar Creek, Oak Ridge, Tennesse," *Remediation*, pp. 119-131, 2012.

[7] U.S. Department of the Interior. U.S. geological Survey (USGS), Mercury in the Environment, 2000, fact sheet 146-00.

[8] U.S. Department of Energy (US DOE), "Record of Decision for Phase I Interim Source Control Actions in Upper East Fork Popler Cereek Characterization Area, Oak Ridge, Tennessee," U.S. Department of Energy, Office of Environmental Management, DOE/OR/01-1951&D3.n Oak Ridge, TN, 2002.

[9] U.S. Department of Energy (US DOE), "Record Decision for Phase II Interim Source Control Actions in Upper East Fork Poplar Creek Characterization Area, Oak Ridge, Tennessee," U.S. Department of Energy, Office of Environmental Management, Oak Ridge, Tennessee, DOE/OR/01-2229%D3.n Oak Ridge, 2006.

[10] H. R. Sorensen, T. V. Jacobsen, J. T. Kjelds, J. Yan, and E. Hopkins, "Application of MIKE SHE and MIKE 11 for Integrated Hydrological Modeling in South Florida," South Florida Water Management District (SFWMD) & Danish Hydraulic Institute (DHI), 2012.

[11] Danish Hydraulic Institute. (2012, May) MIKE by DHI. [Online]. http://www.mikebydhi.com/~/media/Microsite_MIKEbyDHI/Publications/SuccessStories/MIKE%20by%20DHI%20Success%20Story-MSHE-BrowardCounty.ashx

[12] North Carolina Department of Environment and Natural Resources, "Total Maximum Daily Load for Mercury in the Cashie River, North Carolina, Public Review," North Carolina Department of Environment and Natural Resources, 2004.

[13] N. Gandhi et al., "Development of mercury speciation, fate, and biotic uptake (BIOTRANSPEC)," *Environmental Toxicology and Chemisty*, vol. 26, pp. 2260-2273, 2007.

[14] S. Long, "An Integrated Flow and Transport Model to Study the Impact of Mercury

Remediation Strategies for East Fork Poplar Creek Watershed, Oak Ridge, Tennessee," Florida International University, Environmental Engineering Department, Miami, Master Thesis 2009.

[15] Danish Hydraulic Institute (DHI), MIKE 11 Short Descriptions, 2008.

[16] Danish Hydraulic Institute (DHI), MIKE SHE Reference Manual, 2008.

[17] Danish Hydraulic Institute, ECOLAB Reference Manual, 2008.

[18] DOE, "Report on the Remedial Investigation of the Upper East Frok Poplar Creek Characterization Area at the Oak Ridge Y-12 Plant. Volume 1," Oak Ridge, Tennessee, 1998.

[19] USEPA, "Mercury Study Report to Congress. Volume III. Fate and Transport of Mercury in the Environment," EPA-452/R-97-005, 1997.

[20] NC DENR, "North Carolina Department of Environment and Natural Resources. Total Maximum Daily Load for Mercury in the Cashie River, North Carolina. Public Review Draft 7/28/2004," NC DENR. 2004. North Carolina Department of Environment and Natural Resources. Total Maximum Daily Load for Mercury in the Cashie River, North Carolina. Public Review Draft 7/28/2004, North Carolina, 2004.

[21] Barry Moran, Modeling of the Hydrologic Transport of mercury in the Upper East Fork Poplar Creek, December 1996.

[22] DHI, "MIKE 11 Short Descriptions ," Hørsholm, Denmark, 2008.

[23] DOE, "Instream Contaminat Study Task 2, V2. Sediment Characterization.," Office of Natural Resources and Economic Development Tennessee Valey of Authority,

DOE/OR/21444-T1, 1986.

[24] Leo Van Rijn, "Sediment Transport, Part II: Suspended Load Transport," *Journal of Hydraulic Engineering*, vol. 110, no. 11, pp. 1613-1641, November 1984b.

[25] Daniel Levine, William Hargrove, and Hoffman Forrest, "Characterization of Sediments in the Clinch River, Tennessee, Using Remote Sensing and Multidimensional GIS Techniques," , Vancouver, British Columbia, 1995, pp. 548-551.

[26] John Wehr and Robert Sheath, *Fresh water algae of North America, Ecology and classification*. San Diego, CA: Academic Press, 2003.

[27] Michael D LaGrega, Philip L Buckingham, and Jeffrey C Evans, *Hazardous Waste Management*, 2nd ed.: McGraw-Hill, 2001.

[28] Bruce D Honeyman and H Peter Santschi, "Metals in Aquatic Systems," *Environmental Science and Technology*, vol. 22, no. 8, pp. 862-871, 1988.

[29] DOE, "Record of Decision for Phase II Interim Remedial Actions for Contaminated Soils and Scrapyard in Upper East Fork Poplar Creek," Oak Ridge, Tennessee, DOE/OR/01-2229&D3, 2005.

[30] USEPA. (2008, October) Appendix A Chemical Specific Data Delisting Technical Support Document. [Online]. http://www.epa.gov/reg5rcra/wptdiv/hazardous/delisting/appda1.pdf

[31] DOE, "Record of Decision for Soil, Buried Waste, and Subsurface Structure Actions in Zone 2, East Tennessee Technology ParK," Oak Ridge, Tennessee, DOE/OR/01-2161& D2, 2005b.

[32] USEPA, "Guidance on the Development, Evaluation, and Application of Environmental Models," Council for Regulatory Environmental Modeling, U.S. Environmental Protection Agency, Washington, DC, EPA/100/K-09/003, 2009.

[33] James Kuwabara and others, "Flux of Dissolved Forms of Mercury Across the Sediment-water Interface in Lahontan Reservoir, Nevada," U.S. Geological Survey, Nevada, Water Resources Investigations Report 02-4138, 2002.

[34] DOE, "Recommendations to Address Technical Uncertainties in Mitigation and Remediation of Mercury at the Y-12 Plant, Oak Ridge," Office of Environmental Management, Department of Energy, Oak Ridge, Tennessee, 2008.

[35] George Southworth, Max Greeley, Mark Peterson, Kenneth Lowe, and Richard Kettelle, "Sources of Mercury to East Fork Poplar Creek Downstream from the Y-12 National Security Complex: Inventories and Export Rates," Oak Ridge, ORNL/TM-2009/231, 2010.

[36] Nilima Gandhi et al., "Development of a Mercury Speciation, Fate and Biotic Uptake (BIOTRANSPEC) Model; Application to Lahontan Reservoir (NEVADA, USA)," *Environmental Toxicology and Chemistry*, vol. 26, no. 11, pp. 2260–2273, 2007.

[37] Carrie L. Miller, George Southworth, Scott Brooks, and Baohua Gu, "Kinetic Controls in the Complexation between Mercury and Dissolved Organic Matter in a Contaminated Environment," *Environmental Science Technology*, vol. 43, pp. 8548-8553, 2009.

[38] L Van Rijn, "Sediment Transport, Part I, Bed Load Transport," *Journal of*

Hydraulic Engineering, pp. 1431-1456, 1984.

[39] R.J. Garde and K.J. Tanga Raju., *Mechanics of Sediment Transportation and Alluvial Stream Problems*, Second Edition ed.: John Wiley & Sons, 1985.

[40] DOE, "Instream Contaminant Study Task 5, Summary Report," Oak ridge, Tennessee, 1986b.

[41] Cinthia Kaleri, "Implementation Issues: Mercury Transport and Fate. combustion Risk Assessments in Region 6," in *EPA - Proceding of the 12th International conference*, Dallas - Texas, 2000.

[42] Jerry Allison and Terry Allison, "Partition Coefficients for Metals in Surface Water, Soil and Waste ," Office of Research and Development, US Envoironmental Protection Agency, Washington, DC, EPA/600/R-05/074, 2005.

11. APPENDICES

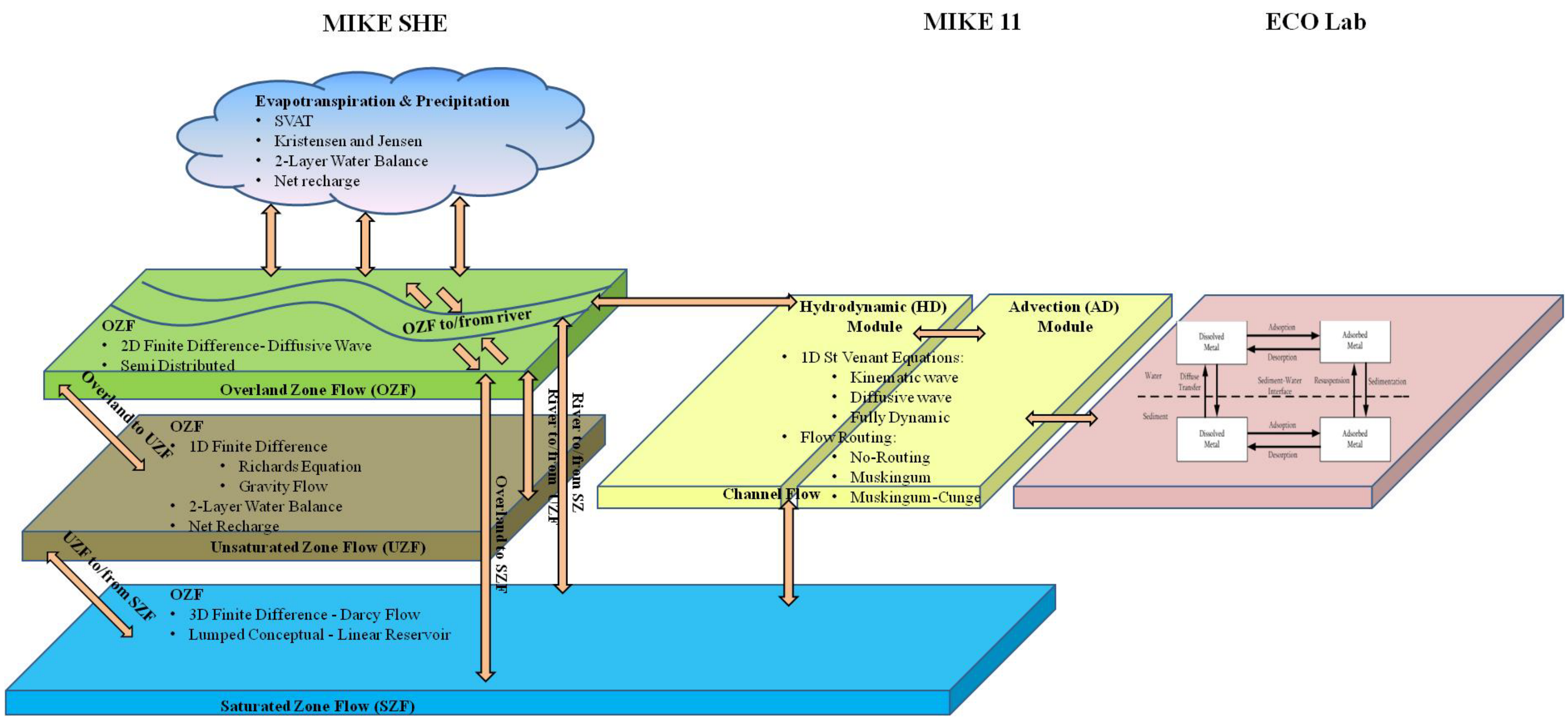

Figure 33 Schematic of the modular set-up and processes of MIKE SHE, MIKE 11, and ECOLAB arranged in accordance to the EFPC model structure. (Concept obtained from DHI [**16**] and modified by Lilian Marrero)

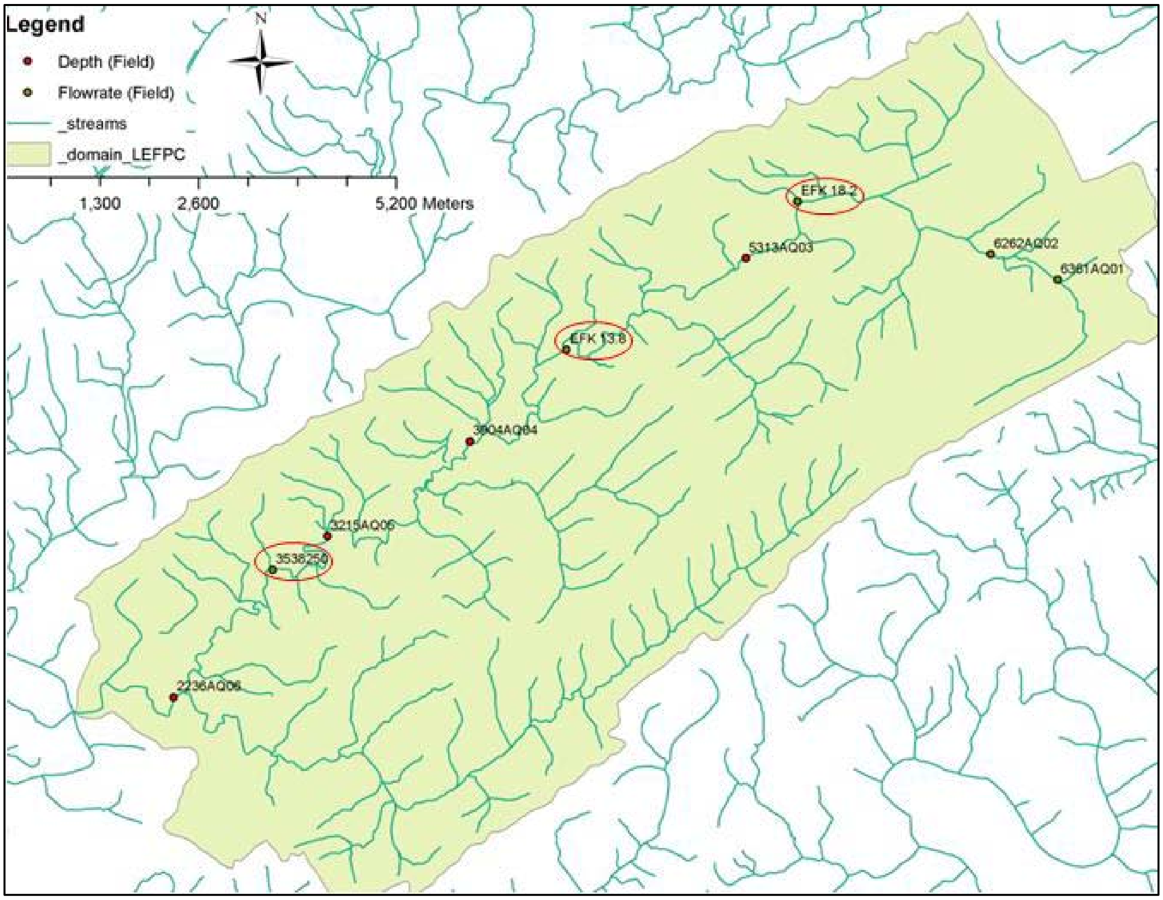

Figure 34 Highlighted stations represent flow data observation points added to the model as timeseries.

Table 6 EFPC Model Network Branches

Name	Downstream Chainage	Downstream Connection Name	Downstream Connection Chainage
BC-A-N01	2627.00852	Bear Creek	9274.97319
BC-A-S01	1731.03357	Bear Creek	8228.22922
Bear Creek	12393.1962	EFPC	23342.328
Branch100	570.515326	Bear Creek	1708.63916
Branch101	645.54787	Bear Creek	1238.53279
Branch102	371.057499	Bear Creek	1994.64616
Branch103	367.130677	Bear Creek	2873.2586
Branch104	676.627975	Bear Creek	502.095608
Branch105	738.47401	Bear Creek	855.648999
Branch106	320.135532	EFPC	17698.0082
Branch107	494.19464	EFPC	20073.4189
Branch108	337.941501	EFPC	20996.8015
Branch109	272.418154	BC-A-N01	1027.66123
Branch110	928.093627	Bear Creek	7040.48431
Branch111	512.962161	Branch110	505.555117
Branch112	407.512497	Branch110	505.555117
Branch113	915.067283	EFPC	9091.23597
Branch18	623.430043	EFPC	3679.62887
Branch19	767.032449	EFPC	4382.24429
Branch20	1562.3612	EFPC	5085.13617
Branch21	747.976283	EFPC-A-S04	1394.2137
Branch22	479.446328	EFPC-A-N04	2412.89544
Branch23	733.906826	EFPC-A-N04	1365.18116
Branch24	1062.82743	EFPC-A-N04-N01	1475.16897
Branch25	574.90101	EFPC-A-N04-N01	755.286944
Branch26	1349.79425	EFPC	7282.7484
Branch27	305.550978	Branch26	645.560017
Branch28	1385.65267	EFPC	7647.66632
Branch29	411.312158	EFPC-A-S04	1078.92038
Branch30	1220.46903	EFPC	8026.57498
Branch31	1100.44229	EFPC-A-S04	1625.79832
Branch32	1119.24833	Milton Branch	2212.74766
Branch33	640.394531	Milton Branch	2215.26565
Branch34	394.470438	Milton Branch	1906.67759
Branch35	1094.31462	Milton Branch	1906.67759
Branch36	555.989773	Branch37	1241.65263
Branch37	1389.40442	Milton Branch	1417.23759
Branch38	258.90626	Milton Branch	299.935879
Branch39	763.967426	Branch37	998.198308
Branch40	349.971877	Branch37	863.709821

Continuation of Table 6

Name	Downstream Chainage	Downstream Connection Name	Downstream Connection Chainage
Branch41	306.896242	Branch39	600.112762
Branch42	648.620057	Milton Branch	893.27888
Branch43	410.206634	EFPC	13730.9602
Branch44	341.965487	EFPC	11930.5444
Branch45	345.398656	EFPC	11105.8086
Branch46	1343.24789	EFPC	10541.2185
Branch47	491.932802	Branch46	635.497021
Branch48	1123.56862	EFPC	12342.9044
Branch49	613.000721	EFPC-A-N03	672.619034
Branch50	1074.72944	EFPC-A-N03	1426.07585
Branch51	1674.47658	EFPC	14936.3057
Branch53	1168.69096	Branch51	1362.24078
Branch54	614.27993	Branch51	1308.53024
Branch55	420.959085	EFPC-A-N02	689.961838
Branch56	1506.09017	EFPC	18288.5517
Branch57	349.039006	Branch56	1036.12
Branch58	367.643714	Branch56	376.299345
Branch59	1362.67434	EFPC	18651.3516
Branch60	785.591557	EFPC	18651.3516
Branch61	455.319439	EFPC-A-N01	509.372774
Branch62	1090.51342	EFPC	20466.32
Branch63	1095.59976	EFPC-A-N01	1615.37626
Branch64	1783.7922	EFPC	24812.5811
Branch65	365.341176	Pinhook Branch	877.595397
Branch66	406.584377	Pinhook Branch	1141.96693
Branch67	565.599776	Pinhook Branch	1141.96693
Branch68	625.023043	Pinhook Branch	467.553892
Branch69	710.859381	Gum Hollow Branch	2607.62585
Branch70	604.115881	GHB-A-S05	875.782043
Branch71	646.687734	GHB-A-S05	1162.66811
Branch72	466.240066	GHB-A-S05	1629.21892
Branch73	1553.5932	Gum Hollow Branch	1495.13032
Branch74	957.998954	Branch73	1304.78772
Branch75	565.605786	Branch73	611.384598
Branch76	386.093979	Gum Hollow Branch	3961.40439
Branch77	757.166531	EFPC-A-S01	1940.3623
Branch78	1180.43707	Bear Creek	10308.0545
Branch79	747.814346	Bear Creek	10203.6514
Branch80	656.335209	Bear Creek	8506.0781
Branch81	1061.41327	Bear Creek	8506.0781

Continuation of Table 6

Name	Downstream Chainage	Downstream Connection Name	Downstream Connection Chainage
Branch82	455.792787	BC-A-S01	813.365846
Branch83	459.796837	Branch82	426.125736
Branch84	1335.56282	Bear Creek	8161.14718
Branch85	287.505808	Branch84	703.608893
Branch86	1598.99258	Bear Creek	8951.6694
Branch87	1219.09375	Bear Creek	7238.97864
Branch88	1504.98443	Bear Creek	6349.44565
Branch89	602.005039	Bear Creek	5917.48305
Branch90	776.620137	Bear Creek	5988.19373
Branch91	508.739969	Bear Creek	5288.30912
Branch92	619.209188	Bear Creek	4969.5992
Branch93	696.968113	Bear Creek	4839.21515
Branch94	628.918276	Bear Creek	4133.97608
Branch95	643.724335	Bear Creek	3766.44731
Branch96	574.72635	Bear Creek	3372.95977
Branch97	643.289247	Bear Creek	2873.2586
Branch98	608.276871	Bear Creek	2496.828
Branch99	568.290615	Bear Creek	2105.09977
EFPC	25485.1953		
EFPC-A-N01	1820.50769	EFPC	21183.8791
EFPC-A-N02	1546.16389	EFPC	14936.3057
EFPC-A-N03	1616.78645	EFPC	12948.7807
EFPC-A-N04	2934.28761	EFPC	6498.75737
EFPC-A-N04-N01	1611.75264	EFPC-A-N04	2100.35832
EFPC-A-S01	2243.13258	EFPC	22905.6146
EFPC-A-S02	1435.42326	EFPC	19750.8333
EFPC-A-S03	1671.92188	EFPC	13831.4589
EFPC-A-S04	2306.03929	EFPC	5746.31448
GHB-A-S05	1829.8496	Gum Hollow Branch	2253.28604
Gum Hollow Branch	4259.9214	EFPC	16319.3026
Milton Branch	3414.31997	EFPC	10778.9293
Pinhook Branch	2016.48484	EFPC	16958.969

Table 7 EFPC Model, network point for branch BC-A-N01 and BC-A-S01

X Coordinate	Y Coordinate	Branch	Chainage Type	Chainage
750360	181500	BC-A-N01	System Defined	0
750190	181600	BC-A-N01	System Defined	197.23083
750060	181510	BC-A-N01	System Defined	355.34471
749940	181500	BC-A-N01	System Defined	475.76066
749930	181420	BC-A-N01	System Defined	556.38324
749710	181260	BC-A-N01	System Defined	828.41265
749520	181200	BC-A-N01	System Defined	1027.6612
749420	181100	BC-A-N01	System Defined	1169.0826
749270	181060	BC-A-N01	System Defined	1324.3243
749210	180930	BC-A-N01	System Defined	1467.5025
749120	180790	BC-A-N01	System Defined	1633.9357
749120	180680	BC-A-N01	System Defined	1743.9357
749100	180430	BC-A-N01	System Defined	1994.7344
749180	180140	BC-A-N01	System Defined	2295.5666
748960	180030	BC-A-N01	System Defined	2541.5341
748940	179980	BC-A-N01	System Defined	2595.3857
748950	179950	BC-A-N01	System Defined	2627.0085
748370	178730	BC-A-S01	System Defined	0
748704.07	178836.58	BC-A-S01	System Defined	350.65372
748941.5	178880.67	BC-A-S01	System Defined	592.14686
749120	178750	BC-A-S01	System Defined	813.36585
749230	178740	BC-A-S01	System Defined	923.81946
749390	178820	BC-A-S01	System Defined	1102.7049
749390	178920	BC-A-S01	System Defined	1202.7049
749450	179000	BC-A-S01	System Defined	1302.7049
749520	179290	BC-A-S01	System Defined	1601.0336
749640	179340	BC-A-S01	System Defined	1731.0336

Table 8 EFPC Model boundary conditions per branch

Boundary Description	Boundary Type	Branch Name	Chainage	Boundary ID
Open	Inflow	Bear Creek	0	N/A
Open	Inflow	Branch100	0	N/A
Open	Inflow	Branch101	0	N/A
Open	Inflow	Branch102	0	N/A
Open	Inflow	Branch103	0	N/A
Open	Inflow	Branch104	0	N/A
Open	Inflow	Branch105	0	N/A
Open	Inflow	Branch106	0	N/A
Open	Inflow	Branch107	0	N/A
Open	Inflow	Branch108	0	N/A
Open	Inflow	Branch109	0	N/A
Open	Inflow	Branch110	0	N/A
Open	Inflow	Branch111	0	N/A
Open	Inflow	Branch112	0	N/A
Open	Inflow	Branch113	0	N/A
Open	Inflow	Branch18	0	N/A
Open	Inflow	Branch19	0	N/A
Open	Inflow	Branch20	0	N/A
Open	Inflow	Branch21	0	N/A
Open	Inflow	Branch22	0	N/A
Open	Inflow	Branch23	0	N/A
Open	Inflow	Branch24	0	N/A
Open	Inflow	Branch25	0	N/A
Open	Inflow	Branch26	0	N/A
Open	Inflow	Branch27	0	N/A
Open	Inflow	Branch28	0	N/A
Open	Inflow	Branch29	0	N/A
Open	Inflow	Branch30	0	N/A
Open	Inflow	Branch31	0	N/A
Open	Inflow	Branch32	0	N/A
Open	Inflow	Branch33	0	N/A
Open	Inflow	Branch34	0	N/A
Open	Inflow	Branch35	0	N/A
Open	Inflow	Branch36	0	N/A
Open	Inflow	Branch37	0	N/A
Open	Inflow	Branch38	0	N/A

Continuation of Table 8

Boundary Description	Boundary Type	Branch Name	Chainage	Boundary ID
Open	Inflow	Branch39	0	N/A
Open	Inflow	Branch40	0	N/A
Open	Inflow	Branch41	0	N/A
Open	Inflow	Branch42	0	N/A
Open	Inflow	Branch43	0	N/A
Open	Inflow	Branch44	0	N/A
Open	Inflow	Branch45	0	N/A
Open	Inflow	Branch46	0	N/A
Open	Inflow	Branch47	0	N/A
Open	Inflow	Branch48	0	N/A
Open	Inflow	Branch49	0	N/A
Open	Inflow	Branch50	0	N/A
Open	Inflow	Branch51	0	N/A
Open	Inflow	Branch53	0	N/A
Open	Inflow	Branch54	0	N/A
Open	Inflow	Branch55	0	N/A
Open	Inflow	Branch56	0	N/A
Open	Inflow	Branch57	0	N/A
Open	Inflow	Branch58	0	N/A
Open	Inflow	Branch59	0	N/A
Open	Inflow	Branch60	0	N/A
Open	Inflow	Branch61	0	N/A
Open	Inflow	Branch62	0	N/A
Open	Inflow	Branch63	0	N/A
Open	Inflow	Branch64	0	N/A
Open	Inflow	Branch65	0	N/A
Open	Inflow	Branch66	0	N/A
Open	Inflow	Branch67	0	N/A
Open	Inflow	Branch68	0	N/A
Open	Inflow	Branch69	0	N/A
Open	Inflow	Branch70	0	N/A
Open	Inflow	Branch71	0	N/A
Open	Inflow	Branch72	0	N/A
Open	Inflow	Branch73	0	N/A
Open	Inflow	Branch74	0	N/A
Open	Inflow	Branch75	0	N/A
Open	Inflow	Branch76	0	N/A
Open	Inflow	Branch77	0	N/A
Open	Inflow	Branch78	0	N/A

Continuation of Table 8

Boundary Description	Boundary Type	Branch Name	Chainage	Boundary ID
Open	Inflow	Branch79	0	N/A
Open	Inflow	Branch80	0	N/A
Open	Inflow	Branch81	0	N/A
Open	Inflow	Branch82	0	N/A
Open	Inflow	Branch83	0	N/A
Open	Inflow	Branch84	0	N/A
Open	Inflow	Branch85	0	N/A
Open	Inflow	Branch86	0	N/A
Open	Inflow	Branch87	0	N/A
Open	Inflow	Branch88	0	N/A
Open	Inflow	Branch89	0	N/A
Open	Inflow	Branch90	0	N/A
Open	Inflow	Branch91	0	N/A
Open	Inflow	Branch92	0	N/A
Open	Inflow	Branch93	0	N/A
Open	Inflow	Branch94	0	N/A
Open	Inflow	Branch95	0	N/A
Open	Inflow	Branch96	0	N/A
Open	Inflow	Branch97	0	N/A
Open	Inflow	Branch98	0	N/A
Open	Inflow	Branch99	0	N/A
Open	Inflow	EFPC	0	N/A
Point Source	Inflow	EFPC	0	N/A
Point Source	Inflow	EFPC	7.69702308	200
Point Source	Inflow	EFPC	15.1815578	135
Point Source	Inflow	EFPC	28.5337035	134
Point Source	Inflow	EFPC	93.2045032	126
Point Source	Inflow	EFPC	99.9074534	125
Point Source	Inflow	EFPC	144.267419	114
Point Source	Inflow	EFPC	253.302757	113
Point Source	Inflow	EFPC	318.675028	110
Point Source	Inflow	EFPC	364.903089	109
Point Source	Inflow	EFPC	370.037803	102
Point Source	Inflow	EFPC	390.364968	99
Point Source	Inflow	EFPC	459.803948	87
Point Source	Inflow	EFPC	459.803948	88
Point Source	Inflow	EFPC	484.094043	86

Continuation of Table 8

Boundary Description	Boundary Type	Branch Name	Chainage	Boundary ID
Point Source	Inflow	EFPC	487.198636	83
Point Source	Inflow	EFPC	551.868787	71
Point Source	Inflow	EFPC	582.150378	67
Point Source	Inflow	EFPC	622.587496	62
Point Source	Inflow	EFPC	628.418544	64
Point Source	Inflow	EFPC	632.571374	63
Point Source	Inflow	EFPC	697.070226	58
Point Source	Inflow	EFPC	701.909704	57
Point Source	Inflow	EFPC	716.780429	55
Point Source	Inflow	EFPC	741.47639	51
Point Source	Inflow	EFPC	764.022982	54
Point Source	Inflow	EFPC	785.40445	48
Point Source	Inflow	EFPC	787.82346	47
Point Source	Inflow	EFPC	804.502318	46
Point Source	Inflow	EFPC	820.952263	44
Point Source	Inflow	EFPC	845.446533	42
Point Source	Inflow	EFPC	883.151953	41
Point Source	Inflow	EFPC	933.004587	34
Point Source	Inflow	EFPC	943.002728	33
Point Source	Inflow	EFPC	1020.78772	21
Point Source	Inflow	EFPC	1059.24245	20
Point Source	Inflow	EFPC	1177.78284	19
Point Source	Inflow	EFPC	1347.73701	16
Point Source	Inflow	EFPC	1399.69678	14
Point Source	Inflow	EFPC	1946.26967	6
Point Source	Inflow	EFPC	2050.32925	7
Point Source	Inflow	EFPC	2398.76723	3
Point Source	Inflow	EFPC	2456.77397	2
Open	Q-h	EFPC	25485.2	N/A
Open	Inflow	EFPC-A-N01	0	N/A
Open	Inflow	EFPC-A-N02	0	N/A
Open	Inflow	EFPC-A-N03	0	N/A
Open	Inflow	EFPC-A-N04	0	N/A
Open	Inflow	EFPC-A-N04-N01	0	N/A
Open	Inflow	EFPC-A-S01	0	N/A
Open	Inflow	EFPC-A-S02	0	N/A
Open	Inflow	EFPC-A-S03	0	N/A
Open	Inflow	EFPC-A-S04	0	N/A
Open	Inflow	GHB-A-S05	0	N/A

Continuation of Table 8

Boundary Description	Boundary Type	Branch Name	Chainage	Boundary ID
Open	Inflow	GHB-A-S05	0	N/A
Open	Inflow	Gum Hollow Branch	0	N/A
Open	Inflow	Milton Branch	0	N/A
Open	Inflow	Pinhook Branch	0	N/A
Closed		BC-A-S01	0	N/A
Closed		BC-A-N01	0	N/A

TECHNICAL REPORT

Remediation and Treatment Technology Development and Support for DOE Oak Ridge Office: A Surface Water Flow and Contaminant Transport Model of the ORNL 4500 Area Using XPSWMM

Date submitted:

March 1, 2013

Principal Investigators:

Leonel E. Lagos, Ph.D., PMP®
David Roelant, Ph.D.

Florida International University Collaborators:

Heidi Henderson, PE (DOE Fellow)
Georgio Tachiev, Ph.D., PE
Angelique Lawrence, MS, GISP

Submitted to:

U.S. Department of Energy
Office of Environmental Management
Under Grant # DE-EM0000598

FIU Applied Research Center
FLORIDA INTERNATIONAL UNIVERSITY

EXECUTIVE SUMMARY

An XPSWWM surface water model was developed to provide a better understanding of the surface water flow rates and water stages during rainfall events for the selected 4500 ORNL area. The specific system of interest, the stormwater collection system up to Outfall 211, is approximately 4.5 acres and encompasses several ORNL buildings. The system is bounded by mostly impervious area (due to roof top runoff through storm drains and pavement to the north, south, east, and west) with minor pervious areas sparsely connected within. Ms. Henderson, the author of this study, conducted an internship during the summer of 2012 and collected information about the physical parameters of the stormwater drainage system. A stormwater hydraulic-hydrologic computer model was developed using XPSWWM software. The objective of the model is to provide detailed information about flow rate and stage timeseries during various stormwater events. ORNL provided monitored timeseries flow rates at OF-211. Dates that rainfall occurred during the monitoring period were noted and simulated through the network for calibration of the model. The model produced results that agreed with the monitored data resulting in credible validation of the model. In addition, a sensitivity analysis was prepared where factual rainfall data was simulated through the network varying Manning's roughness coefficient, infiltration parameters, and percent imperviousness in order to assess the impacts of the variables on the model results. Design storms were simulated and examined. In addition, a hypothetical conservative contaminant was introduced into the system at various locations. The flow rates, concentrations, and loads were fit to a probability distribution which describes the character of the data. The resulting flow rates from the model may be utilized in conjunction with contaminant data to assess where remediation may be necessary within the area of interest.

Contents

LIST OF TABLES

LIST OF FIGURES

1 INTRODUCTION

In the 1940's during World War II, the U.S. initiated its own research and development program—commonly referred to as the Manhattan Project—in a race to create the first atomic bomb. The 33,750 acre Oak Ridge Reservation (ORR) was the first site selected to support the Manhattan Project. This site consists of three major U.S. Department of Energy (DOE) facilities, the East Tennessee Technology Park (ETTP) formerly known as the Oak Ridge Gaseous Diffusion Plant or K-25 (2200-acres), the Y-12 National Security Complex (Y-12 NSC) (800-acres), and the Oak Ridge National Laboratory (ORNL) formerly known as X-10 (4470-acres). The reason for selecting ORR was because it provided the water supply (Clinch River), electricity (Tennessee Valley Authority), and workforce (citizens from the City of Knoxville) necessary for this operation. In addition to the workforce offered by the City of Knoxville, thousands of scientists, engineers, and support personnel relocated to the area in support of this mission (ORNL, 2008).

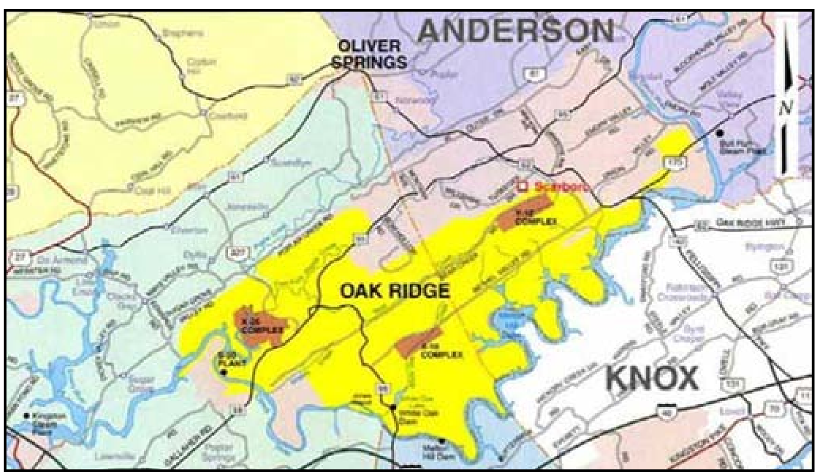

Figure 1 Oak Ridge Reservation (USEPA, 2004)

By the early 1950's, DOE began the production of thermonuclear weapons in support of the Cold War. A key active ingredient in the design of the thermonuclear weapon, or the hydrogen bomb, was lithium-6 (Li-6), which is produced by separating lithium isotopes using an aqueous solution containing mercury (Hg) (Brooks and Southworth, 2011; Ragheb, 2012). In 1953, ORNL Buildings 4501 and 4505 were built to conduct a pilot-scale evaluation of the lithium exchange processes for the development of thermonuclear weapons. Building 4501, the High-Level Radiochemical Laboratory, was a pilot plant for the OREX process. In 1955, Building 4505, the Experimental Engineering Laboratory, was built to house another process named METALLEX. Although ORNL's major concern is Hg contamination, many other pollutants have resulted from the previously described activities. More specifically, radionuclides (strontium-90 and radium-228) and inorganics are also of concern and remediation is needed (Taylor, 1989a).

Figure 2 ORNL Building 4501 and 4505 Location

ORNL is located within the White Oak Creek (WOC) watershed, which is within the Central Bethel Valley watershed (a portion of the Bethel Valley watershed). WOC, a tributary of the Tennessee River, is the main stream running adjacent to ORNL along its south-eastern border and represents a major route for water and contaminant transport (USEPA, 2004; USEPA, 2006). The WOC watershed is comprised of approximately 2,098 acres and collects runoff and treated wastewater discharge from ORNL where it is drained into White Oak Lake and then the Clinch

River (ORNL, 2008; USDOE, 1999). In Figure 3 Oak Ridge Reservation (ChemRisk, 1999a), the location of the area of interest is located within the red circle.

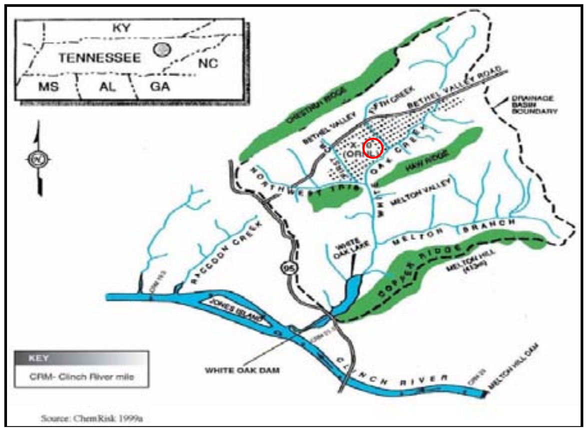

Figure 3 Oak Ridge Reservation (ChemRisk, 1999a)

2 STUDY AREA

The specific system of interest and its drainage area, herein referred to as the stormwater collection system up to Outfall 211, are located within the red circle as shown in Figure 1 and in more detail in Figure 2. It is approximately 4.5 acres and encompasses the following ORNL buildings: 4500N Wings 1, 2, and part of Wing 3, 4500S Wings 1, 2, and part of Wing 3, 4501, 4505, 4507, 4508, and 4556. The system is bounded by mostly impervious land cover (due to roof top runoff through storm drains and pavement to the north, south, east, and west); however, there are minor pervious areas throughout the drainage area.

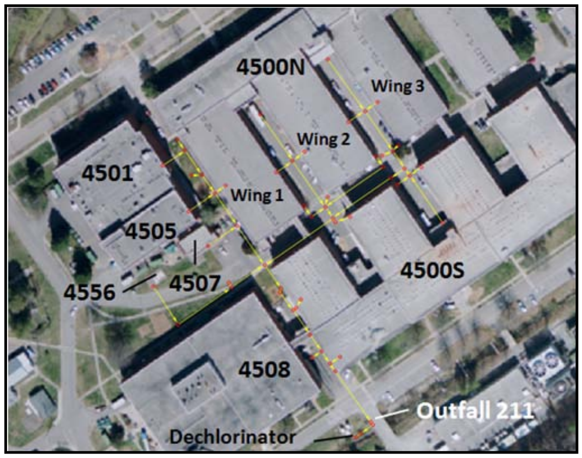

Figure 4 Area of Interest and Building Identification

Figure 5 Area of Interest Boundary

A stormwater model for the contributing drainage areas to Outfall 211 has been developed and consists of 51 link/52 nodes of closed circular conduits discharging into a free surface creek. The node elevations range from 793 ft, NAD to 803 ft, NAD respectively. The system is composed of multiple sub-drainage areas with up to five sub-catchment areas for one inlet. The sub-catchment areas are defined by imperviousness, slope, width, and area. They are linked to a node so that once the rainfall is simulated it is routed into and through the system. Model inputs include topography, pervious and impervious drainage areas of each sub-catchment area, infiltration parameters, slope of sub-catchment areas, length and diameter of pipes, and Manning's coefficient for pipe roughness.

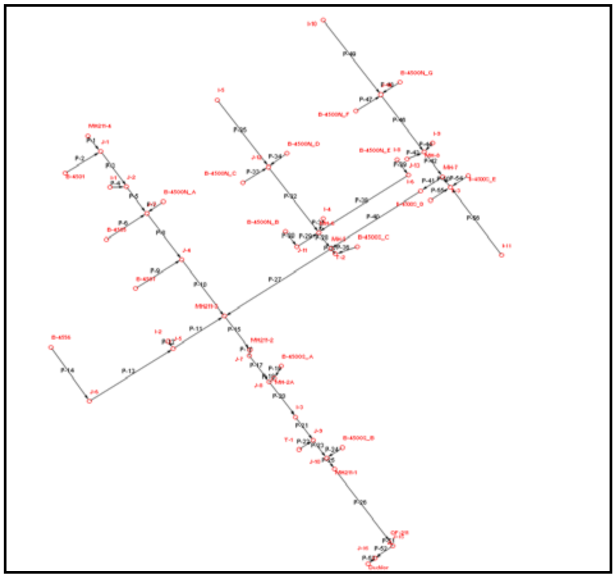

Figure 6 Stormwater Collection System

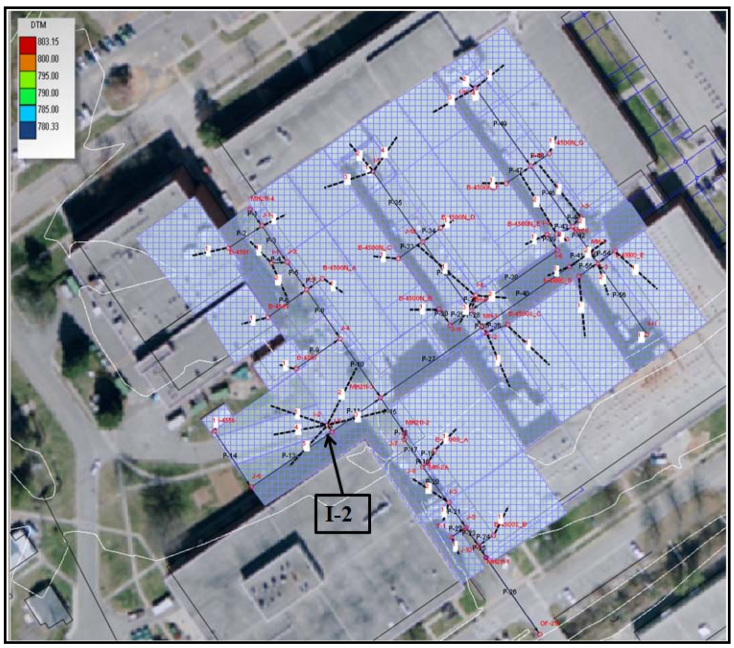

Figure 7 Sub-catchment Delineation of System

The system was modeled as one-dimensional steady flow where a steady uniform rainfall event will be modeled. One-dimensional unsteady non-uniform flow will also be modeled where the rainfall will vary with time. Both synthetic and actual rainfall data from the Oak Ridge area will be modeled through the system.

The storm system is unique in that sources from the adjacent buildings, such as cooling water and condensate from various AC units contribute to the Outfall 211 drainage system as well as process water from the Creep Laboratory (Building 4500S). ORNL receives their water supply, public drinking water and process water, from the Oak Ridge Water Treatment Plant where it is chlorinated for disinfection purposes. Thus, a dechlorinator has been added after Outfall 211 for dechlorination prior to its discharge into WOC.

From Building 4556 a 4” VP connects to a 10” VP which conveys water into MH211-3. MH211-3 is located at the northwest corner of Building 4500S. The main storm line runs west of 4500N and 4500S and contains MH211-1, MH211-2, MH211-2a, MH211-3, MH211-4, and Outfall 211. It begins at MH211-4 and ends at Outfall 211. From MH211-4 to MH211-3, the main storm line is constructed of 15” RCP. South of MH211-3, the line is 30” RCP. Outfall 211 is a culvert located under a bridge. However, prior to its release during dry periods, the water is held back by a 65” long, 13.5” high metal plate accompanied by an 8” PVC orifice. The 8” PVC conveys the water into the dechlorinator. Just prior to the dechlorinator the 8” PVC splits into two 4” PVC as it is directed through the dechlorinator for disinfection prior to its final release into WOC. It seems that only one of the two 4” PVC conveys water through the dechlorinator where the other is closed via a ball valve. This immediately impacts the system by restricting flow from an 8” PVC to a 4” PVC. Thus, for this project the dechlorinator will not be modeled and the point of discharge for the system will be immediately after Outfall 211.

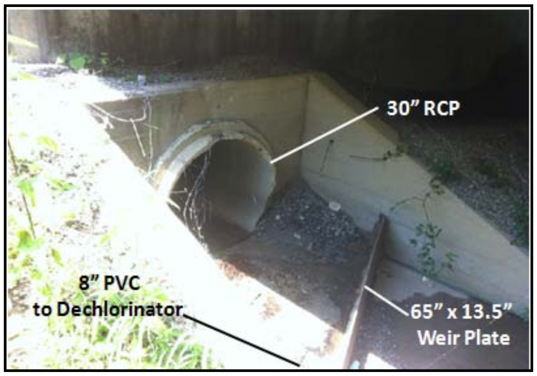

Figure 8 Outfall 211


Figure 9 WOC East of Outfall 211


Figure 10 Dechlorinator in WOC

As an industrial area, ORNL is composed of mostly impervious area with sparse pervious areas and lies within the Tennessee State Plane North American Datum (NAD) 1983. The area bordering the area of interest ranges in elevation from 780 ft NAD to 855 ft NAD as shown on the digital terrain model (DTM). However, the area of interest is relatively flat ranging from 780 ft NAD to 810 ft NAD.

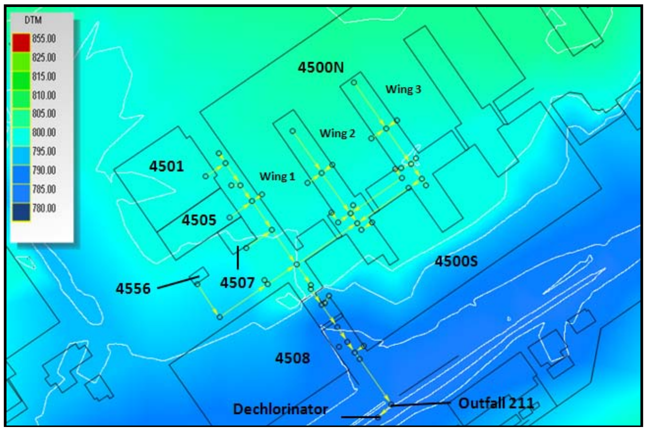

Figure 11 XPSWMM Digital Terrain Model

3 RESEARCH OBJECTIVE

In order to effectively assess the transport of contaminants within the system, it is first important to best understand the flow of water within the system of interest. Thus, the main research objective of this study is to develop a hydrologic-hydraulic model of the stormwater collection system that will be properly calibrated and verified for both steady uniform flow and unsteady non-uniform flow local conditions. If development is successful, it is expected that the model will be capable of supporting an analysis of the system for the following types of simulations in support of decision-making related to design, operation and maintenance of the system:

1. Hydrologic analysis via simulation of various storm events over the site as well as actual rainfall data.
2. Transport analysis by interjecting a conservative contaminant within the system.
3. Determination of the probability exceedance (PE) of the main nodes (inlets, manholes, and junctions) and development of flow duration and load duration functions for each node.

Additional details on the above simulations are presented in the methodology section.

4 SITE ANALYSIS

The model is based upon two sets of drawings and is noted as follows:, 1) the original drawings from the 1950's, and 2) the ATLAS drawings, which are more recent sketches based on what is believed to be underground. Neither set of drawings contain all of the pertinent information for the model. The following assumptions and notes were made based on the information found from the two sets of drawings..

The original drawings indicate that the Outfall 211 drainage system begins from the east between 4500N and 4500S Wings 2 and 3. However, the ATLAS drawings show it interconnected with the drainage system to the east. This model is in accordance with the original drawings where Outfall 211's drainage system stands alone and begins from the east at the manhole (B-4500S_E) located between 4500N and 4500S Wings 2 and 3.

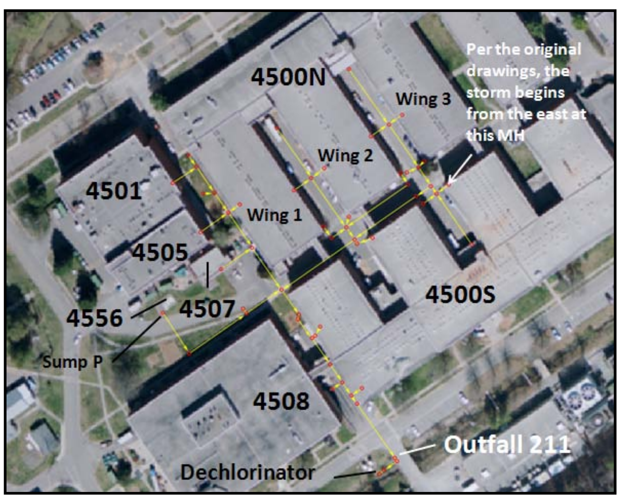

Figure 12 Location of MH B-4500S_E

The ATLAS drawings do not show the existing inlet (I-2) to the west of MH211-3.

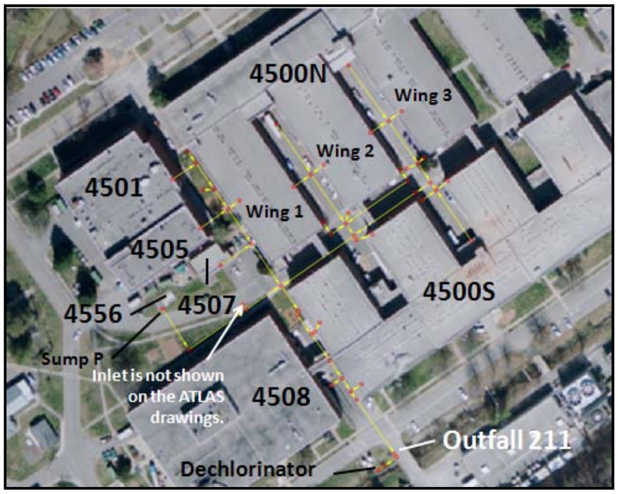

Figure 13 Location of Inlet I-2

The ATLAS drawings indicate that the inlet east of 4500N Wing 1 is shown to the west of the manhole located at the north-south centerline; however, it is located to the east of the north-south centerline (I-4).

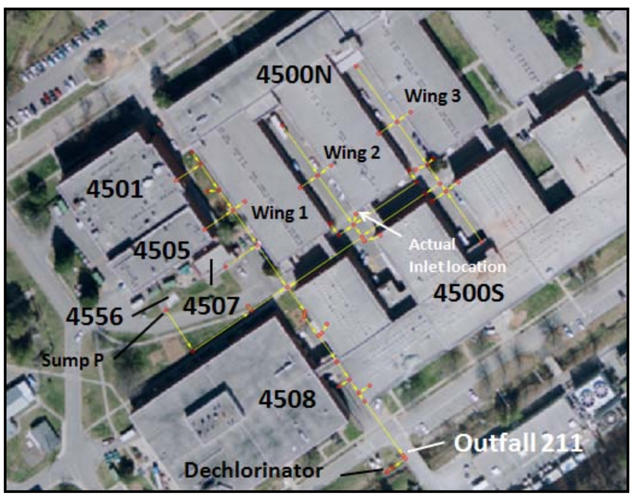

Figure 14 Location of Inlet I-4

The ATLAS drawings do not show the two inlets (I-8 and I-9) located east of 4500N Wing 2.

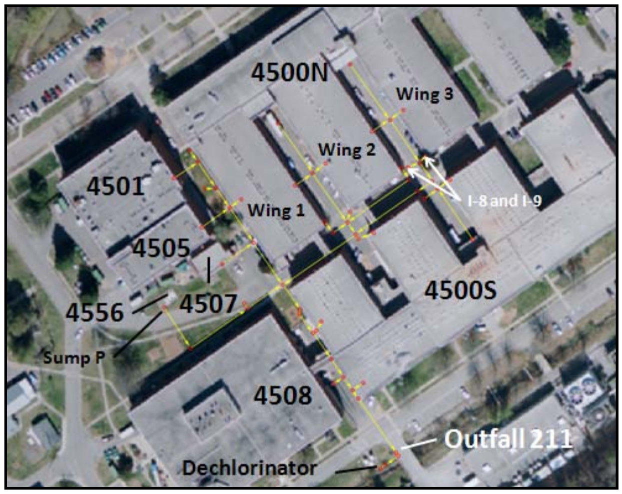

Figure 15 Location of I-8 and I-9

There are unknown inverts, manhole elevations, and inlet elevations throughout the system so reasonable assumptions will be made from analysis of surrounding or like data. Assumptions will be made for the building area contributing to the roof drains.

5 MODEL DEVELOPMENT

The program chosen to develop the stormwater model is XPSWMM, which is the Microsoft Windows version of the Environmental Protection Agency (EPA) stormwater modeling (SWMM) tool (USEPA, 2012). XPSWMM uses a spatially distributed link/node network to analyze the hydraulic, hydrologic, and quality of a stormwater or wastewater system. The XPSWMM software package applies the Saint-Venant equations to solve for the one-dimensional unsteady open channel flow. The Saint-Venant equations are based on the fundamentals of conservation of mass, momentum, and energy (Chanson, 2004). The conservation of mass and momentum is expressed by the continuity equation

$$Q = A_1 * v_1 = A_2 * v_2$$

Where, Q = volumetric flow rate; A = cross sectional area of flow; v = mean velocity.

$$\frac{p}{\gamma} + v2/2g + z = \frac{p}{\gamma} + v2/2g + z$$

XPSWMM is equipped with three modes, the hydraulic, runoff, and sanitary modes, of which only the hydraulic and runoff modes will be utilized in this model (Jacobson, 2011; Elliott and Trowsdale, 2007). The dialogs will request certain information depending on which mode is active. Node data, conduit shapes, control structures and weirs may be modeled in the hydraulic mode. The node dialog requests the spill crest elevation where it can be the manhole elevation for a manhole, inlet elevation for an inlet, or top of pipe for a junction box. For the purpose of this project, a junction box is considered as a point where the storm pipe changes direction without a manhole or inlet, or where the storm drain enters the main storm line. There is a dialog for the conduit information and selection of various shapes of pipe along with an aid to visualizing the conduit profiles.

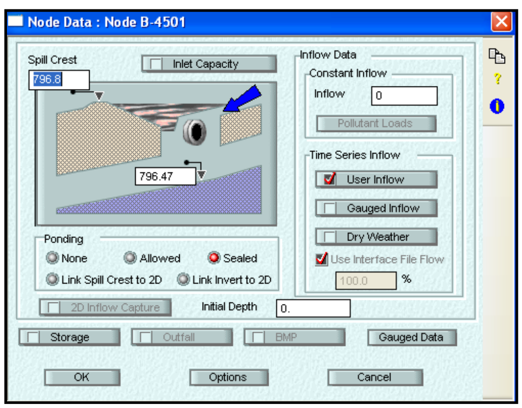

Figure 16 XPSWMM Node Data Dialog

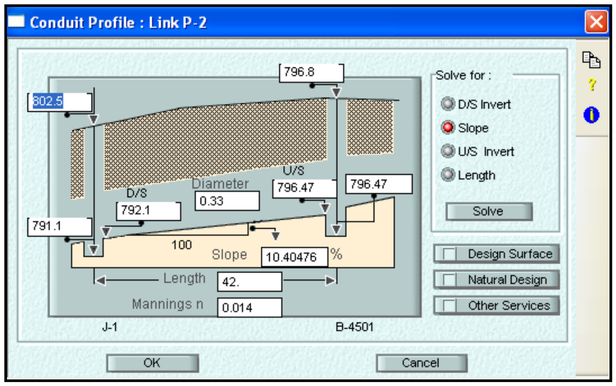

Figure 17 XPSWMM Conduit Profile

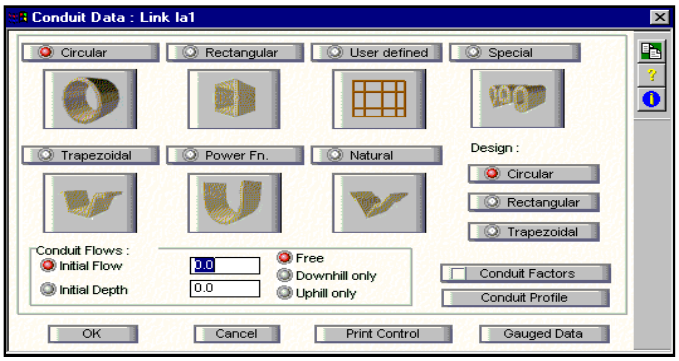

Figure 18 XPSWMM Conduit Shapes

In the runoff mode, drainage areas are delineated for the inlets via sub-catchments. One inlet can have up to five sub-catchment areas where each sub-catchment may have varying areas, impervious percentage, width, and slope. The various sub-catchments will make up the node catch basin incorporating the higher elevation contour surrounding the node. The sub-catchments are the areas that are directly connected to the inlet and will contribute runoff during the simulated rainfall events.

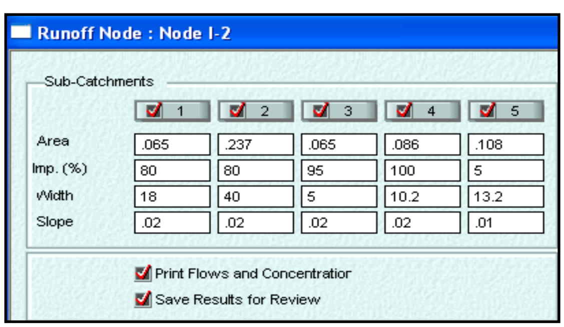

Figure 19 Sub-catchment Dialog

The network is made up of a series of links and nodes, a link being a conduit such as a storm drain, storm pipe, or culvert that conveys water from one node to another. Nodes are considered to intake stormwater or other discharges, and in this case would be the A/C units' condensate and cooling water or the chlorinated discharge water from the Creep Laboratory in Building 4500S, which would be building drains, roof drains, manholes, inlets, or junction boxes. The required input data for the conveyance through the conduits are the Manning's roughness coefficient, slope, downstream invert, upstream invert, pipe length and spill crest elevations.

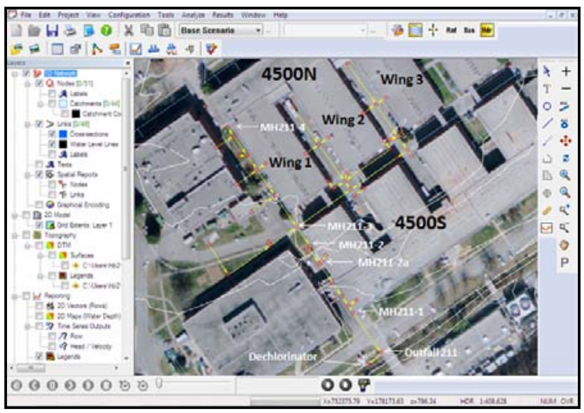

Figure 20 XPSWMM Model Main Storm Line

5.1 Open Channel Flow

The system will be modeled as one-dimensional steady uniform flow as well as unsteady non-uniform flow. The water flow is simulated to operate as partially filled open channel flow because the gravity sewer system is open to atmospheric pressure. However, it is possible that during a large storm event some pipes will encounter full flow.

The conveyance of water within the system is solved by the Manning's formula which originates from the continuity equation. The Manning's formula for uniform open channel flow through the conduits is as follows:

$$v = \frac{1.49}{n} R^{\frac{2}{3}} \sqrt{S}$$

$$Q = v * A$$

$$R = \frac{A}{P}$$

Where Q represents water flow (cfs), v is the velocity (fps), A is the cross-sectional area of flow (sf), n is the Manning's coefficient (dimensionless), R is the hydraulic radius (ft), and S is the slope of the water surface or the linear hydraulic head loss (ft/ft). The hydraulic radius is equal to the cross-sectional area of flow divided by the wetted perimeter (ft) as shown in the third equation above. The wetted perimeter for partially filled circular conduits may be found by the following information and measurements:

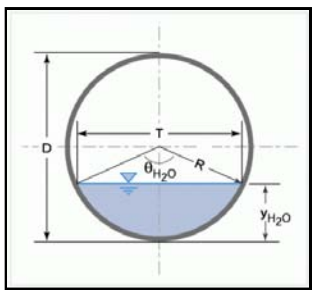

Figure 21 Partially Filled Circular Conduit

Where: Angle from the centerline to the water level, $\theta = cos^{-1}\left(1 - \frac{y}{r}\right)$; Depth of water in culvert, $y = r(1 - \cos\theta)$; Cross-sectional area of flow, $A = r^2(\theta - \cos\theta \sin\theta)$; Wetted Perimeter of water, $P = 2r(\theta)$; Top width of water surface, $T = 2r(\sin\theta)$.

5.2 Routing Method

The runoff routing method was chosen for the simulations as it allowed for the rainfall-runoff process for continuous rainfall simulations. The excess rainfall is defined as the rainfall amount that was not infiltrated into the ground surface and is therefore simulated as overland flow from divided drainage areas and, sub-catchments of the specified basins by taking into account the area, the percent imperviousness, width, and slope of the sub-catchments.

5.3 Green Ampt Infiltration Method

Green Ampt and the Horton's infiltration methods were chosen for the infiltration sensitivity analysis. The ORNL site is composed of buildings, pavement, and minor pervious areas. It is surrounded by ORR's wooded lands. Soils in the area are a mixture of reddish-brown clays and silts resulting from in-situ weathering of shaley limestone bedrock.

The Green Ampt infiltration method was chosen for all of the simulations within the hydrology and transport analyses – Manning's roughness coefficient variations, design storm events, steady uniform flow and unsteady non-uniform flow calibrations, and the three variations within the transport analysis because it is known to simulate unsteady continuous rainfall events. XPSWMM calculates the infiltration rates by utilizing the Green Ampt – Mein Larson equations, the first being the Mein-Larson equation where the soil has yet to become saturated and the Green Ampt equation once saturation of the soil has occurred. The Mein Larson calculations assume that the infiltration rate approaches the rainfall intensity rate then calculates the unsaturated soil's infiltration rate as if the cumulative infiltration volume is less than the required cumulative infiltration volume for the soil to become saturated. The cumulative infiltration volume is then determined by the following formula:

$$Fs = \frac{(\mathrm{Su} * \mathrm{IMD})}{\frac{\mathrm{i}}{\mathrm{Ks}} - 1}$$

Where, Fs = cumulative infiltration volume required to cause surface saturation, ft; Su = average capillary suction at the wetting front, ft water; IMD = initial moisture deficit, ft/ft; i = rainfall intensity, ft/sec; Ks = saturated hydraulic conductivity of soil, ft/sec.

If the soil has been saturated where the infiltration rate approaches the infiltration capacity then the following scenario is run through XPSWMM:

$$Fp = Ks * \left(1 + Su * \left(\frac{IMD}{F}\right)\right)$$

Where, Fp = infiltration capacity, ft/sec; Ks = saturated hydraulic conductivity of soil, ft/sec; Su = average capillary suction at the wetting front, ft water; IMD = initial moisture deficit for the event, ft/ft; F = cumulative infiltration volume, ft.

The Green Ampt parameters and their values based on clay loamy soil consistent with the ORNL 4500 area are shown in the figures below.

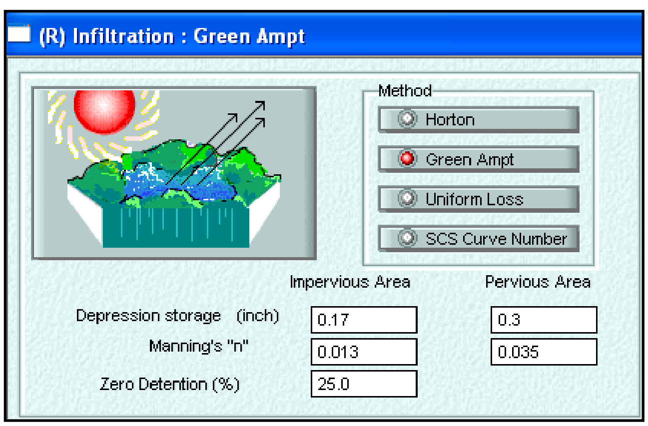

Figure 22 Infiltration Parameters

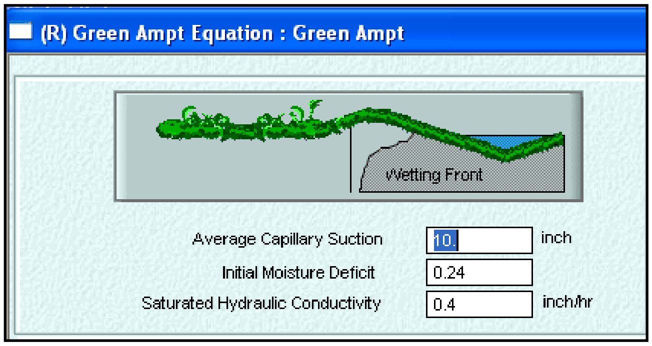

Figure 23 Green Ampt Parameters

5.4 Horton Infiltration Method

The Horton Infiltration Method was chosen as the infiltration method to be compared to the Green Ampt simulations as it may also simulate unsteady continuous rainfall events. The Horton equation indicates infiltration capacity as a function of time is as follows (Verma, 1982):

$$F_p = F_c + (F_0 - F_c)e^{-kt}$$

Where, Fp = infiltration rate into soil, in./hr (mm/hr); Fc = minimum or asymptotic value of Fp, in./hr (mm/hr); Fo = maximum or initial value of Fp, in./hr (mm/hr); t = time from beginning of storm, sec; k = decay coefficient, 1/sec.

Horton's Infiltration Method is known to calculate infiltration rates for single storm events. However, XPSWMM has an option for Horton's infiltration calculations to be regenerated, which is equal to the regeneration specified multiplied by the decay specified. For the Horton simulation a regeneration of 0.01 was used with a decay rate of 0.001.

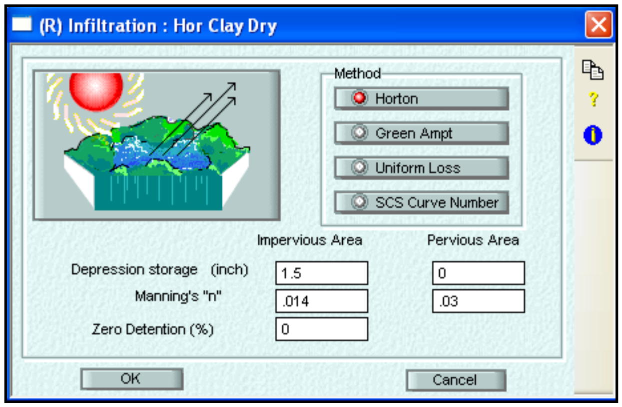

Figure 24 Horton Infiltration Dry Clay Parameter

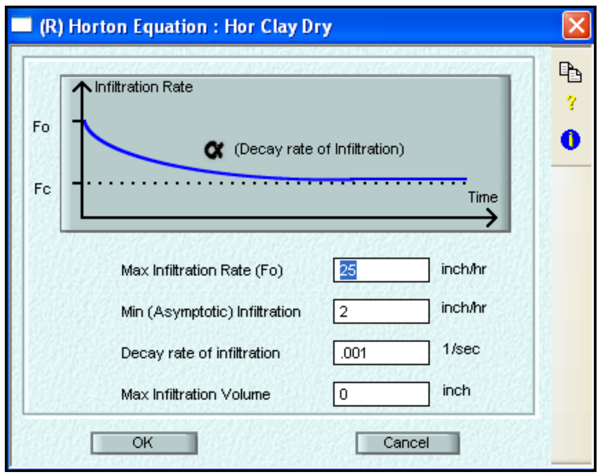

Figure 25 Horton Equation Dry Clay Parameter

6 HYDROLOGY ANALYSIS

A hydrology analysis was performed on the model beginning with a calibration of the model using both synthetic storm events for steady uniform flow conditions and unsteady non-uniform conditions and actual rainfall data. The results of the simulations using actual rainfall data are compared to OF-211 data provided by ORNL in order to validate the model. The hydrology analysis of the model includes the following:

1. Calibration
   a. Calibration of Steady Uniform Flow Conditions
   b. Calibration of Non-steady Non-Uniform Flow Conditions

2. Sensitivity Analysis
    a. Manning's Roughness Coefficients
    b. Green Ampt and Horton's Infiltration Methods
    c. Percent Imperviousness
3. Design Storm Analysis
    a. 5 Year – 24 Hour Design Storm Event
    b. 10 Year – 24 Hour Design Storm Event
    c. 25 Year – 24 Hour Design Storm Event
    d. 100 Year – 24 Hour Design Storm Event

6.1 Steady Uniform Flow Calibrations

The model was calibrated for steady uniform flow conditions where the rainfall intensity remained constant for the duration of the storm event. For the steady uniform flow simulation a hypothetical 24 hour rainfall having an intensity of 0.5 inch/hour as shown in Figure 24 Rainfall Hyetograph for Steady Uniform Flow was simulated through two inlets on the main line.

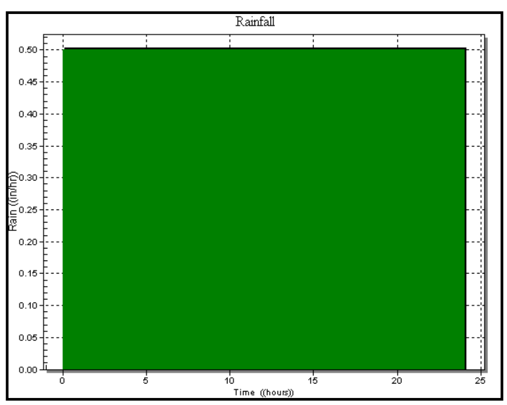

Figure 26 Rainfall Hyetograph for Steady Uniform Flow

Only inlet 1 and the nodes on the main trunk line were active. All other nodes and links were disabled so that flow only entered into inlets 1 and 3 (I-1 and I-3) in order to calibrate the model for steady uniform flow.

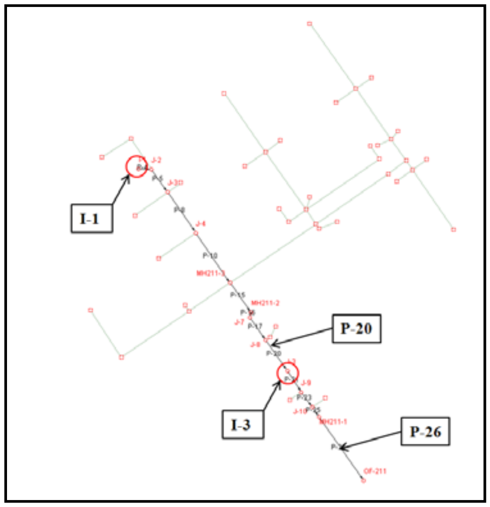

Figure 27 Stormwater Collection System for Steady Uniform Flow

The profile of the pipes included for the steady uniform flow calibration is shown below.

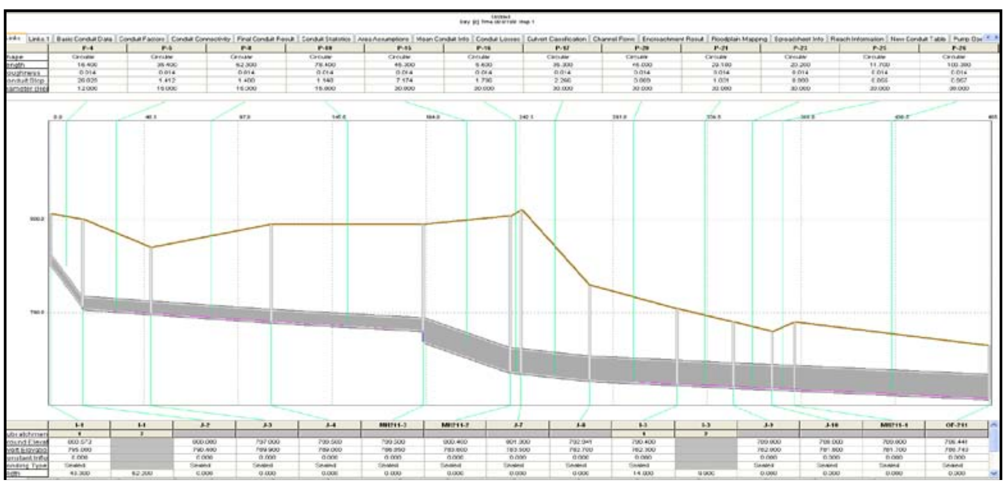
Figure 28 XPSWMM Profile for Links P-2 thru P-26

From the conservation of mass equation, mass in equals mass out, the system was analyzed.

$$m = \rho * Q$$

$$\rho_{I-1} * Q_{I-1} + \rho_{I-3} * Q_{I-3} = \rho_{out} * Q_{out}$$

Where ρ is the density of the surface water in pounds per square foot (lb/sf) and Q is the flow rate of the surface water in cubic feet per second (cfs). Knowing that the density of the surface water is constant, the density can be cancelled out leaving the flow rate of I-1 plus the flow rate of I-3 to equal the flow rate out.

$$Q_{I-1} + Q_{I-3} = Q_{out}$$

Where

$$Q = c * i * A$$

Where c is the dimensionless runoff coefficient in which a copy of the table including typical c values is enclosed in the Appendix, i is the rainfall intensity in inches per hour (in/hr), A is the area of the sub-drainage area in acres (ac). The flow is in cfs and represents the peak flow rate.

The mass balance calculation for the flow rate entering I-1 was calculated as follows:

$$Q_{I-1} = 0.05 * 0.5 \left(\frac{in}{hr}\right) * (0.173\ ac)$$

$$Q_{I-1} = 0.004\ cfs$$

The sub-drainage areas are mostly green space with an estimated impervious area of 5%. A rainfall intensity of 0.5 in/hr and a sub-drainage area total of 0.173 ac were used. A rational runoff coefficient may be estimated as 0.05 to 0.35 for lawns (Corbitt, 1999; Singh, 1992). Based on the flow rate produced by XPSWMM, a runoff coefficient of 0.05 would satisfy the simulation. Dense grass is present in this area. This should be considered as an acceptable approximation for the runoff coefficient. Thus the peak flow rate in P-20 should be equal to that of Q_{I-1}. The XPSWMM hydrograph results in Figure 26 Conduit P-20 Results for Steady Uniform Flow indicate that the peak flow rate is 0.004 cfs, which complies with the mass balance equation for Q_{I-1} that equals 0.004 cfs.

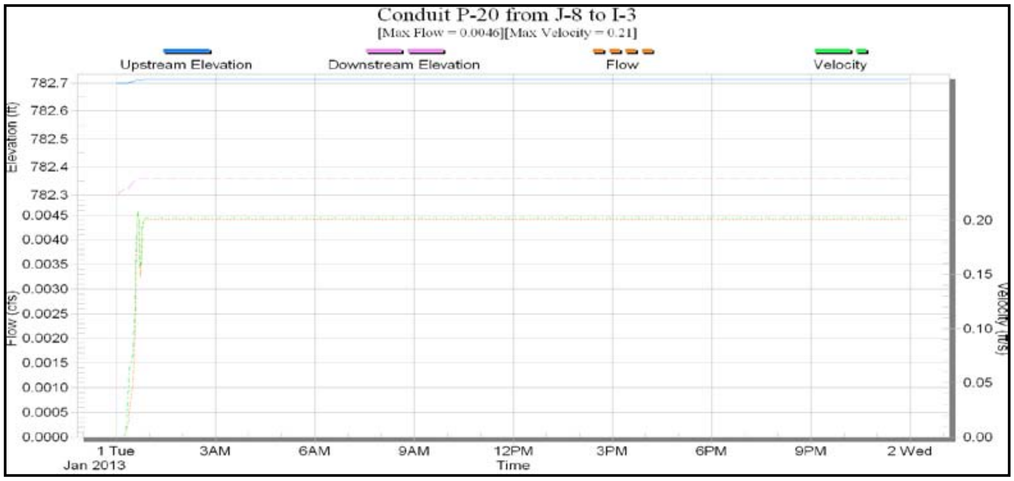

Figure 29 Conduit P-20 Results for Steady Uniform Flow

The mass balance calculation for the flow rate entering I-3 was calculated as follows:

$$Q_{I-3} = 0.95 * 0.5 \left(\frac{in}{hr}\right) * (0.097\, ac)$$

$$Q_{I-3} = 0.046\, cfs$$

$$Q_{out} = Q_{I-1} + Q_{I-3} = 0.05\, cfs$$

I-3 sub-catchments total 0.097 ac, a steady uniform rainfall of 0.5 in/hr, and an assumed rational runoff coefficient of 0.95 for asphalt streets was used as this is an asphalt driveway resulting in a flow rate of 0.046 cfs.

Link P-26 is located immediately before Outfall 211; therefore, the peak flow rate in P-20 should equal that of Q_{out}. The XPSWMM hydrograph results in Figure 27 Conduit P-26 Results for

Steady Uniform Flow indicate that the peak flow rate is 0.05 cfs, which complies with the mass balance equation for Q_{out}.

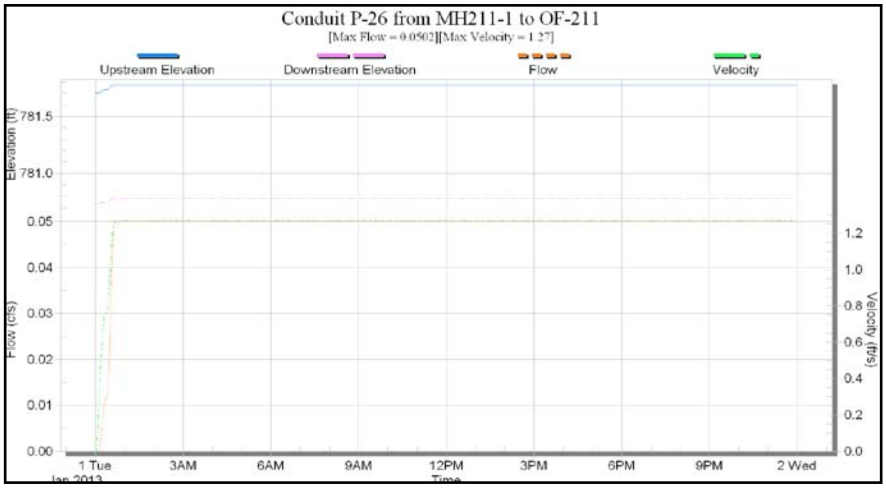

Figure 30 Conduit P-26 Results for Steady Uniform Flow

6.2 Unsteady Non-Uniform Flow Calibration

In order for the ORNL surface water model of the 4500 Area to be considered a valuable source to assess flow rates within the network, it must be calibrated with existing OF-211 data. The non-uniform flow calibration was conducted by simulating actual rainfall that occurred during the timeframe that ORNL provided outfall 211 (OF-211) flow rate data to XPSWMM predicted flow rates. ORNL monitored the OF-211 flow rate discharge from October 21, 2012 11:00 AM to December 19, 2012 9:00 AM. ORNL noted dates and times that precipitation occurred. After review of the ORNL data, the following dates and timeframes (hereby referred to as trials) were used for the calibration based upon peak flow rates indicated by the ORNL hydrographs provided:

1. November 12, 2012 1:00 PM – 10:10 PM
2. November 26, 2012 10:15 PM – November 27, 2012 5:50 AM
3. December 10, 2012 3:25 AM – 6:30 PM

4. December 15, 2012 9:45 PM – December 16, 2012 8:55 PM

After analyzing the OF-211 flow rate data provided by ORNL, an approximate 0.17 cfs base flow was observed. It is known that the OF-211 storm system contains base flow and is defined as once-through cooling water and steam condensate from the adjacent buildings' AC units; however, their exact quantities and locations are unknown. Therefore, a 0.17 cfs has been extracted from the ORNL flow rate data in order to compare the XPSWMM results for calibration purposes due to the fact that exact base flow quantities and locations of entry into the system are unknown. The XPSWMM model only introduces actual 60-minute interval rainfall data that was retrieved from ORNL Tower C monitoring station for calibration purposes.

XPSWMM provides resulting flow rates within each pipe and resulting elevations at each node after the model is solved; thus, flow rates from pipe 26 (P-26), which is the pipe immediately prior to OF-211, were analyzed. The data provided by ORNL is in 5-minute intervals; thus, the XPSWMM P-26 resulting flow rates were extracted in 5-minute intervals, and both data are presented as hydrographs for comparison. The calibration is based on flow rates presented in cubic feet per second (cfs). ORNL provided data in gallons per minute (gpm). A conversion factor of 0.002228 cfs per gpm was used.

For the following calibration trials a Manning's n coefficient of 0.015, the Green Ampt infiltration method, and evaporation default of 0.1"/day were used. The calibrations are based on 24-hour simulations and were conducted by analyzing the ORNL observed flow rate data at OF-211. Rainfall data was retrieved around the time that the data produced peak flow rates. Once the base flow rate was subtracted from the ORNL observed data, the XPSWMM P-26 results were overlain. A timeframe was chosen where the beginning and end times corresponded to flow rates that were zero. Peak flow rates and their corresponding times are noted as well as a summation of flow rates for both the ORNL data and the XPSWMM results during the time of calibration for comparison.

6.2.1 Calibration of Model Trial 1

Sixty-minute interval rainfall data was retrieved from ORNL Tower C and indicates that precipitation occurred on November 12, 2012 between the hours of 12:00 AM and 7:00 PM. The rainfall data was simulated through the network. XPSWMM produced the hyetograph shown to the right based upon the rainfall data.

Tower C Rainfall Data 60 min Intervals			
Time	**Rain (in)**	**Time**	**Rain (in)**
11/12/2012 11:00	0	11/12/2012 16:00	0.12
11/12/2012 12:00	0.01	11/12/2012 17:00	0.08
11/12/2012 13:00	0.04	11/12/2012 18:00	0.06
11/12/2012 14:00	0.07	11/12/2012 19:00	0.03
11/12/2012 15:00	0.24	11/12/2012 20:00	0

Table 1 Rainfall Data for Calibration Trial 1

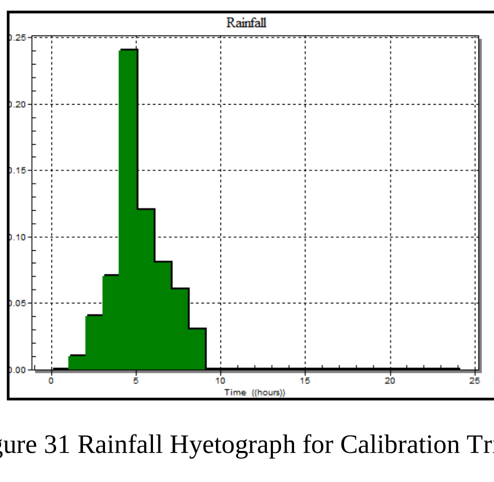

Figure 31 Rainfall Hyetograph for Calibration Trial 1

The timeframe for calibration purposes was chosen as November 12, 2012 from 1:00 PM to 10:10 PM. The figure below shows that the ORNL observed flow rate data has a peak flow rate of 1.73 cfs (excluding 0.17cfs base flow) on November 12, 2012 at 3:50 PM. The XPSWMM hydrograph does not indicate as large of a peak as the ORNL data, however the summation of flow rates under the curve are very similar. The lag time for the model to simulate the rainfall is approximately 25 minutes. This may be considered a successful calibration as the summation of flow rates during the calibration duration are equal, which is shown in the second figure below. The figure is the cumulative flow rate versus time which indicates more clearly the two sets of data summation of flow rates.

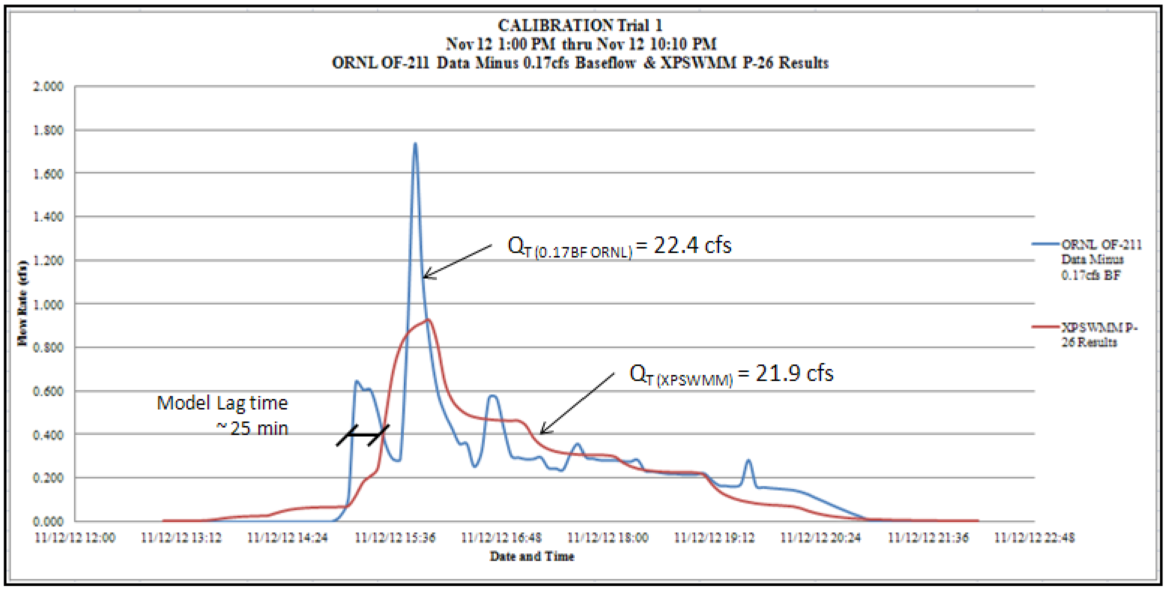

Figure 32 ORNL Data and XPSWMM Results Hydrograph

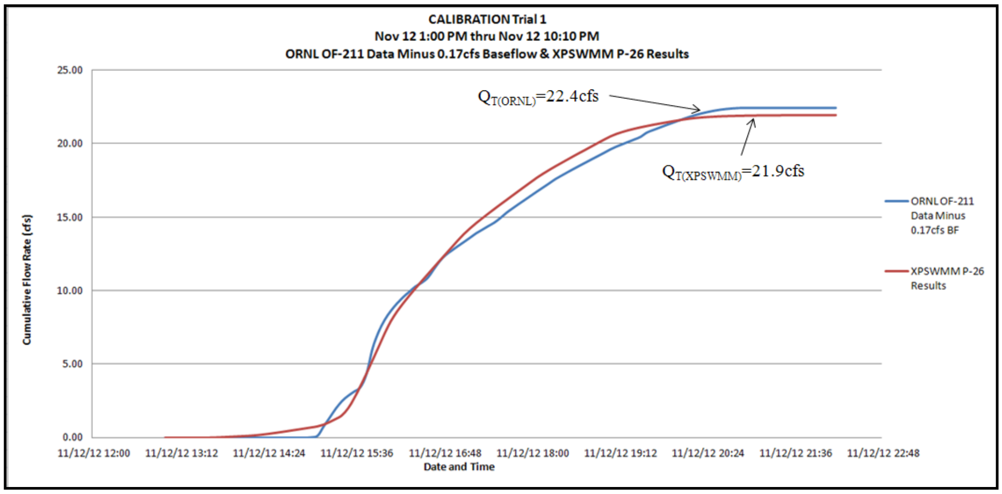

Figure 33 ORNL Data and XPSWMM Results Cumulative Flow Rates

The figure below is a hydrograph of the ORNL OF-211 data including the 0.17 cfs base flow.

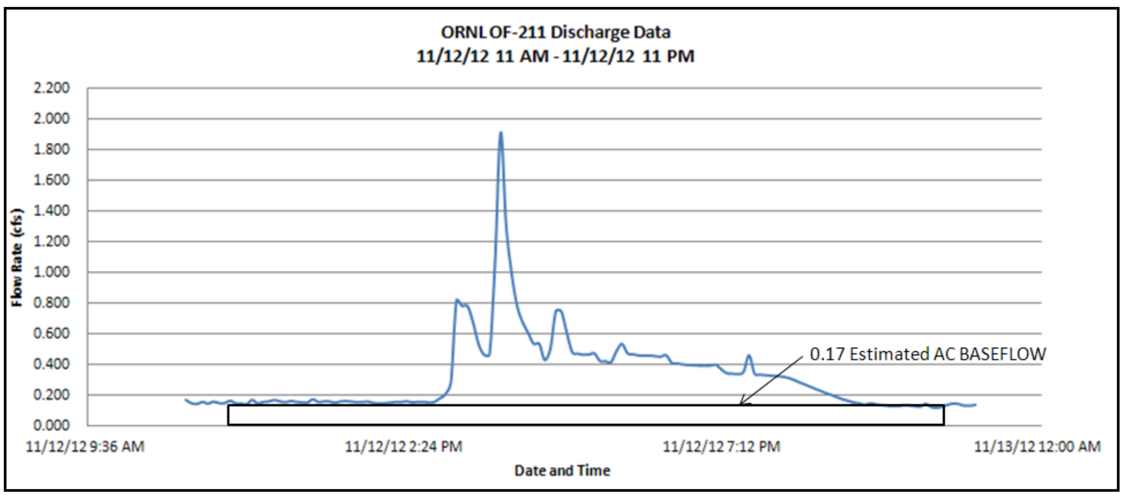

Figure 34 ORNL Data with Base Flow

6.2.2 Calibration of Model Trial 2

The precipitation data beginning on November 26, 2012 at 9PM thru November 27, 2012 at 6AM is shown below and was simulated through the network. XPSWMM produced the hyetograph to the right based upon the data.

Tower C Rainfall Data 60 min Intervals			
Date & Time	**Rain (in)**	**Date & Time**	**Rain (in)**
11/26/2012 21:00	0	11/27/2012 3:00	0.04
11/26/2012 22:00	0.07	11/27/2012 4:00	0
11/26/2012 23:00	0.07	11/27/2012 5:00	0
11/27/2012 0:00	0.12	11/27/2012 6:00	0.01
11/27/2012 1:00	0.04	11/27/2012 7:00	0
11/27/2012 2:00	0.02		

Table 2 Rainfall Data for Calibration Trial 2

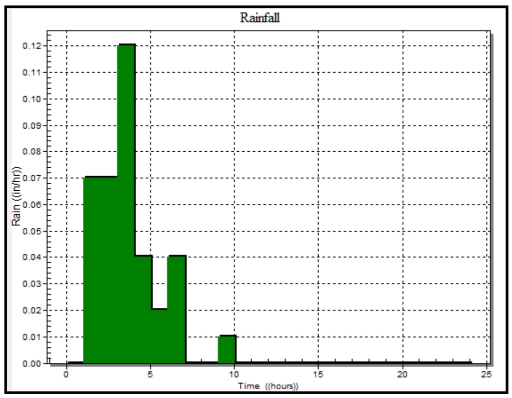

Figure 35 Rainfall Hyetograph for Calibration Trial 2

The timeframe for calibration purposes was chosen as November 26, 2012 10:15 PM - November 27, 2012 6:05 AM. The ORNL observed data indicates a peak flow rate of 0.44 cfs (excludes 0.17 cfs base flow) on November 27, 2012 at 1:15 AM. The XPSWMM hydrograph indicates a peak flow rate of 0.44 cfs at 1:00 AM. A summation of the ORNL OF-211 flow rates and the XPSWMM results are also depicted in the figure below. The peak flow rates are consistent if one accepts that a 0.17 cfs base flow occurs during that timeframe. ORNL's peak falls behind the model results by 15 minutes. However, the XPSWMM model lags behind ORNL data by approximately 55 minutes. The lag time is the difference in time between the two sets of data where the first rainfall interval has been routed through the system. The summation of the flow rates during the calibration timeframe is similar. Below that is a figure indicating the cumulative flow rate versus time which indicates more clearly the two sets of data summation of flow rates during the calibration duration.

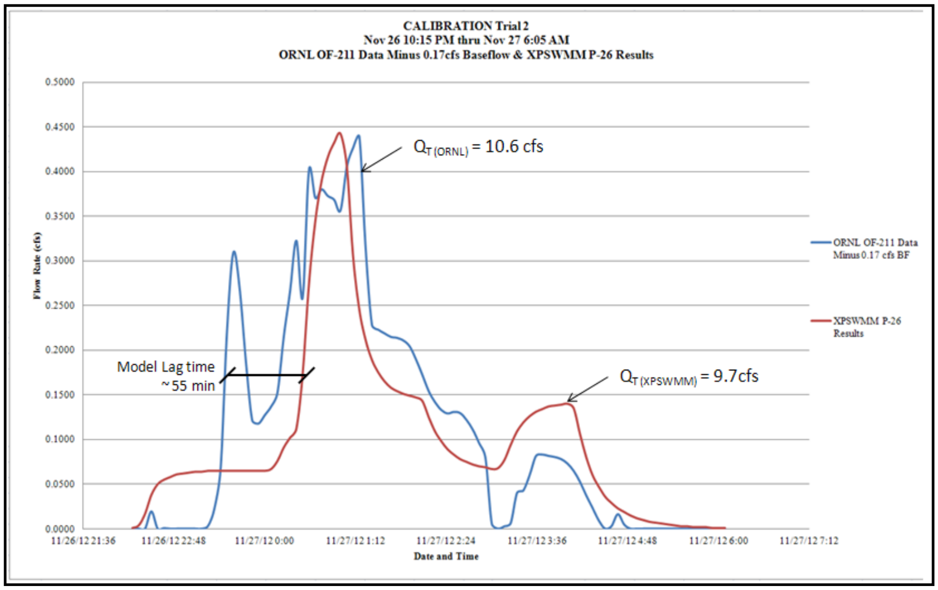

Figure 36 ORNL Data and XPSWMM Results Hydrograph

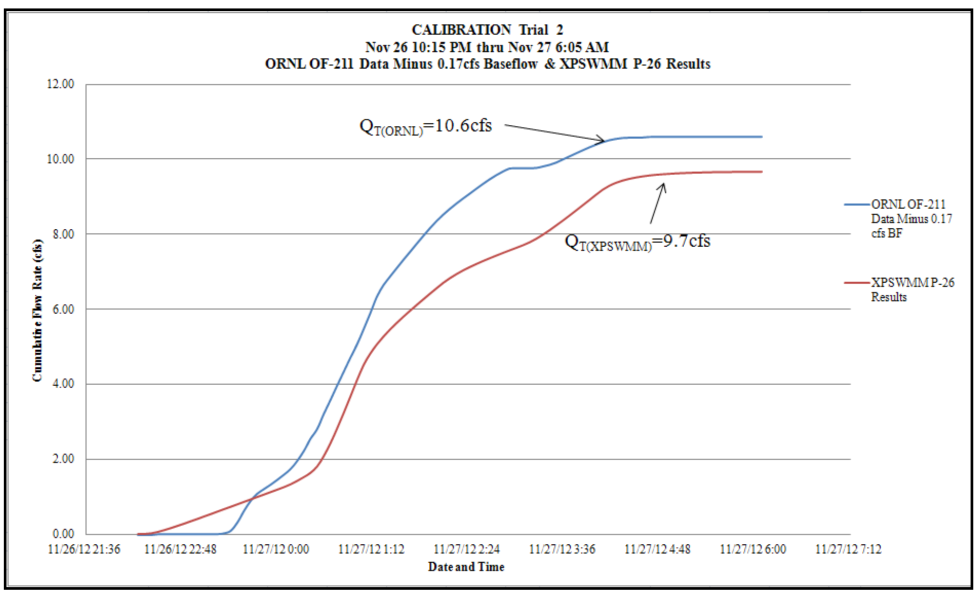

Figure 37 ORNL Data and XPSWMM Results Cumulative Flow Rates

The figure below is a hydrograph of the ORNL OF-211 data including the 0.17 cfs base flow.

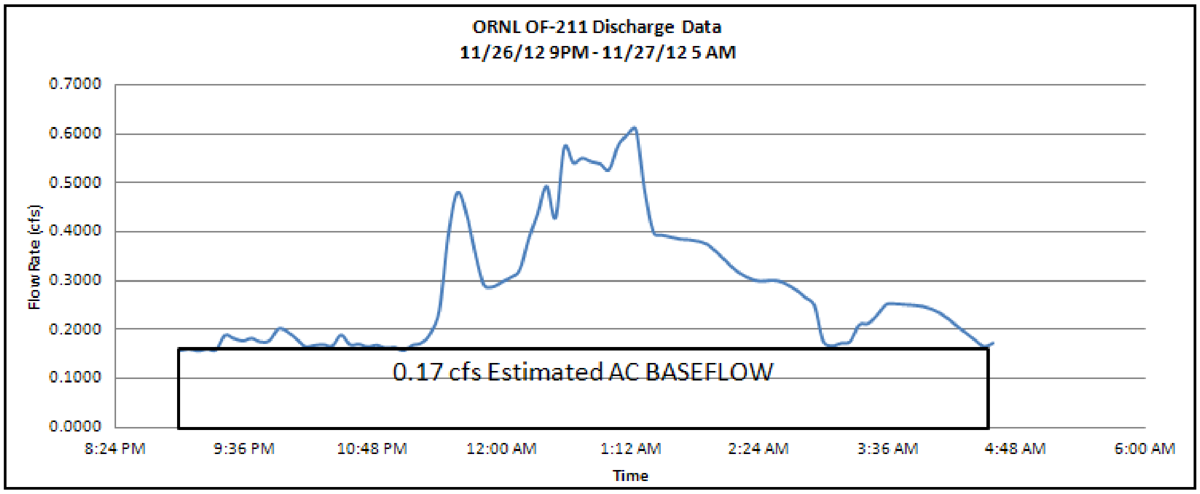

Figure 38 ORNL Data with Base Flow

6.2.3 Calibration of Model Trial 3

Sixty-minute interval rainfall data was retrieved from ORNL Tower C and indicates that precipitation occurred on December 10, 2012 between the hours of 3:00 AM and 4:00 PM. The rainfall was simulated through the network. XPSWMM produced the hyetograph shown to the right based upon the rainfall data.

Tower C Rainfall Data 60 min intervals					
Time	**Rain (in)**	**Time**	**Rain (in)**	**Time**	**Rain (in)**
12/10/2012 2:00	0	12/10/2012 8:00	0.1	12/10/2012 14:00	0
12/10/2012 3:00	0.03	12/10/2012 9:00	0.1	12/10/2012 15:00	0
12/10/2012 4:00	0.12	12/10/2012 10:00	0.05	12/10/2012 16:00	0.01
12/10/2012 5:00	0.02	12/10/2012 11:00	0.02	12/10/2012 17:00	0
12/10/2012 6:00	0.31	12/10/2012 12:00	0.04		
12/10/2012 7:00	0.08	12/10/2012 13:00	0.04		

Table 3 Rainfall Data for Calibration Trial 3

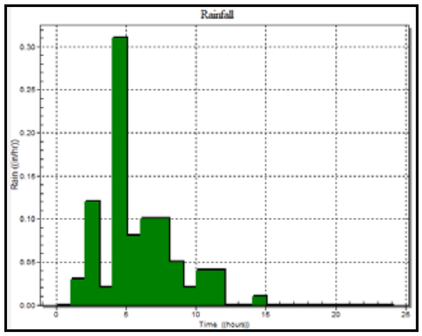

Figure 39 Rainfall Hyetograph for Calibration Trial 3

ORNL OF-211 data provided for calibration is shown in the hydrograph below. The timeframe for calibration purposes was chosen as December 10, 2012 3:25 AM – 6:30 PM. ORNL noted that the 3 cfs peak flow rate may be a faulty reading from the flow rate monitor. The figure below is an overlay of the ORNL data (minus 0.17 cfs base flow) and XPSWMM results. ORNL observed data indicates a peak flow rate of 2.79 cfs (excludes 0.17 base flow) on December 10, 2012 at 7:45 AM. Below that is a figure indicating the cumulative flow rate versus time which indicates more clearly the two sets of data summation of flow rates during the calibration duration. The hydrograph produced by XPSWMM portrays a peak flow rate of 1.22 cfs at 7:00 AM. The lag between the two sets of data is approximately 40 minutes. The total flow rate summation results are relatively close.

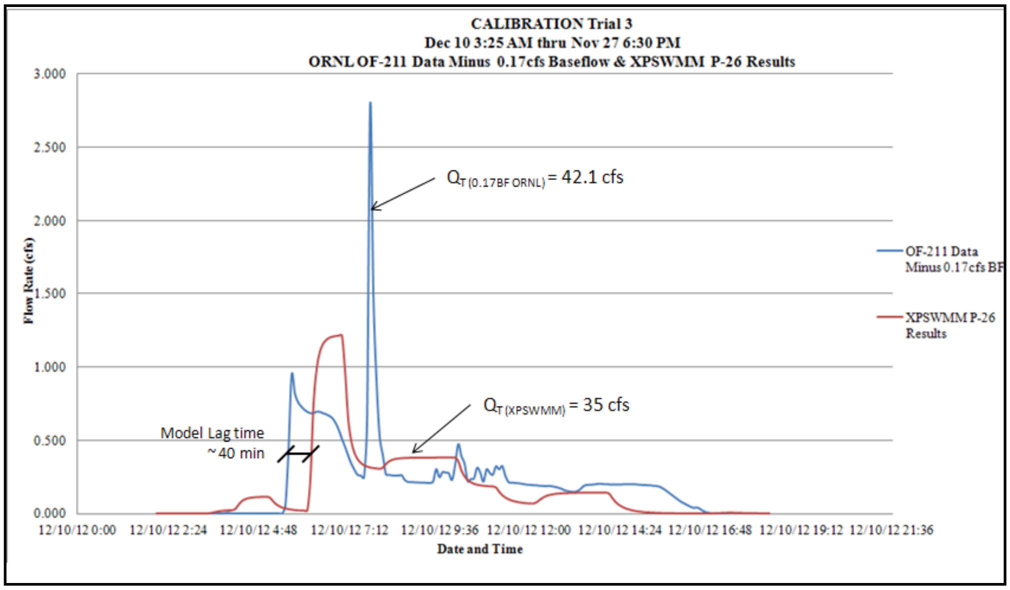

Figure 40 ORNL Data and XPSWMM Results Hydrograph

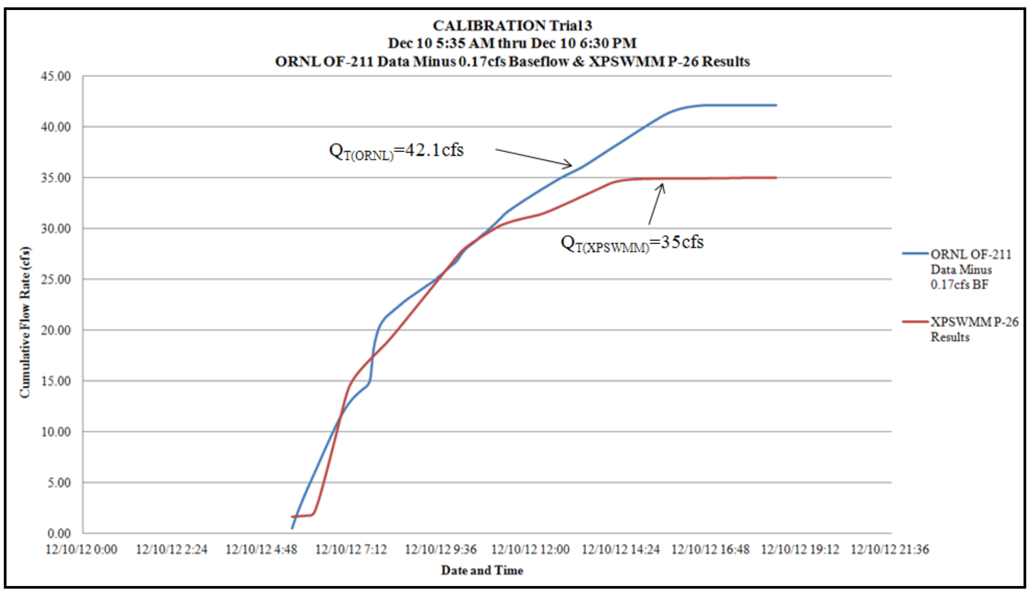

Figure 41 ORNL Data and XPSWMM Results Cumulative Flow Rates

The figure below is a hydrograph of the ORNL OF-211 data including the 0.17 cfs base flow.

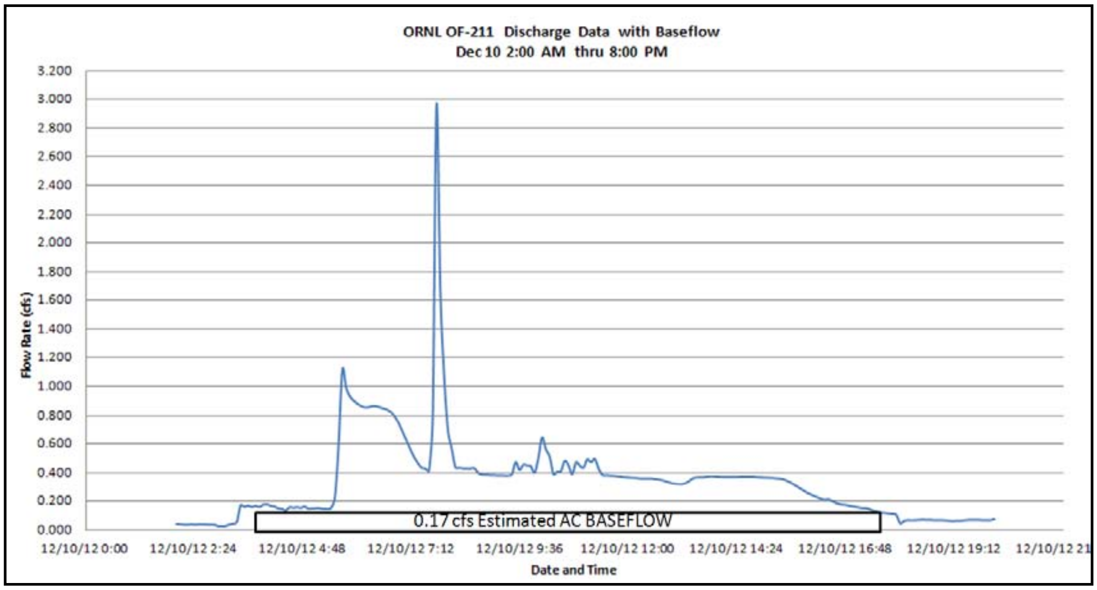

Figure 42 ORNL Data with Base Flow

6.2.4 Calibration of Model Trial 4

Sixty-minute interval rainfall data was retrieved from ORNL Tower C and indicates that precipitation occurred on December 15, 2012 between the hours of 9:00 PM and 8:00 PM. The rainfall was simulated through the network. XPSWMM produced the hyetograph shown to the right based upon the rainfall data.

Tower C Rainfall Data 60 min intervals					
Time	**Rain (in)**	**Time**	**Rain (in)**	**Time**	**Rain (in)**
12/15/2012 20:00	0	12/16/2012 6:00	0.12	12/16/2012 14:00	0
12/15/2012 21:00	0.01	12/16/2012 7:00	0.06	12/16/2012 15:00	0
12/15/2012 22:00	0.1	12/16/2012 8:00	0.09	12/16/2012 16:00	0
12/15/2012 23:00	0.06	12/16/2012 9:00	0.04	12/16/2012 17:00	0.01
12/17/2012 0:00	0.01	12/16/2012 8:00	0.09	12/16/2012 18:00	0.01
12/16/2012 1:00	0.01	12/16/2012 9:00	0.04	12/16/2012 19:00	0.02
12/16/2012 2:00	0	12/16/2012 10:00	0.05	12/16/2012 20:00	0.01
12/16/2012 3:00	0.01	12/16/2012 11:00	0.03	12/16/2012 21:00	0
12/16/2012 4:00	0.26	12/16/2012 12:00	0		
12/16/2012 5:00	0.34	12/16/2012 13:00	0.01		

Figure 43 Rainfall Data for Calibration Trial 4

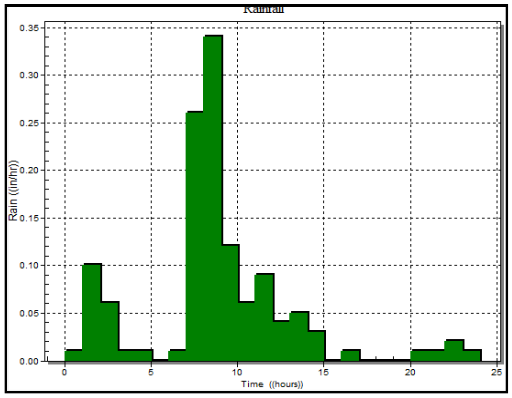

Figure 44 Rainfall Hyetograph for Calibration Trial 4

The timeframe for calibration purposes was chosen as December 15, 2012 9:45 AM – 8:55 PM. The figure below shows that the ORNL observed flow rate data has a peak flow rate of 1.64 cfs (excluding base flow) on December 16, 2012 at 5:35 AM. Similarly, the XPSWMM hydrograph specifies a peak flow rate of 1.34 cfs at 5:50 AM. The lag between the two sets of data is approximately 35 minutes. The total flow rates are relatively close and may be considered that the two sets of data do correlate. Below that is a figure indicating the cumulative flow rate versus time which indicates more clearly the two sets of data summation of flow rates during the calibration duration.

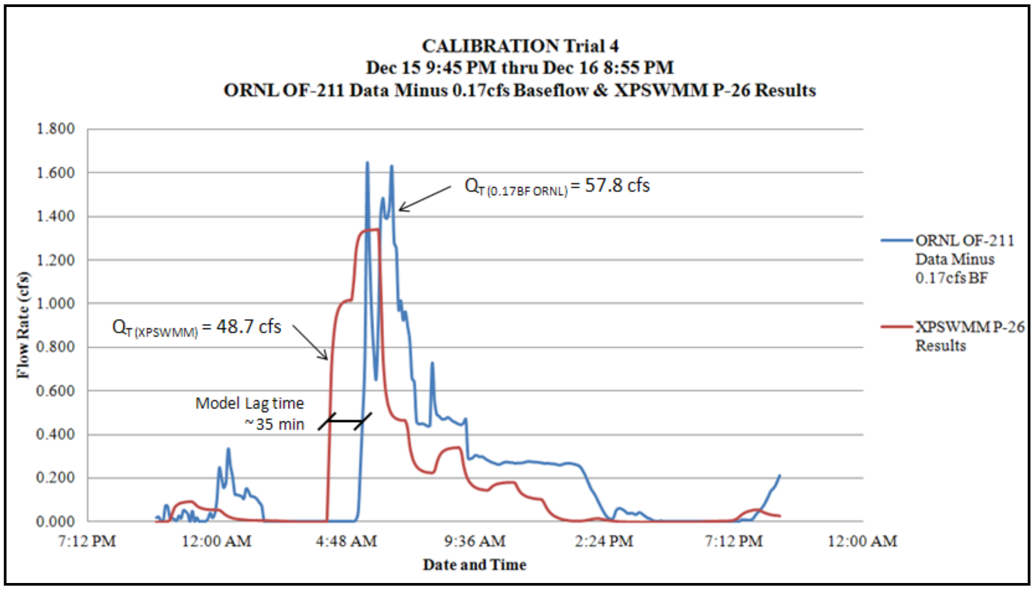

Figure 45 ORNL Data and XPSWMM Results Hydrograph

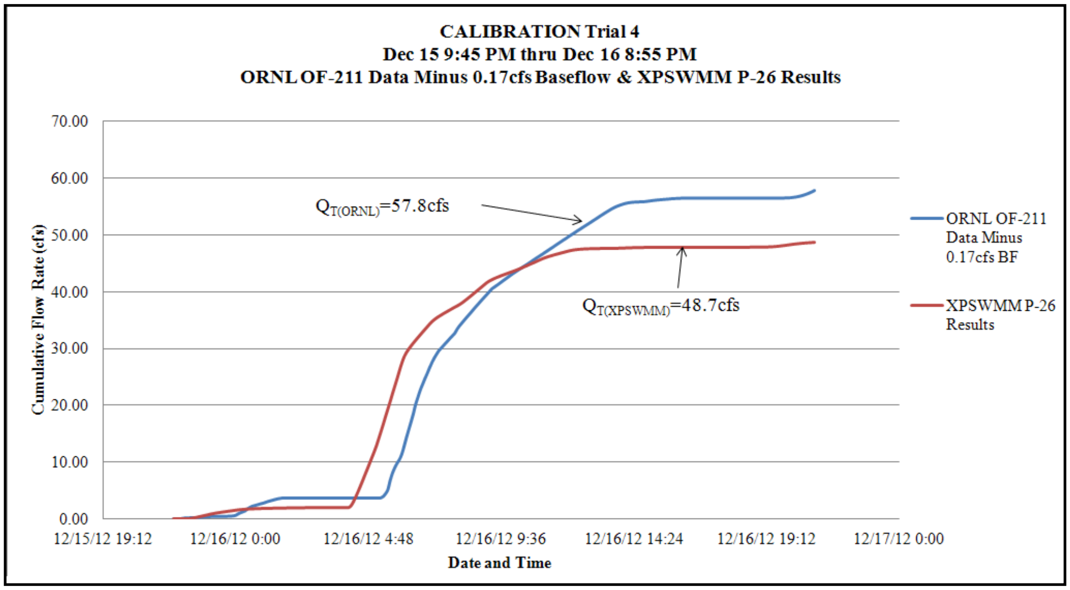

Figure 46 ORNL Data and XPSWMM Results Cumulative Flow Rates

The figure below is a hydrograph of the ORNL OF-211 data including the 0.17 cfs base flow.

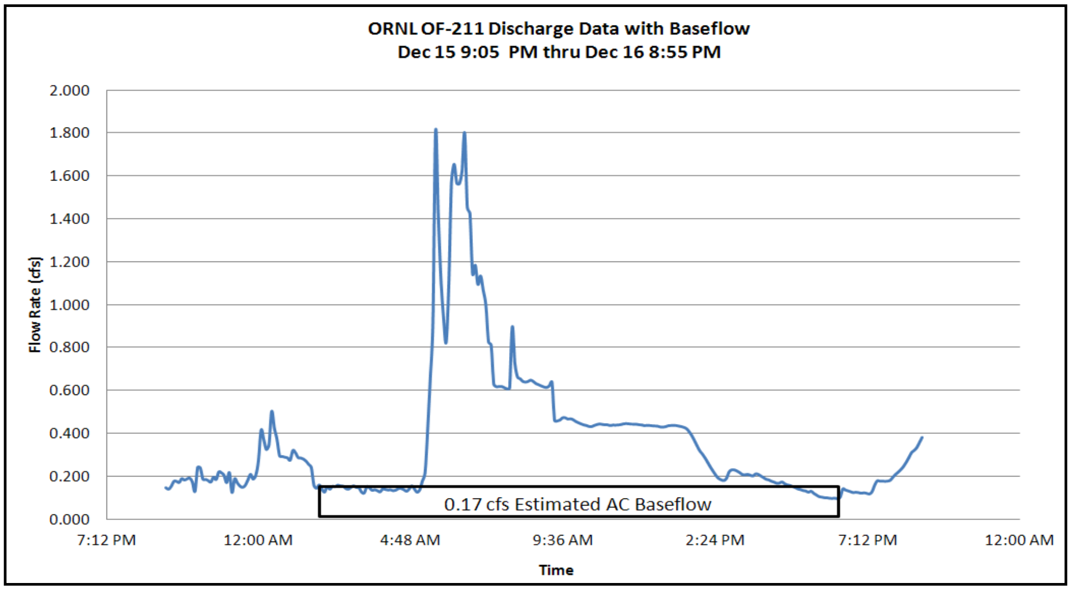

Figure 47 ORNL Data with Base Flow

In conclusion, with respect to calibration, the model does prove to be responsive to the precipitation by indicating relatively similar total flow rates under the hydrograph curves during the calibration timeframes as well as responding to the precipitation within similar timeframes (nominal lag times). Based on the nature of the model and because there are only estimated quantities of the once-through cooling water and steam condensate from the data provided by ORNL, for the purposes of this study, the model should be considered a valid source to aid in the predication of flow rates within the system. To further assess the model's validity, a percent error was calculated based on summation of flow rates of the ORNL data and XPSWMM results during the calibration duration. The percent error is defined as follows:

$$\%\,Error = \left|\frac{\mathrm{T} - \mathrm{E}}{\mathrm{T}}\right| * 100$$

Where T represents the theoretical data which in this case would be the summation of the ORNL observed flow rates, and E represents the experimental data which is the summation of the XPSWMM predicted flow rates. The table below summarizes the results for the four trials.

The model is deemed acceptable based on relatively low percent error values. For this study a percent error of 20% or less has been chosen. All four trials have a 20% percent error or less.

Date of Rainfall Event and Duration of Calibration	ORNL Observed Data			XPSWMM Results		Total Flow During Calibration			Comments
	Peak Flow Rate (cfs)	Peak Flow Rate Minus 0.17 cfs Baseflow (cfs)	Date & Time	Peak Flow Rate (cfs)	Date & Time	ORNL Obs. Data (cfs)	XPSWMM Results (cfs)	Percent Error	
11/12/12 1:00 PM – 10:10 PM	1.9	1.73	11/12/12 3:50 PM	0.92	11/12/12 4:00 PM	22.4	21.9	2.2%	ORNL's peak flow rate is approximately 0.6 cfs larger than the model's; however, the total flow rate under the hydrographs are very similar. SUCCESSFUL.
11/26/12 10:15 PM – 11/27/12 6:05 AM	0.61	0.44	11/27/12 1:15AM	0.44	11/27/12 1:00AM	10.6	9.7	8.5%	Consistent peak flow rates. ORNL's peak lags behind the model results by 15 minutes. Total flow rates are similar. SUCCESSFUL.
12/10/12 3:25 AM – 6:30 PM	2.96	2.79	12/10/12 7:45 AM	1.22	12/10/12 7:00 AM	42.1	35.0	16.9%	The 3 cfs peak is thought to be a faulty reading. The total flows are relatively close. Less than 20% error. May be considered SUCCESSFUL.
12/16/12 4:05 AM – 4:45 PM	1.81	1.64	12/16/12 5:35 AM	1.34	12/16/12 5:50 AM	55	44	20.0%	Similar total flow rates. Right at 20% error. May be considered SUCCESSFUL.

Figure 48 Results of Calibration

6.3 Probability Exceedance

The simulations run for the sensitivity and transport analysis generate a large amount of data due to the fact that there are 52 nodes and 51 links in the network. XPSWMM generates six variables for each simulation run for the hydrology analysis - node depth, node elevation, link velocity, link upstream elevation and link downstream elevation. However, this study focuses on the node elevations of MH211-3 and OF-211 and the links P-10, P-11, P-15, P-26, and P-27 as shown in the figure below for both the hydrology and transport analyses. Thus, there is a need for a program to read the results and plot the data in a timely manner for data analysis. MATLAB was chosen for the task. MATLAB produced plots for each variable versus time and their probability exceedance (PE) curves.

The simulations were run where the data was saved every 300 minutes throughout the yearly simulation. Thus, 1 year saved every 300 minute interval gives 1748 intervals. When analyzing a peak flow rate for a specified pipe it may be difficult to sort through the 1748 intervals of flow rates for that single pipe. Thus, the PE has been calculated for all pipes and nodes within the remaining simulations in order to find the maximum flow rate within a pipe and for what percent of the time it remains at that flow rate. For instance, if a node meets or exceeds its inlet elevation (link flow rate) for 90% of the duration of the storm event, then it may be necessary for improvements to be considered. When producing PE curves time is not a factor and is calculated as follows, where the rank from largest to smallest and the number of intervals which equals 1748 for the sensitivity analysis and transport analysis, are considered:

$$Probability\ Exceedance = Rank/(Total\ Number\ of\ Values + 1)$$

MATLAB was utilized for the production of the hodographs (flow versus time), pollutographs (pollutant concentration versus time), PE curves, and the following PD: Generalized Extreme Value (GEV), Logistic, Log-Logistic, and Exponential. The PD that fits the data best has been chosen for the transport analysis. Timeseries data for all nodes and links was extracted from XPSWMM. For the sensitivity analysis, hydrographs with the variables node depth, node elevation, link velocity, link upstream elevation, link downstream elevation as well as their PE curves were produced via MATLAB. The idea is to have the varying parameters on one hydrograph in order to see the various impacts it has on the node or link. For instance, for the sensitivity analysis for the Manning's roughness coefficient, MATLAB is able to graph all five of the various coefficients on one hydrograph where XPSWMM cannot. For the transport analysis, MATLAB produces timeseries pollutant loads (L) by multiplying timeseries flow rates (Q) in cfs and timeseries concentrations (C) in mg/L multiplied by a conversion factor of 5.39 lb/day. MATLAB computes the various transport simulations on one graph, similar to the sensitivity analysis. In addition, the Q, C, and L PE curves were produced via MATLAB.

6.4 Sensitivity Analysis

Multiple sensitivity analyses were run and analyzed in order to understand the impacts of the various parameters on the system. They were produced where actual continuous rainfall data from year 2010 (January 1, 2010 thru December 31, 2010) was simulated and the Manning's roughness coefficients, infiltration parameters, and percent imperviousness. Year 2010 rainfall data was retrieved from ORNL's Tower C monitoring station in 15 minute intervals as shown below.

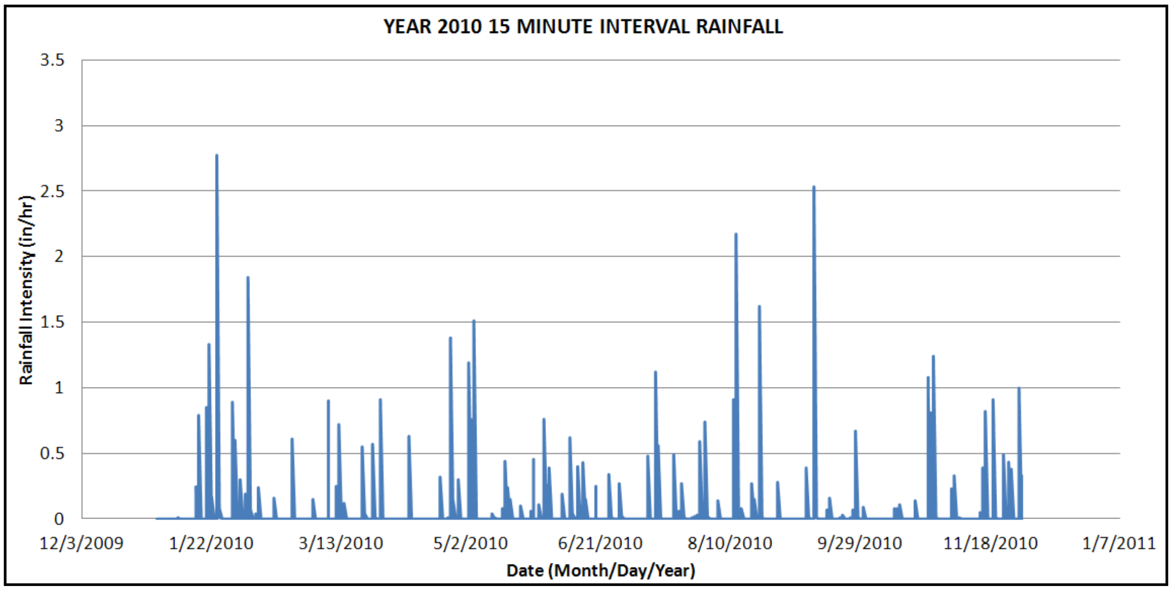

Figure 49 Year 2010 Rainfall Data

For the purpose of demonstrating the effects the various parameters have on the network, the nodes MH211-3 and OF-211and the links P-10, P-11, P-15, P-27, and P-26 will be used. However, not all are used in each section to avoid redundancy.

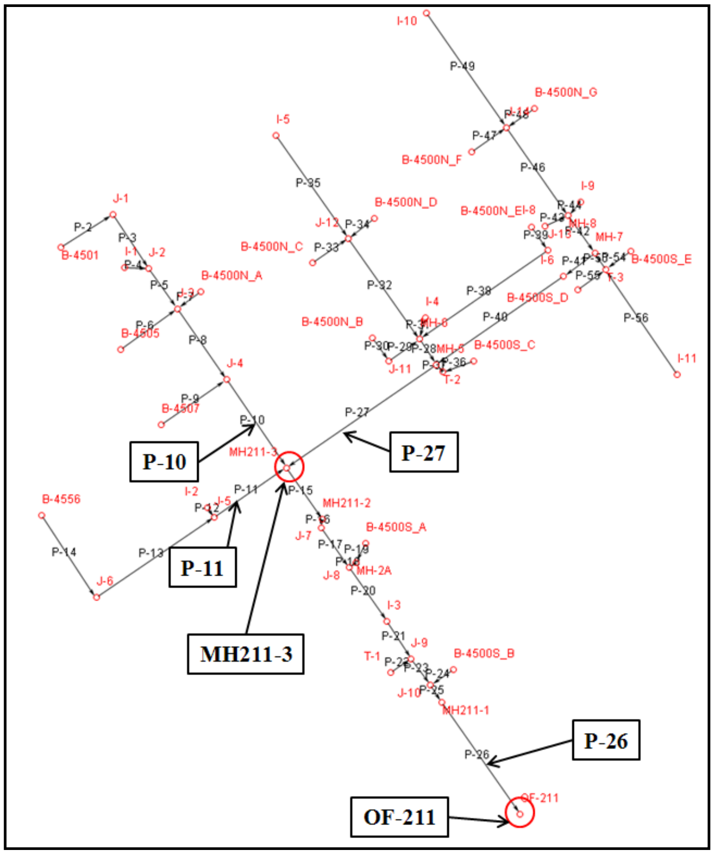

Figure 50 Storm System

The reason these nodes and pipes were chosen is that P-10 conveys the inflow from the north, P-11 from the west, P-27 from the east into the node MH211-3. P-15 then collects those waters and conveys them south to P-26 which is the last pipe prior to the discharge OF-211.

6.4.1 Manning's Roughness Sensitivity Analysis

The Manning's roughness coefficient is based on the material of the pipe or the type of channel. It is inversely proportional to the flow rate where the smaller the coefficient the larger the flow due to the friction caused by the channels roughness. The network contains the following types of pipes: wrought iron (WI), vitrified clay pipe (VP), concrete pipe (CP), reinforced concrete pipe (RCP), and polyvinyl chloride (PVC).

The following are the results from varying the Manning's roughness coefficient, n, by 0.011, 0.013, 0.05, 0.017, and 0.035 where continuous rainfall of year 2010 was simulated, the Green Ampt method used, and an evaporation default of 0.1"/day assumed.

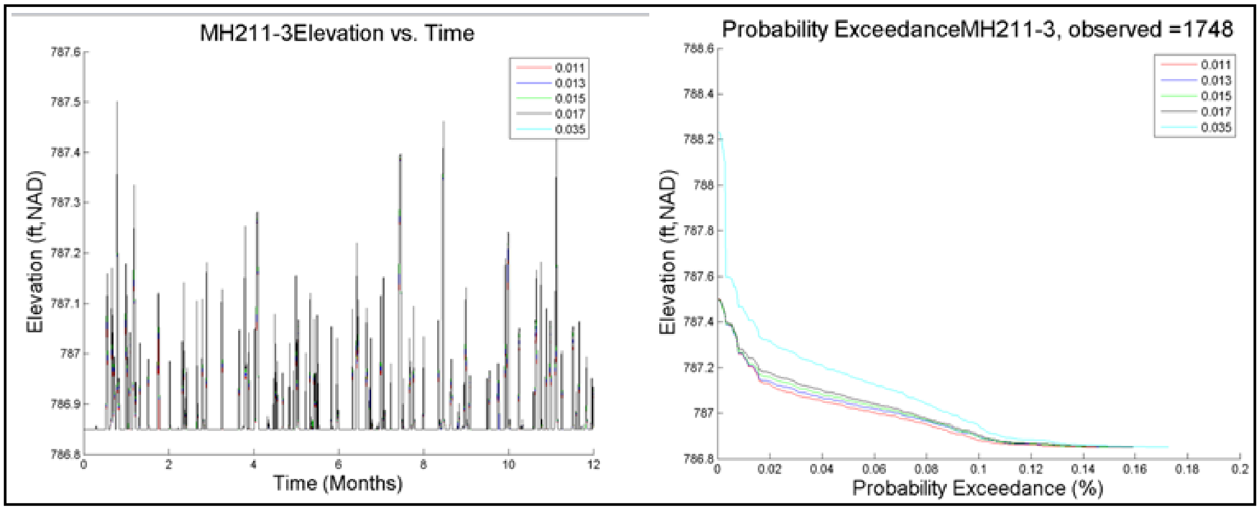

Figure 51 MH211-3 Hydrograph and PE Curves for Manning's Roughness Coefficient Sensitivity Analysis

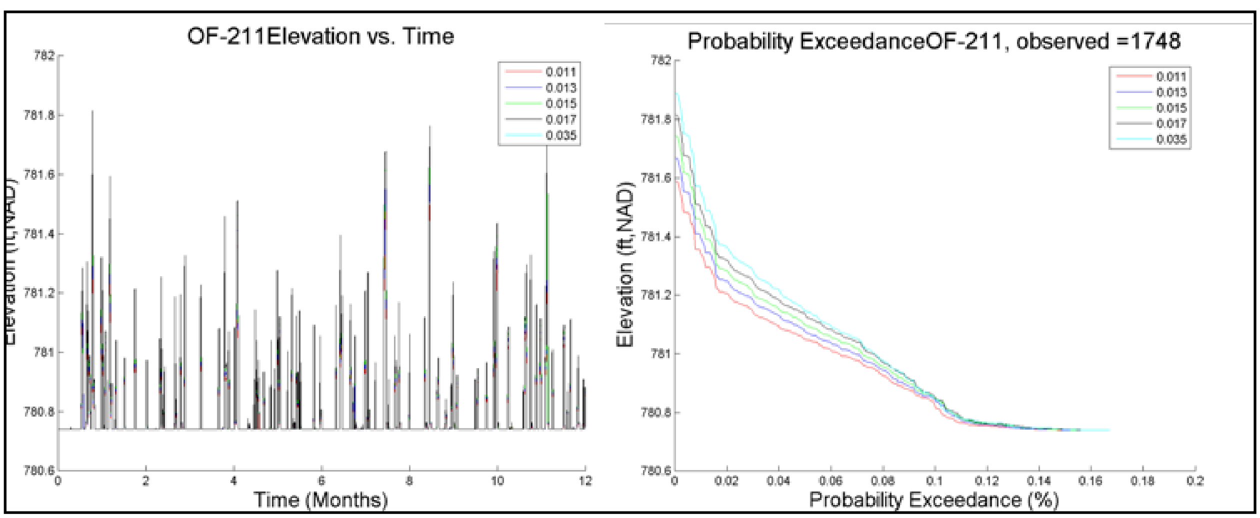

Figure 52 OF-211 Hydrograph and PE Curves for Manning's Roughness Coefficient Sensitivity Analysis

The results indicate minor changes if any in the flow rate through the specified pipes; however, node elevations are shown to vary via the hydrographs and more so on the probability exceedance curves. Although Manning's coefficient of 0.035 is specific to grassy areas, it was used in order to assess the sensitivity of the simulation. As one would expect, it does have a larger impact than the 0.017, 0.015, etc. Also note the PE x-axis was decreased from 1 (100%) to 0.2 (20%) with the purpose of demonstrating that the roughness coefficients do make a difference; however, too minor to take into account for this study. Thus, the coefficient 0.015 for the remaining simulations was chosen due to the fact that the typical value for closed conduits flowing through partly full concrete sewer gravity pipes is 0.015, as indicated in the Manning's n for Closed Conduits Flowing Partly Full (Chow, 1988) table located under the Appendices.

6.4.2 Green Ampt vs. Horton Infiltration Method Sensitivity Analysis

Yearly simulations were run where the Manning's roughness coefficient of 0.015 was held constant, and an evaporation default of 0.1"/ day was assumed.

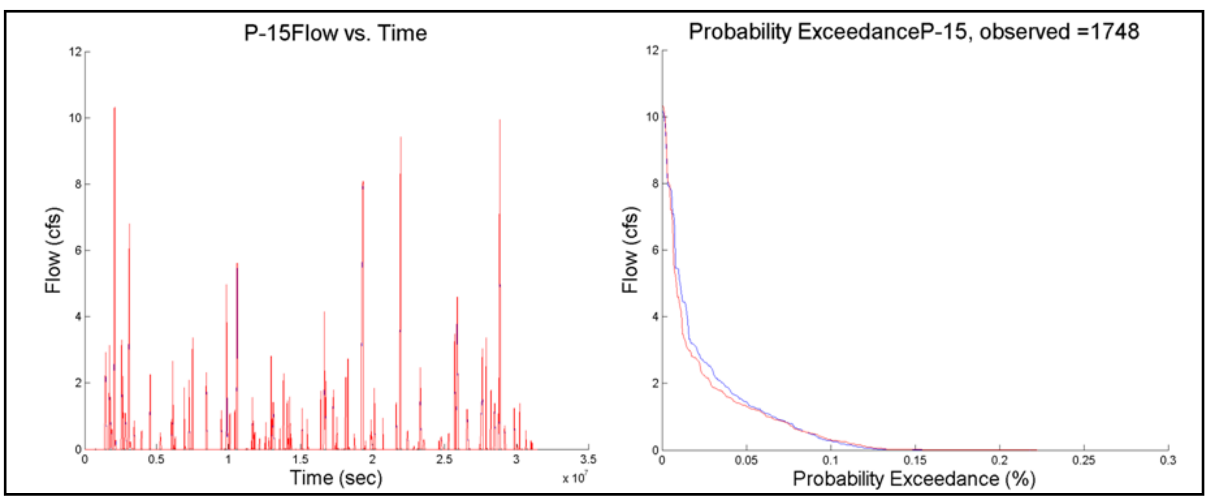

Figure 53 P-15 Hydrograph and PE Curves for Infiltration Sensitivity Analysis

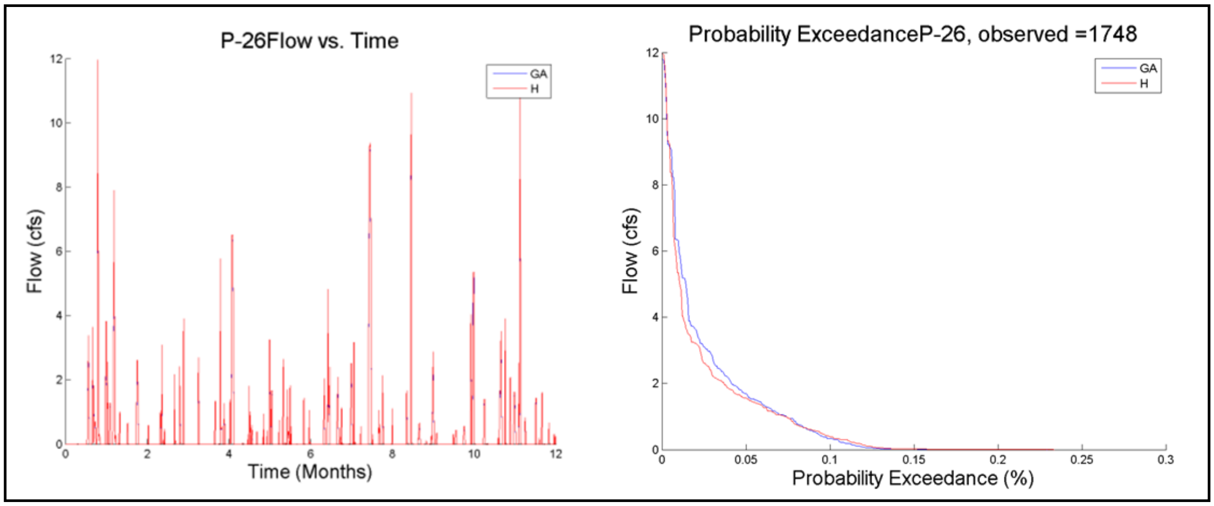

Figure 54 P-26 Hydrograph and PE Curves for Infiltration Sensitivity Analysis

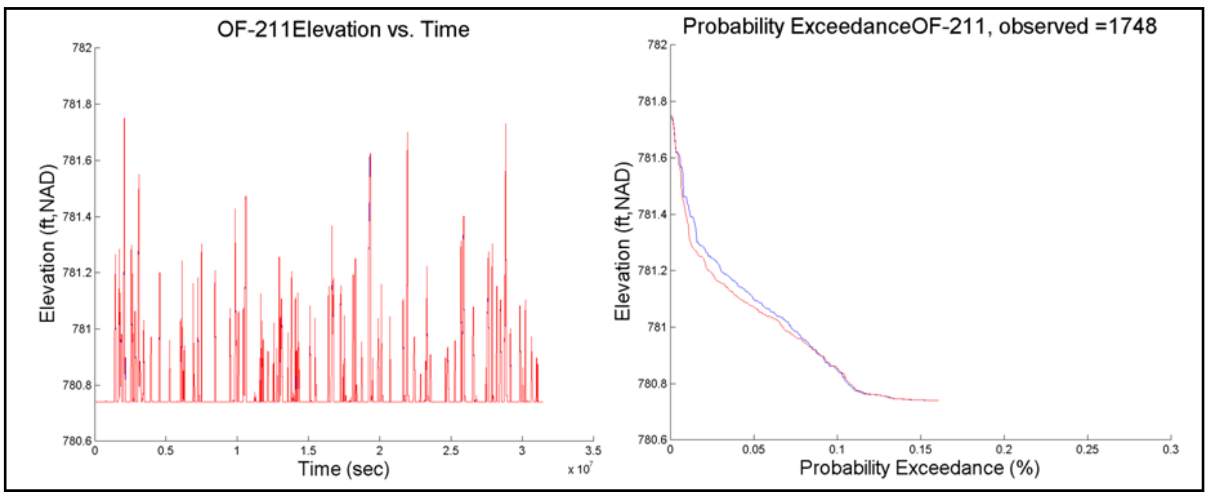

Figure 55 OF-211 Hydrograph and PE Curves for Infiltration Sensitivity Analysis

The results indicate minor differences in the hydrographs and minor differences in the node elevations. This could be that the Horton's default regeneration rate of 0.01 and/or decay rate of 0.001 were not large enough to produce a significant regeneration throughout the continuous rainfall. Studies have found that the Green Ampt method simulates one dimensional unsteady continuous rainfall events effectively and due to the fact there are only minor differences in the two methods, Green Ampt infiltration parameters have been chosen for the remaining simulations (Risse, 1994).

6.4.3 Percent Impervious Sensitivity Analysis

The assumed percent imperviousness was visual inspection during the site inspections. An increase of imperviousness on a basin will impact the surface water runoff as there will be a larger quantity of runoff due to less infiltration. The time of concentration will also lessen and impact the peak of the hydrographs as the runoff will approach the inlet at an increased speed.

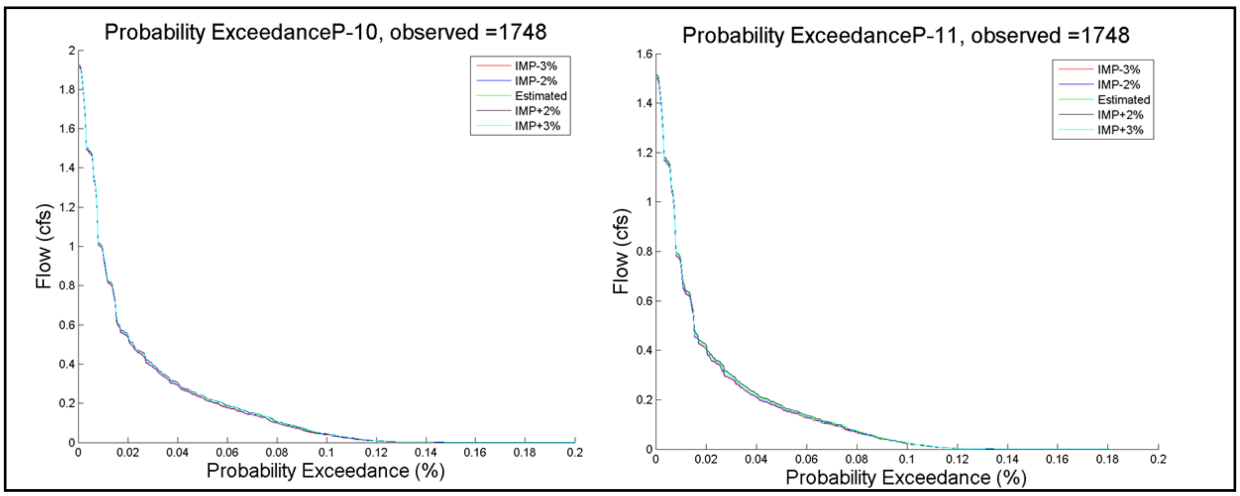

Figure 56 P-10 and P-11 PE Curves for Percent Imperviousness Sensitivity Analysis

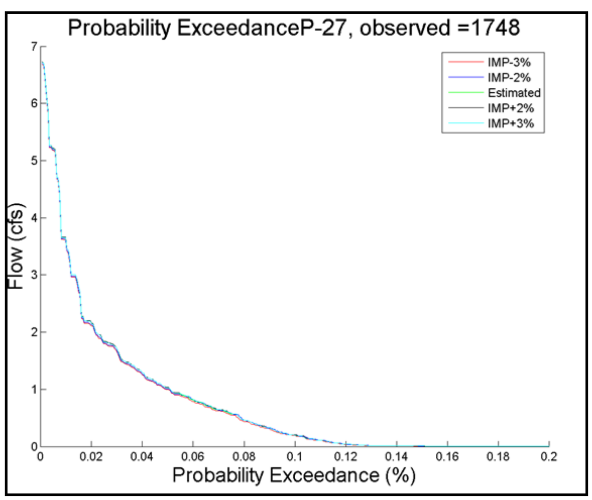

Figure 57 P-27 PE Curves for Percent Imperviousness Sensitivity Analysis

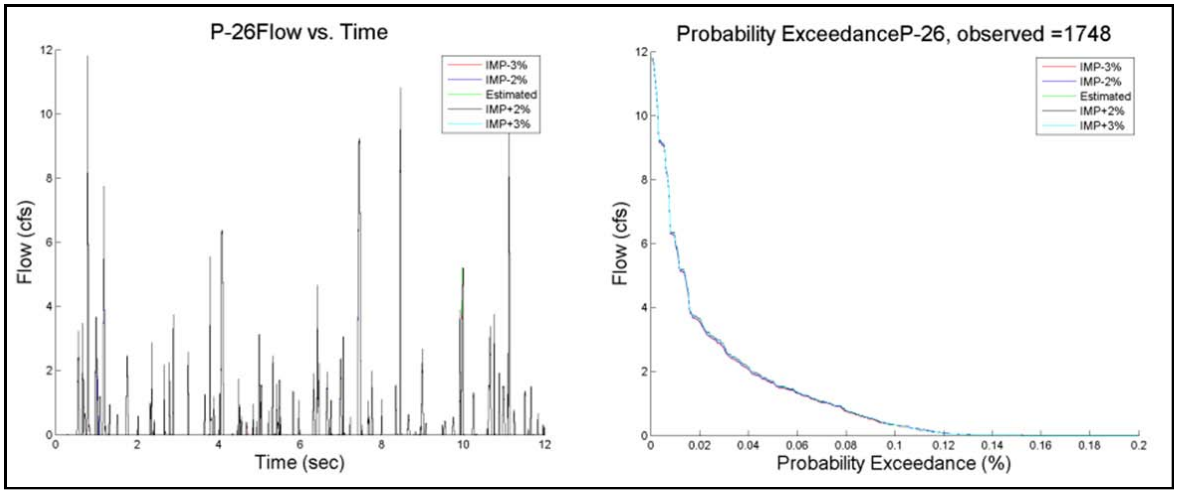

Figure 58 P-26 Hydrograph and PE Curves for Percent Imperviousness Sensitivity Analysis

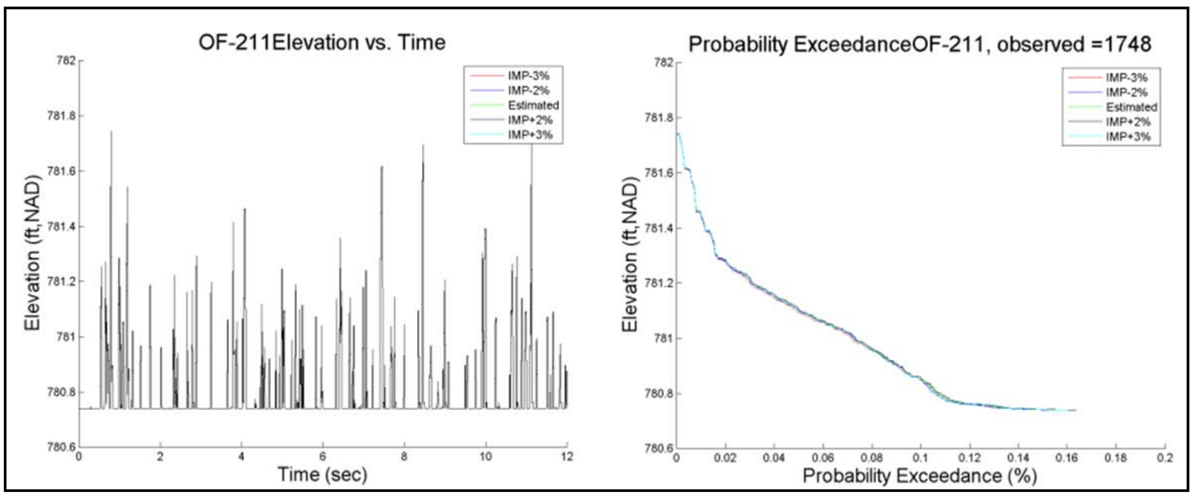

Figure 59 OF-211 Hydrograph and PE Curves for Percent Imperviousness Sensitivity Analysis

The amount of imperviousness a basin has is directly connected to the volume of runoff. There are only subtle differences between the variations of percent imperviousness. When an increase in imperviousness occurs, the PE curves falls flatter, which indicates that a higher flow rate will occur for a longer time.

One base simulation was held consistent through all three sensitivity analyses and is used for the base of the simulations in the transport analysis, which was the simulation using Manning's n roughness coefficient of 0.015, the Green Ampt infiltration parameters, evaporation default of 0.1"/day, and the estimated percent imperviousness. The figure below is a snapshot of the north-south main trunk line which includes the following pipes: P-2, P-3, P-4, P-5, P-8, P-10, P-15, P-16, P-17, P-20, P-21, P-23, P-25, and P-26 and indicates that the system on day 23 hour 23:00:00 which encounters its first peak throughout the yearly continuous rainfall events. The first pipe, P-2, is a 4" diameter storm lateral from building 4501 and nearly reaches capacity due to the peak in rainfall intensity. Also to be noted, according to the rainfall intensity simulated through the system, the first peak occurs on January 24, 2010 at hour 20:00:00 which is a day after the model predicts its first peak.

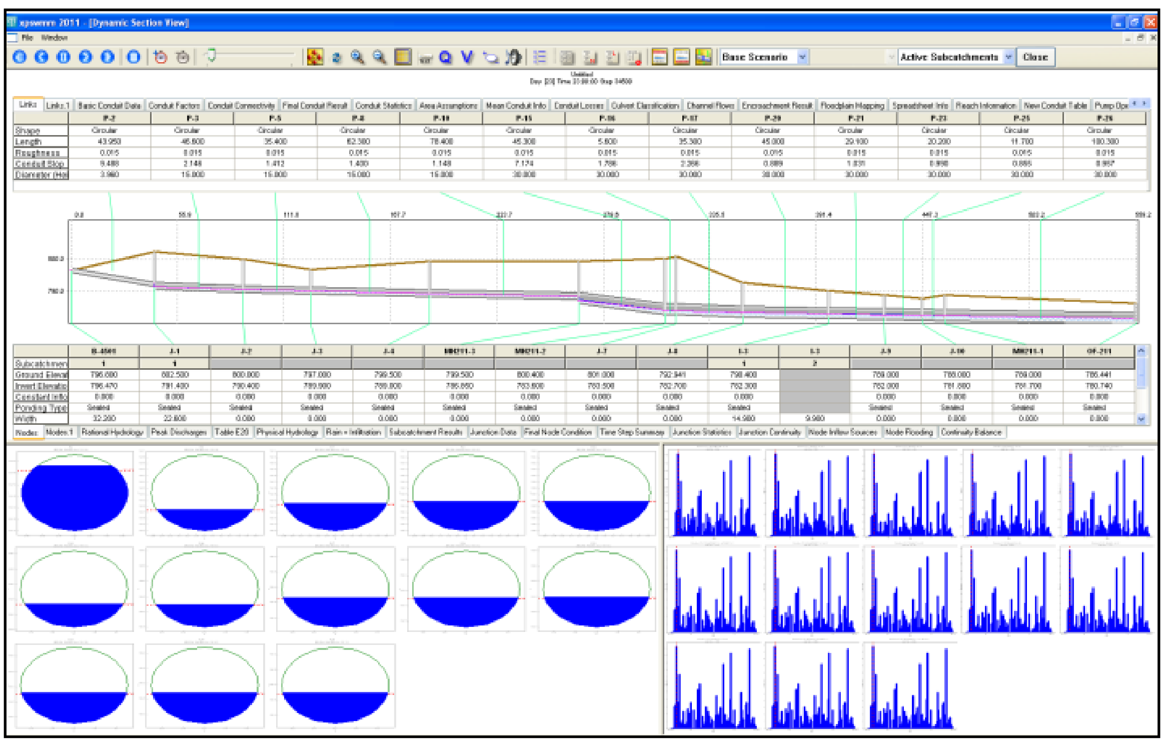

Figure 60 XPSWMM North-South Storm Line Results for Base Conditions

Similarly to the north/south main trunk line, XPSWMM estimates a peak to occur in the east-west trunk lines (I-10 thru B-4556) on day 23; however at the 18:00:00 hour. The east/west main trunk line is defined as the following pipes: P-14, P-11, P-27, P-40, P-41, P-42, P-46, and P-49 and is shown in the figure below.

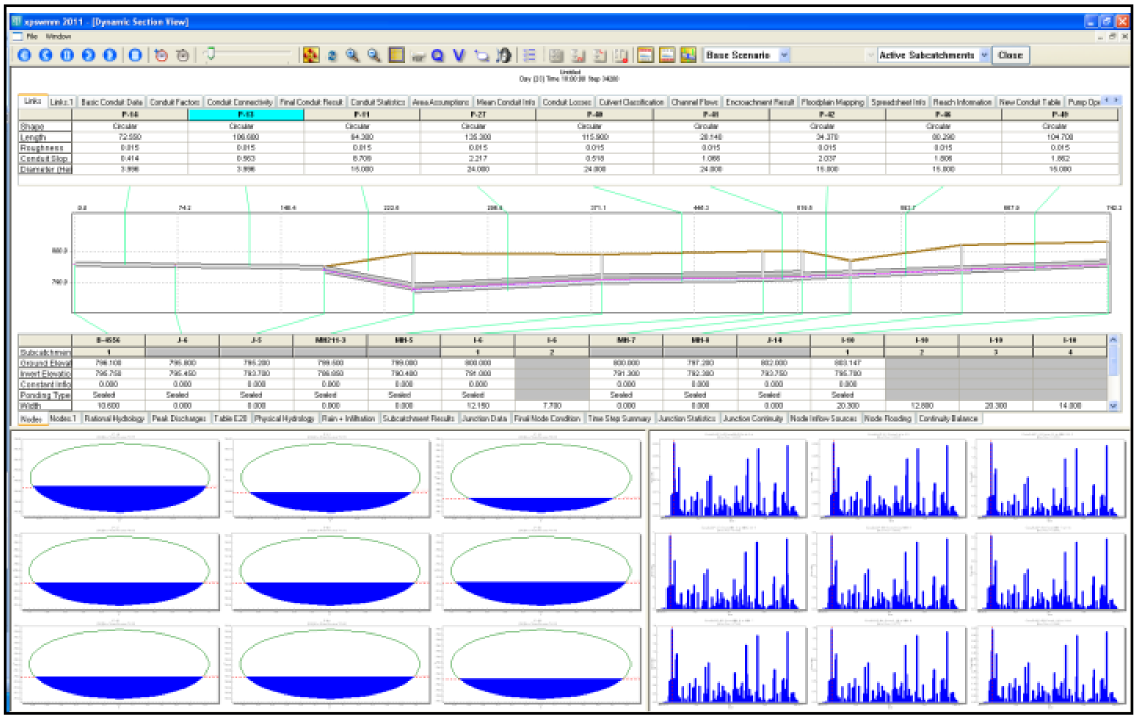

Figure 61 XPSWMM East-West Storm Line Results for Base Conditions

The system does indicate during the first peak in rainfall intensity that minor flooding occurs between nodes I-3 to OF-211 as the hydraulic grade line approaches the ground elevation, as shown in the figure below.

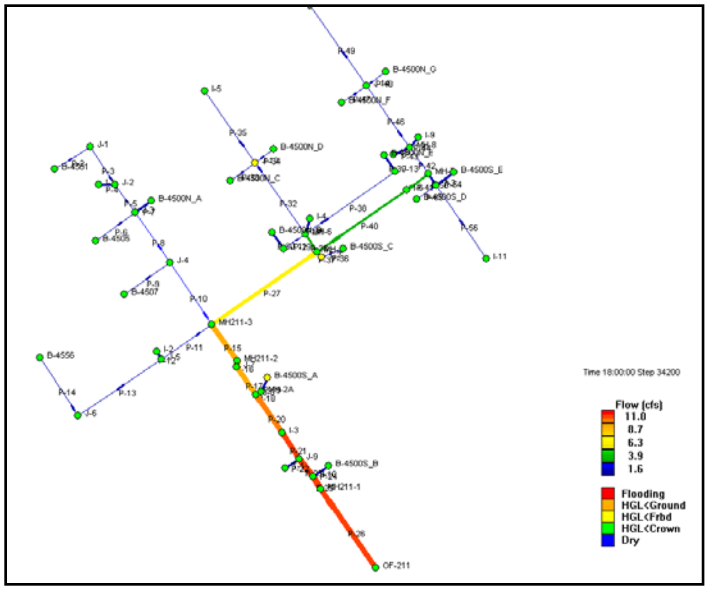

Figure 62 XPSWMM Results for Base Conditions

6.5 Design Storm Simulation Results

The U.S. Natural Resources Conservation Service (NRCS), formerly known as the U.S. Soil Conservation Services (SCS) method, is used to compute rainfall distributions. NRCS has divided the United States into four main regions where Type II distribution represents rainfall for the Tennessee Valley (ECE, 1991; City of Knoxville, 2012). For the design storms, the SCS Type II unit-hyetograph (shown in the figure below) will be multiplied by a precipitation corresponding to its storm event in order to duplicate flow rates and water elevations corresponding to the magnitude of the storm event throughout the site for analysis.

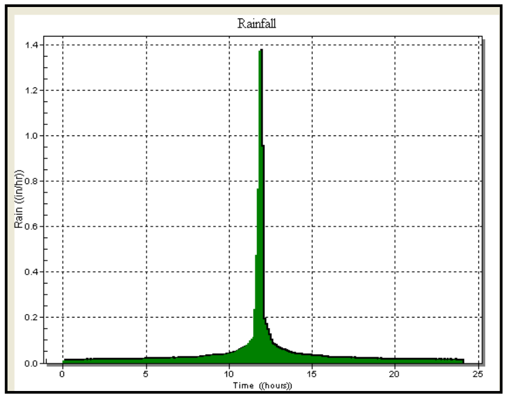

Figure 63 SCS Type II Unit Hyetograph

When a piece of land is developed, design storms are simulated for pre-development and post-development conditions to ensure that the post conditions do not exceed the pre-conditions. If they did, then during a heavy rainfall they would flood their neighbor. The 5 year storm event is run to assess the parking lot elevation, the 10 year storm event for roadways, the 25 year storm event for the properties berm elevation (to keep the excess rain on their property so that they would not flood their neighbor), and the 100 year storm event for the building's finish floor. It is dependent on which municipality the land resides under as to the duration (24 hour or 72 hour) of the storms required for analysis. For this reason, these design storms have been simulated over the network. The table below indicates the single design storm events and their corresponding precipitation that the unit-hyetograph will be multiplied by in order to run the design storm specific to its region (NOAA, 2006).

Storm Event	Precipitation
5 year - 24 hour	4.1”
10 year - 24 hour	4.7”
25 year - 24 hour	5.5”
100 year - 24 hour	6.8”

Table 4 NOAA Precipitation

The design simulations are based on a Manning’s roughness coefficient of 0.015, Green Ampt infiltration method, and the estimated percent imperviousness from site visits. Below are the hydrographs and PE curves for nodes MH211-3 and OF-211 and for links P-10, P-11, P-26, and P-27.

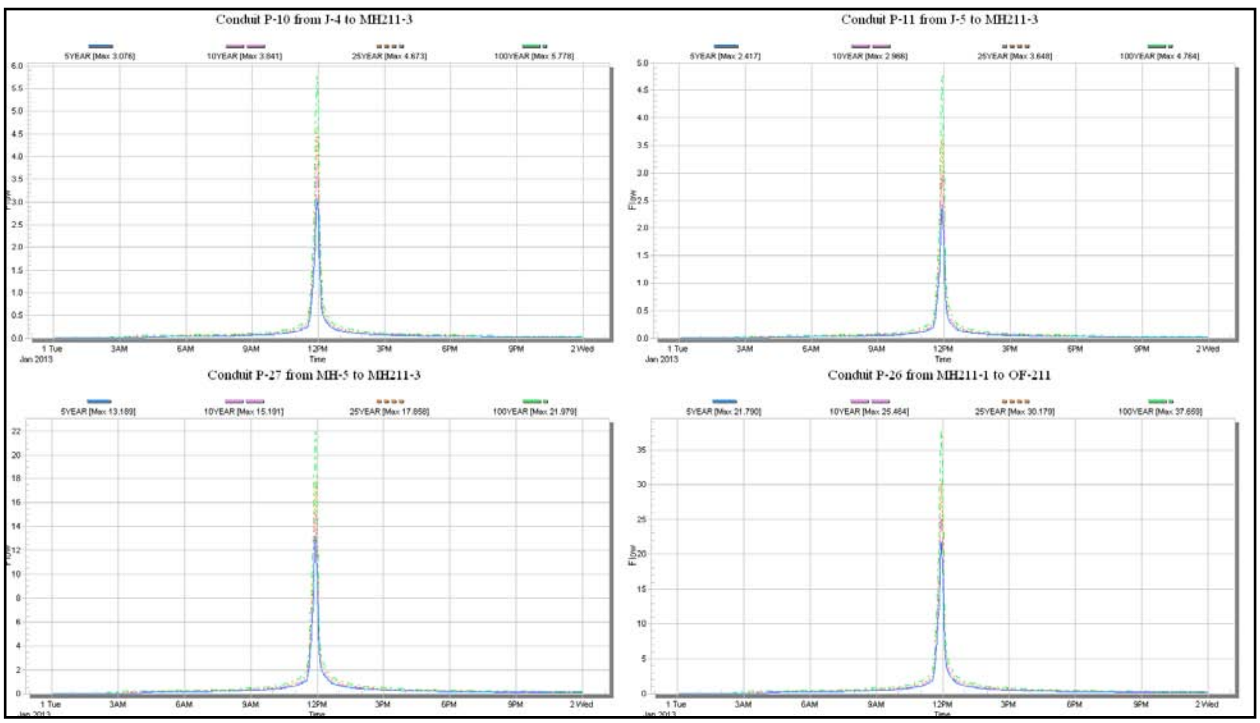

Figure 64 XPSWMM Design Storm Hydrographs

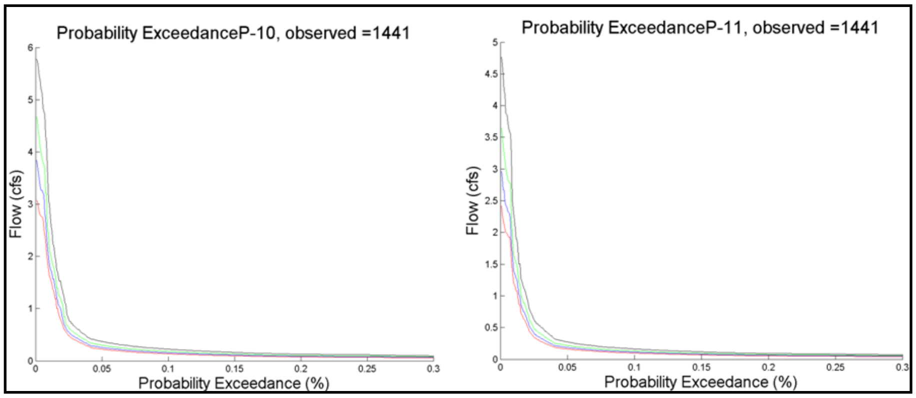

Figure 65 P-10 PE Curves for Design Storm Events

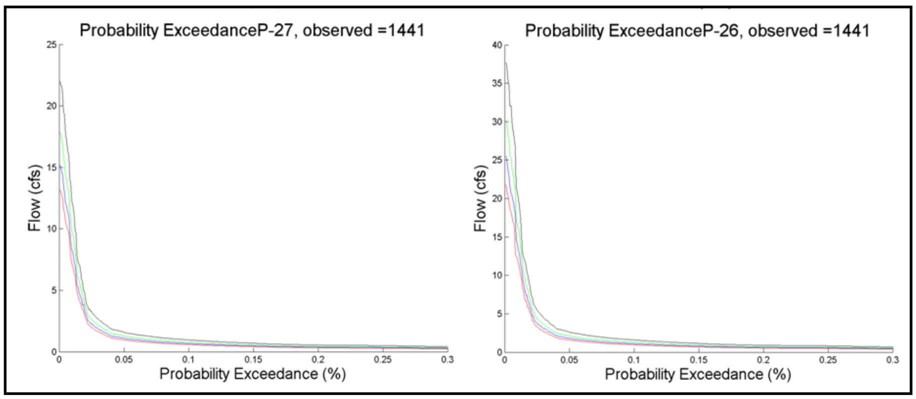

Figure 66 P-27 PE Curves for Design Storm Events

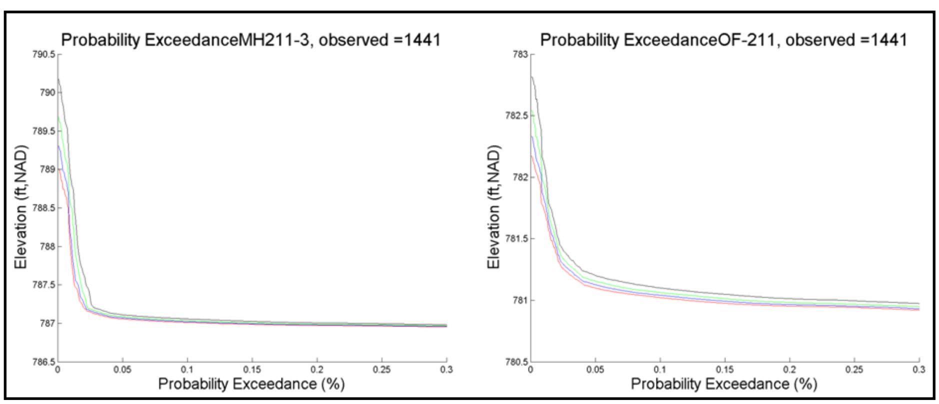

Figure 67 MH211-3 PE Curves for Design Storm Events

The table below is a summary of the maximum stages (elevations) and flow rates for the chosen nodes and links. Due to the fact that the design storms precipitation amounts vary in magnitude almost an inch, a difference in node elevations and link stages throughout the events are observed as shown in the hydrographs and PE curves.

Design Storm	**Peak Stage (ft, NAD)**		**Peak Flow Rate (cfs)**			
	MH211-3	**OF-211**	**P-10**	**P-11**	**P-26**	**P-27**
5 yr - 24 hour	789	782.2	3.1	2.4	21.8	13.2
10 yr - 24 hour	789.3	782.3	3.8	3	25.5	15.2
25 yr - 24 hour	789.7	782.5	4.7	3.6	17.9	30.2
100 yr - 24 hour	790.2	782.8	5.8	4.8	22	37.7

Table 5 Design Storm Stage and Flow Rate Results

For the simulations, the hydraulic grade line (HGL) and flow quantities and capacities of the main conduits have been evaluated to determine the extent of overflow. The 5 year and 10 year – 24 year storm events do not encounter flooding. The HGL is shown in the figure below for the main trunk line beginning at P-10 to P-26. The HGL rose higher for the 10 year storm event than the 5 year storm event due to the fact that less precipitation was simulated over the site. The figures below indicate that the water does not exceed the top of the pipe; thus, no flooding is expected to occur as the water is contained within the pipes for both the 5 year and 10 year – 24 hour storm events.

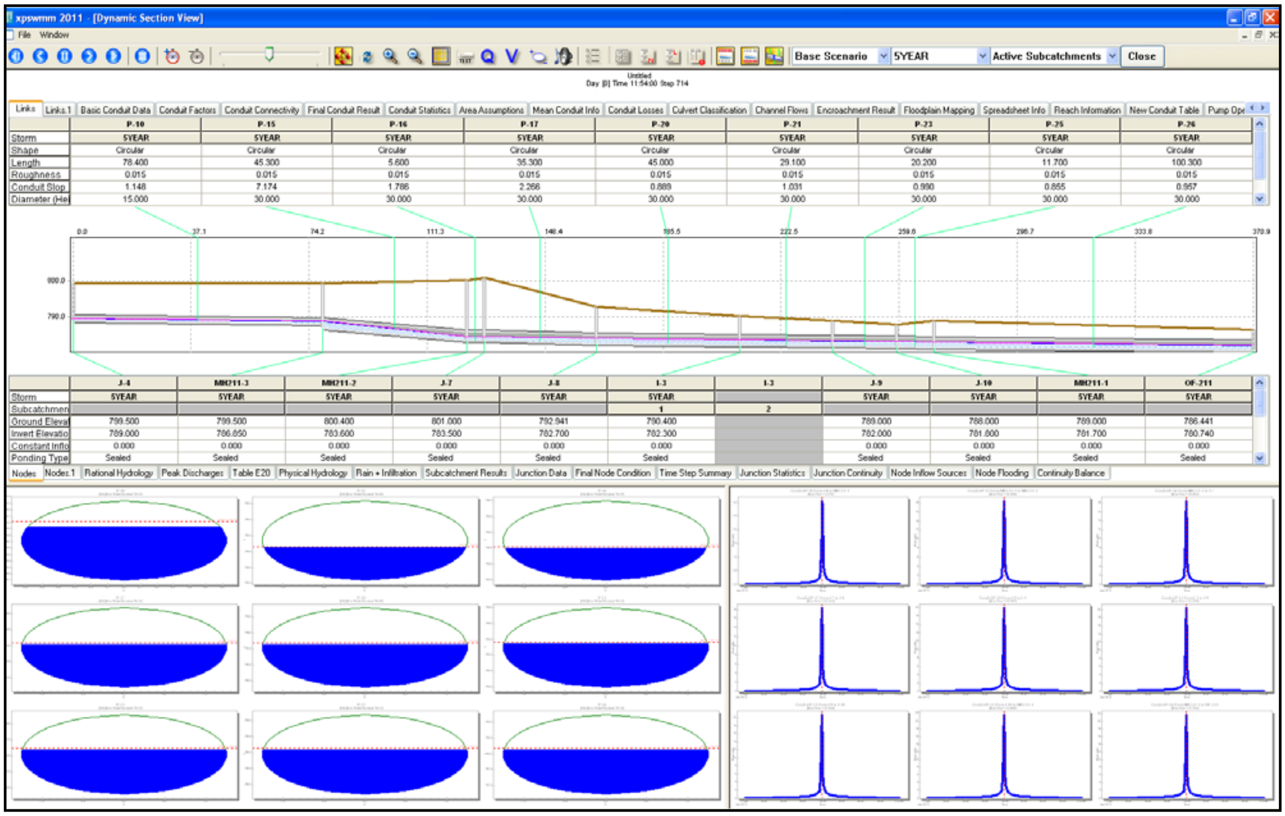

Figure 68 XPSWMM 5-Year 24-Hour Storm Event

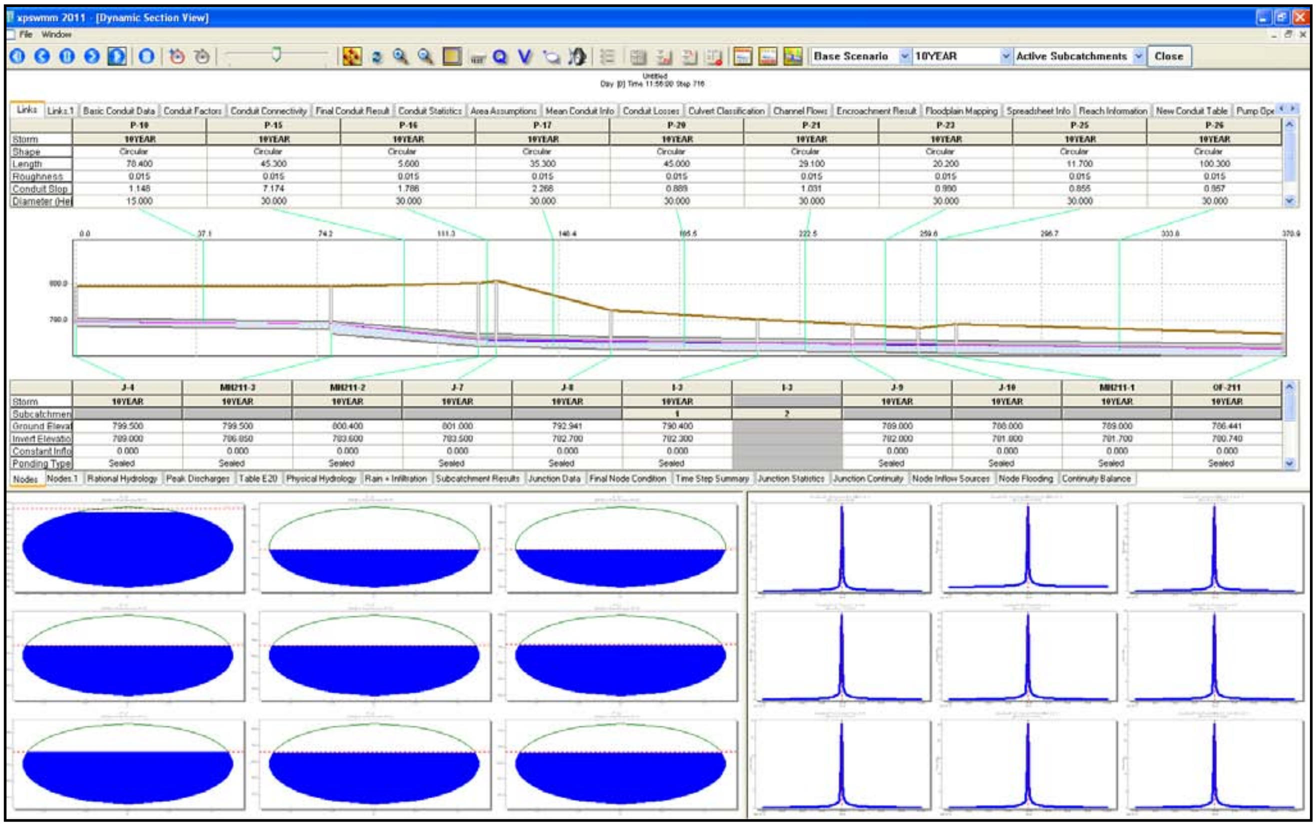

Figure 69 XPSWMM 10-Year 24-Hour Storm Event

However, the 25 year and 100 year – 24 hour storm events do cause flooding to occur within the system. As would be expected, the 100 year storm produced a larger runoff excess than the 25 year storm event. The figures below indicate that P-10 exceeds its maximum capacity, which indicates there would be ponding on the pavement.

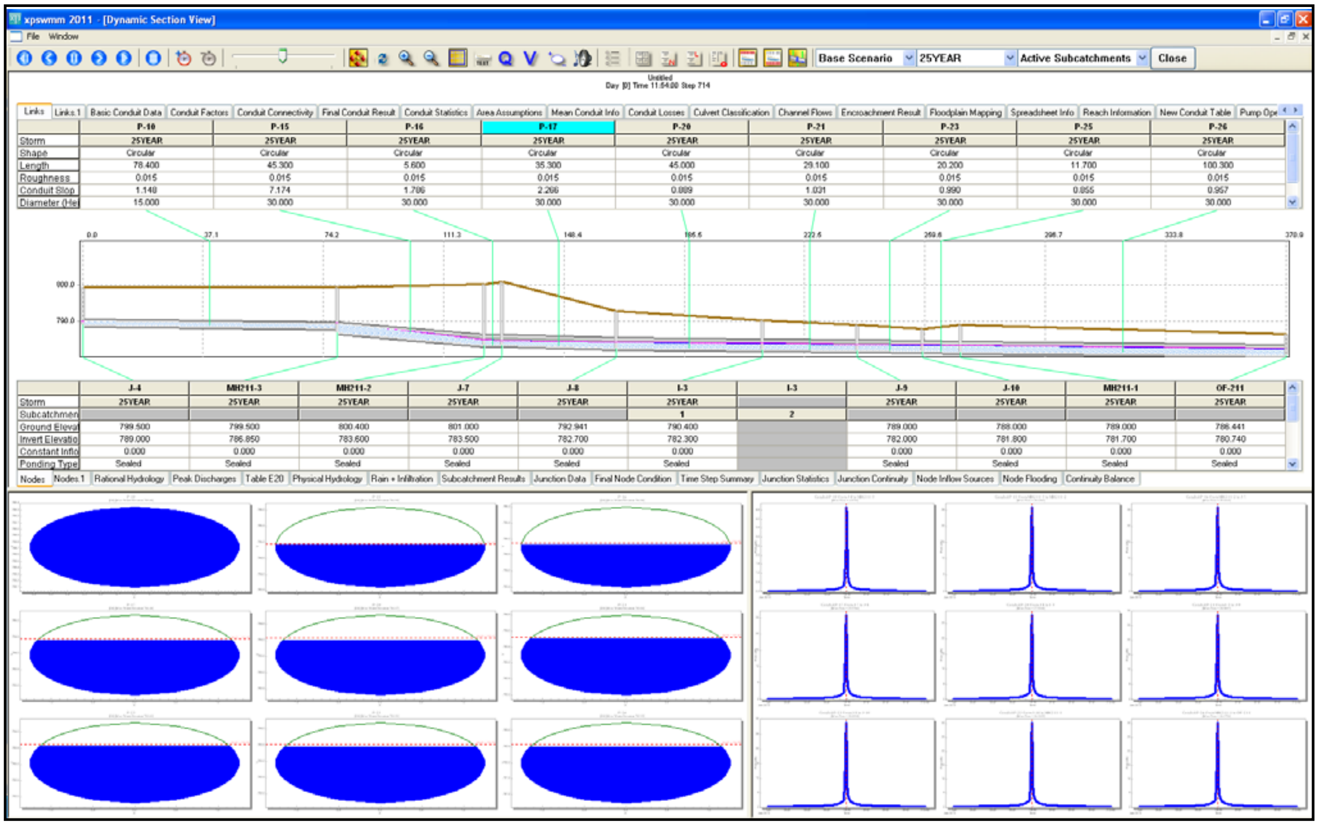

Figure 70 XPSWMM 25-Year 24-Hour Storm Event

The figure below is a schematic of the system indicating where the flooding occurred and its quantity. The links (P-21, P-22, and P-26) that are red represent that the flow rate has met or exceeded 28.2 cfs, and the nodes (B-4501, J-12, B-4500_S, B-4500S_D, and B-4500S_E) that are red represent flooding in which the HGL was exceeded and there was insufficient capacity within the pipes.

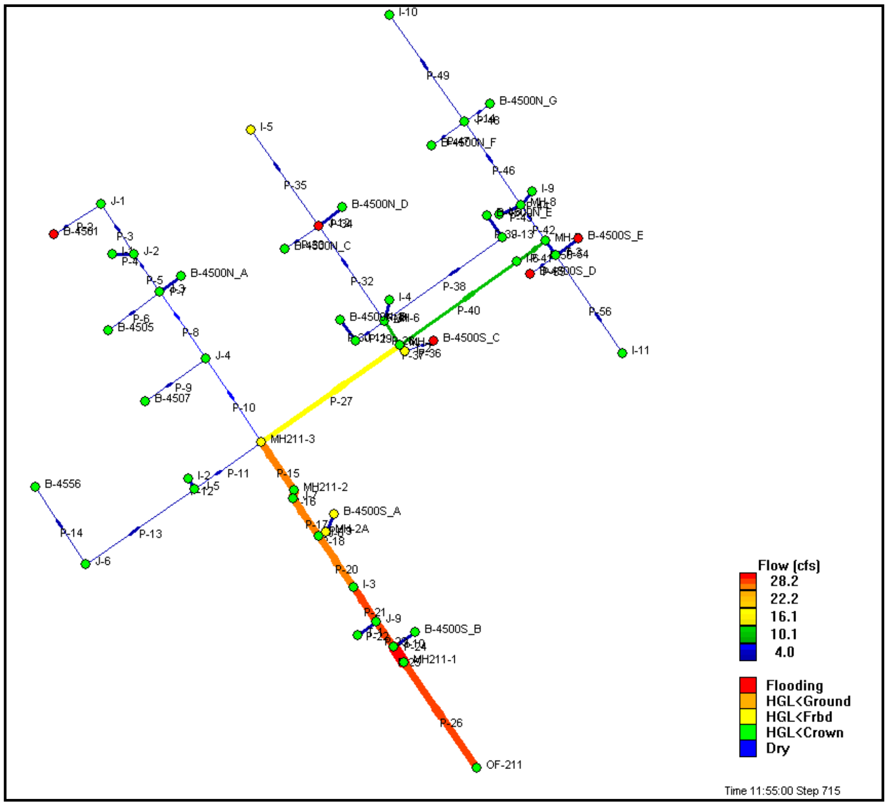

Figure 71 XPSWMM 25-Year 24-Hour Storm Event Areas of Flooding

Below are the 100 year – 24 hour design storm event results which are similar to the 25 year storm results. The major difference is that the flow rate is higher, reaching up to 35.1 cfs in the pipes leading up to OF-211. In addition, flooding occurs in the storm lateral, B-4500S_A.

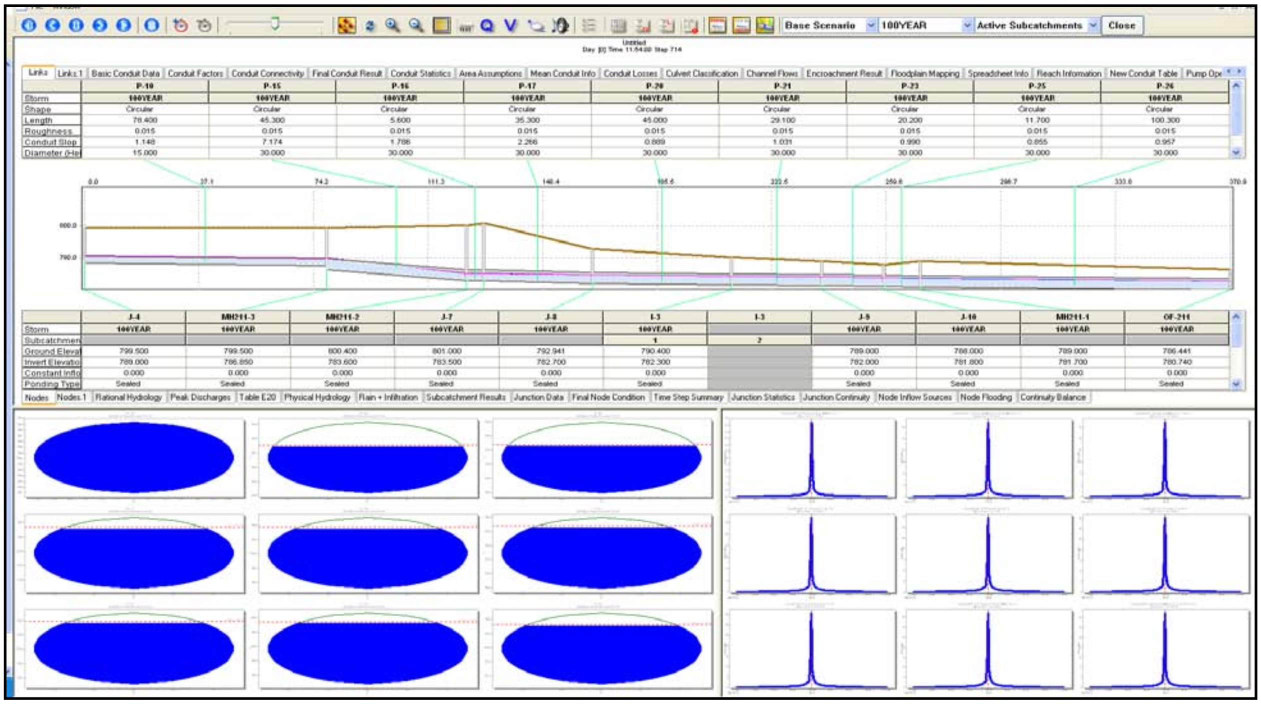

Figure 72 XPSWMM 100-Year 24-Hour Storm Event

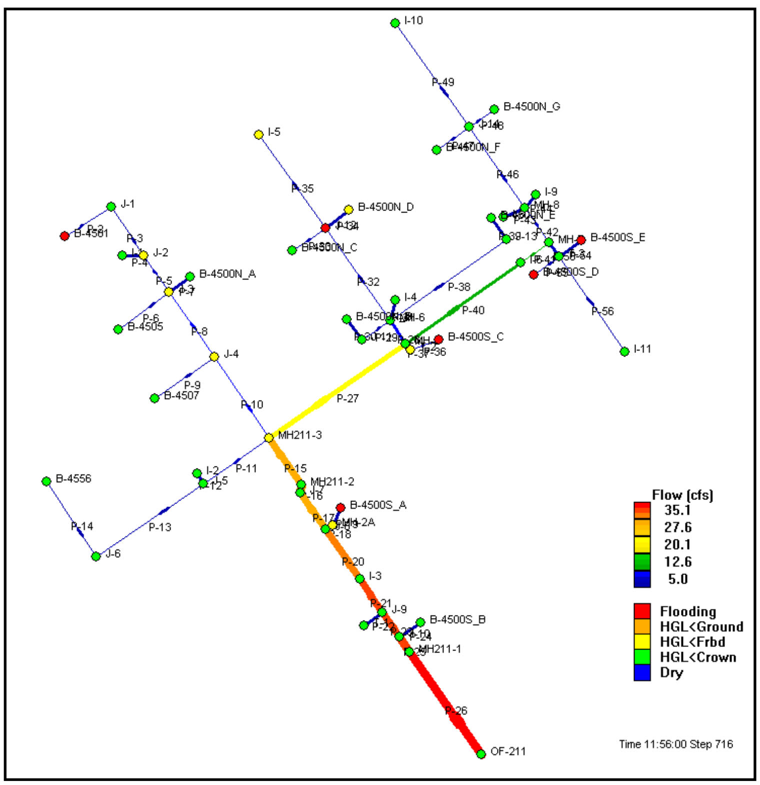

Figure 73XPSWMM 100-Year 24-Hour Storm Event Areas of Flooding

7 TRANSPORT ANALYSIS

The transport analysis has been conducted by introducing a hypothetical conservative contaminant into the system. Examples of conservative contaminants are bromine, nitrate, technetium-99, and dye, as opposed to a non-conservative contaminant where adsorption/desorption would occur. The conservative contaminant (described as 'pollutant' by XPSWMM) may be routed via the Hydraulics or the Runoff mode within XPSWMM. Introducing the pollutant via the Hydraulics mode may be interpreted as having a residual contaminant within an existing pipe and/or inlet within the system. Four variations of the Hydraulics mode simulations were run. This study focuses on injecting a pollutant into the Hydraulics mode specifically as user timeseries inflow at various nodes, as shown in the interface below.

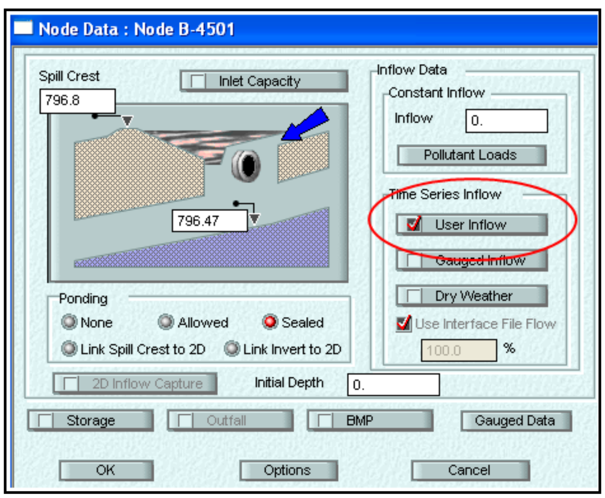

Figure 74 XPSWMM User Inflow

Similarly to the sensitivity analysis, the simulations were run using the following parameters: actual 15 minute interval rainfall data, year 2010; Manning's roughness coefficient, n, of 0.015; Green Ampt infiltration parameters for loamy clay soil; an evaporation default of 0.1"/day; and estimated percent imperviousness from site visits. The following describes the various simulations run in order to assess the effects of a hypothetical pollutant entering the system as a residual contaminant existing within the pipes. Four timeseries were used for the simulations (one steady flow and concentration, and three varied flow and concentration). The first is the timeseries containing a constant flow of 0.17 cfs and a constant pollutant concentration of 0.1 mg/L, which from here onwards will be referred to as the 'steady timeseries' followed by three varied flow rate and concentration timeseries for a duration of 24 hours. The pollutant concentrations are hypothetical; however, the flow rates resemble the base flow rate found during the calibration of the model which is approximately 0.17 cfs in the system due to the once through cooling water for the AC units. The hypothetical scenarios used for the simulations are listed below:

1. HYD Scenario 1: Steady timeseries A was introduced into the system at both locations B-4501 and B-4500N_G
2. HYD Scenario 2: Steady timeseries A was introduced into the system at B-4556 and varied timeseries B into I-5
3. HYD Simulation 3: Varied timeseries B was introduced into the system at I-11 and varied timeseries C at I-10
4. HYD Scenario 4: Varied timeseries C was introduced into the system at B-4500S_C and varied timeseries D at T-1

The following table depicts the steady timeseries (A) and the three varied timeseries (B), (C), and (D) that were introduced into the system for the four various simulations.

Hydraulics Mode Simulation Timeseries Input											
(A)			(B)			(C)			(D)		
Time (hr)	Q (cfs)	C (mg/L)	Time (hr)	Q (cfs)	C (mg/L)	Time (hr)	Q (cfs)	C (mg/L)	Time (hr)	Q (cfs)	C (mg/L)
0	0.17	0.1	0	0.14	0.1	0	0.11	0.2	0	0.17	0.5
3	0.17	0.1	3	0.15	0.5	2	0.13	0.3	4	0.14	0.2
6	0.17	0.1	6	0.16	0.7	6	0.12	0.1	9	0.13	0.4
9	0.17	0.1	9	0.17	0.4	8	0.15	0.25	16	0.15	0.15
12	0.17	0.1	12	0.13	0.2	15	0.18	0.5	18	0.16	0.6
15	0.17	0.1	15	0.15	0.15	21	0.16	0.4	20	0.18	0.15
18	0.17	0.1	20	0.14	0.3	23	0.15	0.35	22	0.11	0.3
24	0.17	0.1	24	0.13	0.1	24	0.14	0.1	24	0.13	0.25

Table 6 Transport Simulations Hypothetical Timeseries

The following table summarizes the location and which timeseries (steady or varied) were introduced into the system. Two timeseries were entered for each simulation.

Hydraulics Mode Simulation Name	Node 1	Input 1	Node 2	Input 2
HYD 1	B-4501	A	B-4500N_G	A
HYD 2	B-4556	A	I-5	B
HYD 3	I-11	B	I-10	C
HYD 4	B-4500S_C	C	T-1	D

Table 7 Transport Simulation Scenarios

The simulations ran in the Hydraulics mode take into account an assumed event mean concentration of 0.1 mg/L, with a standard deviation of 0.01 mg/L and an assumed initial pollutant concentration of 0.1 mg/L. No buildup is assumed for these simulations, only washoff of the pollutant which is calculated via the event mean concentration rating curve approach with a coefficient of 1. The event mean concentration approach assumes that the quantity of the pollutant plus or minus its standard deviation is proportional to the quantity of runoff.

7.1 Transport Analysis Scenario 1

The flow and pollutant steady timeseries (A) was injected at the two nodes B-4501 and B-4500N_G as shown below.

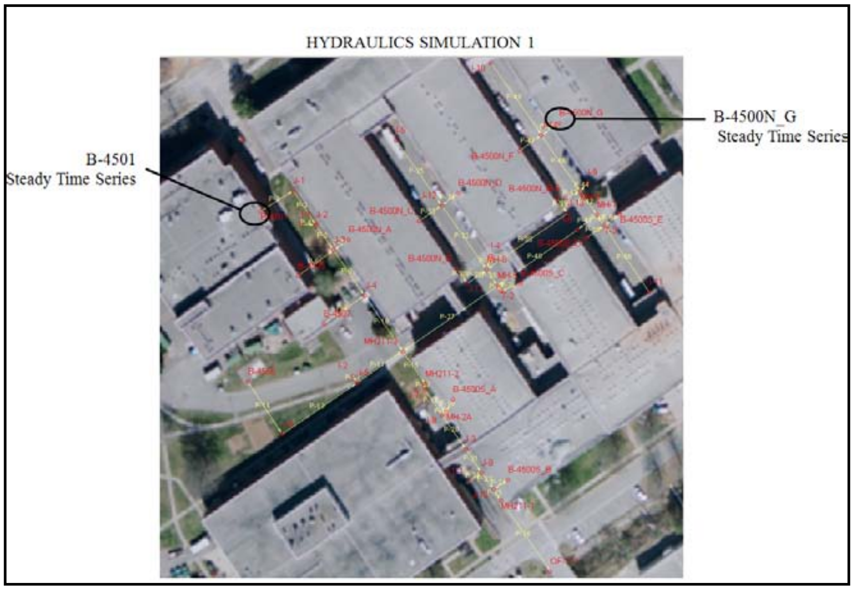

Figure 75 Transport Scenario 1 Entrance of Pollutant Location

Thus, a pollutant load is expected to occur from the north from B-4501 and seen in P-10 and the east from B-4500S_G in P-27. No load was introduced into nodes located west of MH211-3. The load within P-15 will depict a combination of the two loads from P-10 and P-27. The following are the hydrographs and pollutographs (concentration versus time and load versus time) for the first scenario for links P-10, P-11, P-15, P-26 and P-27. Make note that P-10 collects water from the north, P-11 from the east, and P-27 from the west, then the water is conveyed via MH211-3 into P-15, then P-26 and into OF-211. In addition, the XPSWMM model specifies the velocity on the hydrographs. These velocities are cumulative velocities hence their magnitude. In addition, the loads shown on the pollutographs are also cumulative load values represented by a diagonal line.

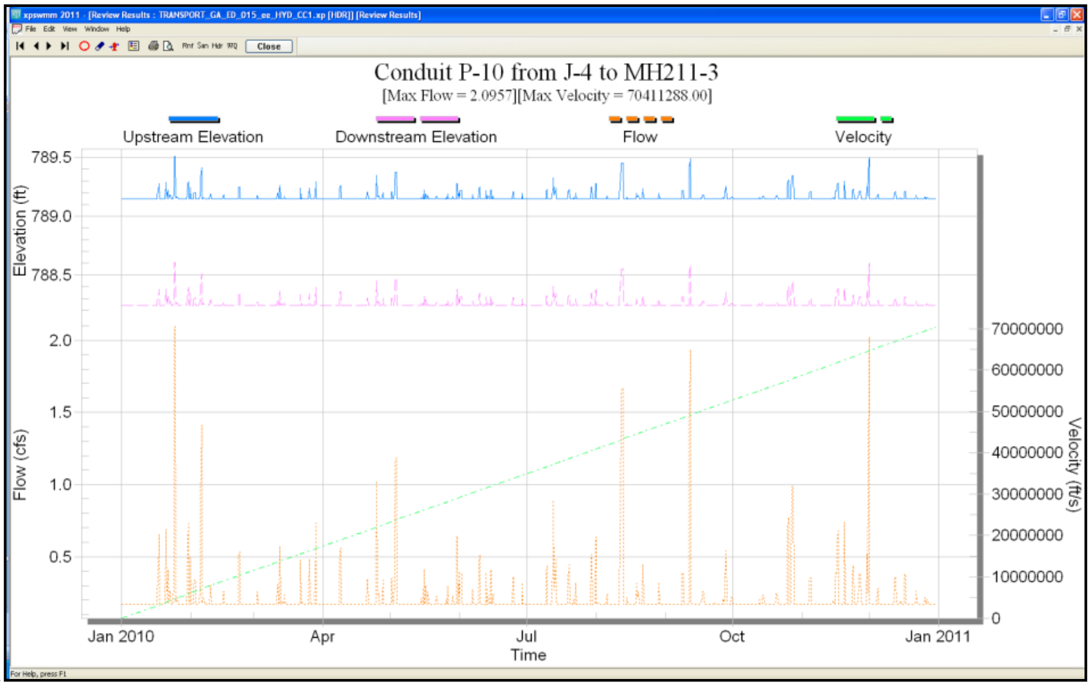

Figure 76 XPSWMM P-10 Hydrograph

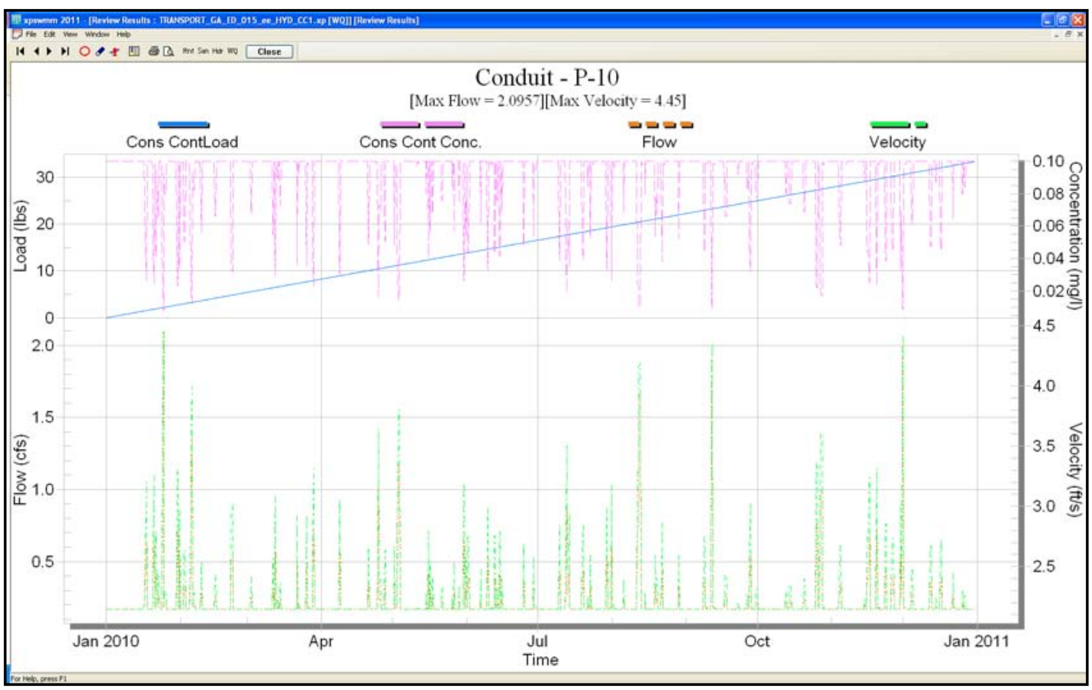

Figure 77 XPSWMM P-10 Pollutograph

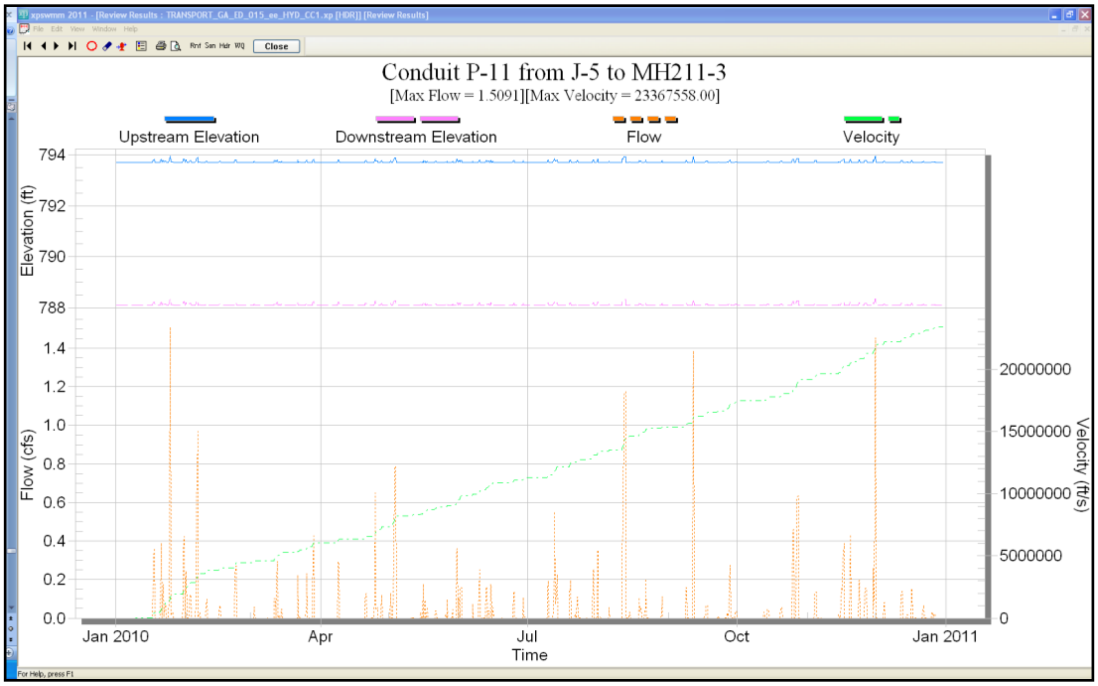

Figure 78 XPSWMM P-11 Hydrograph

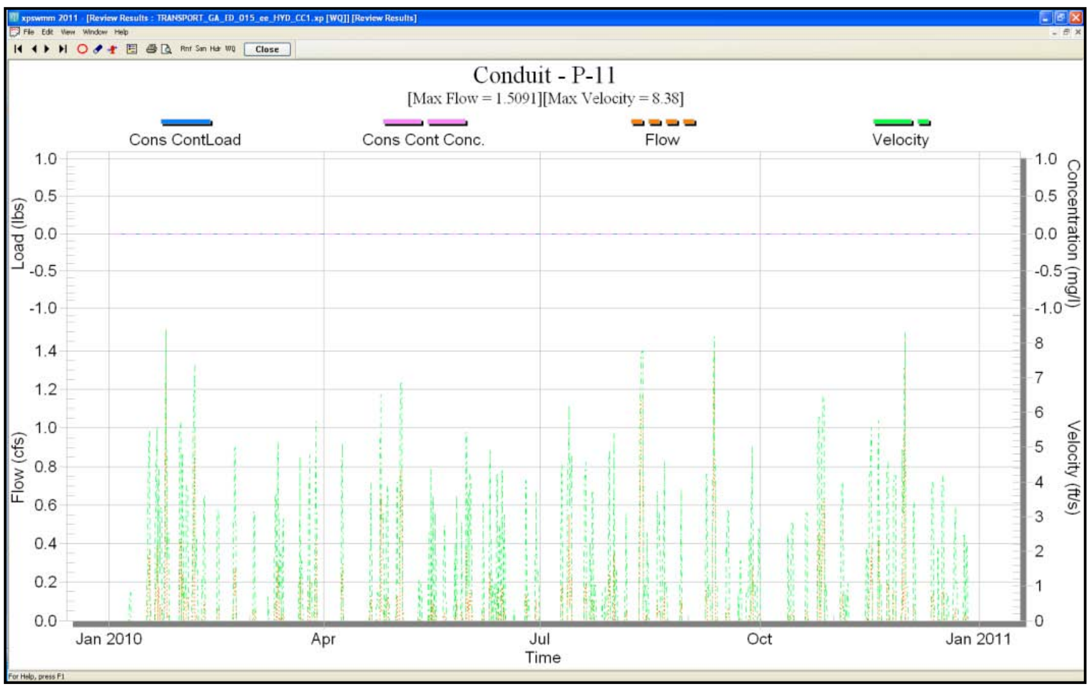

Figure 79 XPSWMM P-11 Pollutograph

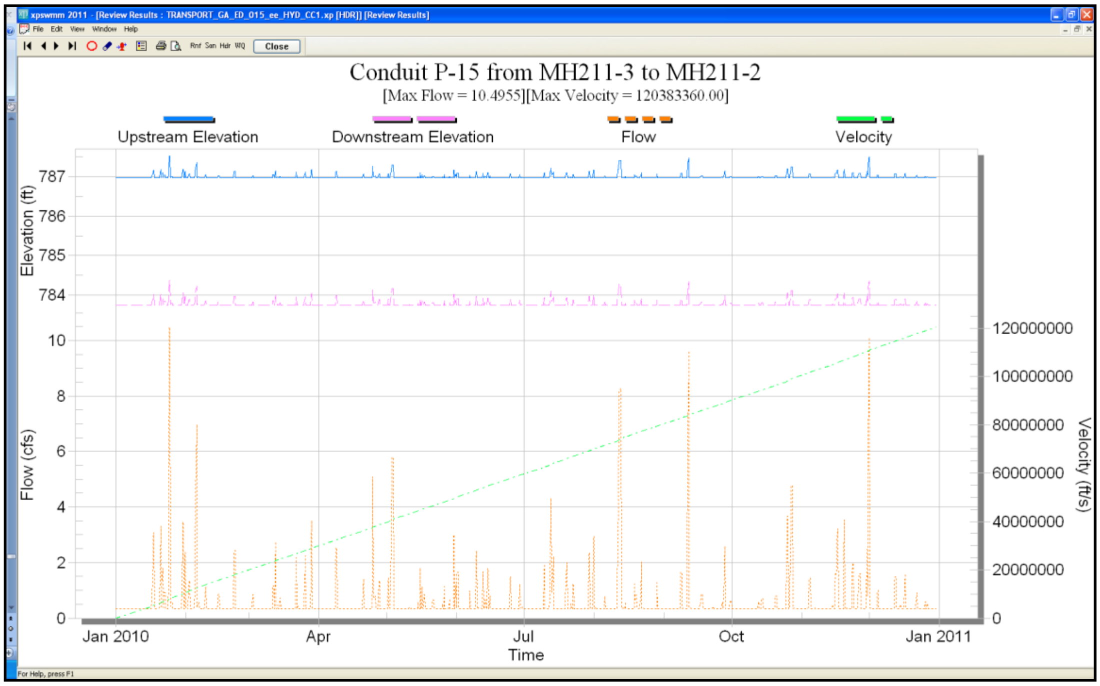

Figure 80 XPSWMM P-15 Hydrograph

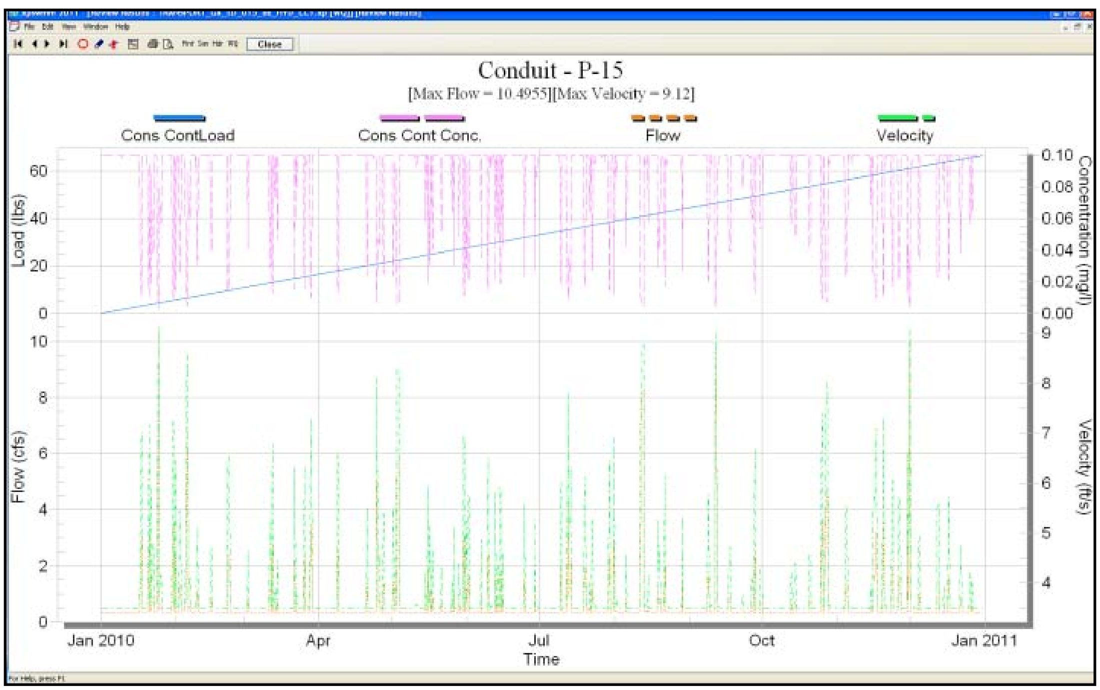

Figure 81 XPSWMM P-15 Pollutograph

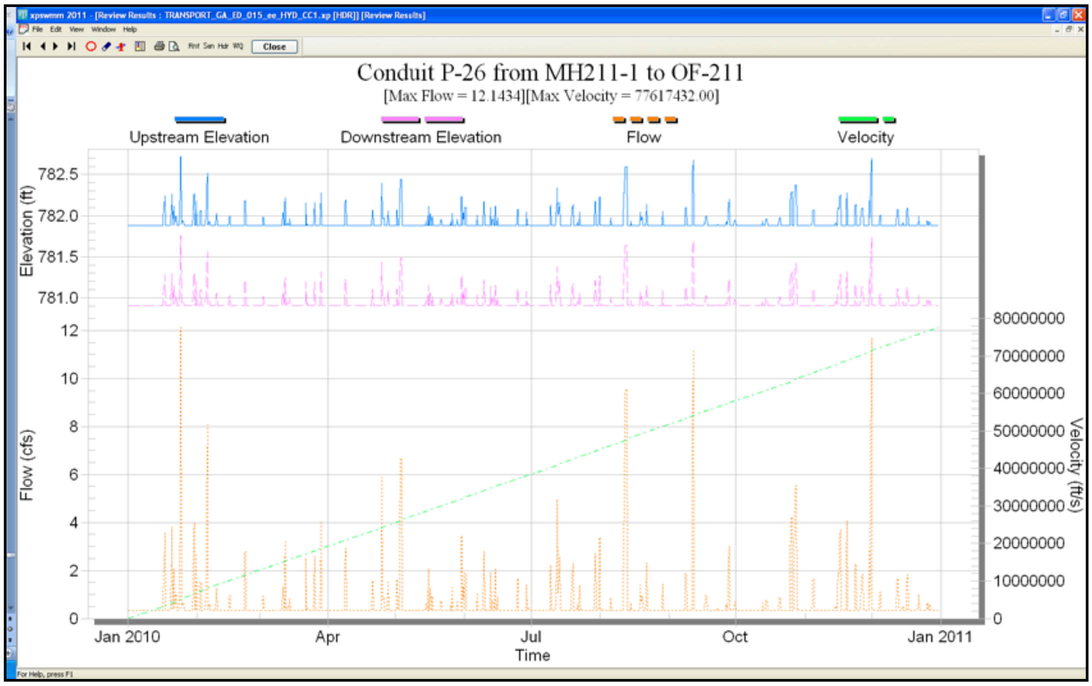

Figure 82 XPSWMM P-26 Hydrograph

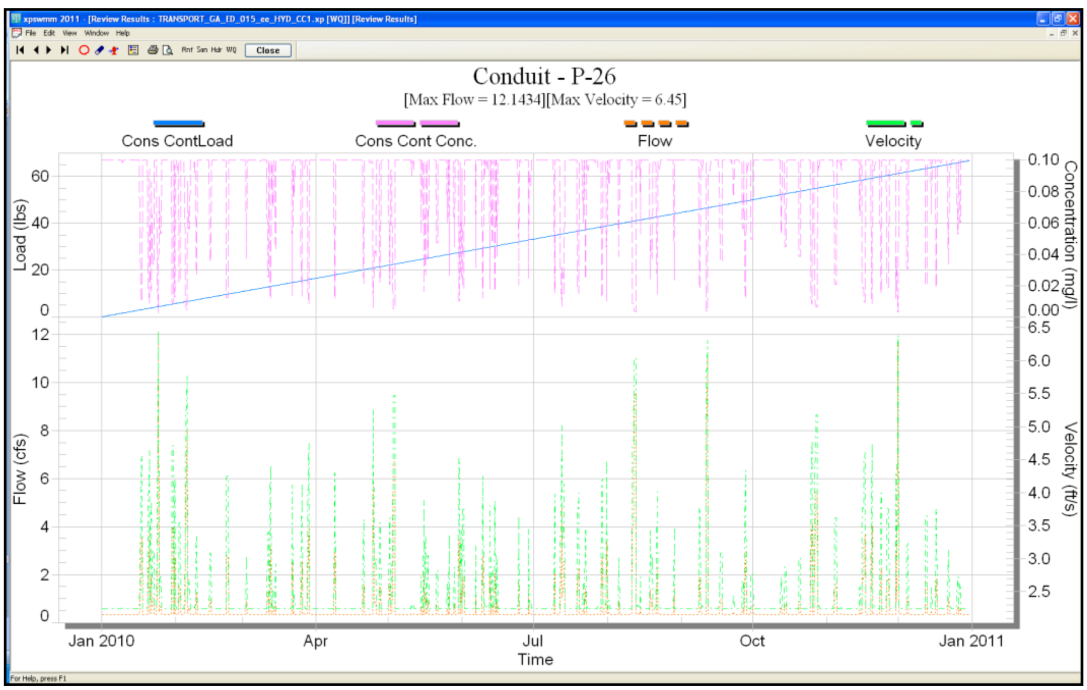

Figure 83 XPSWMM P-26 Pollutograph

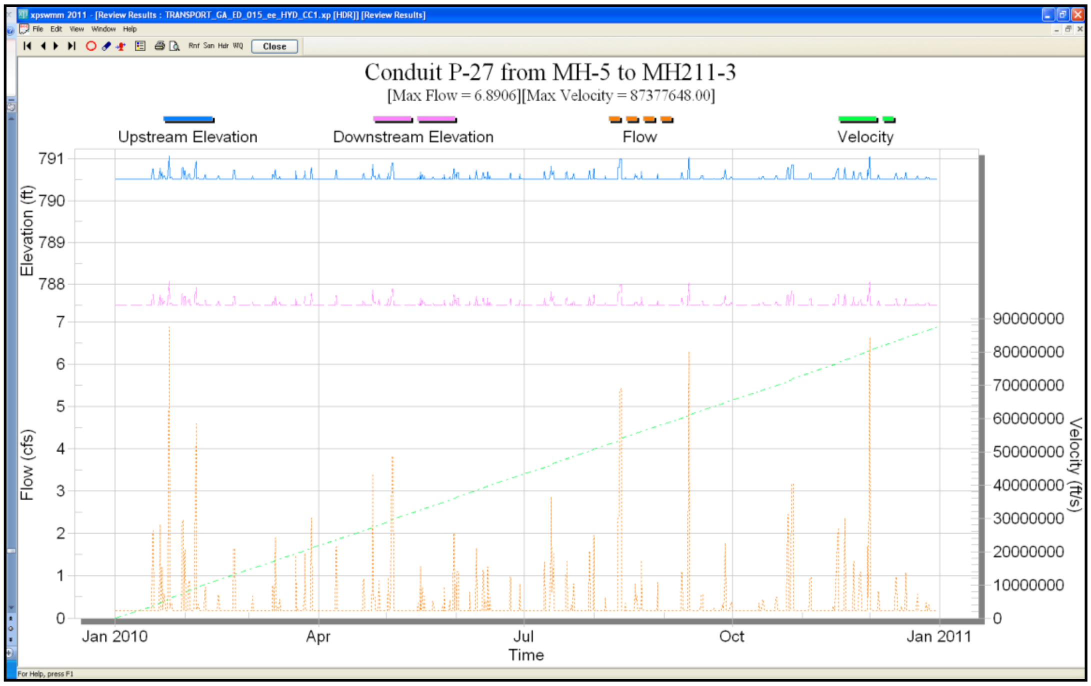

Figure 84 XPSWMM P-27 Hydrograph

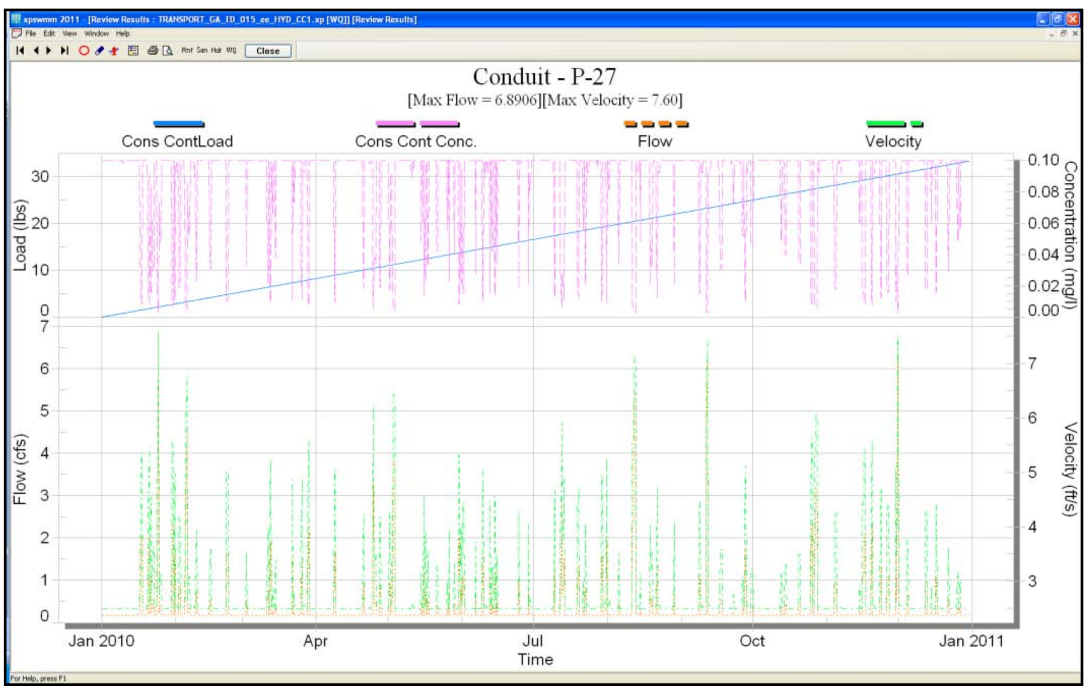

Figure 85 XPSWMM P-27 Pollutograph

As expected, loads were present in links P-10, P-15, P-26, and P-27; however, none was found in P-10 as no load was introduced west of MH211-3. The constant 0.1 mg/L concentration entered into B-4501 and B-4500N_G appears as the maximum concentration of 0.1 mg/L. The concentration lessens as runoff is introduced into the system as it responds to the yearly rainfall. Links P-10 and P-27 hydrographs and pollutographs respond to the steady flow rate timeseries entered. This is shown to be the minimum constant base flow of 0.17 cfs. No additional flow was entered into the system west of P-11; thus, no base flow is indicated. P-15 flow rate agrees with the flow rates entered into node MH211-3, and indicates a base flow of 0.34 cfs which agrees with the 0.17 cfs from P-10 and P-27. P-26 also indicates a base flow of 0.34 cfs and has a larger flow rate than in P-15, as it should due to the runoff entering the system south of P-15. The simulation results accurately respond to the first scenario. The maximum flow rate within link P-26 is 12.1 cfs and the maximum elevation in node OF-211 is 781.8 ft, NAD. The cumulative load in P-26 is estimated to be 65 lb.

7.2 Transport Analysis Scenario 2

The second scenario introduces a steady timeseries flow and concentration into node B-4556 and a varied timeseries in node I-5.

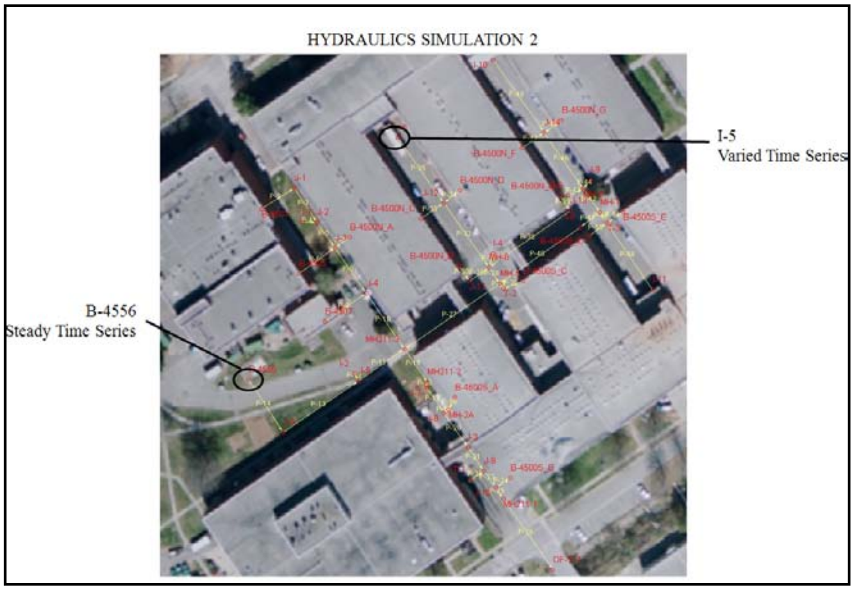

Figure 86 Transport Analysis Scenario 2 Pollutant Entrance Locations

A pollutant load is expected to occur in P-11 due to the introduction of the steady timeseries into B-4556 as well as to the east in P-27 where a hypothetical flow and concentration varied timeseries was entered. The following are the resulting hydrographs and pollutographs for the HYD2 simulation.

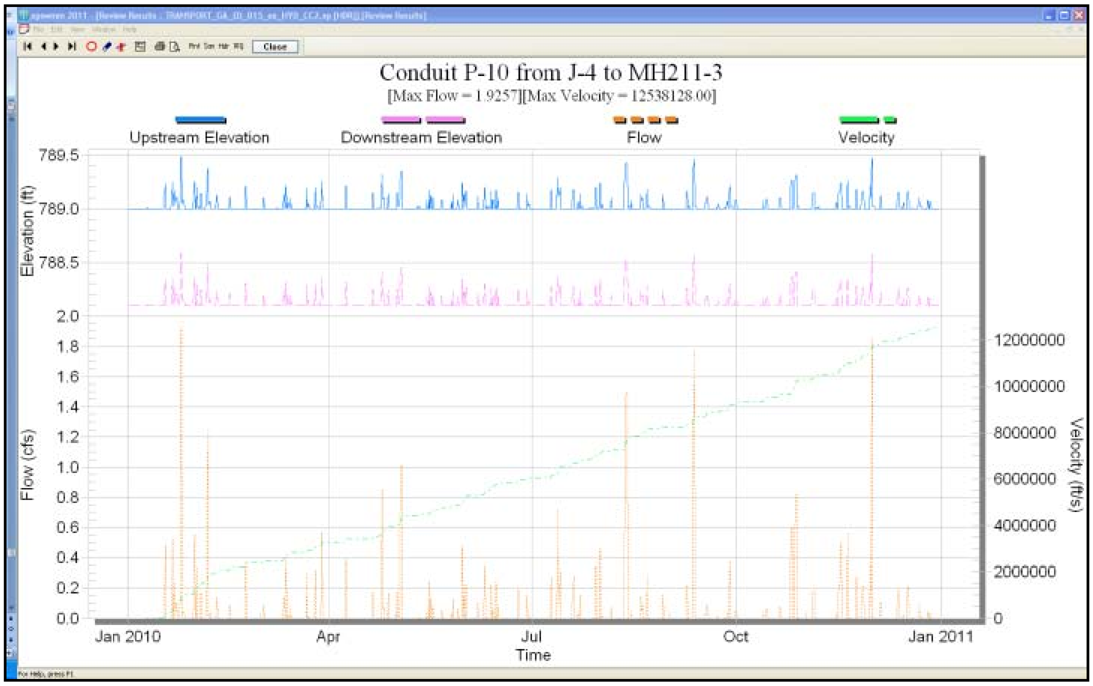

Figure 87 XPSWMM P-10 Hydrograph

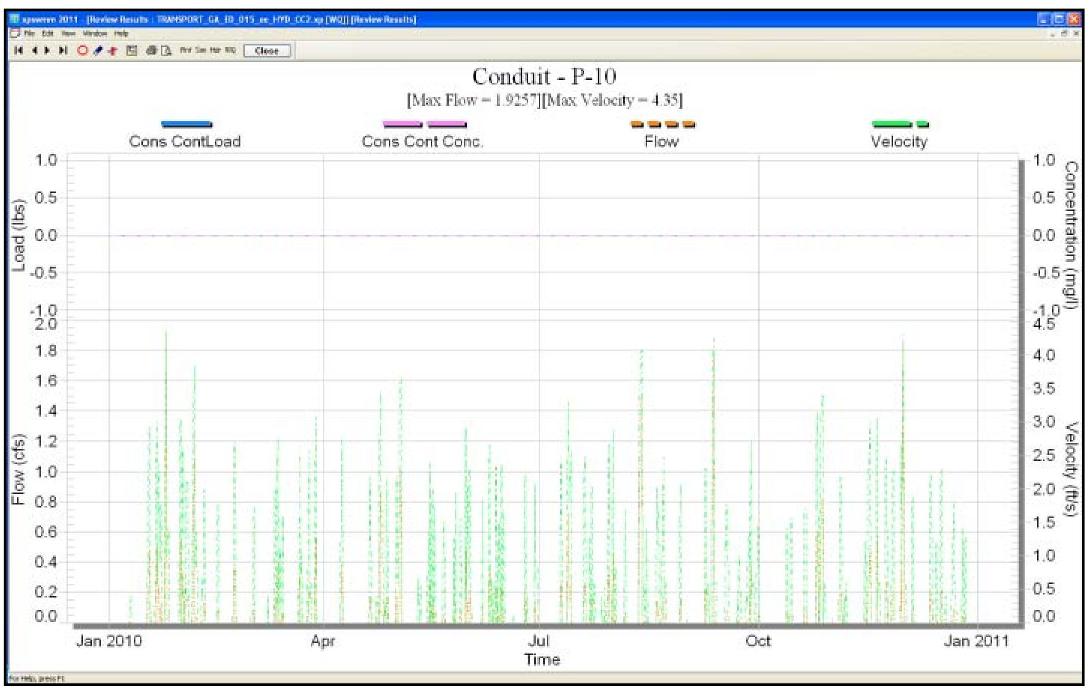

Figure 88 XPSWMM P-10 Pollutograph

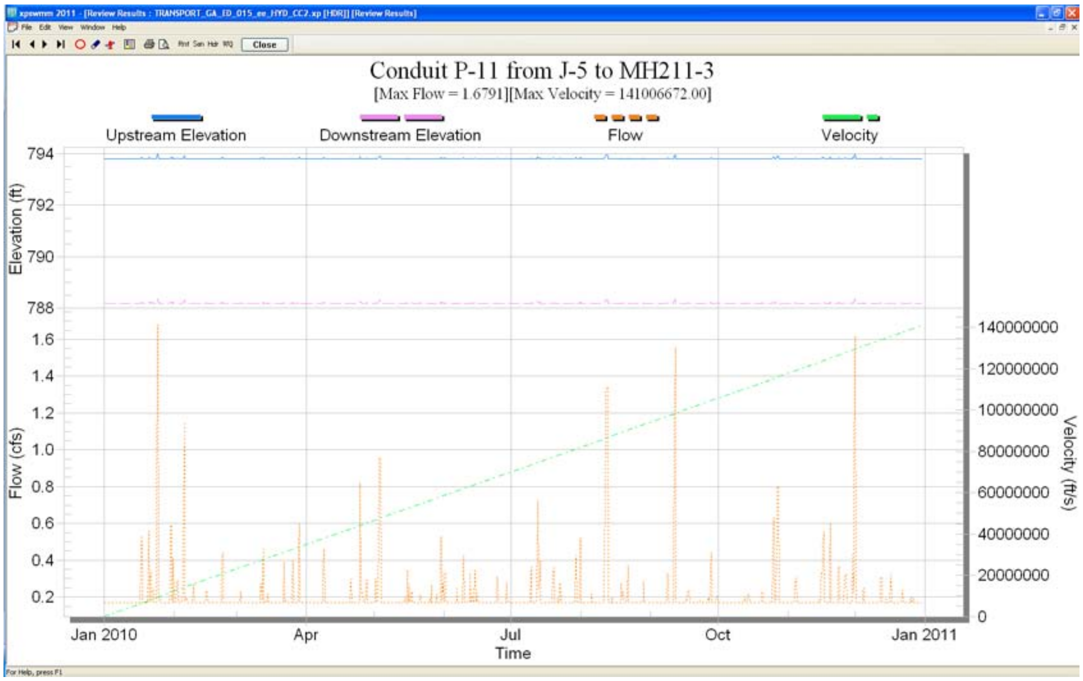

Figure 89 XPSWMM P-11 Hydrograph

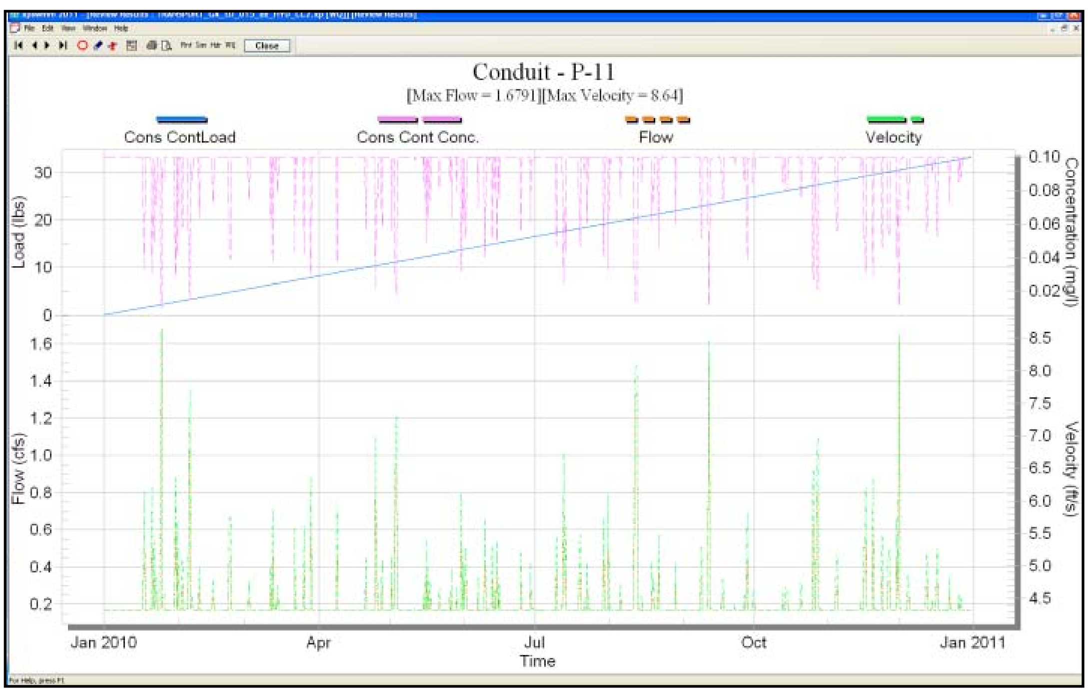

Figure 90 XPSWMM P-11 Pollutograph

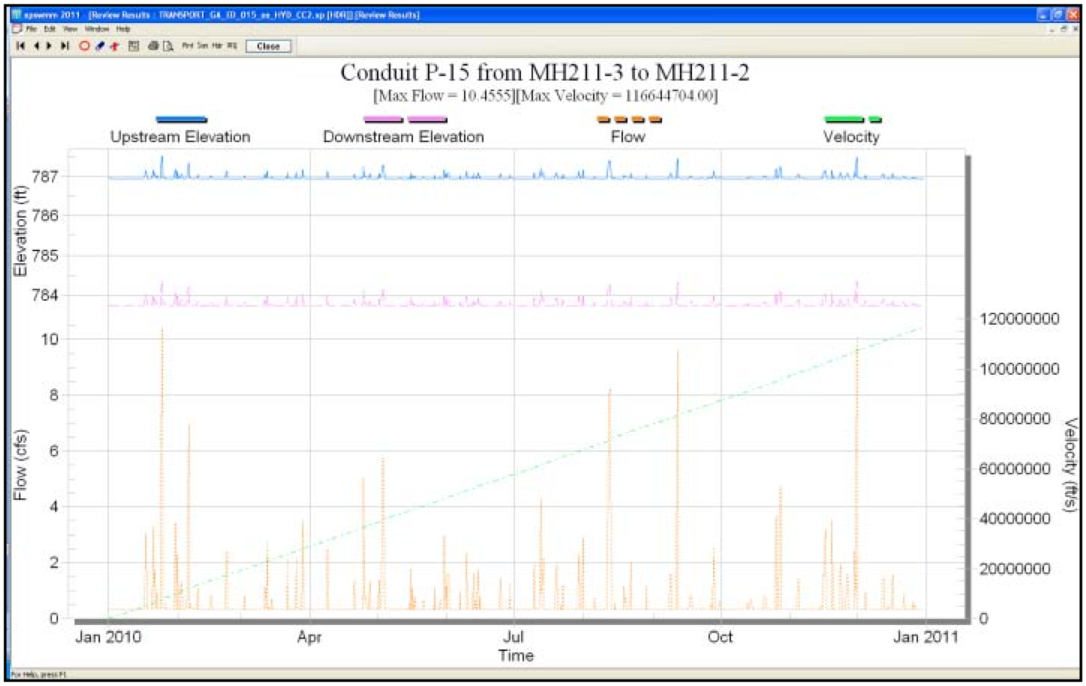

Figure 91 XPSWMM P-15 Hydrograph

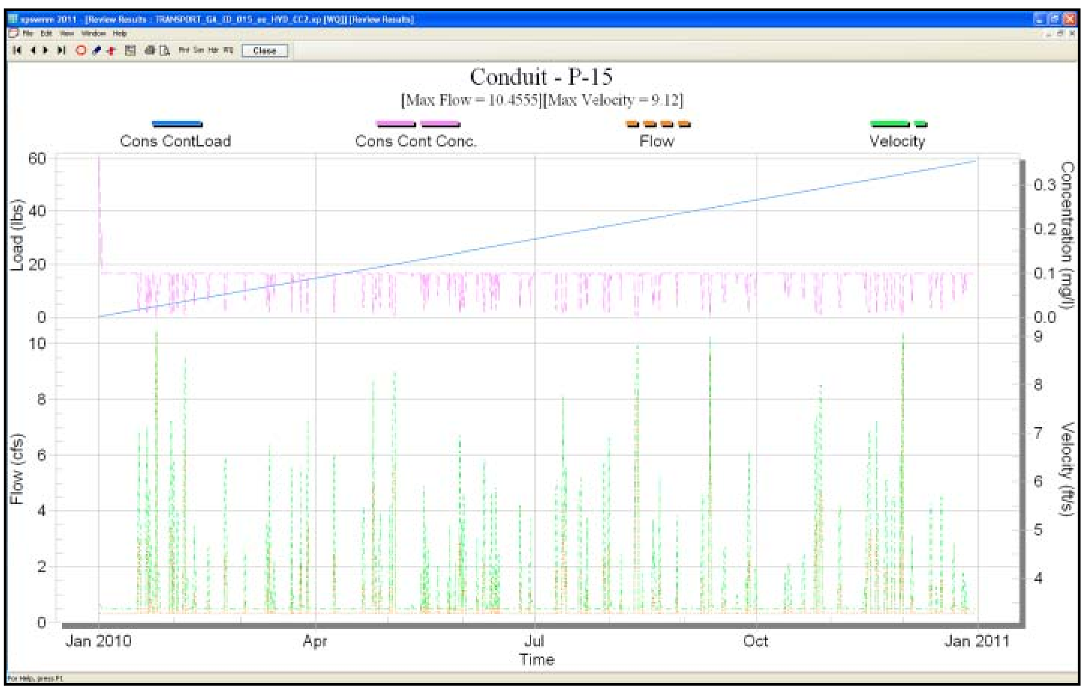

Figure 92 XPSWMM P-15 Hydrograph

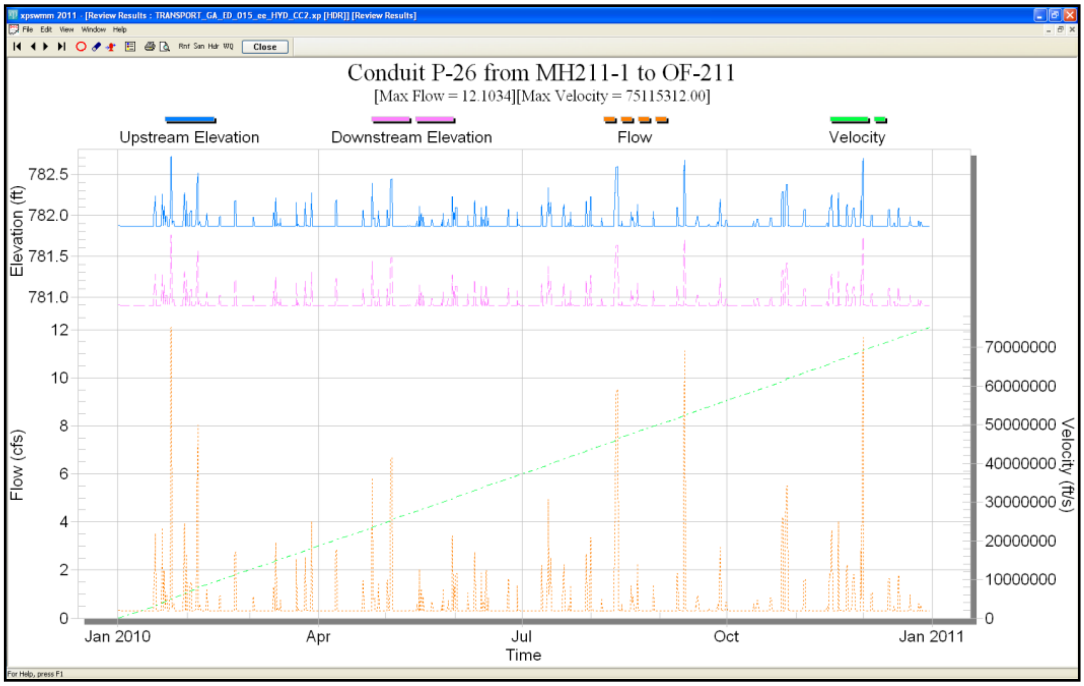

Figure 93 XPSWMM P-26 Hydrograph

Figure 94 XPSWMM P-26 Pollutograph

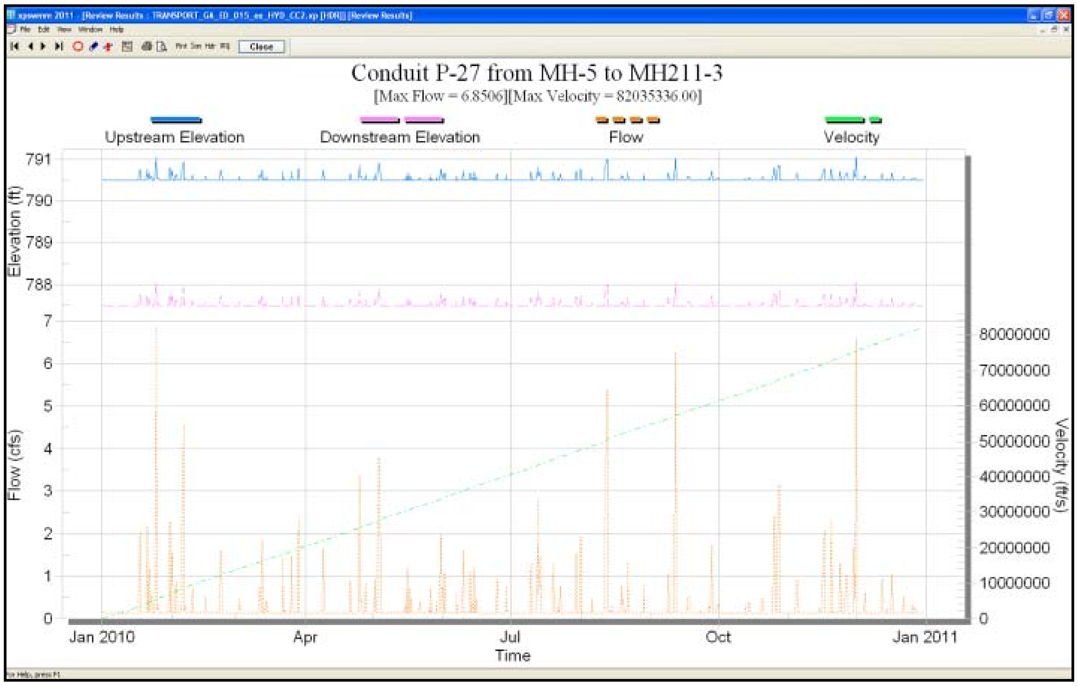

Figure 95 XPSWMM P-27 Hydrograph

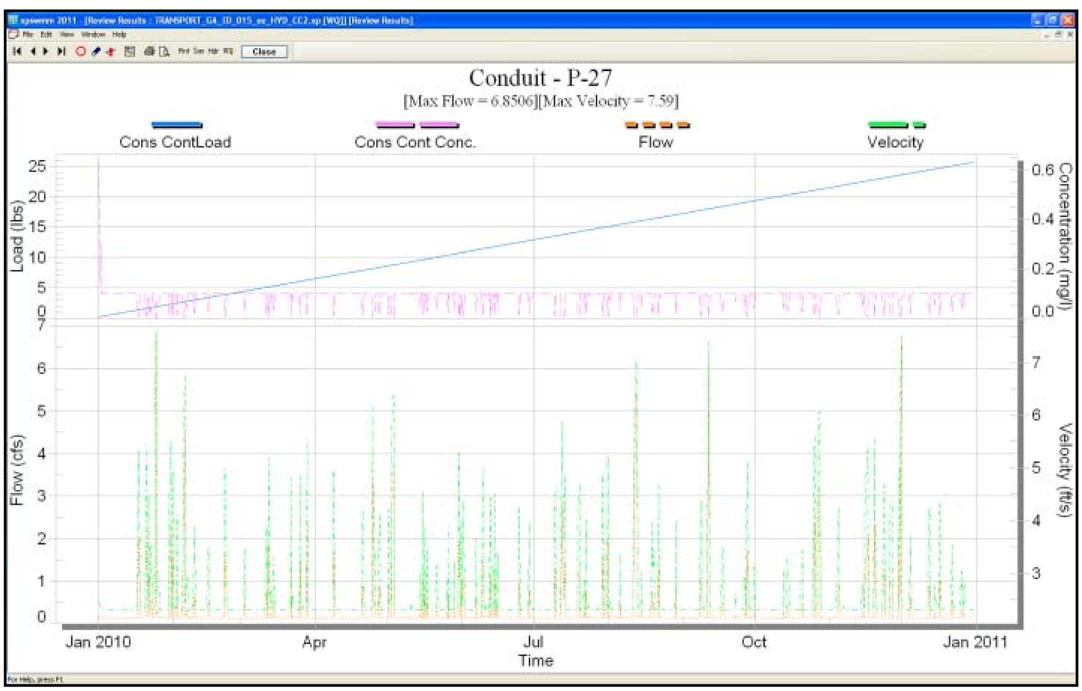

Figure 96 XPSWMM P-27 Pollutograph

Scenario 2 varies from Scenario 1 as steady timeseries is entered at the west and varied timeseries to the east. As expected, P-10 does not indicate a pollutant load and P-11, P-15, P-26, and P-27 do. Similarly to Scenario 1 where a constant concentration of 0.1 mg/L is entered into the system, the pollutograph indicates a maximum concentration of 0.1 mg/L. The concentration remains constant during the event except when runoff is encountered, then the concentration is decreased. Link P-27 spikes at the concentration of 0.63 mg/L at the beginning of the pollutograph, which responds to the varied timeseries (B) entered. The timeseries (B) ends at hour 24 with a concentration of 0.1 mg/L. The model holds the concentration constant at 0.1 mg/L throughout the remaining storm event except when runoff is encountered, then the concentration is decreased. A base flow rate of 0.17 cfs is represented in P-11 and a base flow rate of 0.13 cfs in P-27. P-15 and P-26 indicate a base flow of 0.1 cfs from the yearly rainfall and the additional flow rates entered into the system. The maximum flow rate within link P-26 is 12.1 cfs and the maximum elevation in node OF-211 is 781.8 ft, NAD. The cumulative load is estimated to be 26 lbs.

7.3 Transport Analysis Scenario 3

Scenario 3 introduces varied flow and concentration timeseries (B) into node I-11 and varied flow and concentration (C) data into node I-10. No pollutant was introduced into the north and west wings of the system; therefore, no pollutant load should appear in links P-10 and P-11.

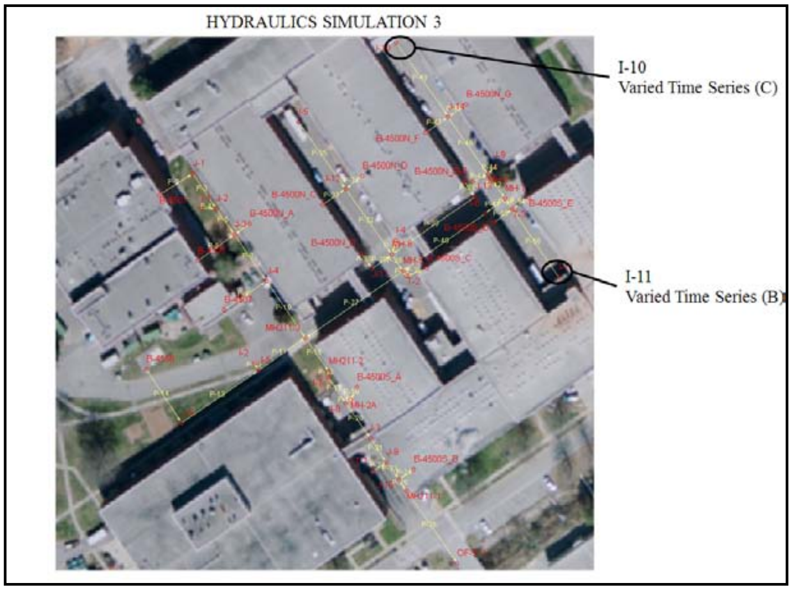

Figure 97 Transport Analysis Scenario 3 Entrance of Pollutant

The following are the resulting hydrographs and pollutographs for the HYD3 simulation.

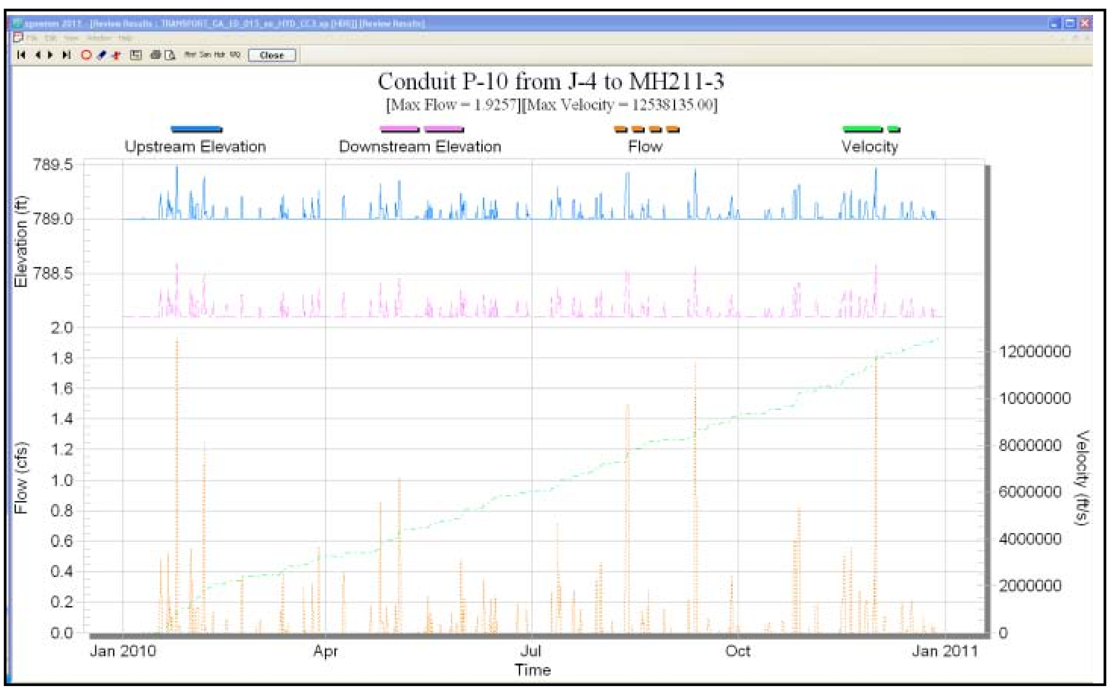

Figure 98 XPSWMM P-10 Hydrograph

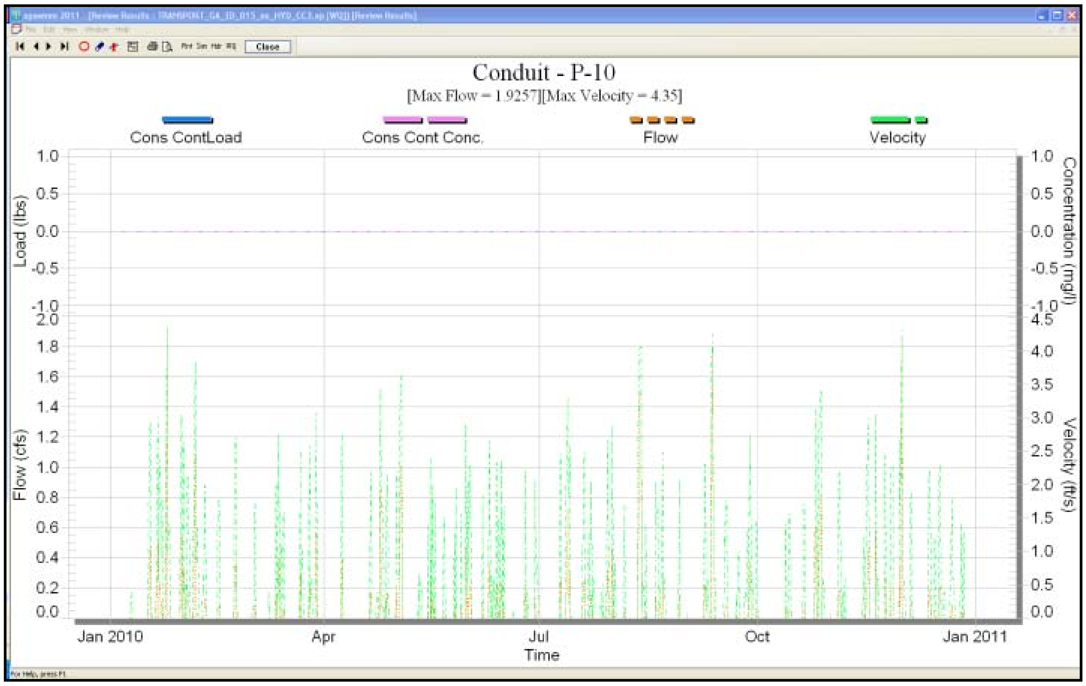

Figure 99 XPSWMM P-10 Pollutograph

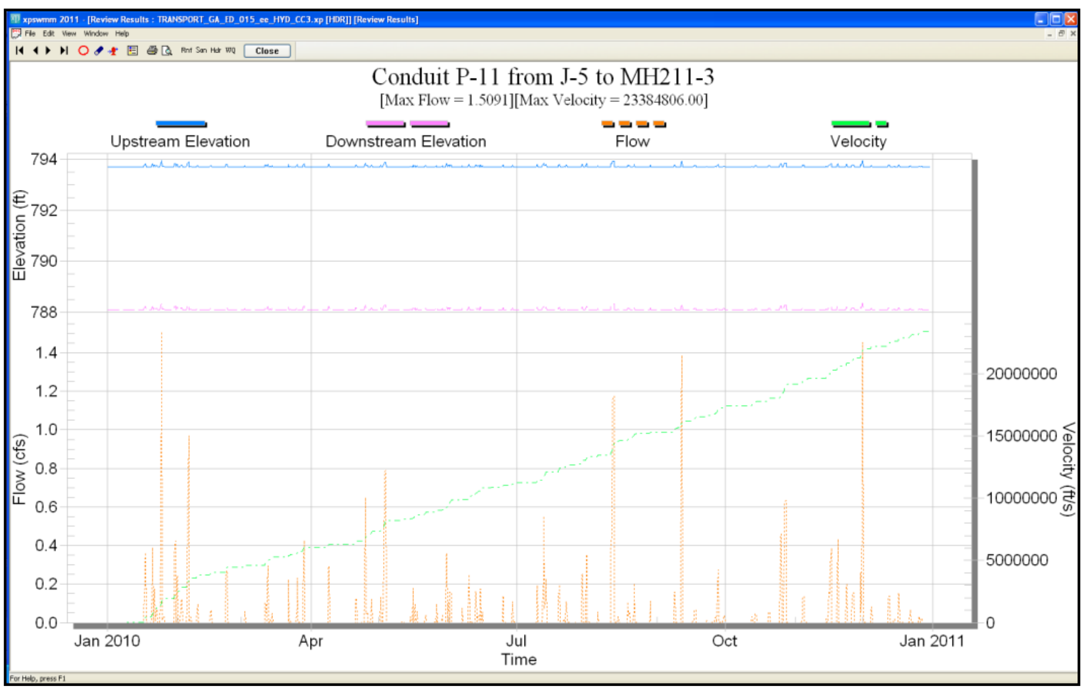

Figure 100 XPSWMM P-11 Hydrograph

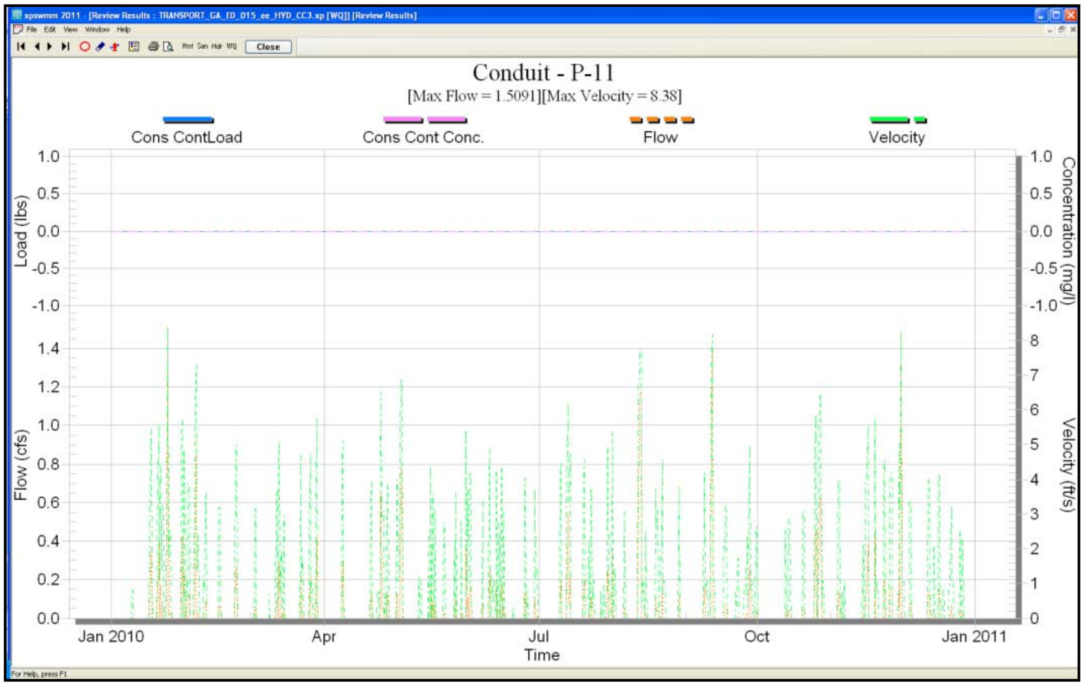

Figure 101 XPSWMM P-11 Pollutograph

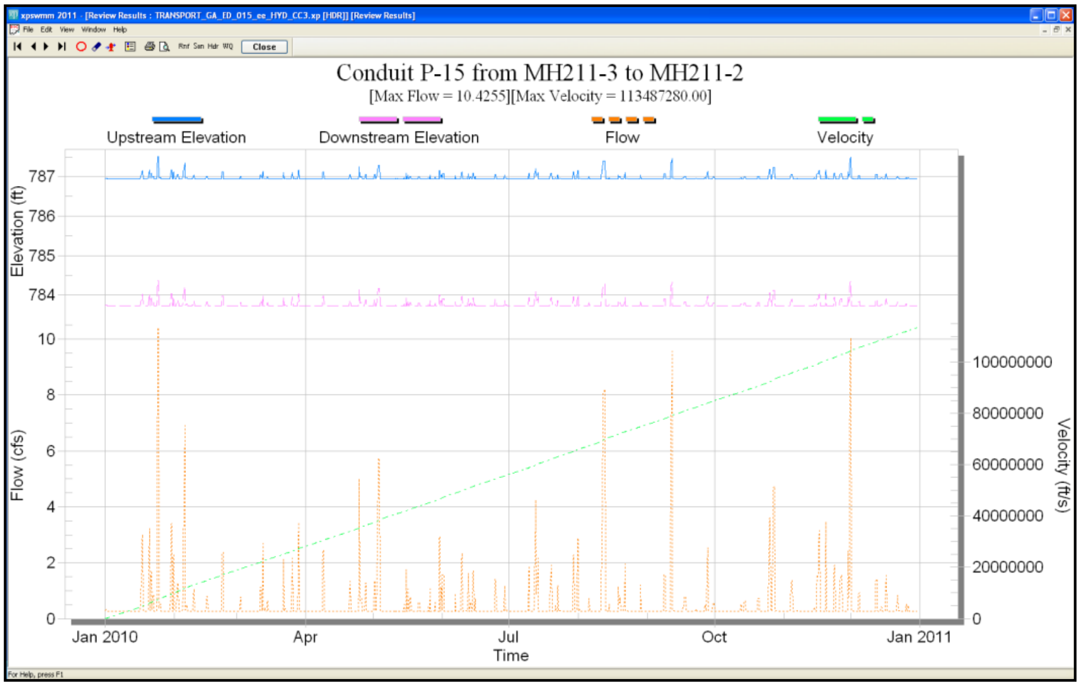

Figure 102 XPSWMM P-15 Hydrograph

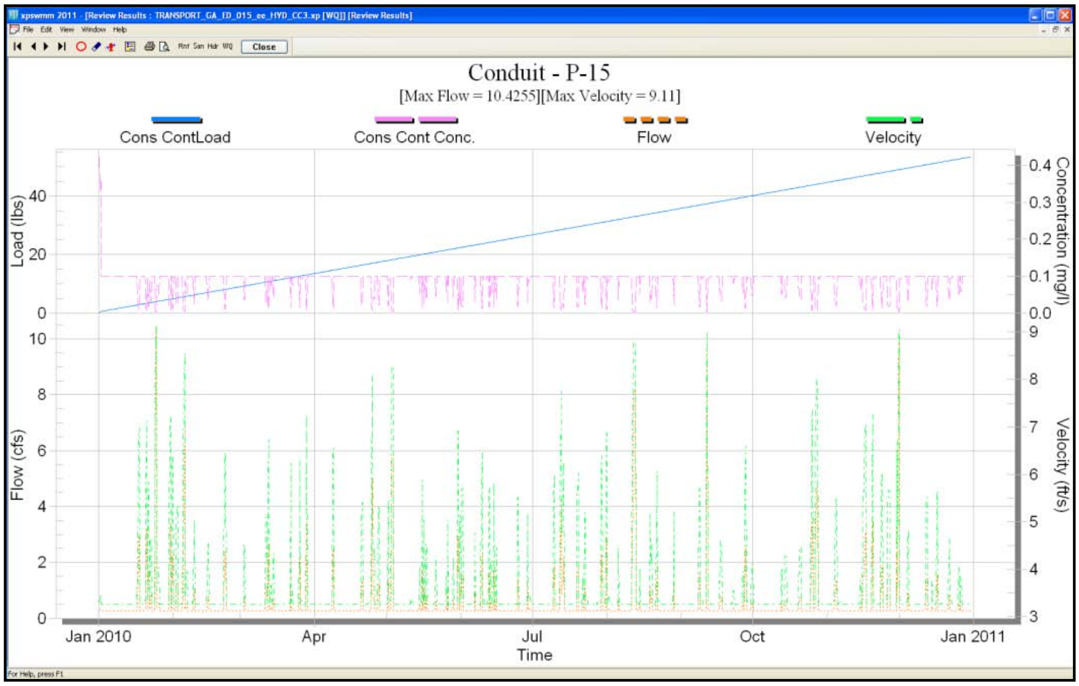

Figure 103 XPSWMM P-15 Pollutograph

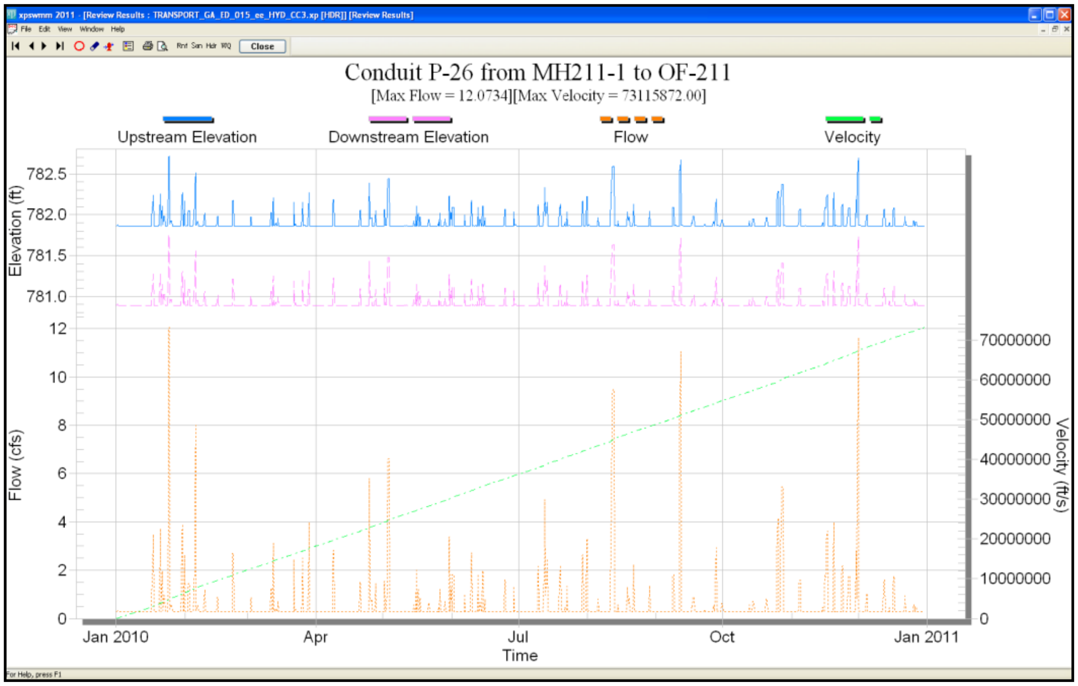

Figure 104 XPSWMM P-26 Hydrograph

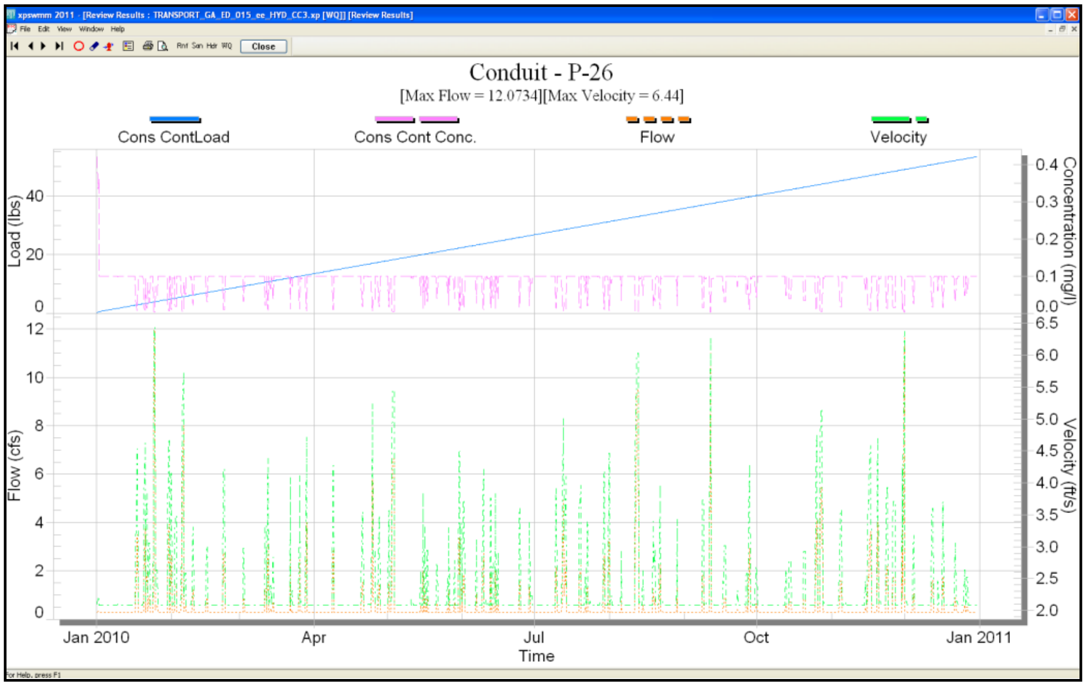

Figure 105 XPSWMM P-26 Pollutograph

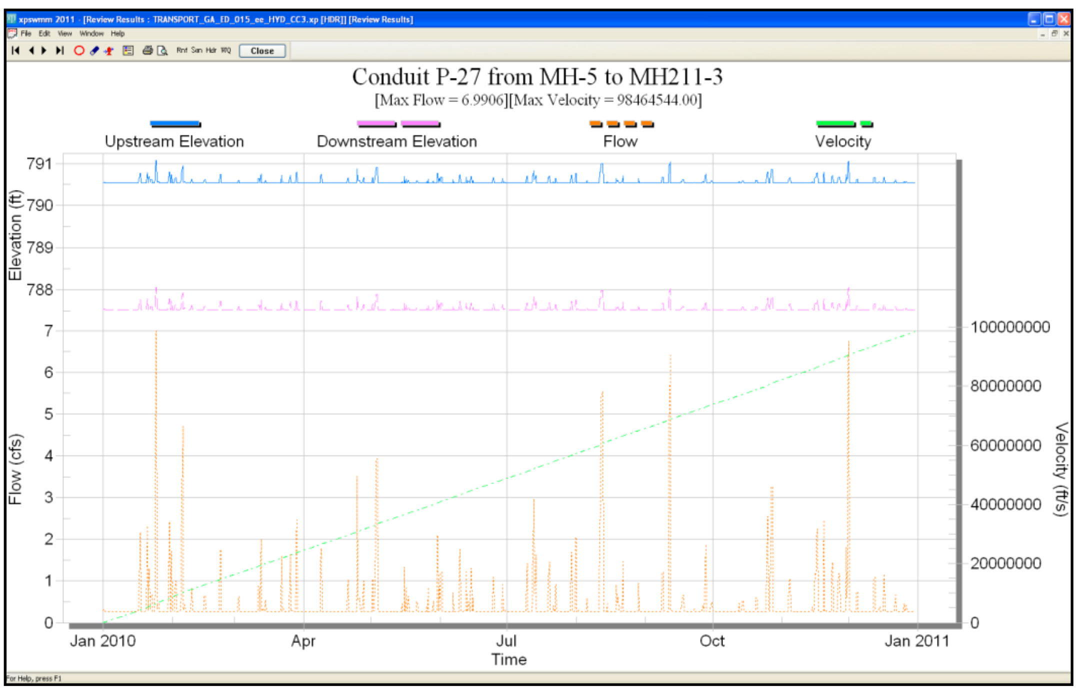

Figure 106 XPSWMM P-27 Hydrograph

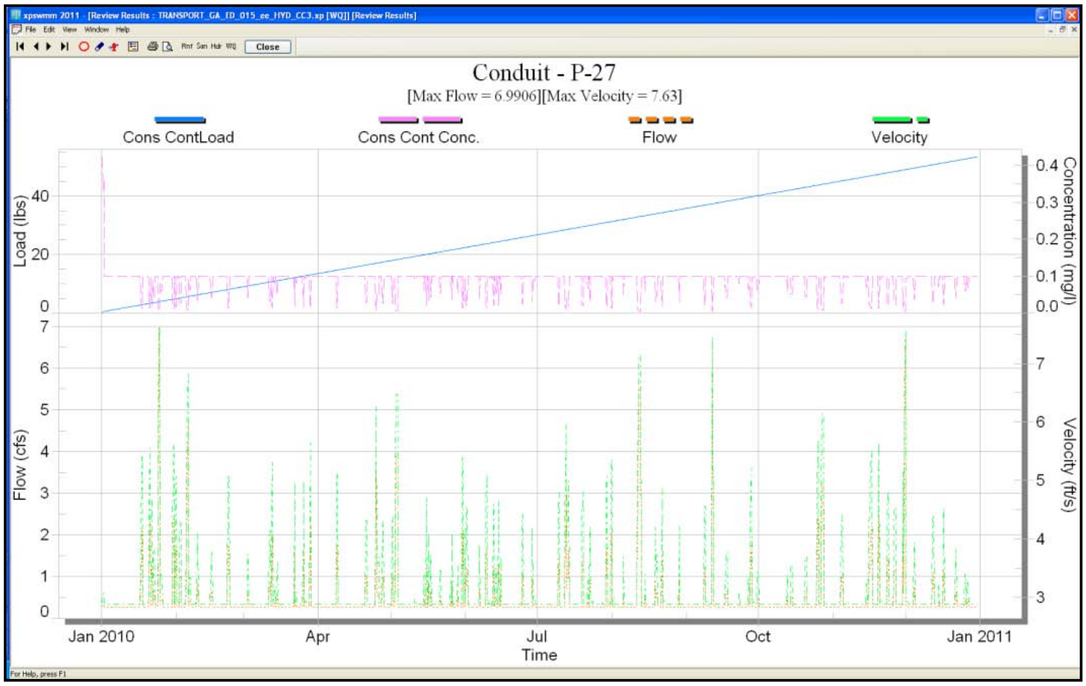

Figure 107 XPSWMM P-27 Pollutograph

Scenario 3 is focused on the system west and south of MH211-3. Link P-27 represents the combination of the two varied timeseries (B) and (C) in I-11 and I-10. Links P-15, P-26, and P-27 indicate a base flow of 0.27 cfs and a base pollutant of 0.1 mg/L from the two. The flow rate within the links increases as runoff enters the system and the concentration decreases as expected. The maximum flow rate within link P-26 is 12.1 cfs and the maximum elevation in node OF-211 is 781.8 ft, NAD. The cumulative load is estimated to be 50 mg/L.

7.4 Transport Analysis Scenario 4

The last scenario, Scenario 4, introduces varied flow and concentration timeseries (C) into node B-4500S_C, and varied flow and concentration (D) data into node T-1. No pollutant was introduced into the north and west wings of the system; therefore, no pollutant load should appear in links P-10 and P-11.

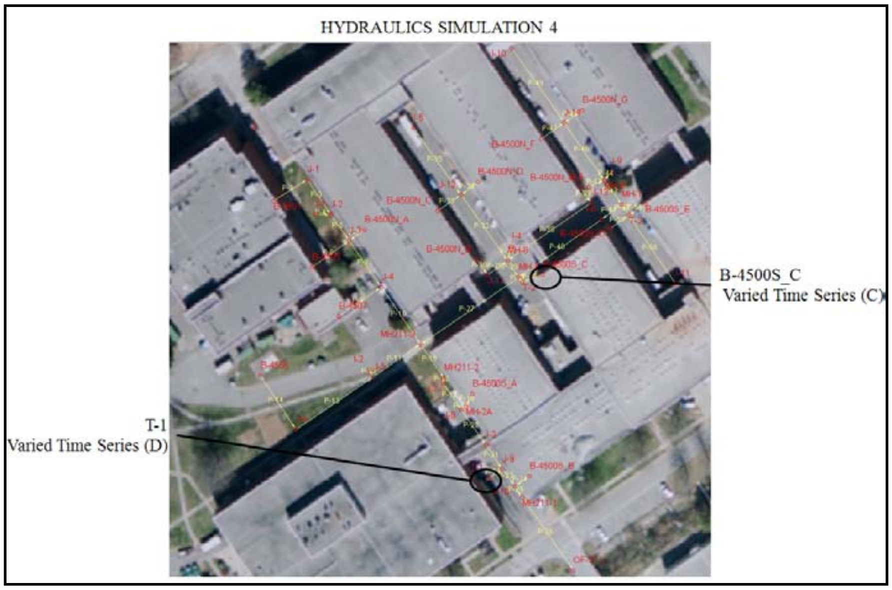

Figure 108 Transport Analysis Scenario 4 Pollutant Entrance Locations

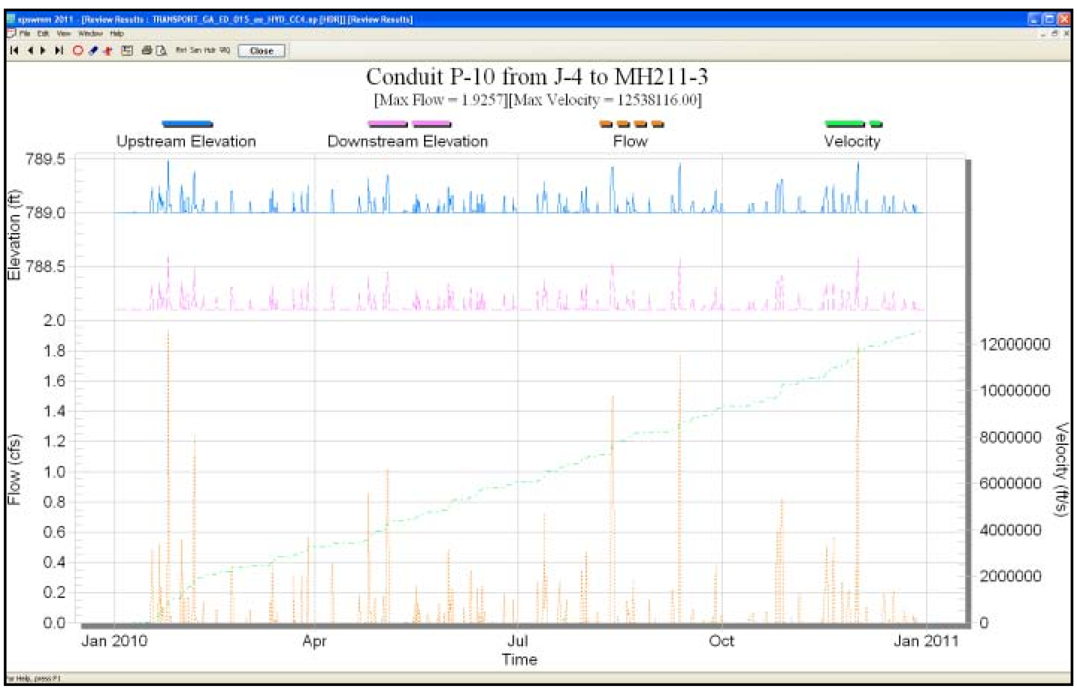

Figure 109 XPSWMM P-10 Hydrograph

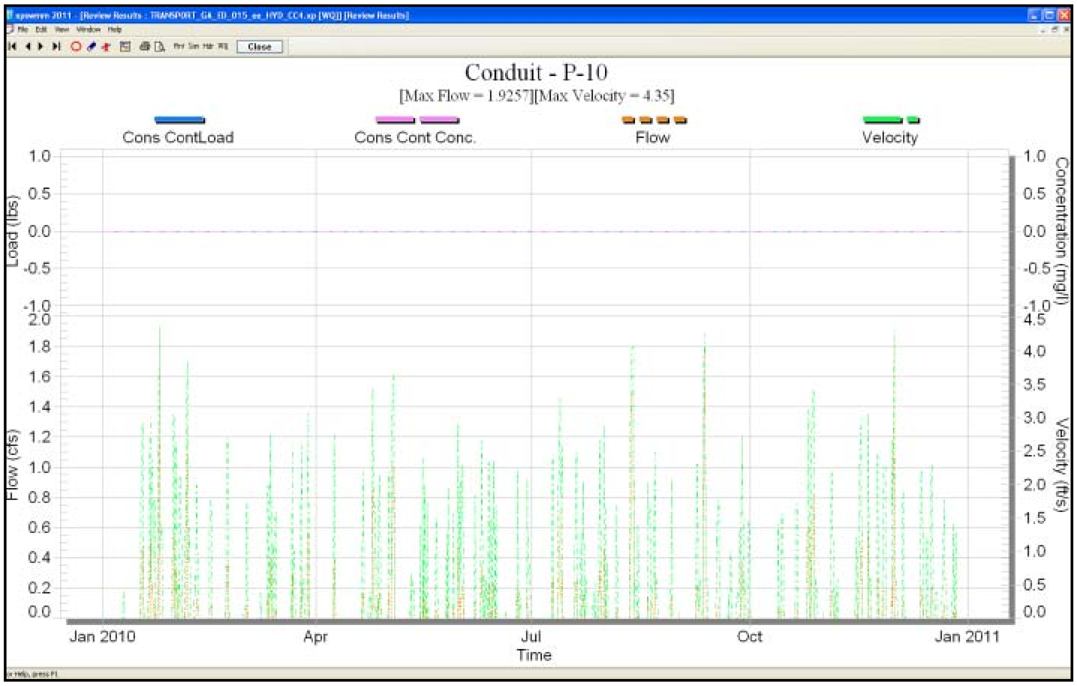

Figure 110 XPSWMM P-10 Pollutograph

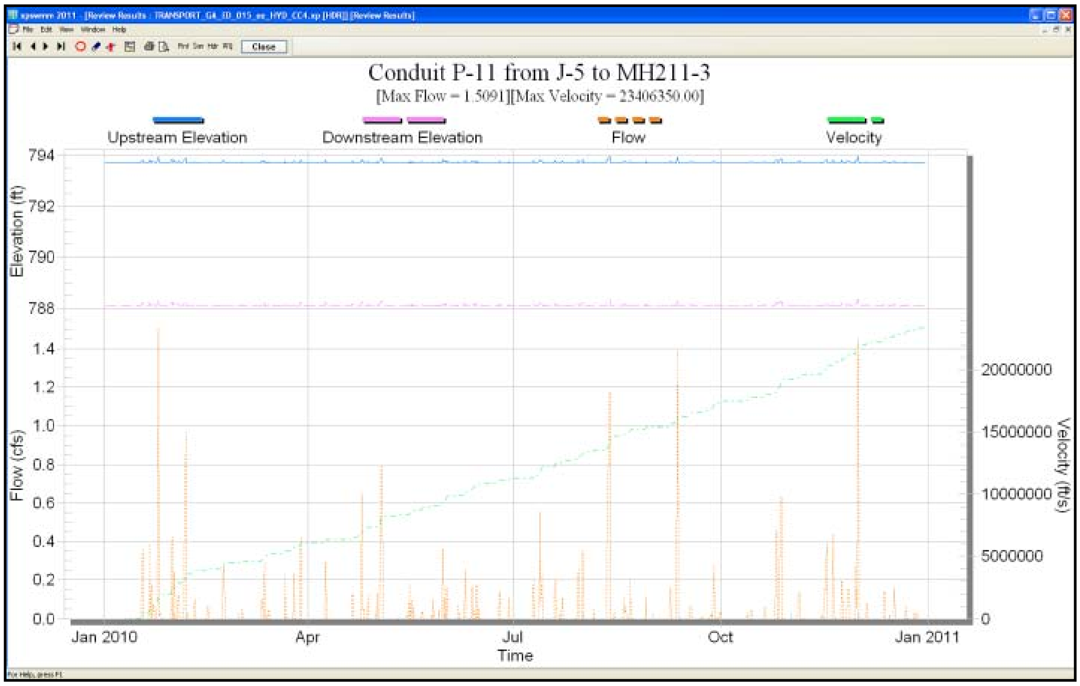

Figure 111 XPSWMM P-11 Hydrograph

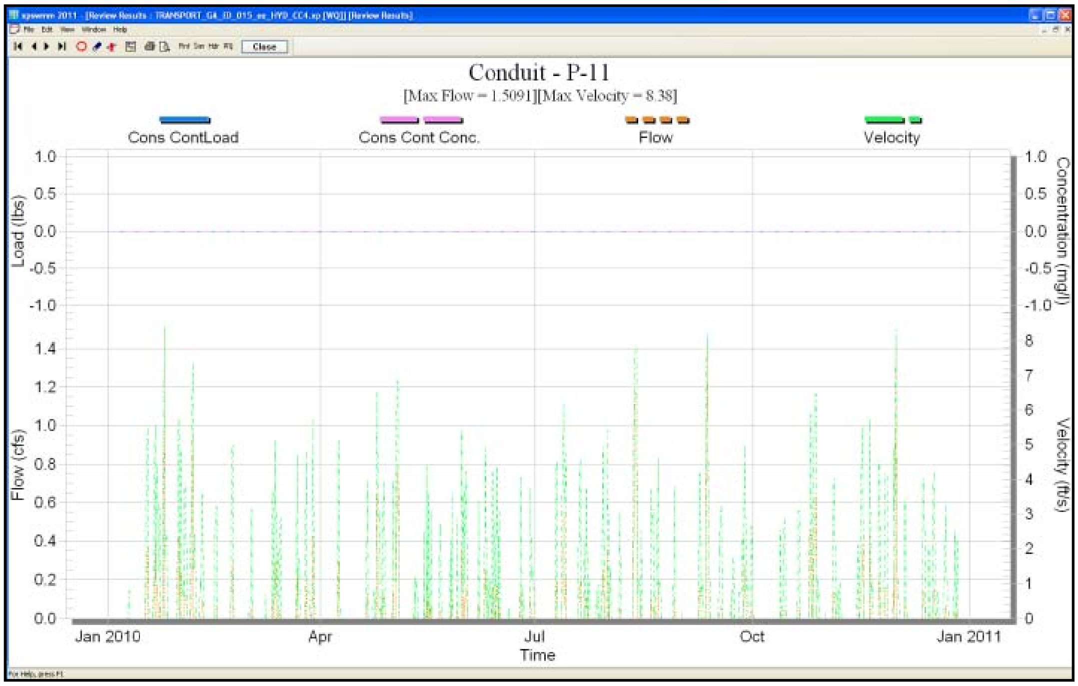

Figure 112 XPSWMM P-11 Pollutograph

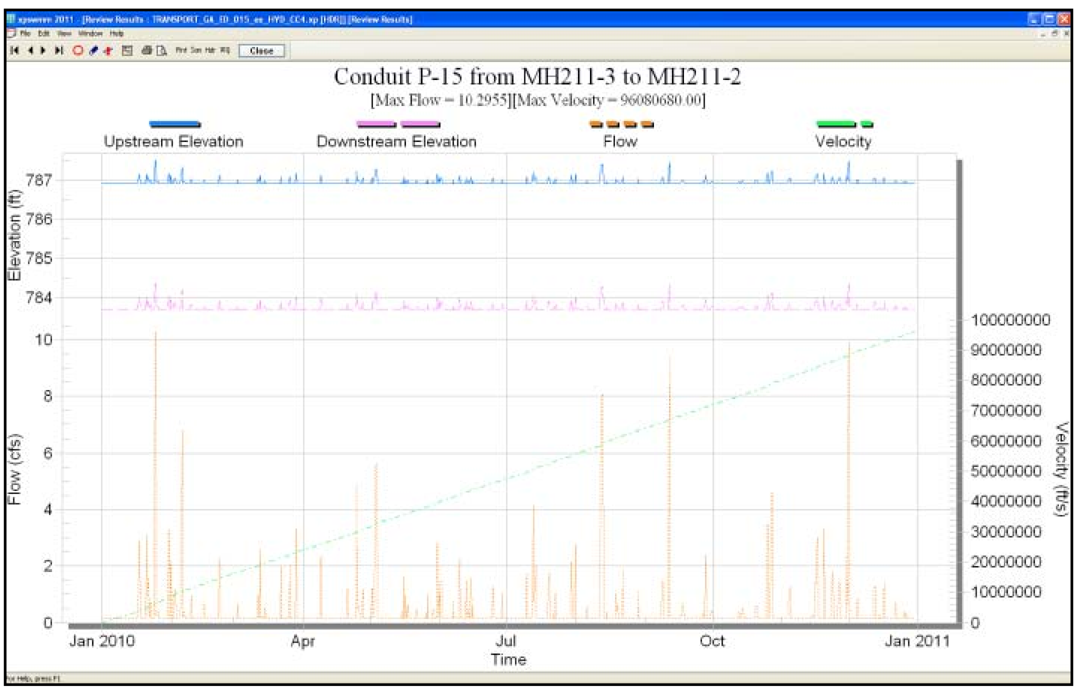

Figure 113 XPSWMM P-15 Hydrograph

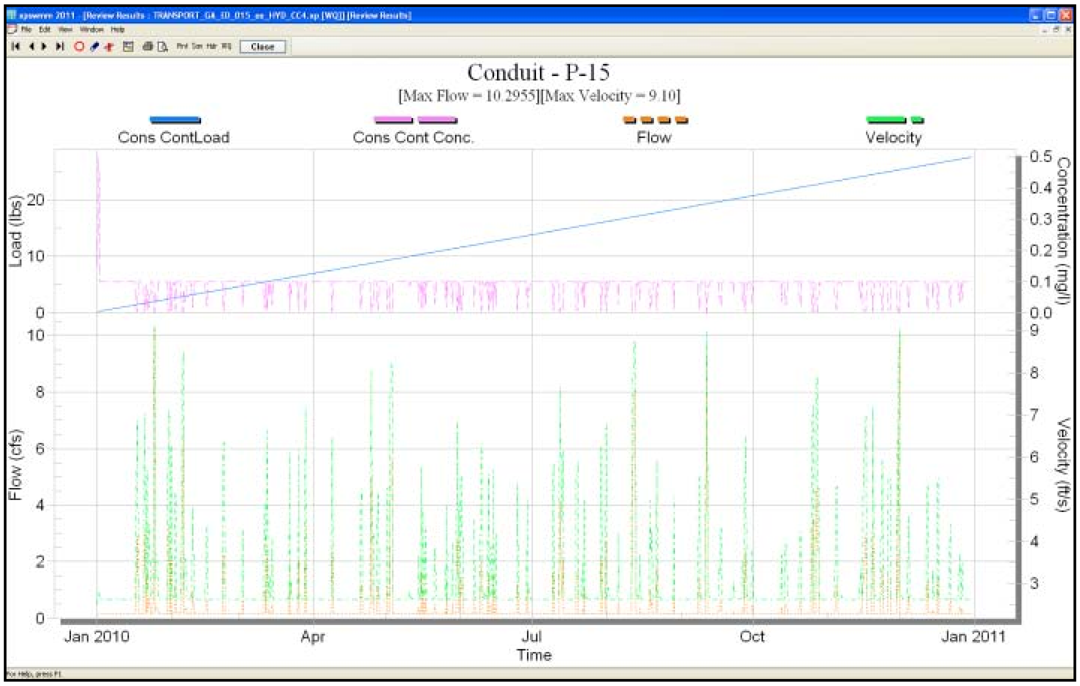

Figure 114 XPSWMM P-15 Pollutograph

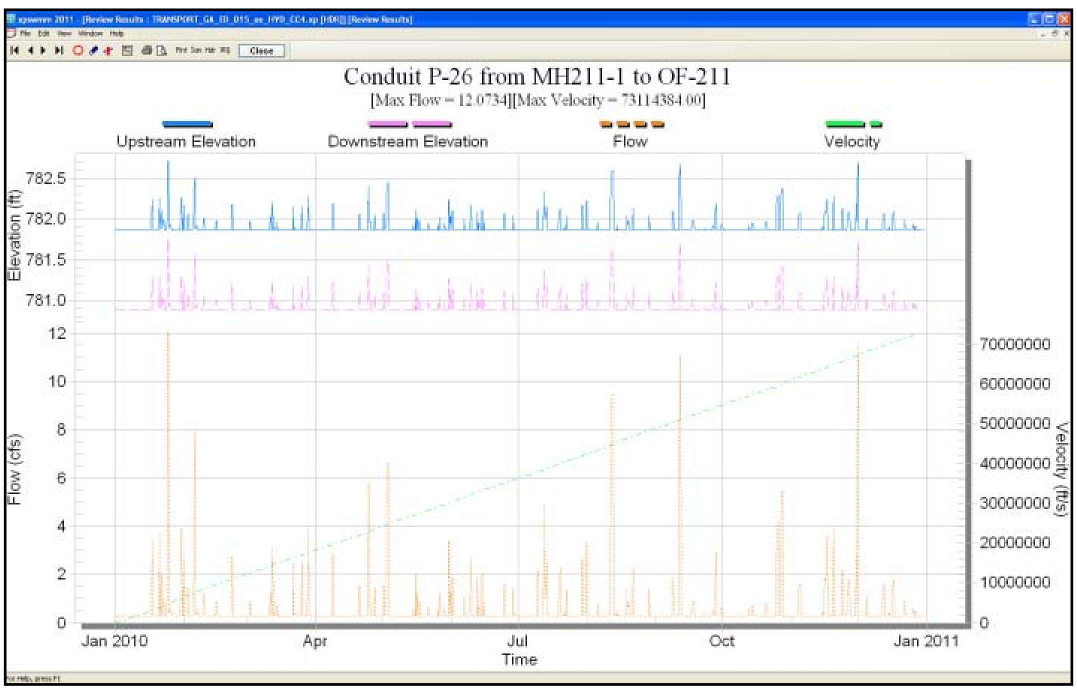

Figure 115 XPSWMM P-26 Hydrograph

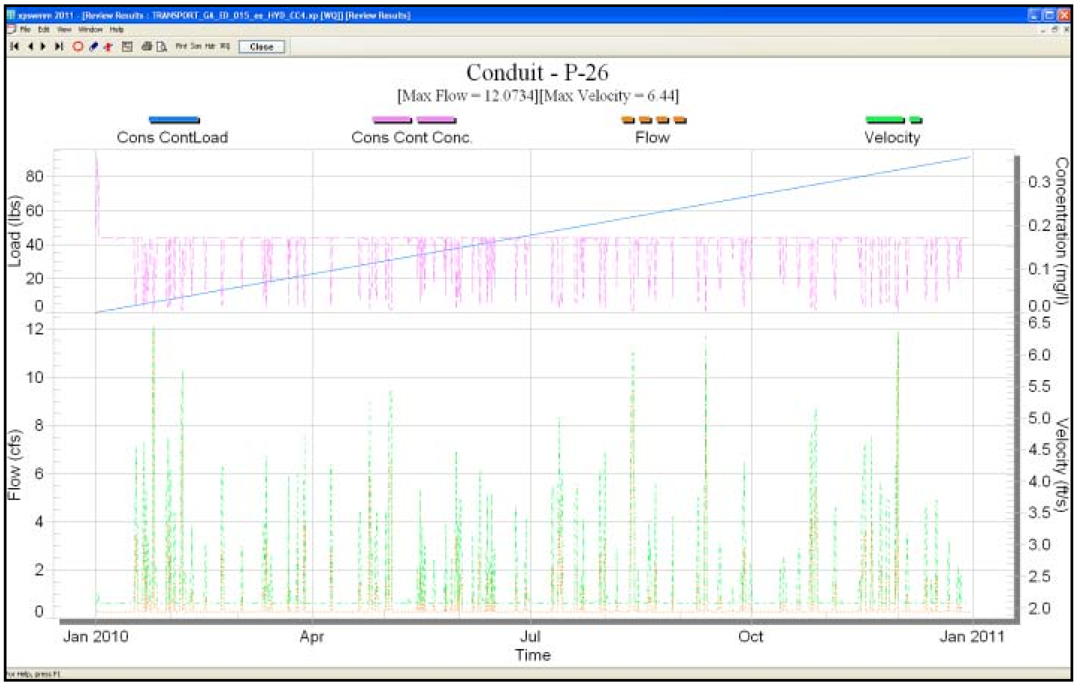

Figure 116 XPSWMM P-26 Pollutograph

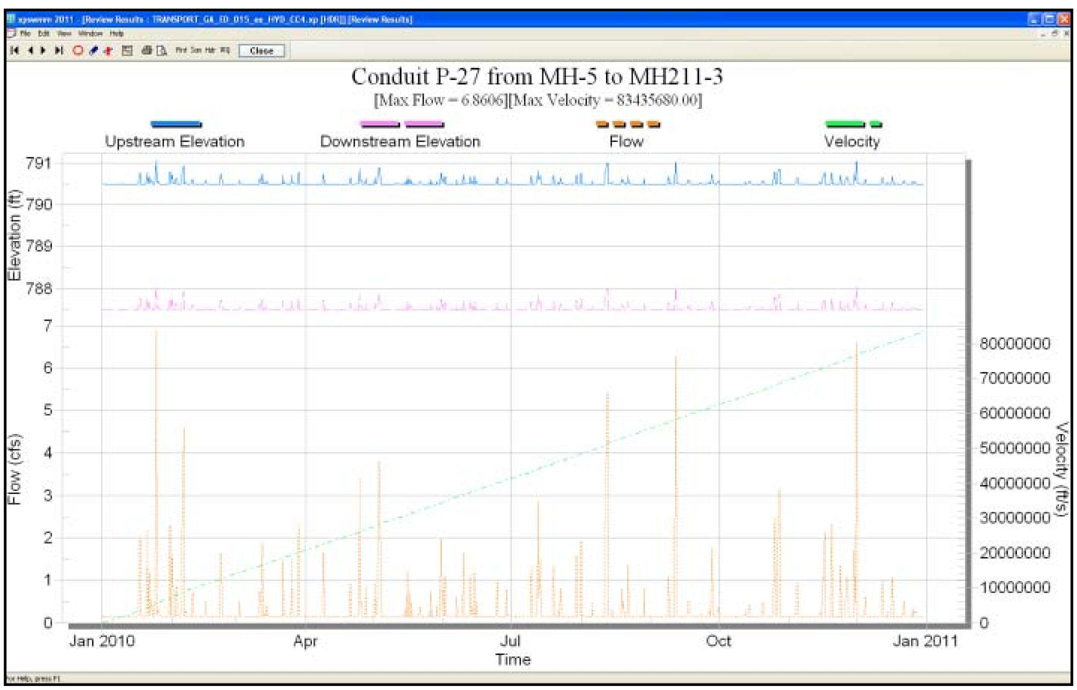

Figure 117 XPSWMM P-27 Hydrograph

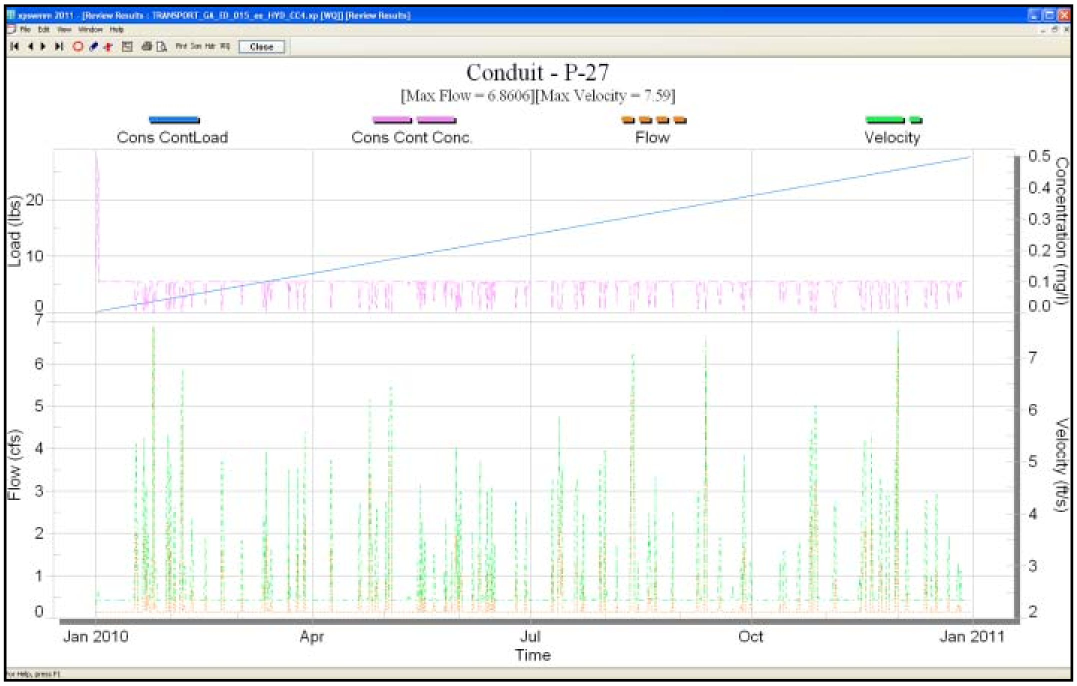

Figure 118 XPSWMM P-27 Pollutograph

Similar to Scenario 3, Scenario 4 introduces varied timeseries in two different locations and P-27 represents the combination of the two. A 0.14 cfs base flow and a 0.1 mg/L pollutant base concentration are indicated in links P-27 and P-15. Link P-26 estimates a base flow rate of 0.27 cfs and a 0.172 mg/L base pollutant concentration throughout the event. The maximum flow rate within link P-26 is 12.1 cfs and the maximum elevation in node OF-211 is 781.8 ft, NAD. The cumulative pollutant load for the year is estimated at 90 lbs.

The following figures are hydrographs representing all four scenarios, and to the right are their probability exceedance curves. P-10 and P-11 show a larger variance in PE; however, the PE indicates roughly 18% of the time there is a variance. These are minor changes in flow rate due to the introduction of base flow. P-15, P-26 and P-27 indicate even smaller variances in flow rate.

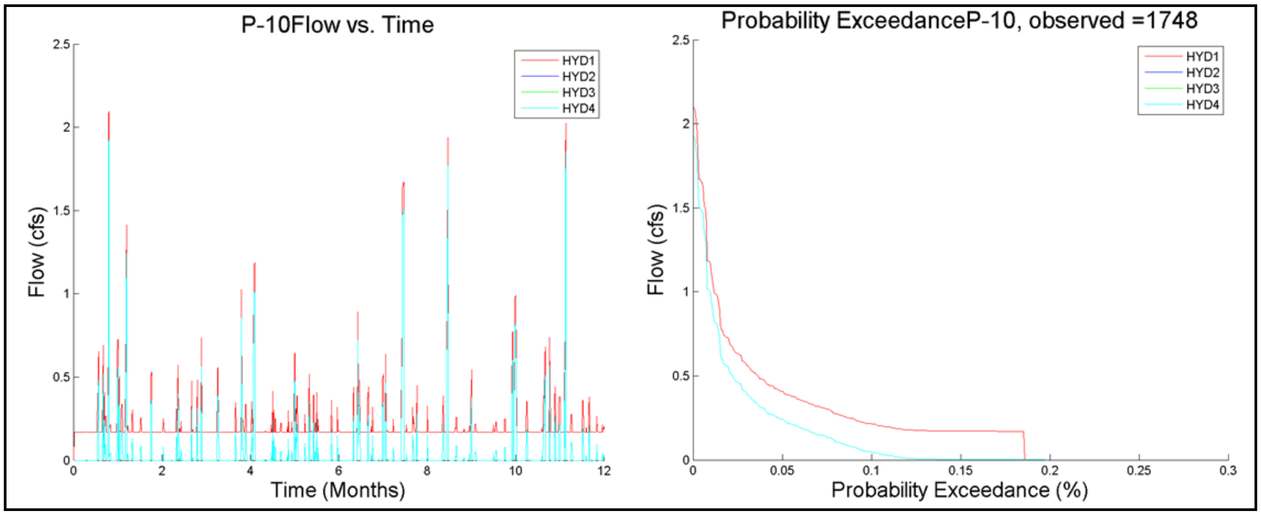

Figure 119 P-10 Hydrographs Indicating Scenarios 1-4 and their PE Curves

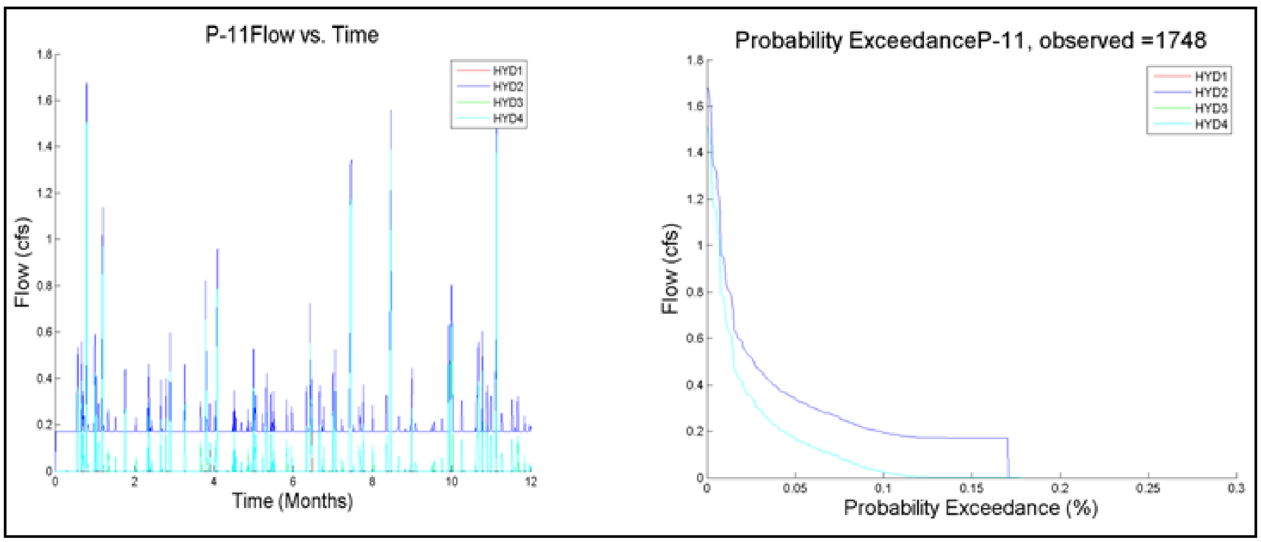

Figure 120 -11 Hydrographs Indicating Scenarios 1-4 and their PE Curves

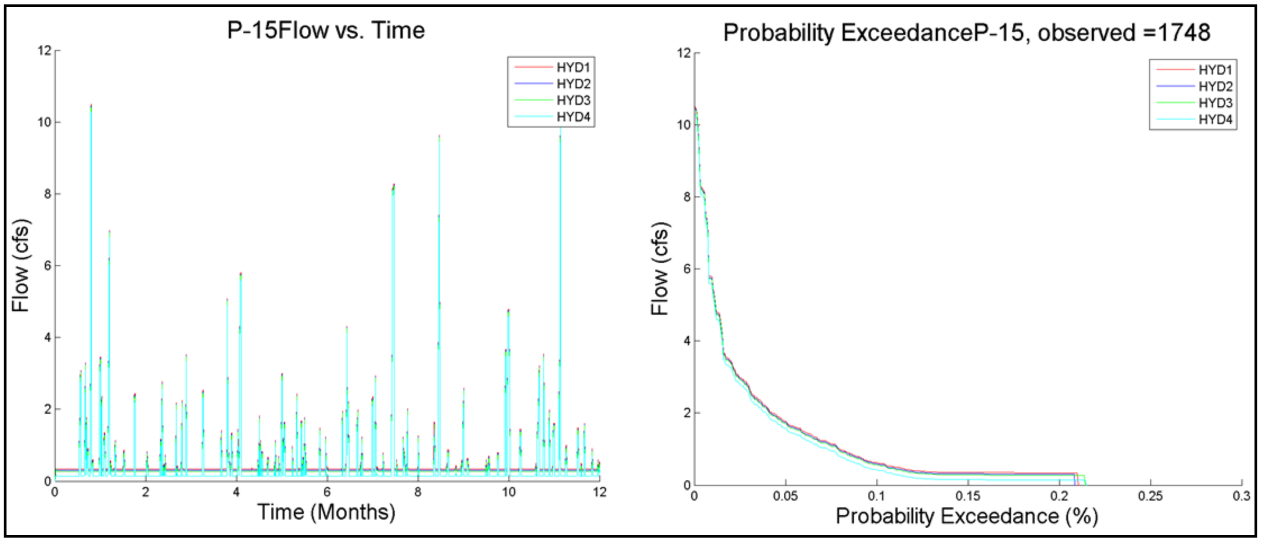

Figure 121 -15 Hydrographs Indicating Scenarios 1-4 and their PE Curves

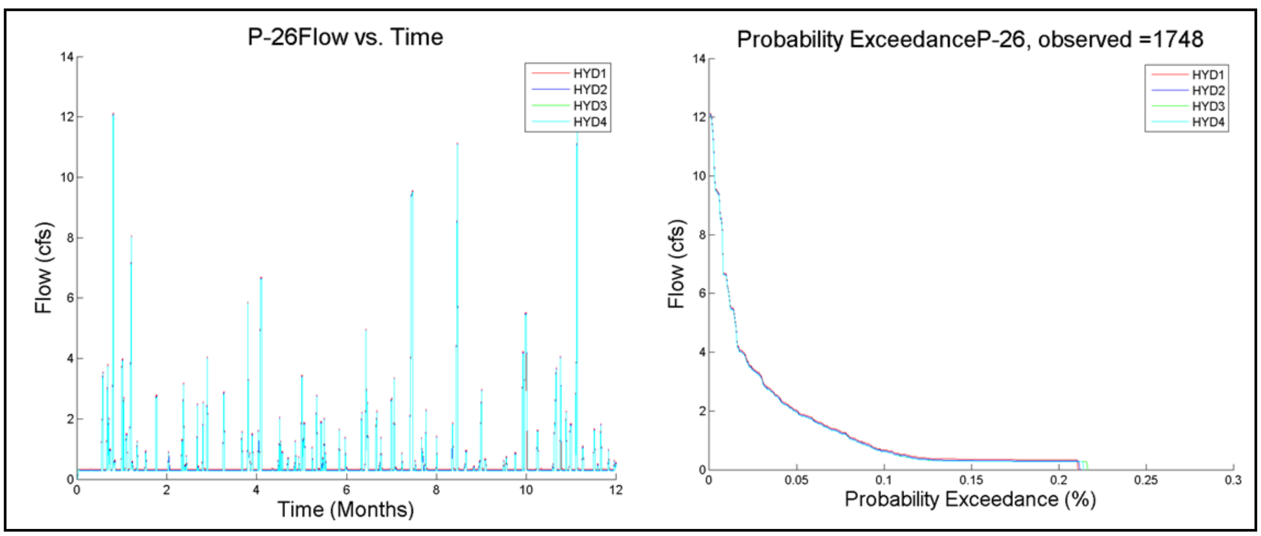

Figure 122 P-26 Hydrographs Indicating Scenarios 1-4 and their PE Curves

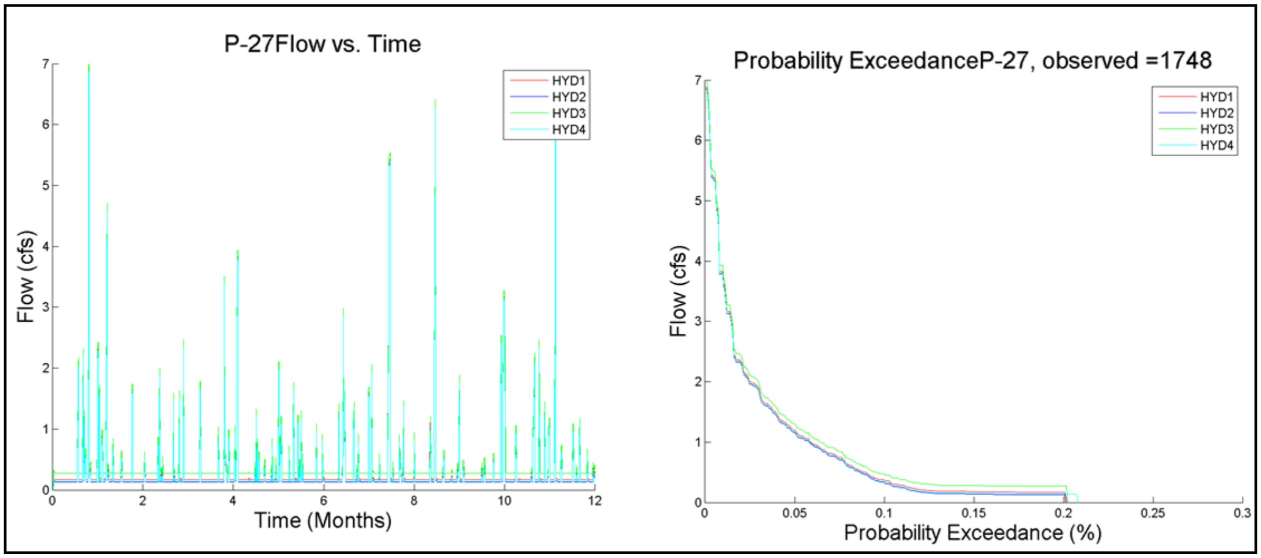

Figure 123 P-27 Hydrographs Indicating Scenarios 1-4 and their PE Curves

7.5 Probability Distribution (PD) Fitting

It is known that hydrological data follow a pattern (Hanson, 2008; Kroll, 2002; Mahdavi, 2010; Vogel, 1996). Thus, the input and output data are fit to suitable PDs for comparison. Hydrological timeseries data can be lengthy and numerous; thus, fitting the data allows the data to be characterized by its high and low distributions, which reduces the level of risk and uncertainty of results and allows for better understanding of data parameters when they are analyzed as a whole and fitted to a PD. This permits the extrapolation of data, for example in special situations such as defective monitoring equipment, on the basis or assumption the hydrological parameters at that given location are consistent with nearby outfalls, and may permit an educated guess with some certainty the data is realistic.

More specifically, low stream flow and rainfall depth are two hydrological data types that are continually analyzed and fit to probability distributions to better understand their patterns

(Hanson, 2008; Kroll, 2002; Vogel, 2002). The introduction of low stream flow and rainfall depth distributions at foreign locations may be used in order to determine the impact it has on that system. For instance, this past October 2012, Hurricane Sandy went over New York, raising water elevations and devastating Staten Island. Perhaps for the rebuilding of Staten Island, storms such as Hurricane Sandy and Hurricane Katrina could be analyzed and fit to a PD and simulated through Staten Island's proposed stormwater system with the purpose of providing a safer infrastructure for the public.

A timeseries analysis for the mercury (Hg) concentrations, surface flow rates, and Hg loads provides a means of identifying the nature of the phenomenon by the sequence of observations and allows for the forecasting of the timeseries variable by analysis of the data using different probability distribution functions and fitting it to the best probability distribution curve. Thus, the hydrograph and pollutograph timeseries data from the transport simulations were entered into the EasyFit 5.5 tool where it fit the data to numerous probability distribution functions and ranked them according to Komogorov Smirnov, Anderson Darling, and Chi-Squared methods. The distribution fits were ranked highest by the Komogorov Smirnov method for this study.

The first ranked distributions were chosen for the majority of the parameters, but were not chosen for all due to the fact that the best fit distribution is not widely known. For instance, for Scenario 1, P-11 flow was best fit to a hypersecant distribution; however, the second ranked Beta distribution, was chosen for the purpose of this study. If there is not a note for the rank, then it may be assumed the distribution stated is the first rank in the 'goodness of fit' test. The following tables display the resulting distributions from the 'goodness of fit' test for the four scenarios.

HYDRAULICS SCENARIO 1 'GOODNESS OF FIT' RESULTS				
Pipe	**Q**	**C**	**L**	**Comments**
P-10	Log-Logistic	GEV	Log-Logistic	Flow: Normal distribution ranked first Log-Logistic third.
P-11	Logistic	N/A	N/A	Pollutant data was not entered to the west.
P-15	Inv. Gaussian	GEV	Log-Logistic	Load: Burr distribution ranked first Log-Logistic second.
P-26	Inv. Gaussian	GEV	Inv. Gaussian	Flow: Fatigue Life first Inv. Gaussian fourth.
P-27	GEV	Beta	GEV	Flow: Generalized Pareto ranked first GEV second. Concentration: Burr first Beta eighth. Load: Log-Logistic (3P) first GEV second.

Table 8 Scenario 1 'Goodness of Fit' Results

Scenario 1 demonstrates that two out of the four flow rates were matched to Inverse Gaussian, three out of the four concentrations entered are characterized by the generalized extreme value (GEV) distribution, and two out of the four loads are characterized by Log-Logistic distribution.

HYDRAULICS SCENARIO 2 'GOODNESS OF FIT' RESULTS				
Pipe	**Q**	**C**	**L**	**Comments**
P-10	Logistic	N/A	N/A	Pollutant data was not entered to the north. Flow: Normal distribution ranked first Log-Logistic third.
P-11	Log-Logistic	Inv. Gaussian	Log-Logistic	Load: Frechet first Log-Logistic second.
P-15	Lognormal	GEV	Log-Logistic	Concentration: Johnson SU first GEV second.
P-26	Log-Logistic	Gamma	Log-Logistic	Flow: Person 6 first Log-Logistic sixth.
P-27	GEV	Log-Logistic	Log-Logistic	Flow: Frechet first GEV third. Load: Burr fist Log-Logistic fourth.

Table 9 Scenario 2 'Goodness of Fit' Results

Scenario 2's 'goodness of fit' results conclude that the flow rate in P-11 and P-26 may be characterized by the Log-Logistic distribution. There are no trends found for the concentration timeseries data in Scenario 2; however, all four load data fit to the Log-Logistic distribution and are characterized by that distribution.

HYDRAULICS SIMULATION 3 'GOODNESS OF FIT' RESULTS				
Pipe	**Q**	**C**	**L**	**Comments**
P-10	Logistic	N/A	N/A	Pollutant data was not entered to the north. Flow: Normal distribution ranked first Logistic third.
P-11	Logistic	N/A	N/A	Pollutant data was not entered to the west. Flow: Normal distribution ranked first Logistic third.
P-15	Exponential	Beta	Log-Logistic	Flow: Kumaraswany distribution ranked first Logistic third. Concentration: Uniform first Beta second.
P-26	Log-Logistic	Log-Logistic	Log-Logistic	Concentration: Generalized Pareto ranked first Log-Logistic second.
P-27	Log-Logistic	Exponential	Log-Logistic	

Table 10 Scenario 3 'Goodness of Fit' Results

Scenario 3 links, P-10 and P-11, contain runoff only and share the Logistic distribution fit. P-26 and P-27 share the Log-Logistic distribution. No trend is found for the concentration data; however, the loads follow a Log-Logistic trend similar to the flow rates.

HYDRAULICS SCENARIO 4 'GOODNESS OF FIT' RESULTS				
Pipe	**Q**	**C**	**L**	**Comments**
P-10	Logistic	N/A	N/A	Pollutant data was not entered to the north. Flow: Normal distribution ranked first Logistic third.
P-11	Logistic	N/A	N/A	Pollutant data was not entered to the west. Flow: Normal distribution ranked first Logistic third.
P-15	Lognormal	GEV	Log-Logistic	Load: Dagum distribution first Log-Logistic third.
P-26	Log-Logistic	Log-Logistic	Log-Logistic	Concentration: Gumbel Minimum first Log-Logistic fifth.
P-27	Log-Logistic	Log-Logistic	Log-Logistic	Concentration: Dagum distribution first Log-Logistic third. Load: Burr first Log-Logistic third.

Table 11 Scenario 4 'Goodness of Fit' Results

Similar to Scenario 3, Scenario 4 P-10 and P-11 flow rates containing only runoff share the Logistic distribution, and P-26 and P-27 the Log-Logistic distribution. Their concentrations and their loads also follow the Log-Logistic distribution.

Looking at all four scenarios as a whole, the following is apparent: when runoff was encountered and no base flow was introduced, the Logistic distribution best fit the data. The combination of runoff and base flow may be characterized by the Log-Logistic distribution. The generalized extreme value distribution was the most apparent trend in the concentrations. Lastly, the loads are mainly characterized by the Log-Logistic distribution.

8 CONCLUSION

The model was demonstrated to be an effective tool as it properly responds to rainfall data as shown by the calibration. The sensitivity analysis proves that the model is sensitive to the various Manning's roughness coefficients, infiltration parameters, and adjusted imperviousness of the sub-catchment areas; however, not enough to alter the flow rates in the system. As one would expect, flooding within the system does occur during the 25 year and 100 year – 24 hour storm events due to the fact that the storms are for designing of a system and do not resemble ordinary precipitation events throughout the year. The transport analysis has provided insight into how a conservative contaminant would react within the system if introduced at the various locations. The flow rates, concentration, and loads were fit to a probability distribution in order to characterize the data. The PE curves provide insight into the percentage of time that any node's elevation (link's flow rate) will be met or exceeded during a storm event. The runoff flow rates were found to follow the Logistic distribution; runoff and base flow are characterized by

Log-Logistic distribution, concentrations to the generalized extreme value, and the loads to the Log-Logistic distribution.

Ultimately, ORNL is concerned with residual mercury contamination within the area. Understanding the flow characteristics is fundamental for estimating contaminant transport, which directly correlates to flow. The resulting flow estimates from this model may also be used in support of other models, such as flow and transport models, for the assessment of mercury transport scenarios. In addition, it should also assist in implementing the most appropriate remediation programs, including permits to comply with regulatory guidelines.

9 REFERENCES

Bonnin, D.M., Lin, B., Parzybok, T., Yekta, M., and Riley, D. 2006. Precipitation-Frequency Atlas of the United States. NOAA Atlas 14, Volume 2, Version 3.0. NOAA, National Weather Service, Silver Spring, Maryland.

Brooks, S.C., Southworth, G.R. 2011. “History of mercury use and environmental contamination at the Oak Ridge Y-12 Plant.” Environmental Pollution Volume 159. Issue 1: 219-228. Print.

Chanson, H. 2004. Environmental Hydraulics of Open Channel Flows, Burlington: Elsevier Butterworth-Heinemann.

ChemRisk. (1999a). Radionuclide Releases to the Clinch River from WOC on the Oak Ridge Reservation—An Assessment of Historical Quantities Released, Off-site Radiation Doses, and Health Risks, Task 4. Reports of the Oak Ridge Dose Reconstruction, Volume 4. Tennessee Department of Health.

Chow, Ven Te, David R. Maidment, and Larry W. Mays. 1988. Applied Hydrology. McGraw-Hill.

City of Knoxville. 2005. Land Development Manual, Chapter 22.5 Stormwater and Street Ordinance. Accessed September 2012.

Elliott, A. H., and Trowsdale, S. A., 2007. “A review of models for low impact urban stormwater drainage”, *Environmental Modelling and Software*, 22, 394-405.

Environmental Consulting Engineers, Inc. (ECE) 1991. Functional Requirements for Waste Area Grouping 6 Monitoring Station 3 Upgrade. Knoxville, TN.

Franzetti, S. M. 2005. Background and History of Stormwater Regulations. Franzetti Law Firm P.C. Oak Brook, Illinois.

Hanson, Lars S. and Vogel, Richard. 2008. “The Probability Distribution of Daily Rainfall in the United States,” World Environmental and Water Resources Congress 2008, pp1-10.

Hossein, E, Rottle, N., Batten, Leslie. 2012. Stormwater Estimation For Management In Urban Watersheds: A Landuse-Based GIS Model. 2012 AWRA Spring Specialty Conference.

Jacobson, C. R., 2011. “Identification and Quantification of the Hydrological Impacts of Imperviousness in Urban Catchments: A Review”, *Journal of Environmental Management*, 92, 1438-1448.

Kroll, Charles N. and Vogel, Richard M. 2002. “Probality distribution of low streamflow series in the United States,” Journal of Hydrologic Engineering, Vol 7: 137-146.

Mahdavi, Mohammad; Osati, Khaled; Sadeghi, Sayed Ali Naghi; Karimi Bakhtiar; and Mobaraki, Jalil. 2010. “Determining Suitable Probability Distribution Models for Annual

Precipitation Data (A Case Study of Mazandaran and Golestan Provinces)," Journal of Sustainable Development Vol. 3, No.1, pp159-168.

Morss, R. E., Wilhelmi, O. V., Downton, M. W., and Gruntfest E. 2005. Flood Risk, Uncertainty, and Scientific Information for Decision Making: Lessons from an Interdisciplinary Project. National Center for Atmospheric Research. Boulder Colorado: Gruntfest.

Oak Ridge National Laboratory (ORNL). 2008. "Oak Ridge Reservation Annual Site Environmental Report 2007: Chapter 1 Introduction to the Oak Ridge Reservation." Home of the Oak Ridge Reservation Annual Site Environmental Report. Oak Ridge National Laboratory September 2008. UT-Battelle, LLC, for the Department of Energy. July 22, 2012

Ragheb, M. Nuclear Power Engineering: Chapter 10 Isotope Separation and Enrichment. March 9, 2012. University of Illinois. March 28, 2012 http://bit.ly/T9YVnJ

Risse, L. M., Nearing, M. A., and Savabi, M. R. Determingin the Green-Ampt Effective Hydraulic Conductivity From Rainfall-Runoff Data For the WEPP Model. Journal of the American Society of Agricultural Engineers Vol. 37(2):411-418.

Taylor, Jr., Fred G. 1989. "Mercury Monitoring of Water and Sediment in Oak Ridge National Laboratory Streams During 1989." ORNL Environmental and Health Protection Operated by Martin Marietta Energy Systems, Inc. for the United States Department of Energy: 1989.

United States Department of Energy (USDOE). 1999. Remedial Investigation/Feasibility Study for Bethel Valley Watershed at Oak Ridge National Laboratory. Report# DOE/OR/01-1748/V1&D2.

United States Environmental Protection Agency (USEPA). 2004. Federal Facilities Assessment Branch Division of Health Assessment and Consultation Agency for Toxic Substances and Disease Registry. "Health Assessment: Y-12 Uranium Releases" (USDOE) Oak Ridge, Roane County, Tennessee."

United States Environmental Protection Agency (USEPA). 2006. Federal Facilities Assessment Branch Division of Health Assessment and Consultation Agency for Toxic Substances and Disease Registry. "Public Health Assessment White Oak Creek Radionuclide Releases Oak Ridge Reservation (USDOE) Oak Ridge, Roane County, Tennessee."

United States Environmental Protection Agency (USEPA). 2012. "Stormwater Management Model (SWMM)." Risk Management Water Research. [Available online at http://www.epa.gov/nrmrl/wswrd/wq/models/swmm/, accessed September 2012].

Verma, S. C., 1982. "Modified Horton's Infiltration Equation", Journal of Hydrology, 58, 383-388.

Vogel, R. M., and Wilson, I. (1996). "Probability distribution of annual maximum, mean, and minimum streamflows in the United States," Journal of Hydrologic Engineering, 1 (2), 69–76.a3j

10 APPENDICES

Rational Method Runoff Coefficients (Chow, 1988)	
Ground Cover	**Runoff Coefficient, c**
Lawns	0.05 - 0.35
Forest	0.05 - 0.25
Cultivated land	0.08-0.41
Meadow	0.1 - 0.5
Parks, cemeteries	0.1 - 0.25
Unimproved areas	0.1 - 0.3
Pasture	0.12 - 0.62
Residential areas	0.3 - 0.75
Business areas	0.5 - 0.95
Industrial areas	0.5 - 0.9
Asphalt streets	0.7 - 0.95
Brick streets	0.7 - 0.85
Roofs	0.75 - 0.95
Concrete streets	0.7 - 0.95

Manning's n for Closed Conduits Flowing Partly Full Table (Chow, 1988)			
Type of Conduit and Description	**Minimum**	**Normal**	**Maximum**
1. Brass, smooth:	0.009	0.010	0.013
2. Steel:			
Lockbar and welded	0.010	0.012	0.014
Riveted and spiral	0.013	0.016	0.017
3. Cast Iron:			
Coated	0.010	0.013	0.014
Uncoated	0.011	0.014	0.016
4. Wrought Iron:			
Black	0.012	0.014	0.015
Galvanized	0.013	0.016	0.017
5. Corrugated Metal:			
Subdrain	0.017	0.019	0.021
Stormdrain	0.021	0.024	0.030
6. Cement:			
Neat Surface	0.010	0.011	0.013
Mortar	0.011	0.013	0.015
7. Concrete:			
Culvert, straight and free of debris	0.010	0.011	0.013
Culvert with bends, connections, and some debris	0.011	0.013	0.014
Finished	0.011	0.012	0.014
Sewer with manholes, inlet, etc., straight	0.013	0.015	0.017
Unfinished, steel form	0.012	0.013	0.014
Unfinished, smooth wood form	0.012	0.014	0.016
Unfinished, rough wood form	0.015	0.017	0.020
8. Wood:			
Stave	0.010	0.012	0.014
Laminated, treated	0.015	0.017	0.020
9. Clay:			
Common drainage tile	0.011	0.013	0.017
Vitrified sewer	0.011	0.014	0.017
Vitrified sewer with manholes, inlet, etc.	0.013	0.015	0.017
Vitrified Subdrain with open joint	0.014	0.016	0.018
10. Brickwork:			
Glazed	0.011	0.013	0.015
Lined with cement mortar	0.012	0.015	0.017
Sanitary sewers coated with sewage slime with bends and connections	0.012	0.013	0.016
Paved invert, sewer, smooth bottom	0.016	0.019	0.020
Rubble masonry, cemented	0.018	0.025	0.030